

NASA Contract NAS9-13882
DRL No. T-945, Item 9
DRD No. MA-1291 Rev. B
R-9840

NASA CR.

150991

SPACE SHUTTLE
PROTOTYPE CHECK VALVE DEVELOPMENT

September 1976

(NASA-CR-150991) SPACE SHUTTLE PROTOTYPE
CHECK VALVE DEVELOPMENT (Rocketdyne) 297 p
HC \$9.25 CSCL 13K

N76-32560

Unclas
G3/37 05358

Prepared by
G. F. Tellier

Prepared for
National Aeronautics and Space Administration
Johnson Spacecraft Center
Houston, Texas 77058

Rocketdyne Division
Rockwell International Corporation
Canoga Park, California 91304



NASA Contract NAS9-13882
DRL No. T-945, Item 9
DRD No. MA-129T Rev. B
R-9840

SPACE SHUTTLE
PROTOTYPE CHECK VALVE DEVELOPMENT

September 1976

Prepared by
G. F. Tellier

Approved
R. D. Paster
Program Manager

Prepared for
National Aeronautics and Space Administration
Johnson Spacecraft Center
Houston, Texas 77058

Rocketdyne Division
Rockwell International Corporation
Canoga Park, California 91304

FOREWORD

This final report was prepared in compliance with NASA contract NAS9-13882 covering a period of performance from 1 March 1974 through 24 September 1975.

Principal Rocketdyne investigators were G. F. Tellier, Principal Engineer, and G. M. Smith. Materials and process advice and assistance was provided by R. Mowers (polymers) and W. Taggart who suggested RFNA for accelerated corrosion screening of cutter seal specimens. Major design effort was provided by W. A. Gillon. Program Managers were R. W. Helsel succeeded by R. D. Paster.

The program was sponsored and administered by NASA Lyndon B. Johnson Space Center, Propulsion and Power Division, Houston, Texas, with John W. Griffin as Project Engineer.

Specialized fabrication and preparation of test models, fixtures, and the prototype check valve were contracted with L. A. Gauge Company, Sun Valley, California, whose cooperation and interest is gratefully acknowledged.

This report is assigned Rocketdyne Report No. R-9840.

ABSTRACT

Presented herein are detail results of analytical and experimental investigations to develop contaminant resistant seal designs and a dynamically stable prototype check valve for the orbital maneuvering and reaction control helium pressurization systems of the Space Shuttle. Polymer and carbide seal models were designed and tested. Perfluoroelastomers compatible with N_2O_4 and N_2H_4 types were evaluated and compared with Teflon in flat and captive seal models. Carbide cutter seals of proven long life were compared with the polymer seals in low load sealing and contamination resistance which demonstrated cutter seal superiority. Ceramic and carbide materials were evaluated for N_2O_4 service using exposure to RFNA as a worst case screen; chemically vapor deposited tungsten carbide was shown to be impervious to the acid after 6 months immersion. A unique carbide shell poppet/cutter seat check valve was designed and tested to demonstrate low cracking pressure (<2.0 psid), dynamic stability under all test bench flow conditions, contamination resistance (0.001 inch CRES wires cut with <1.5 pound seat load) and long life of 100,000 cycles (leakage <1.0 scc/hr helium from 0.1 to 400 psig).

CONTENTS

| | |
|---|------|
| Introduction | 1-1 |
| Program Objective | 1-1 |
| Technical Approach | 1-1 |
| Technical Guidelines | 1-2 |
| Summary | 1-5 |
| Leakage Analysis | 1-5 |
| Test Models | 1-6 |
| Materials Investigation | 1-6 |
| Model Seal Tests | 1-8 |
| Check Valve Development | 1-9 |
| Conclusions | 1-13 |
| Recommendations | 1-15 |
| Leakage Analysis | 2-1 |
| Nomenclature and Units | 2-1 |
| Modes of Leakage Flow | 2-3 |
| Transition Molecular and Laminar Flow | 2-6 |
| Numerical Example | 2-8 |
| OMS Check Valve Leakage | 2-9 |
| Test Models | 3-1 |
| Concent Design and Trade Study | 3-1 |
| Model Description | 3-2 |
| Model Preparation | 3-6 |
| Model Inspection | 3-8 |
| Materials Investigation | 4-1 |
| Cutter Seal Materials | 4-1 |
| Structural Materials | 4-24 |
| Polymer Materials | 4-27 |
| Model Seal Tests | 5-1 |
| General Approach | 5-1 |
| Data Presentation | 5-3 |
| Cutter Model Tests | 5-4 |
| Flat Polymer Model Tests | 5-48 |

| | |
|--|------|
| Captive Polymer Model Tests | 5-63 |
| Observations | 5-66 |
| Check Valve Development | 6-1 |
| Trade Study | 6-1 |
| Performance Analysis | 6-18 |
| Fabrication | 6-21 |
| Test Program | 6-23 |
| Spare Parts Testing | 6-30 |
| Projected Quad Valve Performance | 6-38 |
| References | 7-1 |
| <u>Appendix A</u> | |
| General Technical Guidelines | A-1 |
| <u>Appendix B</u> | |
| Seal Model Concepts and Detail Designs | B-1 |
| <u>Appendix C</u> | |
| Polymer Seal Fabrication | C-1 |
| <u>Appendix D</u> | |
| Seal Model Tester, System and Operational Procedures | D-1 |

ILLUSTRATIONS

| | | |
|-------|---|------|
| 1-1. | Prototype Value Analysis and Design | 1-10 |
| 2-1. | Parallel Plate Model Flow | 2-13 |
| 2-2. | Circular Hole Model Flow | 2-15 |
| 2-3. | Check Valve Leakage Model | 2-19 |
| 2-4. | Model Gap for Narrow Land (0.0002 inch) | 2-21 |
| 2-5. | Model Gap for Wide Land (0.0006 inch) | 2-22 |
| 2-6. | N ₂ O ₄ Liquid Leakage Correlation | 2-24 |
| 2-7. | MMH Liquid Leakage Correlation | 2-25 |
| 2-8. | H ₂ O Liquid Leakage Correlation | 2-26 |
| 2-9. | Seat Gap Versus Force Hypothesis | 2-28 |
| 2-10. | NO ₂ Vapor Leakage Correlation | 2-29 |
| 2-11. | H ₂ O Vapor Leakage Correlation | 2-30 |
| 3-1. | Cutter Seal Model | 3-4 |
| 3-2. | Flat Polymer Seal Model | 3-5 |
| 3-3. | Captive Polymer Seal Model | 3-7 |
| 3-4. | Leitz Interference Microscope | 3-9 |
| 4-1. | Edge Fracturability Test of Typical Cutter Material Specimens (462X Interference Photos) | 4-6 |
| 4-2. | Head of Common House Ant (500X SEM Photo) | 4-10 |
| 4-3. | Razor Blade Edge (SEM Photos) | 4-11 |
| 4-4. | Specimen No. 1 Sapphire | 4-12 |
| 4-5. | Specimen No. 2 Ruby | 4-13 |
| 4-6. | Specimen No. 3 Chromium Carbide, CA815 (15% Nickel) | 4-14 |
| 4-7. | Specimen No. 4 Silicon Nitride | 4-16 |
| 4-8. | Specimen No. 5 Tungsten Carbide, CA315 (15% Cobalt) | 4-17 |
| 4-9. | Specimen No. 6 Tungsten Carbide, KZ801 (6% Nickel) | 4-18 |
| 4-10. | Specimen No. 7 Tungsten Carbide, CM-500 (Vapor Deposited) | 4-19 |
| 4-11. | Specimen No. 7 Tungsten Carbide, CM-500 (Vapor Deposited) | 4-20 |
| 4-12. | Specimen No. 8 Tungsten Carbide, 883 (6% Cobalt) | 4-21 |
| 4-13. | Specimen No. 9 Alumina (Superwearox) | 4-22 |

| | | |
|-------|--|------|
| 4-14. | Specimen No. 10 Tantalum-Tungsten Carbide (K602) | 4-23 |
| 4-15. | Specimen No. 11 Boron Carbide | 4-25 |
| 4-16. | Specimen No. 12 304L CRES | 4-26 |
| 4-17. | Specimen No. 15 17-4PH CRES | 4-28 |
| 4-18. | Specimen No. 16 Stooddy No. 2 Alloy | 4-29 |
| 4-19. | Specimen No. 17 Inconel 718 | 4-30 |
| 4-20. | Typical Surface Texture of Molded AF-E-124X Filled Elastomer (91X Interference Photo) | 4-33 |
| 4-21. | TFE Molded at 350F (462X Interference Photo) | 4-35 |
| 4-22. | FEP Molded at 400F (462X Interference Photo) | 4-35 |
| 4-23. | FEP Die Molded at 540F (462X Interference Photo) | 4-35 |
| 5-1. | Leakage Data for Model 101, Test No. 1 Through 3 | 5-8 |
| 5-2. | Model 101 Computed Seat Gap, Test No. 1 (Clean) | 5-9 |
| 5-3. | Model 101 Computed Seat Gap, Test No. 2 (0.0004 Inch CRES Wire) | 5-10 |
| 5-4. | Model 101 Computed Leakage, Test No. 2 (0.0004 Inch CRES Wire) | 5-11 |
| 5-5. | Leakage Data for Model 101, Tests 3 Through 5 | 5-12 |
| 5-6. | Model 101 Seat Gap, Test 4 (0.001 Copper Wire) | 5-13 |
| 5-7. | Model 101 Computed Leakage, Test 4 (0.001 Inch Copper Wire) | 5-14 |
| 5-8. | Leakage Data for Model 101, Tests 5 Through 7 | 5-15 |
| 5-9. | Model 101 Computed Seat Gap, Test 6 (0.003 Inch Copper Wire) | 5-16 |
| 5-10. | Leakage Data for Model 101, Tests 7 Through 9 | 5-17 |
| 5-11. | Model 101 Computed Seat Gap, Test 8 (0.001 Inch CRES Wire) | 5-18 |
| 5-12. | Leakage Data for Model 101, Tests 9 Through 11 | 5-19 |
| 5-13. | Computed Seat Gap, Test 10 (0.003 Inch CRES Wire) | 5-20 |
| 5-14. | Model 101 Seat Showing Groove From 0.004 Inch CRES Wire (462X Interference Photo) | 5-21 |
| 5-15. | Model 101 Seat (Repeat 462X Interference Photo) | 5-21 |
| 5-16. | Model 101 Test 2 0.0004 Inch CRES Wire (462X Interference Photo) | 5-21 |
| 5-17. | Model 101 Test 6 0.003 Inch Copper Wire (462X Plain Photo) | 5-21 |

| | | |
|-------|---|------|
| 5-18. | Model 101 Seat Showing Groove From 0.001 Inch CRES Wire (462X Interference Photo) | 5-22 |
| 5-19. | Model 101 Test 8 0.001 Inch CRES Wire (462X Interference Photo) | 5-22 |
| 5-20. | Model 101 Seat Showing Crown (462X Interference Photo) | 5-22 |
| 5-21. | Model 101 Poppet Showing Seat Groove (462X Interference Photo) | 5-22 |
| 5-22. | Model 102 Seat Showing Dent From 0.003 Inch CRES Wire (462X Interference Photo) | 5-24 |
| 5-23. | Model 102 Test 2 0.003 Inch CRES Wire (91X Plain Photo) | 5-24 |
| 5-24. | Leakage Data for Model 103, Test No. 1 Through 3 | 5-26 |
| 5-25. | Model 103 Computed Seat Gap, Test No. 1 (Clean) | 5-27 |
| 5-26. | Leakage Data for Model 103, Tests 3 Through 5 | 5-28 |
| 5-27. | Leakage Data for Model 103, Tests 5 Through 7 | 5-29 |
| 5-28. | Leakage Data for Model 103, Test 7 Through 9 | 5-30 |
| 5-29. | Leakage Data for Model 103, Tests 9 Through 11 | 5-31 |
| 5-30. | Model 103 Seat Land (462X Interference Photo) | 5-32 |
| 5-31. | Model 103 Test 2 0.0004 Inch CRES Wire (462X Interference Photo) | 5-32 |
| 5-32. | Model 103 Test 4 0.001 Inch Copper Wire (462X Plain Photo) | 5-32 |
| 5-33. | Model 103 Test 10 0.003 Inch CRES Wire (462X Interference Photo) | 5-32 |
| 5-35. | Leakage Data for Model 104, Tests 1 Through 3 | 5-33 |
| 5-36. | Model 104 Computed Seat Gap, Test 1 (Clean) | 5-34 |
| 5-37. | Computed Seat Gap, Test 2 (0.0004 Inch CRES Wire) | 5-35 |
| 5-38. | Model 104 Computed Leakage, Test 2 (0.0004 Inch CRES Wire) | 5-36 |
| 5-39. | Leakage Data for Model 104, Tests 3 Through 5 | 5-37 |
| 5-40. | Model 104 Computed Seat Gap, Test 4 (0.001 Inch Copper Wire) | 5-38 |
| 5-41. | Model 104 Computed Leakage, Test 4 (0.001 Inch Copper Wire) | 5-39 |
| 5-42. | Leakage Data for Model 104, Tests 5 Through 7 | 5-40 |

| | | |
|-------|--|------|
| 5-43. | Model 104 Computed Seat Gap, Test 6 (0.004 Inch Copper Wire) | 5-41 |
| 5-44. | Model 104 Computed Leakage, Test 6 (0.003 Inch Copper Wire) | 5-42 |
| 5-45. | Leakage Data for Model 104, Tests 7 Through 9 | 5-43 |
| 5-46. | Leakage Data for Model 104, Tests 9 Through 11 | 5-44 |
| 5-47. | Model 104 Seat Showing Groove from 0.0004 Inch CRES Wire (462X Interference Photo) | 5-45 |
| 5-48. | Model 104 Test 2 0.0004 Inch CRES Wire (462X Interference Photo) | 5-45 |
| 5-49. | Model 104 Seat Showing Depression from 0.001 Inch Copper Wire (462X Interference Photo) | 5-45 |
| 5-50. | Model 104 Test 4 0.001 Inch Copper Wire (462X Interference Photo) | 5-45 |
| 5-51. | Model 104 Seat Showing Groove from 0.001 Inch CRES Wire (462X Interference Photo) | 5-46 |
| 5-52. | Model 104 Test 8 0.001 Inch CRES Wire (462X Interference Photo) | 5-46 |
| 5-53. | Model 104 Seat Showing Groove From 0.003 Inch CRES Wire (462X Interference Photo) | 5-46 |
| 5-54. | Model 104 Test 10 0.003 Inch CRES Wire (462X Plain Photo) | 5-46 |
| 5-55. | Leakage Correlation Plot, Model 105 | 5-49 |
| 5-56. | Relative Helium Leakage and Closure Load | 5-50 |
| 5-57. | Seal Serration Force Deflection | 5-54 |
| 5-58. | Flat Seal Force Deflection | 5-55 |
| 5-59. | Leakage Data for Model 201, Tests 1 Through 3 | 5-56 |
| 5-60. | Leakage Data for Model 202, Tests 1 Through 3 | 5-57 |
| 5-61. | Leakage Data for Model 203, Tests 1 Through 10 | 5-58 |
| 5-62. | Leakage Data for Model 204, Tests 1 Through 5 | 5-60 |
| 5-63. | Leakage Data for Model 207, Tests 1 and 2 | 5-61 |
| 5-64. | Leakage Data for Model 208, Tests 1 Through 3 | 5-62 |
| 5-65. | Leakage Data for Model 206, Tests 1 and 2 | 5-64 |
| 5-66. | Leakage Data for Model 304, Tests 1 Through 5 | 5-67 |
| 5-67. | Leakage Data for Model 305, Test No. 1 Through 8 | 5-68 |
| 5-68. | Leakage Data for Model 306, Tests 1 Through 3 | 5-69 |

| | | |
|-------|--|------|
| 6-1. | Apollo Technology (SPS Oxidizer Quad Check Valve) | 6-2 |
| 6-2. | Check Valve Conceptual Design and Selection | 6-5 |
| 6-3. | Prototype Check Valve | 6-6 |
| 6-4. | Spring Cantilever | 6-7 |
| 6-5. | Check Valve Guide | 6-8 |
| 6-6. | Check Valve Poppet | 6-9 |
| 6-7. | Check Valve Spring | 6-10 |
| 6-8. | Check Valve Seat | 6-11 |
| 6-9. | Check Valve Pin | 6-12 |
| 6-10. | Check Valve Plug | 6-13 |
| 6-11. | Check Valve Body | 6-14 |
| 6-12. | Check Valve Base | 6-15 |
| 6-13. | Prototype Valve Details | 6-16 |
| 6-14. | Prototype Valve Seat | 6-17 |
| 6-15. | Leak and Cycle Test Setup | 6-24 |
| 6-16. | Prototype Cycle Test No. 1 | 6-27 |
| 6-17. | Test No. 1 Poppet Showing Groove From Seat (462X Interference Photo) | 6-27 |
| 6-18. | Test No. 1 Seat Showing Deformed Land (462X Interference Photo) | 6-27 |
| 6-19. | Prototype Cycle Test No. 2 | 6-28 |
| 6-20. | Test No. 2 Poppet Showing Groove From Seat (462X Interference Photo) | 6-28 |
| 6-21. | Test No. 2 Seat Showing Deformed Land (462X Interference Photo) | 6-28 |
| 6-22. | Prototype No. 2 Computed Seat Gap (Start) | 6-31 |
| 6-23. | Predicted NO ₂ Vapor Leakage (Prototype Check Valve, Test No. 2) | 6-32 |
| 6-24. | Check Valve Poppet ("A" Change) | 6-34 |

TABLES

| | |
|--|------|
| 2-1. Nomenclature for Leakage Flow Equations | 2-2 |
| 2-2. Gas Leakage Equations | 2-4 |
| 2-3. Liquid Leakage Equations | 2-5 |
| 2-4. Parallel Plate Model Molecular-Laminar Flow | 2-10 |
| 2-5. Parallel Plate Model Turbulent-Nozzle Flow | 2-11 |
| 2-6. Circular Hole Model Flow | 2-12 |
| 2-7. Fluid Properties at Standard Temperature and Pressure | 2-20 |
| 4-1. Cutter Material Samples | 4-3 |
| 4-2. Preliminary Cutter Material Tests | 4-5 |
| 4-3. Cutter Materials Hardness Test Data | 4-8 |
| 4-4. Structural Materials Hardness Test Data | 4-27 |
| 5-1. Cutter Model Tests | 5-5 |
| 5-2. Leakage Correlation Data, Model 105 | 5-47 |
| 5-3. Flat Polymer Model Tests | 5-51 |
| 5-4. Captive Polymer Model Tests | 5-65 |
| 6-1. Prototype Check Valve Design Data | 6-18 |
| 6-2. 50,000-Cycle Test | 6-37 |
| 6-3. Wire Cutting Test Results | 6-39 |

PRECEDING PAGE BLANK NOT FILMED

INTRODUCTION

Historically, schedule constraints and complex development problems have resulted in very minimal effort being placed on check valves. As a result, the state of the art in check valve design has not been sufficiently advanced to meet the multiple-reuse, high-reliability, and low-maintenance requirements of the Orbit Maneuvering and Reaction Control Propulsion Systems (OMS/RCS) of the Space Shuttle Orbiter. This lag in the state of the art was evidenced in the Apollo propulsion system check valves, which also utilized nitrogen tetroxide (N_2O_4) and hydrazine (N_2H_4)-base propellants. Consistent leakage performance, dynamic stability, contamination tolerance, and propellant compatibility were not satisfactorily attained. Thus, these Apollo quad check valves, designed for a single mission usage, do not contain the design features required for the Space Shuttle, where a reusable valve with extended operational life is required.

PROGRAM OBJECTIVE

The objective of this program was to develop the necessary data, through analytical and experimental evaluation, of different sealing concepts and materials, to provide the means of optimizing the quad propellant check valve design for OMS/RCS application. Specifically, the program was designed to provide data on contamination-resistant sealing concepts and valve concepts that would prevent recurrence in Space Shuttle hardware of problem areas encountered with Apollo quad check valves. The major valve design objectives of this effort were: (1) contamination-resistant sealing in the presence of propellant reaction products as well as particulate matter, (2) elimination or severe limitation of sliding fits, (3) no critical orificing or small clearances susceptible to fouling, (4) dynamic stability, (5) compatibility with oxidizer (N_2O_4) and fuels (N_2H_4 types) separately as well as in combination with each other and with moisture, (6) minimum and consistent pressure drop, and (7) resolution of the unique problems that result from the extended Space Shuttle operational life.

TECHNICAL APPROACH

The technical approach to this program was based upon the precept that analysis, coupled with detail observation and measurement of the physical and geometrical parameters causing seal leakage, leads to dimensions and designs for reducing leakage. This has been the basis for similar metal-to-metal closure research at Rocketdyne (Ref. 1 through 3) and has resulted in advance closures, and methods for evaluating these closures in controlled contamination environments. Recently completed Space Shuttle Auxiliary Propulsion System (SS/APS) valve research (Ref. 4) has demonstrated the advantages of captive plastic and carbide cutter seals in resisting contamination and achieving low leakage for 1,000,000 scrubbing-impact closures cycles. Also, a recently completed TRW effort (Ref. 5), characterizing AF-E-124D elastomer and demonstrating its compatibility with earth storable propellants, has provided a potential basis for improved sealing performance.

Combining these technological breakthroughs in sealing concepts useful for Space Shuttle components, and particularly the OMS quad check valves, was a primary aim of this effort. This was achieved by systematic evaluation of selected sealing concepts and materials under precisely controlled conditions, correlating cause with effect and comparing results with analytical predictions. Results of this work provided the basis for design of a candidate quad check valve. Verification of the selected design was accomplished by fabricating and testing a prototype check valve.

Elements of the work accomplished are shown in the following program structure. These tasks were performed more or less in the order listed and are reported herein in similar order.

1. Sealing Investigation
 - a. Leakage analysis
 - b. Test model conceptual analysis, design, and fabrication
 - c. Materials investigation
 - d. Test system and methods
 - e. Model seal tests
2. Check Valve Development
 - a. Conceptual design
 - b. Prototype analysis and design
 - c. Prototype fabrication
 - d. Prototype development testing

TECHNICAL GUIDELINES

General guidelines for performing the work were based on the OMS check valve requirements as then currently defined. While the intent of the effort was to develop new technology, sufficient similarity between the research and the flight program was required to allow utilization of the results. Thus, the goals established for the OMS check valve formed the basis and standards for closure designs examined in the Sealing Investigations tasks. While all closure types were evaluated in tradeoff studies, emphasis was placed on the recognized state-of-the-art concepts most likely to meet the exacting compatibility and low-load sealing requirements of the OMS check valve; these were: (1) cutter seal (Ref. 3 and 4), (2) AF-E-124D elastomer seal (Ref. 5), and (3) captive Teflon seals (Ref. 4). General technical guidelines extracted from the contract Statement of Work are covered in Appendix I. A summary listing of the quad valve primary performance goals follows:

| | |
|-------------------------|--|
| Fluid Media | N ₂ O ₄ , MMH, inert gases |
| Contamination Tolerance | 150 microns |
| Temperature | ±150 F gas, -20 to +150 F unit |

| | |
|---------------|---|
| Flow | 1.2 lb/min helium at 70 F |
| Pressure | 200 to 275 psi |
| Pressure Drop | 3.5 psi maximum |
| Stability | No on-seat chatter allowable |
| Leakage | 1.0 scc/hr helium (0.001 scim) maximum |
| Vibration | 2 g ² /cps (liftoff) |
| Cycle Life | 10-year mission (10,000 cycle, estimated) |

Toward the program conclusion, requirements established for the OMS/RCS check valve indicated a common design to satisfy both requirements. The major consideration was the greater cyclic requirement for the RCS application of 100,000 cycles that would therefore be imposed on the valve.

SUMMARY

To meet program objectives for optimizing the OMS/RCS check valve, major effort was devoted to sealing investigations in which seal materials were evaluated and carefully controlled seal model tests were performed in precision test fixtures. Facilities available from previous poppet and seat research programs were utilized to evaluate these advanced seal concepts. Polymer and ceramic cutter materials were studied with emphasis on means for fabrication and capability with storable propellants. Data from the sealing investigations led to design and development of a unique prototype check valve which demonstrated, by analysis and test, compliance with all program goals and requirements.

The program work and results are summarized by section in essentially the order performed and reported herein.

LEAKAGE ANALYSIS

Leakage analyses have provided the basis for relating fabricated surface geometry with measured leakage. These analyses have also been instrumental in this and previous programs for guiding seat designs toward improved sealing performance through identification of major leak paths.

A summary of leakage equations covering molecular, laminar, turbulent, and orifice flow regimes is presented for parallel plate and tubular flow paths. Included are application examples to show the range of each equation and the solution method.

The laminar-molecular flow equations are used to predict the equivalent parallel plate gap required to allow specification leakages over a range of pressures from 0.1 to 1000 psig for a valve seat having a 0.0002- or 0.006-inch wide sealing lands and mean diameter the same as the fabricated prototype valve (1.02 inch). Propellant leakages are predicted based on the resulting analytical model. The analysis shows that liquid leakage is significant, but less than vapor leakage, which for NO_2 is about 7 times greater than the equivalent leakage of helium at 0.5 psid. The NO_2 vapor leakage is high because of a 14.8 psi vapor pressure (at 70 F) which does not provide added seat load. Consequently, under conditions of near or partial cracking where the valve seat is nearly unloaded, vapor leakage could be substantial if the closure design tends to open excessively due to nonflat sealing surfaces, such as with polymer seals. It is concluded that without frequent helium purging some NO_2 vapor will be present upstream of a check valve meeting the program requirement of 10 scc/hr leakage.

The predominant leakage mode at low pressure drops is molecular in the 10 scc/hr range. On the other hand, liquid leakage is entirely laminar and varies with the cube of the equivalent gap. Because molecular leakage varies as the gap squared, the liquid leakage past a wide (0.006 inch) land is on the order of 5 times that of a narrow (0.0002 inch) land for the same equivalent helium leakage.

The gap correlation analyses were further used throughout the model test effort to predict the effect of variable seat load based on the check valve data wherein both inlet pressure, and thus load, were varied to measure seal leakage. A specific correlation test was performed indicating fair agreement with the analyses.

TEST MODELS

The concept of evaluating critical poppet and seat sealing parameters in precision test fixtures proved extremely successful in previous research efforts. Sealing loads, position, pressures, and leakage were precisely controlled and measured, usually with an accuracy better than 0.1 percent. Test models were designed and fabricated in this program to evaluate polymer seals in comparison with cutter seal models that were available for rework from the previous APS program (Ref. 4). Basic size of the model seals was the same as with models tested in previous programs (Ref. 1 through 4); i.e., 0.470 inch mean diameter and 0.03 inch land width, except that the cutter seal land was varied from 0.0002 inch to 0.002 inch to evaluate contaminant cutting loads.

Two types of polymer models were designed for evaluation of the AF-E-124 variety perfluoroelastomers and TFE, FEP Teflons; a flat model incorporating a thin (0.03 inch thick) seal disk clamped at the periphery, and a captive seal model. The flat model was a "workhorse" configuration designed to allow evaluation of a variety of seal insert material configurations in both composition and surface geometry. The captive polymer seal was patterned somewhat after the "captive plastic" closure of the SS/APS program. No other polymer materials were considered because of limited compatibility with storable propellants.

MATERIALS INVESTIGATION

Definition of cutter material compatibility with N_2O_4 and final selection for the prototype check valve, along with experiments in molding and machining polymer seals proved to be a major task in the program.

Cutter Materials

What little data was available from the literature indicated that typical sintered carbides were possibly compatible with N_2O_4 but not with the nitric acid that was certain to be present from water contamination. For the cutter seal to be successful in long-term contact with N_2O_4 , the seal material had to be literally impervious to any corrosive byproducts of the propellant. Program scope and time limited the value of propellant testing, therefore, immersion in RFNA was used as a rigorous screen of candidate specimens.

Material acceptability criteria were based on examination and microhardness test of 11 carbide and ceramic material samples with razor sharp edges using plain, interference, and scanning electron microscope (SEM). Observations and hardness tests were made following 1 hour, 1 day, 15 days and 169 days (6 months) exposure. Scanning electron microscope photographs at 500X and 5000X were obtained at the start and after 15 and 169 day periods.

This study showed that aluminum oxide materials (sapphire, ruby, sintered ceramics), boron carbide, silicon nitride, Kennametal K602 tantalum-tungsten carbide, and chemically vapor deposited tungsten carbide alloy (CM-500 by Chemetal Corporation) were not significantly affected by 6 months exposure to RFNA. Minor etching of the K602 material was visible, probably from the nominal 1.5 percent cobalt binder. Nickel and cobalt binders in all other sintered carbides were severely attacked.

Further investigation of the CM-500 material revealed the potential of outstanding properties: (1) hardness variable from 500 to 3000 Vickers depending upon processing and percentage of raw tungsten in the alloy, (2) transverse rupture strengths to 1,000,000 psi, (3) edge strength exceeding all sintered carbides, (4) grain size less than 100 angstrom, and (5) extreme wear resistance. With eventual selection of the cutter seal concept and CM-500 for the poppet and seat material, additional processing, fabrication, and performance data became available which uncovered potential (fabrication and processing) problems, but provided added confidence in use of the material.

Polymer Materials

The unknown quantity with polymer seals was how smooth did the seal need to be to meet leakage requirements, particularly at low temperature? Early discussions with TRW led to fabrication of a precision, polished mold to produce 3.5-inch-diameter sheets of AF-E-124D elastomer, both 0.03- and 0.04-inch thick. Difficulty was experienced by TRW in obtaining smooth surfaces, therefore, AFML and DuPont were contacted and supplied interim quantities of the elastomer, but of insufficient as-molded smoothness to meet sealing requirements. After many variations of the perfluoroelastomer were evaluated in the first half of the program, it was concluded that AF-E-124D could not be molded with a sufficiently smooth surface.

This led to machining experiments to produce flat, smooth elastomer surfaces. Machining was performed using a high-speed diamond fly cutting process that produced surfaces flat and parallel within 50 microinches. Unfortunately, the surface finish lay crossed the sealing land and was too rough to seal at low temperature or with very light load. Cold (-20 F) lapping was attempted with the AF-E-124D material, but it was soon apparent that no better finish than could be attained with soft metals (e.g., aluminum) was practically possible. In conjunction with current (poor) leak test results it was concluded that a glassy molded surface was required.

Molding experiments by TRW eventually led to the use of a white titanium dioxide filler in a variation of the basic AF-E-124D material. After several trials and variations, one 3.5-inch-OD sheet of material, 0.045-inch thick, was received which had an overall glassy, surface finish. Most of the material was wavy on both sides from gases entrapped in the mold, but about 30 percent of one side was reasonably flat. This material was used for the major test series of both polymer models and yielded promising results.

Teflon seals were machined by fly cutting, but again the surface was too rough. This led to several molding experiments using the captive model, a pair of carbide plates, and an enclosed cylindrical die. The entire results were less than satisfactory, but did lead to the conclusion that unlike TFE, FEP could be molded to a glassy smooth surface in a totally contained die. However, the surface was quite fragile and easily scratched which indicated the need for sufficient seal load to provide a substantial degree of plastic flow to overcome contaminant entrapments.

MODEL SEAL TESTS

Model seal tests were performed in the modified APS tester (Ref. 4) and were limited to static load-leakage tests in the check valve mode with added force from the tester piston, as required. Selected polymer seal models were tested at a temperature of -15 F.

Cutter Models

Cutter seal models were tested with land widths of 0.0002, 0.0005, 0.001 and 0.002 inch to determine the load required to cut or mash CRES and copper wires (0.0004-, 0.001-, and 0.003-inch-diameter CRES; 0.001- and 0.003-inch-diameter copper). These tests also demonstrated the cutter seal's capability for sealing at the 1.0 scc/hr level with negligible load, provided the surfaces were sufficiently flat.

Wire cutting tests showed that a 0.0002-inch land width was required to mash or cut all but the 0.003-inch-diameter CRES wire with less than 1.5 pound load and less than 10 scc/hr helium leakage. A load of 3.9 pounds was required to cut the 0.003-inch-diameter CRES wire. In all cases, following wire cutting or mashing with a seat load of up to 87 pounds, leakage was less than 10 scc/hr at low pressure, indicating negligible after-effect of the wire entrapment.

Polymer Models

Initial model tests were performed with flat AF-E-124D seals fly cut on both surfaces with a roughness of about 16 microinches AA. By most standards, sealing could be considered excellent at room temperature with leakage less than 1.0 scc/hr at 10 psid, equivalent to a seat load of 1.7 pounds. Effects of excessive surface roughness and waviness were evident, however, with much greater leakage at lower loads and grossly excessive leakage at -15 F. These results verified the need for a glassy, smooth, molded surface with a precision approaching lapped metal surfaces to meet leakage requirements at low temperature.

This objective was more or less attained by one molded sheet of material, designated as AF-E-124X by TRW, which was a variant of the AF-E-124D elastomer containing a white filler. This sheet was fly cut on one side and seals of proper thickness were cut from selected areas for the flat and captive models. Test results with both models were similar, with room temperature and -15 F leakage less than 0.1 scc/hr. For the cold test, the model was chilled under load to keep the polymer surface flat. In one cold test of the flat seal, the model was chilled open and required a load of 1.0 pound to seal to the noted leakage level. Although not tested, it is reasonably certain that this load would increase with rougher surfaces or reduction in temperature.

Tests with a 0.001-inch-diameter wire entrapped in the flat and captive polymer seal models indicated that the leakage requirement could not be met with the wire entrapped, but the surface did reheal and seal reasonably after its removal, both at room temperature and -15 F.

Tests with TFE and FEP seals in both models were less than satisfactory, mainly because of the inability to produce precision sealing surface and the corresponding relatively high loads required to obtain low leakage. As with the elastomer seals, the Teflon models could not seal with a 0.001-inch-diameter CRES wire entrapped. Moreover, leakage after removal of the wire was excessive because of the resultant permanent groove across the sealing surface.

In comparison between flat and captive models, it was determined that the captive model was the best design for seal containment and retention. However, it was found necessary to ensure that the retainers did not interfere with the natural position of the seal because of the resultant distortion to the sealing surface. This requirement presents formidable dimensional problems with swell from propellant exposure and shrinkage at low temperature.

CHECK VALVE DEVELOPMENT

While model tests of the AF-E-124X seals were encouraging, many questions remained unanswered. It was apparent that extensive added research was required to define long-term compatibility and the effects of propellant exposure on sealing properties that were yet to be quantitatively established. Also, the loss of elastic resilience below +20 F dictated the need for extreme dimensional control of both the elastomeric and seal retention surfaces. Finally, process control in the polymer formulation, molding, and curing was undefined at the program conclusion. This was evidenced by receipt of purportedly duplicate material from TRW which did not have the surface texture, glassy smoothness, flatness, or pure white color of the previously received material.

On the other hand, the cutter seal had demonstrated the capability of meeting all goals and the CM-500 chemically vapor deposited tungsten carbide provided the material means for long-range compatibility. Thus, the cutter seal was selected for application in the prototype check valve.

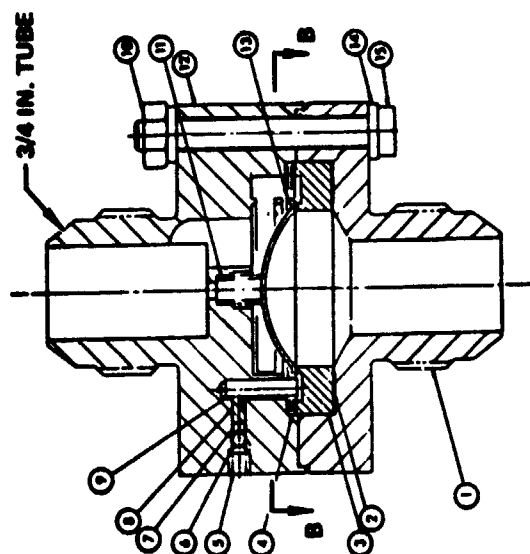
Valve Design

A trade study of candidate valve designs was made considering past art and the OMS/RCS check valve requirements. Having achieved low leakage, long life, and contamination resistance with the cutter seal, primary drivers in the design selection and preliminary analyses were dynamic stability and resistance to vibration.

As shown in Fig. 1-1, these requirements were met by a unique design of a hemispherical shell poppet of 0.03-inch-thick, CM-500 carbide, axially guided by three equally spaced carbide guide pins, one of which is a cantilever spring producing a lateral force of 1.0 pound between the poppet and the other two guides. With

DESIGN DATA

| | |
|--------------------------------------|--------------------|
| NOMINAL SEAT DIAMETERS, IN. | 1.02, 1.08 |
| NOMINAL LAND WIDTHS (2), IN. | 0.0002 |
| STROKE, IN. | 0.029 |
| SEATING SPRING FORCE, LB | 1.48 |
| LATERAL SPRING FORCE, LB | 1.0 ^(a) |
| MAXIMUM CRACKING PRESSURE, PSID | 2.0 |
| MAXIMUM FULL OPEN ΔP , PSID | 2.6 |
| POPPET WEIGHT, LB | 0.021 |
| AXIAL ACCELERATION RESISTANCE, G'S | 70 |
| LATERAL ACCELERATION RESISTANCE, G'S | 60 |
| POPPET/SPRING RESONANT FREQUENCY, HZ | 60 |
| PRESSURE DROP @ 116 SCFM HE, PSID | 2.6 |



(a) 0.41 LB USED IN TEST; SEE CHECK VALVE DEVELOPMENT

Figure 1-1. Prototype Value Analysis and Design

a relatively large seat diameter, the required valve stroke is only 0.029 inch. Rubbing between the carbide guides and poppet rim provides sufficient coulomb friction to critically damp the poppet against flow induced oscillations and also provide extreme resistance to vibration accelerations. Precision guidance of the poppet is not required because of minimal impact force and a secondary 0.0002-inch-wide seal land 0.03 inch outside of the inner seat land which acts as a bumper to align the poppet during clamshell closure.

Fabrication

Two seats and poppets were initially fabricated. The seats were made from 15 percent cobalt based, sintered micrograin, tungsten carbide and then coated with 0.001 inch of CM-500. Lapping the CM-500 proved exceedingly difficult compared with the sintered carbide because of the material's extreme toughness and hardness. As a consequence, each part was annealed to a final hardness of 1200 Vickers and finish lapped to produce sealing lands of between 0.0002 and 0.0003 inch in width.

Desired poppet hardness was on the order of 2100 Vickers, however, it was determined in machining the first two poppets that hardness varied with processing and machined depth. Because variable amounts were removed from these parts, their final hardness was 1000 and 1200 Vickers. Tests with the 1200 Vickers part were not entirely satisfactory because the seat cut into the poppet several microinches and displaced material which, upon subsequent high-pressure loading, caused similar depressions in the seat land. Three additional poppets were deposited with minor changes in sealing land geometry to avoid excessive machining. Of these, one was successfully fabricated with 1700 Vickers hardness and used in final testing. Problems in controlling hardness at depth have shown that strict process control is necessary to duplicate deposition geometry, hardness, and strength.

Preliminary Tests

Initial assembly of the valve indicated that the friction between the 1.0-pound lateral spring and the poppet rim was excessive. This was believed to be caused by the K602 carbide guides (at approximately 2000 Vickers) scratching the softer poppet rim. All further tests were therefore run with a lateral spring force of 0.41 pound.

Crack and reseal tests were performed with and without the lateral spring. With an axial spring force of 1.34 pounds, the cracking and reseal pressures without the lateral spring were identical at 1.4 psid, and with the lateral spring were 1.6 and 1.2 psid, respectively. Flow stability tests were performed which showed the valve to be stable and chatter free from cracking, to full open, and back to reseal. Without the lateral spring, the valve buzzed at low flow and chattered violently at higher flows.

Cycle Test

Two 20,000 cycle tests were performed with the same seat and poppet each having a hardness of 1200 Vickers. Both sealing surfaces were refinished between tests. Initial leakage, on the order of 1.0 scc/hr, increased with cycles to a maximum

**ORIGINAL PAGE IS
OF POOR QUALITY**

of 60 scc/hr in the first test and 10 scc/hr in the second test. The leakage increase was caused by material upset between the poppet and seat because of the soft poppet.

A harder poppet was fabricated with a sealing face of 1700 Vickers. The previously cycled seat was refinished and used to run 50,000 cycles. Leakage throughout this test remained essentially unchanged at less than 10 scc/hr and there was no visual evidenced surface upset.

As previously noted, two additional poppets were deposited in attempting to obtain the desired hardness of 2000 to 2200 Vickers, but process changes and human error precluded their use. The second seat was therefore finished and used with the 1700 Vickers poppet to run a 100,000 cycle test. As with the 50,000 cycle test, leakage was not significantly affected by cycling and remained throughout the test at less than 1.0 scc/hr from 0.1 to 400 psig. Again, microscopic inspection of the sealing surface did not show evidence of material upset or wear.

Unlike the first two 20,000 cycle tests wherein crack and reseal pressures remained unchanged, additional cycling uncovered a minor wear problem between the K602 guide pins and 1700 Vickers poppet rim. During the 50,000 cycle test, cracking pressure after 30,000 cycles raised to approximately 2.0 psig and was caused by a granular interlocking type of wear between the bearing surfaces. The same problem occurred at 20,000- and 30,000 cycles after refinishng the guide pins for the 100,000 cycle, but not thereafter. It was concluded that redesign of the guide pin bearing area and material was necessary to avoid granular wear of both surfaces.

CONCLUSIONS

Based on program results and defined goals, the cutter seal concept with a 0.0002-inch-wide land is the best choice for the OMS/RCS check valve. This approach was made possible by the outstanding material properties and corrosion resistance of the Chemetal CM-500 chemically vapor deposited tungsten carbide alloy that was employed with technology established over the past decade of research (Ref. 1 through 4).

As second choice, AF-E-124(?) polymer seal technology has indicated promising results, but significantly more research effort is needed to define (1) required surface geometry, (2) seal load/stress/leakage characteristics, (3) temperature and chemical properties effects, and (4) chemical composition and mold processing variables. Moreover, it is unlikely that the material can seal at low temperature with required low cracking pressure loads. Also, contamination resistance of the seal material is limited to temperatures above +20 F, but even then, 25 micron particles bridging the seal land will cause excessive leakage. These limitations indicate that revision of the OMS/RCS check valve requirements would be necessary for successful application of a perfluoroelastomer seal. Teflon seals are not recommended for the check valve.

The unique shell poppet check valve design has demonstrated the capability of meeting all program goals and requirements. Having performed 100,000 cycles of operation with less than 1.0 scc/hr leakage, and clearly demonstrating primary program objectives of contamination resistance and dynamic stability with low cracking pressure, the design provides a strong basis for the flightweight quad check valve.

Lastly, leakage analyses and correlation tests performed have shown that accurate correlation between helium and propellant leakages can be obtained and depends upon the precise definition and repeatability of the leak path at a dimensional level commensurate with the leak rate. For most aerospace valves this dimension is equivalent to a seal gap of from 1.0 to 50.0 microinches.

ORIGINAL PAGE IS
OF POOR QUALITY

RECOMMENLATIONS

It is recommended that the shell poppet and cutter seal concepts, as defined herein, be incorporated into a flight-type quad check valve which will satisfy both the OMS and RCS requirements. To successfully accomplish this objective, additional work is required to define (1) the process controls necessary for repeatable deposition and machining of CM-500 parts, (2) the production design and mechanical lapping processes for competitive fabrication of the seat and poppet sealing surfaces, (3) a pin guide bearing/material design capable of sustaining the required cycling without a granular type of wear and (4) dynamic analyses of the quad valve in conjunction with vibration testing to verify vibratory dynamic stability and seal wear resistance.

Recommendations for further work with polymer seals follow from the conclusions. Additional effort in molding and process control is required to consistently produce glassy surfaces, flat within 10 μ in./in. This program has barely scratched the surface in definition of the load/stress/leakage characteristics of polymer seals, and a complete parametric program is required to provide the detail design criteria that is currently lacking in the aerospace valving industry.

Finally, correlation of leakages between gases and liquids has been attempted by many, but with limited success. This was caused by the inability to produce (and reproduce) a precisely defined leak path. Metal sealing technology of this and past programs has evolved methods for fabrication and measurement of separable, and thus repeatable, leaks. A program to provide gas/gas, gas/vapor, and gas/liquid leakage correlation is recommended as both economically feasible and necessary to allow accurate definition of cryogenic and storable propellant leak rates in terms of the usual helium/nitrogen leakage acceptance criteria.

ORIGINAL PAGE IS
OF POOR QUALITY

LEAKAGE ANALYSIS

All seals, valve seats and even hermetic seals leak contained fluid to some degree. Often there is no visible or audible evidence of leakage and the incorrect assumption is that there is "zero" leakage. Accepting the premise of some degree of fluid leakage, the analytical approach is to postulate the leakage mechanism and define a suitable analytical model. The analytical model provides the basis for (1) relating the maximum leak requirement to the seal geometry, (2) defining surface defects in relation to failure leaks, (3) correlating leak rates of different fluids and (4) understanding specific seal-leakage peculiarities and phenomena with changes in pressure, load, and temperature.

Analysis of seal leakage can be simple or exceedingly complex depending upon the degree of compressibility and the flow regime. Deviation from perfect gas law and variable viscosity are added complications necessitating an iterative computer solution to leakage problems.

Over moderate pressure and temperature ranges, perfect gas laws are usually adequate and viscosity can be assumed constant across the leak path; such has been assumed herein. The purpose of this presentation is to provide a basis for data correlation and practical application. Therefore, equation derivations are not included but may be found in Ref. 6 through 11.

Units of leakage are often confusing; the discussion is therefore initiated with a definition of units. The various mechanisms of leakage flow are discussed and demonstrated with detailed numerical analysis of a valve seat model. Concluding, is a leakage analysis of a hypothetical OMS check valve. The purpose of this analysis is to provide a broad view of the potential extremes of gaseous and propellant leakage that corresponds with the OMS check valve guidelines and requirements.

NOMENCLATURE AND UNITS

Equation nomenclature is presented in Table 2-1. Units of leakage are usually expressed volumetrically such as cc or cubic inches per minute at STP (standard temperature and pressure, usually 70 F and 14.7 psia). To avoid unit errors all parameters should be in a consistent set of units. For this discussion the pound mass, inch, minute system is used.

Volumetric flow (Q) at defined (standard) conditions is directly related to weight flow (\dot{W}) by the density at standard conditions. For gases the density can be defined from the equation of state.

$$PV_{01} = W_m RT$$

$$\frac{W_m}{t} = \dot{W} = \frac{P_s}{RT_s} \cdot \frac{\text{volume}}{\text{time}}$$

$$\dot{W} = \rho_s Q$$

TABLE 2-1. NOMENCLATURE FOR LEAKAGE FLOW EQUATIONS

| Symbols | |
|----------------|--|
| AA | = arithmetic average surface roughness, inch |
| A | = flow area; normal to flow direction, in. ² |
| C _v | = velocity of sound, in./min ² |
| C | = discharge coefficient |
| d | = hole or hydraulic diameter, inch |
| D | = seat mean diameter, inch |
| e | = peak to valley surface roughness, inch |
| f | = Darcy friction factor |
| g | = gravitational constant $1.39 \times 10^6 \frac{\text{lb}_m}{\text{lb}_f} \text{ in./min}^2$ |
| h _e | = equivalent parallel plate gap, inch |
| h _p | = parallel plate channel height (gap), inch |
| K | = ratio of specific heats |
| K _f | = resistance factor |
| K _N | = Knudsen No. |
| K _p | = permeability constant |
| L | = channel length, inch |
| M | = Mach No. |
| P | = pressure, psia |
| ΔP | = pressure drop, psi |
| Q | = volumetric flow at S.T.P. (14.7, 70°F and 14.7 psia) acim scim = cubic cm/hr at STP (scf/hr)/984 |
| r | = downstream to upstream static pressure ratio |
| R | = gas constant, $\frac{\text{lb}_f}{\text{lb}_m} \text{ in./R}$ |
| Re | = Reynolds' No. |
| T | = temperature, degrees Rankine (R) |
| V | = velocity, in./min |
| W | = weight flowrate, lb/min |
| W | = channel width or perimeter, inch |
| W _m | = mass weight, lbm |
| Greek Symbols | |
| μ | = viscosity, $\frac{\text{lb}_f\text{-min}}{\text{in.}^2}$ $\frac{\text{lb}_f\text{-min}}{\text{in.}^2} = 0.999260 \times \frac{\text{lbm}}{\text{ft-hr}}$ $= 2.41730 \times 10^{-9} \times \text{centipoise}$ |
| ρ | = density, lb/in. ³ |
| λ | = mean molecular free path, inch |
| Subscripts | |
| a | ambient conditions |
| i | inlet or entrance conditions |
| 2 | downstream conditions |
| o | stagnation conditions |
| * | choked conditions (M = 1) |
| E | exit conditions |
| S | standard conditions |
| L | liquid |
| G | gas |

ORIGINAL PAGE IS
OF POOR QUALITY

Vacuum technology texts usually express leakage in pressure x volume per unit time units (q); e.g., Torr x liter per second, psi x cubic inches per minute or atmospheric x cubic centimeters per second. This also is an expression of weight flow because leakage is at a defined pressure (P_s) with the assumption of gas temperature at the flowing conditions. The relationships between volumetric flow at STP and q is shown as follows:

$$q = P_s Q \cdot \frac{T}{T_s} = \dot{w}RT$$

$$\frac{\text{lb force}}{\text{in.}^2} \cdot \frac{\text{in.}^3}{\text{min}} = \frac{\text{lb mass}}{\text{min}} \cdot \frac{\text{lb force}}{\text{lb mass}} \cdot \frac{\text{in.}}{R} \cdot R$$

$$Q = \frac{\dot{q} T_s}{P_s T}$$

MODES OF LEAKAGE FLOW

The leakage of fluids can occur through one or more of the following mechanisms:

1. permeation
2. molecular flow
3. transition flow
4. laminar flow
5. turbulent flow
6. nozzle flow

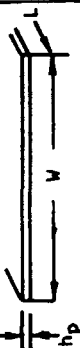

Each of these mechanisms is discussed in the following paragraphs. Equations and boundary conditions are summarized in Tables 2-2 and 2-3. These equations are derived for a circular hole of diameter (d) and a parallel plate leak path model of width (W), gap, (h_p), and with pressure drop over length (L) for each path.

Permeation, turbulent flow and nozzle flow are proportional to flow area, thus, circular or other flow paths can be substituted. The hydraulic diameter (d) is used to determine applicable Reynolds No. and friction factor. On the other hand, molecular and laminar flow are integrated equations involving the path geometry; therefore, the noted constants will differ as shown in Tables 2-2 and 2-3.

Permeation Leaks

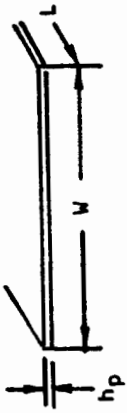
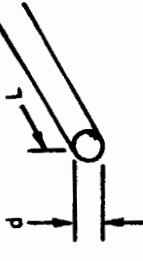
These leaks occur by a process of gas absorption on a surface film, diffusion through the bulk, and desorption on the low-pressure side. Large surface areas and organic materials are usually required to achieve significant leakage. A typical example of material with high permeability is natural rubber to helium and water vapor. Metals are unpermeable to the rare gases, although hydrogen gas can diffuse into most metals, often with loss of strength. Unless leakage in the mass spectrometer range ($<10^{-5}$ scim or 10^{-2} scc/hr) is important, permeation

TABLE 2-2. GAS LEAKAGE EQUATIONS

| Flow Regime | Flow Equations | | Boundary Parameters |
|-----------------------|---|---|---|
| Permeation | $\dot{w} = \frac{KA(P_1 - P_2)}{L}$ K_p is a function of seal material, fluid and temperature | | No boundary; leak rate varies exponentially with temperature |
| Molecular Flow |  $\dot{w} = \frac{4}{3} \sqrt{\frac{2g}{\pi RT}} \frac{w h^2}{L} (P_1 - P_2)$ |  $\dot{w} = \frac{1}{6} \sqrt{\frac{2g}{RT}} \frac{d^3}{L} (P_1 - P_2)$ | $K_N = \frac{\lambda}{h_p}$ or $\frac{\lambda}{d} > 1.0$ $\lambda = \frac{3.6\mu}{P_1 + P_2} \sqrt{RTG}$ |
| Laminar Flow | $\dot{w} = \frac{w h^3 (P_1^2 - P_2^2)}{24\mu LRT}$ | $\dot{w} = \frac{\pi d^4 (P_1^2 - P_2^2)}{256\mu LRT}$ | $K_N < 0.01$, $Re < 500$ $Re = \frac{2\dot{w}}{\mu g} = \frac{4\dot{w}}{\pi d \mu g}$ |
| Choked Turbulent Flow | $\dot{w} = AP_1 M_1 \sqrt{\frac{Kg}{RT_1}}, \beta_1 = 1 + \frac{K-1}{2} M_1^2$ $T_1 = T_0/\beta_1; T^* = 2\beta_1 T_1 / (K+1); P_1 = P_0/\beta_1 \exp \frac{K}{K-1}$ $P^* = M_1 P_1 \sqrt{\frac{T^*}{T_1}}, f = \left\{ 2 \log \frac{d}{e} + 1.14 - 2 \log \left[1 + \frac{9.28}{Re \left(\frac{e}{d} \sqrt{f} \right)} \right] \right\}^{-2}$ $d = 2 h_p \text{ in } f \text{ equation for plate flow, } e \approx 3 \text{ (AA)}$ $A = w h_p = \pi d^2/4, Re \text{ (see above)}$ $L \equiv L^* = \frac{2h}{f} \left[\frac{1 - M_1^2}{KM_1^2} + \frac{K+1}{2K} \ln \frac{(K+1) M_1^2}{2\beta_1} \right], (2 h_p = d \text{ for hole})$ | | (1) $500 < Re < 2000$ For plates $f = 96/Re$ For hole $f = 64/Re$ (2) $Re > 2000$ $f = \text{function } e/d$ (3) L/d or $L/h_p > 10$ |
| Nozzle Flow | $\dot{w} = \frac{CAP}{RT_0} \sqrt{gK \left(\frac{2}{K+1} \right) \exp \frac{K}{K-1}}, C \text{ is function of entrance geometry and } L/d$ | | L/d or $L/h_p < 10$ |

ORIGINAL PAGE IS
OF POOR QUALITY

TABLE 2-3. LIQUID LEAKAGE EQUATIONS

| Flow Regime | Flow Equations | | Boundary Parameters |
|----------------|---|--|--|
| Laminar Flow |  $\dot{w} = \frac{\rho W h_p^3 \Delta P}{12 \mu L}$ |  $\dot{w} = \frac{\pi \rho d^4 \Delta P}{128 \mu L}$ | <p>Re < 2000</p> $Re = \frac{2\dot{w}}{\mu W g} = \frac{4\dot{w}}{\pi d \mu g}$ |
| Turbulent Flow | $\dot{w} = A \sqrt{\frac{2 \rho C \Delta P}{K_{f1} + f L/d + K_{fE}}}$ $f = \left\{ 2 \log \frac{d}{e} + 1.14 - 2 \log \left[1 + \frac{9.28}{Re \left(\frac{e}{d} \right) \sqrt{f}} \right] \right\}^{-2}$ <p>$d = 2h_p$ in f equation for plate flow, $e \approx 3(AA)$</p> <p>$A = Wh_p = \pi d^2/4$, Re (see above)</p> | | <p>Re > 2000</p> <p>L/d or $L/h_p > 10$</p> |
| Nozzle Flow | $\dot{w} = CA \sqrt{2 \rho \Delta P}$ $A = Wh_p = \pi d^2/4$ <p>C is function of entrance geometry and L/d</p> | | <p>L/d or $L/h_p < 10$</p> |

ORIGINAL PAGE IS
OF POOR QUALITY

leakage is usually insignificant. Note, however, that other modes of flow can occur through physical openings in the same or opposite direction as the permeation leakage. Consequently, it is difficult in the low leakage range to differentiate between leak modes.

Molecular Flow

When gas pressure is sufficiently low and/or the leak path is small so that gas molecules encounter the walls more frequently than other molecules, the flow is termed molecular. This type of flow results when the mean free path (λ) is greater than the leakage gap (h_p). The condition is defined by the Knudsen No. as follows:

$$K_n = \frac{\lambda}{h_p} > 1.0$$

Molecular flow results from a greater concentration of molecules on one side of a barrier than on the other. The driving force for flow is therefore the partial pressure differential existing across a given leak path. As example, with 1 atmosphere pressure helium on one side of an opening and a like pressure of nitrogen on the other side, there would be a molecular flow transfer of each gas in opposite directions across the same leak path.

TRANSITION MOLECULAR AND LAMINAR FLOW

When the mean free path of the molecule is small with respect to the distance between walls, laminar flow results and the flow is governed by bulk fluid properties, primarily viscosity. The Knudsen No. for the lower boundary of laminar flow is

$$K_n = \frac{\lambda}{h_p} < .01$$

In this case, the channel is full and flow prevails only from higher to lower pressure.

Between laminar and molecular flow exists a transition region whereing combined molecular and laminar flow characteristics exist. As will be seen, the easiest treatment is to simply add the two types of flow, or, if sufficiently high flow exists, to ignore the molecular component and vice versa.

In laminar flow, the stream lines are governed by the viscous forces between the fluid particles resulting in a predictable velocity profile from zero velocity at the boundary to a maximum velocity between boundaries. The profile is termed parabolic because it follows a second degree curve (parabola). As the flow velocity is increased, the inertial forces between fluid particles become greater than the

viscous forces and a transition to turbulent flow begins. The defining parameter is Reynolds number, the ratio of inertial to viscous forces

$$Re = \frac{\rho V^2 d^2}{\mu V d g} = \frac{\rho V d}{\mu g}$$

From tests of valve seats, gaseous laminar flow exists for Reynolds number less than 500. Flow velocities are usually low enough to assume infinite heat transfer, or isothermal flow. For Reynolds number approaching 500, gas exit velocities become very high due to expansion and reduced density and the isothermal assumption is not valid, although the results may be sufficiently accurate for most analysis. As will be shown in the example calculation, Reynolds number can be lower than 500 with an exit velocity near the sonic velocity. From the literature, liquid laminar flow prevails with Reynolds numbers up to 2000.

Turbulent Flow

In the turbulent regime, laminar flow exists only in a narrow boundary near the walls. The velocity profile is nearly flat and the flow characteristics are defined by both theoretical and empirical information. Basically, flowrate is a function of internal and surface fluid friction resulting over the length of path. Under some conditions of incompressible flow, entrance and exit losses can exceed the friction loss, and these factors must be considered in computing the leakage flow.

For gas flows, thermodynamic considerations are employed to define fluid conditions and the flow is considered to be adiabatic; i.e., no heat transfer. Consequently, temperature will decrease as the gas expands to an exit pressure. The exit pressure will either be greater than the ambient for sonic flow or equal to the ambient for subsonic flow.

Nozzle Flow

As the flow path is shortened, friction losses become negligible and flow pressure drop is expended in a turbulent jet. In this case the flowrate is governed by the velocity, head and an empirically defined flow coefficient that is largely a function of the entrance geometry and length of path to gap ratio (L/h_p).

Compressibility Effects

Compressibility effects exist in most modes of gas leakage flow. The most significantly affected regions are the turbulent and nozzle regimes. With constant area leak paths, the exit velocity is limited by a phenomenon known as "choking." This condition results when the exit velocity equals the acoustic velocity. A measure of compressibility effects and an important parameter in gas dynamics is the Mach number, defined as the ratio of the average fluid velocity (V) to the speed of sound (C_v) at the same conditions, i.e.,

$$M = \frac{V}{C_v}$$

Compressibility effects can usually be neglected with Mach number less than about 0.4. This corresponds to a pressure drop less than 10 percent of the upstream pressure. This case will seldom be seen with seal leakage because the supply pressure is usually several times greater than the ambient or downstream back pressure.

Volumetric vs Weight Flow

Gas leakage is usually specified as volumetric units at standard conditions. In comparison between various gases, the volumetric leak rates in the orifice and molecular flow regimes vary with the molecular weight; i.e., the gas constant. In the laminar flow regime the flow is governed by viscosity, and gases such as nitrogen and helium will leak at nearly the same rate. In other regimes, helium leakage (in scim) will be about 2.6 times that of nitrogen.

NUMERICAL EXAMPLE

The preceding flow regimes are most easily viewed from the basis of a specific numerical example of gas leakage. The model leak path is a parallel plate gap (h_p) of width (W) and length in the direction of pressure drop (L). The path with (W) can be viewed as the entire periphery of a valve seat (πD) or as a portion of a larger seat produced by some imaginary flaw. In either case, the width is assumed to be much greater than the gap (for molecular and laminar flow). Also, the path length (L) is small with respect to seat diameter so that radial divergence can be neglected. A circular hole leak path is also analyzed. Note that total leakage from either geometry is n times the leakage from a single path. This simple concept shows the tie-in between scratch or flaw leakage and parallel plate gap leakage.

Test data for a variety of leak paths are presented in Refs. 1 through 3. The same seal model used in these prior tests will be analyzed herein. Due to the special nature of permeation flow it will not be included in the analysis. The leakage model dimensions and fluid conditions are as follows:

Model Geometry

$D = 0.470$ inch
 $W = \pi D = 1.4765$ inch
 $L = 0.03$ inch
 $h_p = 10^{-8}$ to 0.01 inch
 $d = 10^{-7}$ to 0.01 inch
 $C = 1.0$
 $K_f =$ gas leakage neglected
 $AA = 10^{-6}$ inch ($e \approx 3.0 \times 10^{-6}$ inch)

Fluid Conditions for Nitrogen

$P_o = 30$ psig = 44.7 psia
 $P_a = 14.7$ psia
 $T_o = 70$ F = 530 R

$$\begin{aligned}
 K &= 1.4 \\
 \mu &= 4.4 \times 10^{-11} \text{ lb-min/in.}^2 \\
 R &= 661.7 \text{ in./R} \\
 \rho_s &= 4.1917 \times 10^{-5} \text{ lb/in.}^3 \text{ at } P_s = 14.7 \text{ psia and } T_s = 530 \text{ R}
 \end{aligned}$$

Flow Analysis

The equations in Table 2-2 display a complete picture of the analytical scope involved in solution of the subject model. Molecular, laminar and nozzle flow can be determined by direct substitution versus gap or diameter. The numerical and plotted results are displayed in Tables 2-4 through 2-6 and Fig. 2-1 and 2-2. As shown, the slope of the molecular and laminar flow components are such that, outside the transition region, one becomes negligible with respect to the other. Within the laminar-molecular transition region, each component adds to produce the total flow.

Between the laminar and nozzle flow regions is the turbulent regime, the major computational problem. From Table 2-2 it can be seen that several equations must be satisfied at any given gap to obtain the flow. Furthermore, the flowrate will be limited at the exit by choking and P_E will be greater than P_a . Trial and error solution within the turbulent regime is as follows:

1. Calculate A
2. Assume M_1
3. Calculate P_1 , T_1 , and \dot{w} from P_0 , T_0 and isentropic flow equations
4. Calculate Re
5. Calculate f from Re and e/d
6. Calculate L^*
7. Adjust M_1 to obtain $L^* = L$
8. Calculate $P_E = P^*$ to ensure $P_E = P_a$; if $P_E < P_a$, flow is subsonic and a function of P_a , also, $L < L^*$

The repeated nature of the preceding calculation is best handled by a programmable computer. The Moody diagram equation is also easily solved with a digital computer in the form shown because rough estimates of f result in a rapid convergence on f for a given Reynolds number. Note that for $Re < 2000$, f is constant (substitution of this expression into the incompressible turbulent flow equation results in the laminar flow equation, neglecting K_f).

The data of Tables 2-4 through 2-6 show that, between nozzle and laminar flow, the equations do not provide an exact match of flowrate. Specific flow tests in which correcting coefficients are carefully derived would be necessary to obtain a closer correlation. Nevertheless, for leakage computations, the accuracy demonstrated is usually adequate.

OMS CHECK VALVE LEAKAGE

Leakage range for the OMS check valve is between 1.0- and 10.-scm/hr (0.00102- to 0.0102-scm) helium, and other shuttle components may have significantly higher allowable leakage. The question to be answered is how these requirements relate

TABLE 2-4. PARALLEL PLATE MODEL MOLECULAR-LAMINAR FLOW

| h_p | Q | K_n | R_E | P_e | M_E |
|---|------------------------|------------------------|------------------------|-------|------------------------|
| Molecular Flow ($K_n > 1.0$) | | | | | |
| 10^{-8} | 7.46×10^{-9} | 1.86×10^2 | -- | 14.7 | 6.12×10^{-7} |
| 10^{-7} | $\times 10^{-7}$ | $\times 10^1$ | -- | ↓ | $\times 10^{-6}$ |
| 10^{-6} | $\times 10^{-5}$ | $\times 10^0$ | -- | | $\times 10^{-5}$ |
| 10^{-5} | $\times 10^{-3}$ | $\times 10^{-1}$ | -- | | $\times 10^{-4}$ |
| 10^{-4} | $\times 10^{-1}$ | $\times 10^{-2}$ | -- | ↓ | $\times 10^{-3}$ |
| Laminar Flow ($K_n < 0.01$, $R_E < 500$) | | | | | |
| 10^{-8} | 5.65×10^{-12} | -- | 5.25×10^{-12} | 14.7 | 4.63×10^{-10} |
| 10^{-7} | $\times 10^{-9}$ | -- | $\times 10^{-9}$ | ↓ | $\times 10^{-8}$ |
| 10^{-6} | $\times 10^{-6}$ | -- | $\times 10^{-6}$ | | $\times 10^{-6}$ |
| 10^{-5} | $\times 10^{-3}$ | -- | $\times 10^{-3}$ | | $\times 10^{-4}$ |
| 10^{-4} | $\times 10^0$ | 1.86×10^{-2} | $\times 10^0$ | | $\times 10^{-2}$ |
| 2.0×10^{-4} | 45.2 | 0.931×10^{-2} | 42.0 | | 0.185 |
| 3.0×10^{-4} | 153.0 | -- | 142.0 | | 0.417 |
| 4.0×10^{-4} | 362.0 | -- | 336.0 | | 0.741 |
| 4.5×10^{-4} | 515.0 | -- | 478.0 | | 0.938 |
| 4.6×10^{-4} | 550.0 | -- | 511.0 | ↓ | 0.980 |
| 4.7×10^{-4} | 584.0 | -- | 542.0 | 14.97 | 1.0 |
| Combined Laminar - Molecular Flow | | | | | |
| 10^{-8} | 7.46×10^{-9} | 1.86×10^2 | -- | 14.7 | -- |
| 10^{-7} | $\times 10^{-7}$ | $\times 10^1$ | -- | ↓ | -- |
| 10^{-6} | 8.03×10^{-5} | $\times 10^0$ | -- | | -- |
| 10^{-5} | 13.11×10^{-3} | $\times 10^{-1}$ | 1.22×10^{-2} | | -- |
| 10^{-4} | 64.0×10^{-1} | $\times 10^2$ | 5.94×10^0 | ↓ | 5.25×10^{-2} |
| $>10^{-4}$ | Laminar Flow | | | | |
| NOTE: $p_s = 4.1917 \times 10^{-5}$ lb/in. ³ for N_2 at 14.7 psia and 70 F | | | | | |

TABLE 2-5. PARALLEL PLATE MODEL TURBULENT-NOZZLE FLOW

| h_p | M_1 | P_1 | T_1 | Q | $P_E = P^*$ | M_E | R_e | f | L/h_p |
|--------------------------|-------|-------|-------|----------|-------------|-------|--------|--------|---------|
| Turbulent Flow | | | | | | | | | |
| 4.0×10^{-4} | 0.212 | 43.3 | 525.0 | 306 | 8.4 | 1.0 | 284.0 | 0.338 | 75.0 |
| 7.0×10^{-4} | 0.398 | 40.1 | 514.0 | 940 | 14.8 | 1.0 | 873.0 | 0.110 | 42.9 |
| 1.0×10^{-3} | 0.516 | 37.3 | 503.0 | 1638 | 18.0 | 1.0 | 1520.0 | 0.0631 | 30.0 |
| 2.0×10^{-3} | 0.656 | 33.5 | 488.0 | 3800 | 20.9 | 1.0 | 3530.0 | 0.0410 | 15.0 |
| 3.0×10^{-3} | 0.716 | 31.8 | 481.0 | 5940 | 21.8 | 1.0 | 5520.0 | 0.0360 | 10.0 |
| (T* = 441.7 R = -18.3 F) | | | | | | | | | |
| Nozzle Flow | | | | | | | | | |
| 2.0×10^{-3} | 1.0 | P_o | T_o | 4,290.0 | -- | - | -- | -- | 15.0 |
| 3.0×10^{-3} | | | | 6,440.0 | -- | - | -- | -- | 10.0 |
| 4.0×10^{-3} | | | | 8,590.0 | -- | - | -- | -- | 7.5 |
| 1.0×10^{-2} | | | | 21,500.0 | -- | - | -- | -- | 3.0 |

TABLE 2-6. CIRCULAR HOLE MODEL FLOW

| d | Q | K _N | R _e | P _E | M _E |
|--|---------------------------|--------------------------|--------------------------|----------------|-------------------------|
| Molecular Flow (K _n > 1.0) | | | | | |
| 10 ⁻⁷ | 1.984 × 10 ⁻¹⁴ | 1.862 × 10 ¹ | -- | 14.7 | 3.06 × 10 ⁻⁶ |
| 10 ⁻⁶ | × 10 ⁻¹¹ | × 10 ⁰ | -- | ↓ | × 10 ⁻⁵ |
| 10 ⁻⁵ | × 10 ⁻⁸ | × 10 ⁻¹ | -- | | × 10 ⁻⁴ |
| 10 ⁻⁴ | × 10 ⁻⁵ | × 10 ⁻² | -- | ↓ | × 10 ⁻³ |
| Laminar Flow (K _n < 0.01, R _e < 500) | | | | | |
| 10 ⁻⁷ | 1.127 × 10 ⁻¹⁶ | -- | 0.983 × 10 ⁻⁹ | 14.7 | 1.74 × 10 ⁻⁸ |
| 10 ⁻⁶ | × 10 ⁻¹² | -- | × 10 ⁻⁶ | ↓ | × 10 ⁻⁶ |
| 10 ⁻⁵ | × 10 ⁻⁸ | -- | × 10 ⁻³ | | × 10 ⁻⁴ |
| 10 ⁻⁴ | × 10 ⁻⁴ | 1.862 × 10 ⁻² | × 10 ⁰ | ↓ | × 10 ⁻² |
| 6.0 × 10 ⁻⁴ | 0.146 | -- | 212.0 | ↓ | 0.625 |

| d | M ₁ | P ₁ | T ₁ | Q | P* | M _E | R _e | f | L/d |
|---|----------------|----------------|----------------|-------|-------|----------------|----------------|---------|------|
| Turbulent Flow (R _e > 500, L/d > 10) | | | | | | | | | |
| 0.001 | 0.351 | 41.1 | 517.0 | 0.644 | 13.33 | 1.0 | 562 | 0.1138 | 30.0 |
| 0.002 | 0.578 | 35.7 | 497.0 | 3.76 | 19.43 | 1.0 | 1639 | 0.03904 | 15.0 |
| 0.003 | 0.608 | 34.8 | 494.0 | 8.72 | 20.03 | 1.0 | 2536 | 0.0460 | 10.0 |
| Nozzle Flow | | | | | | | | | |
| 0.001 | 1.0 | P ₀ | T ₀ | 1.14 | -- | - | -- | -- | 30.0 |
| 0.003 | ↓ | ↓ | ↓ | 10.3 | -- | - | -- | -- | 10.0 |
| 0.010 | ↓ | ↓ | ↓ | 114.0 | -- | - | -- | -- | 3.0 |

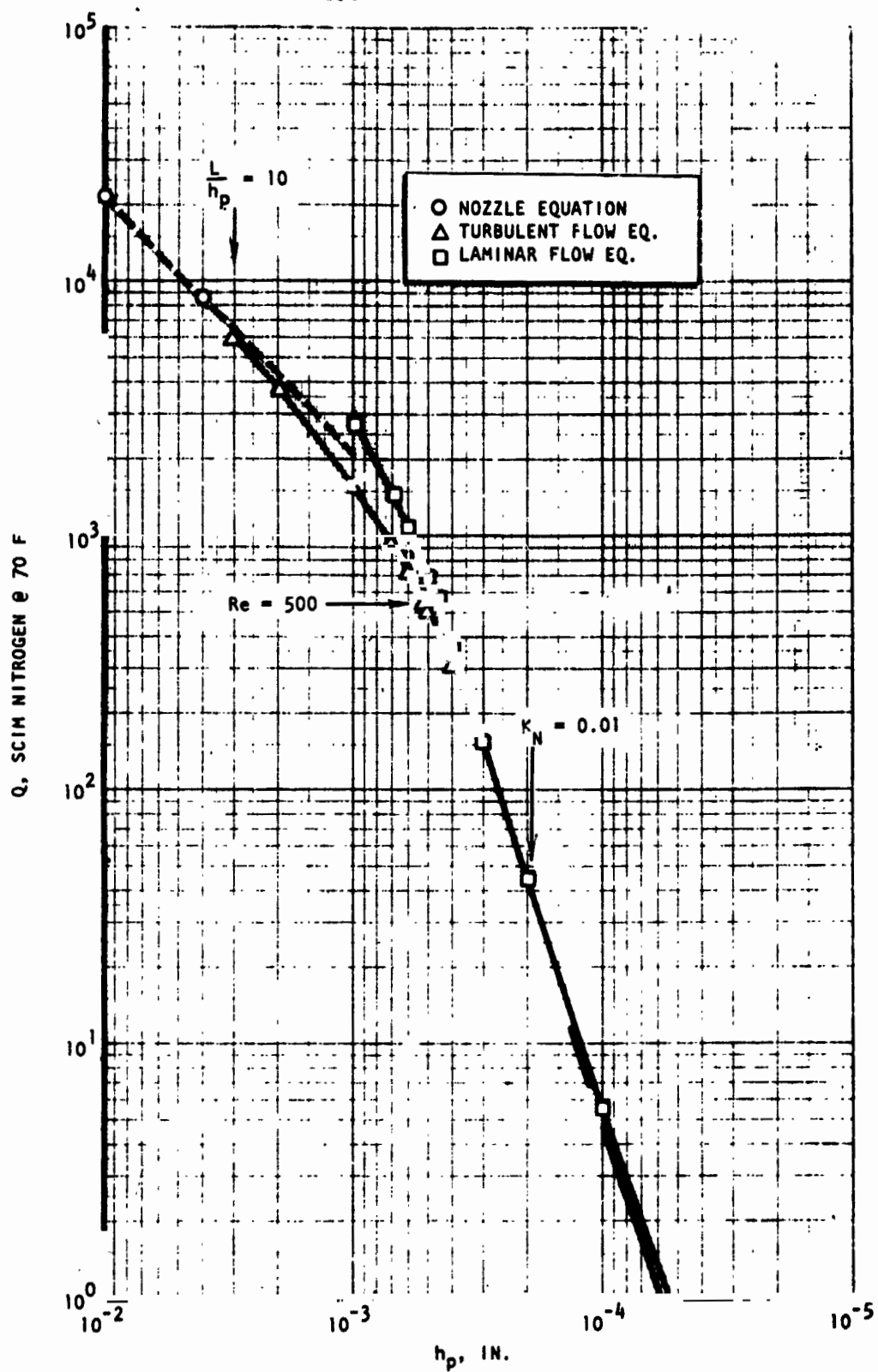


Figure 2-1. Parallel Plate Model Flow

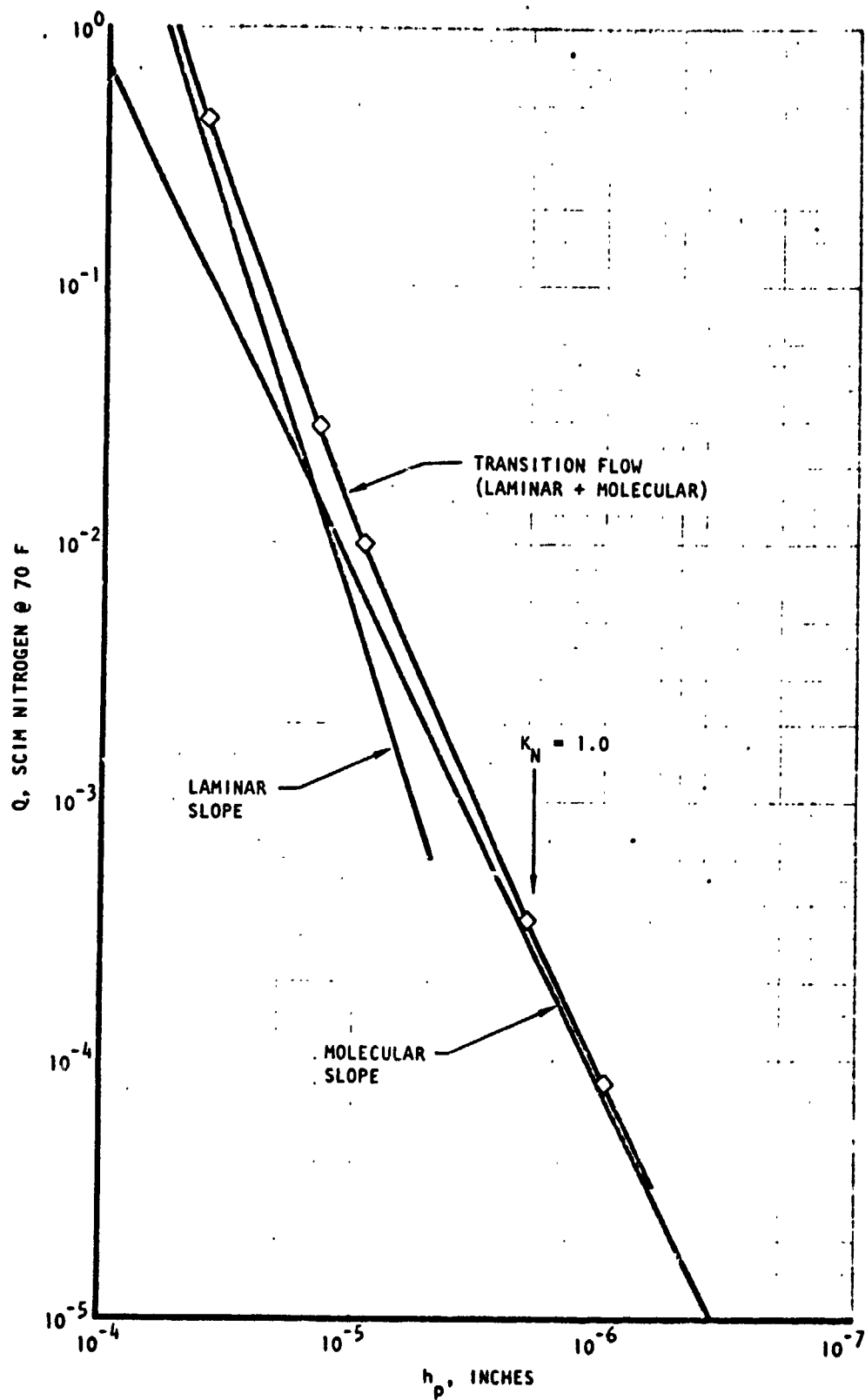


Figure 2-1. (Concluded)

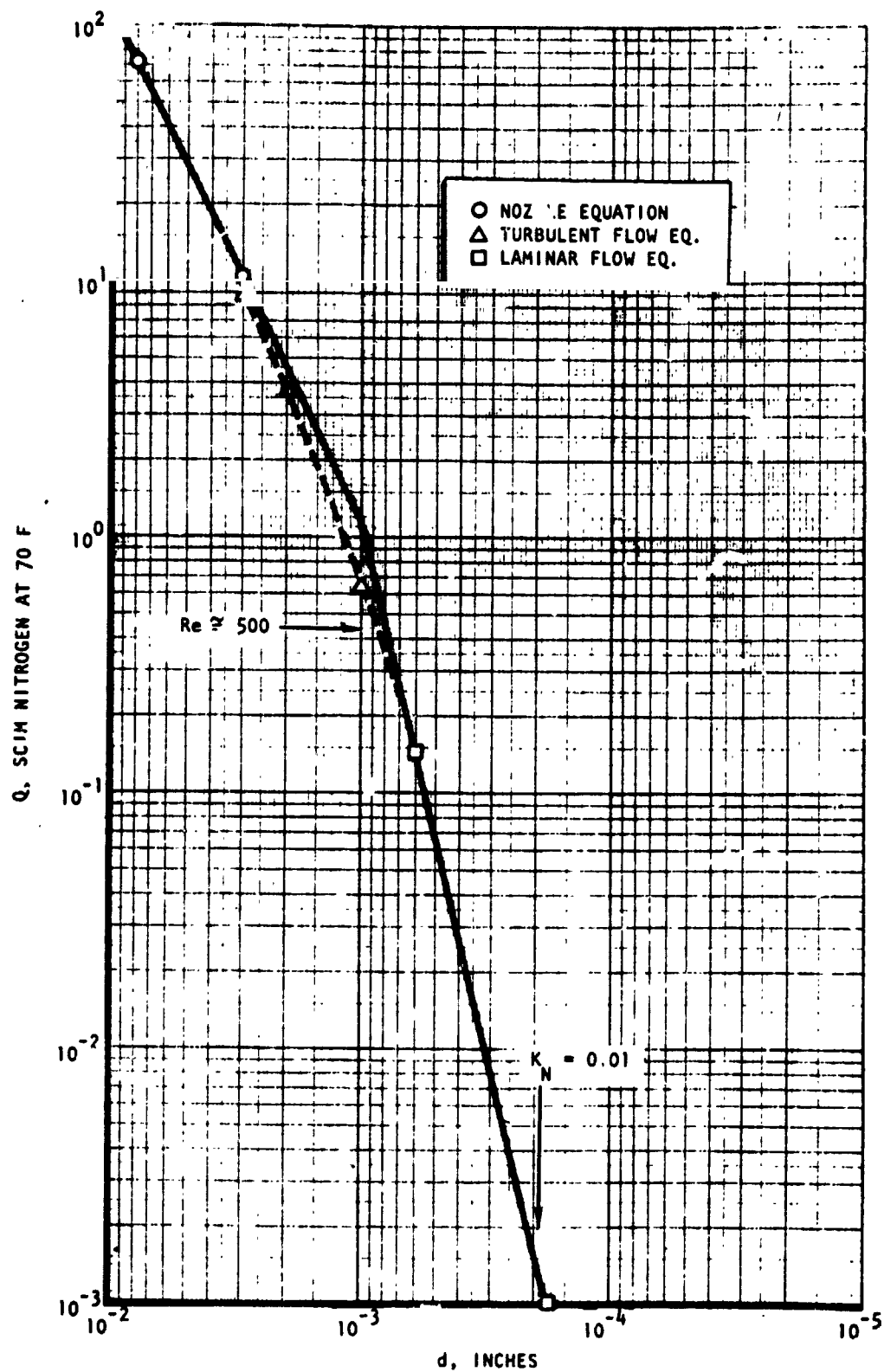


Figure 2-2. Circular Hole Model Flow

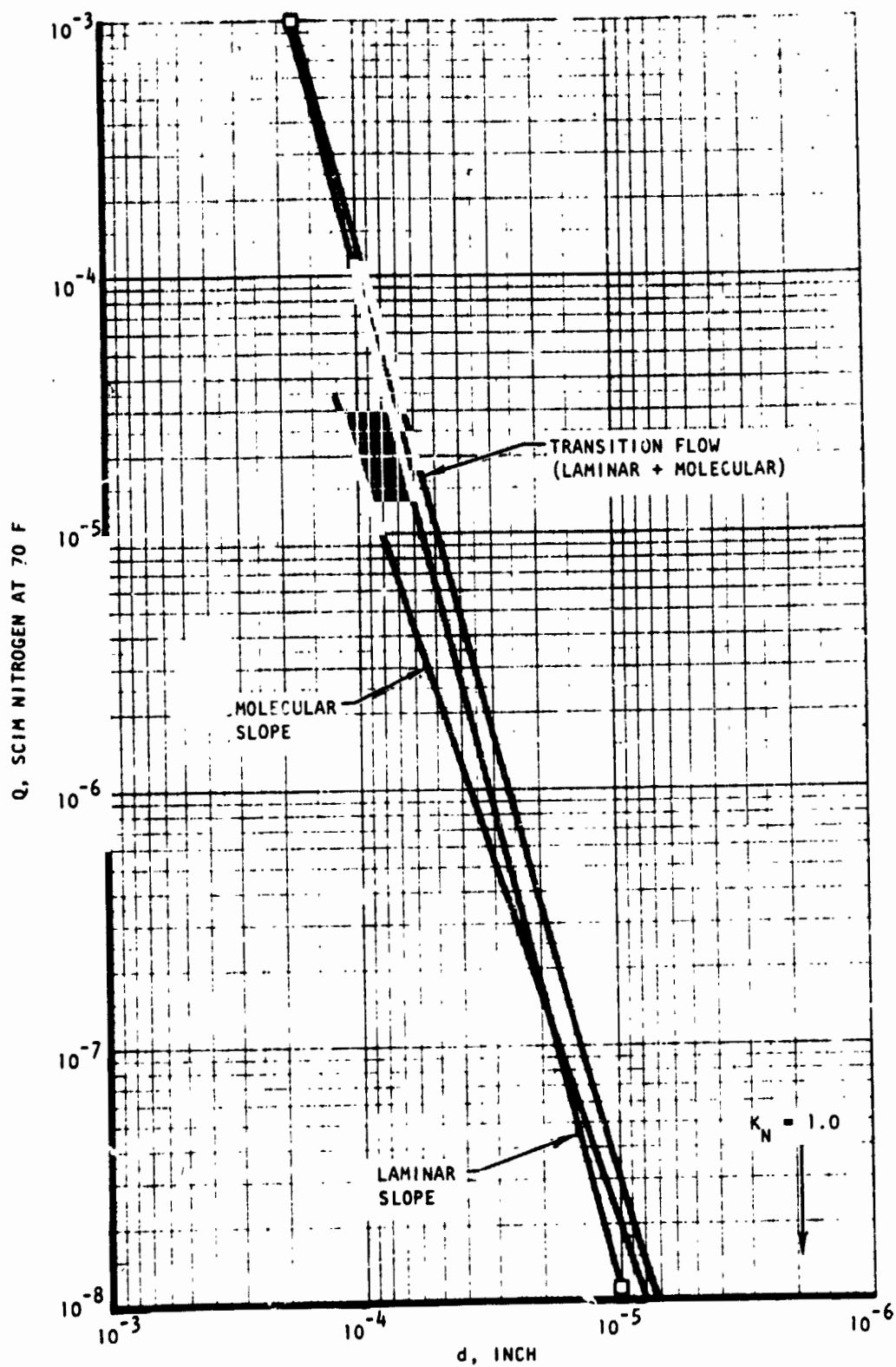


Figure 2-2. (Concluded)

to actual OMS check valve leakage performance under a broad spectrum of environmental influence, fluids, pressure change, etc.

Metal-to-metal closures have been performance characterized to provide a wide range of leakage predictability for a given seal design with and without entrapped contaminants (Ref. 1 through 3). These data have been extended to include the cutter seal. Knowledge of the basic seal dimensions and source of predominant leakage provides the basis for an analytical model of the leak path. The two most simple and usual paths are (1) equivalent parallel plate gap generated by surface deviations or a cocked poppet and (2) one or more grooves or scratches. In the first case the model width is the seal periphery and in the second it is the sum of the scratch widths of approximately the same average depth.

This simple model can be extended to empirically include load variation effects on the leak path for specific seal configurations. This approach provides detail leak data for specific closure models which can then be compared with established requirements. On the other hand, the seal closure model characteristic leak dimensions (i.e., the "path") can be hypothesized on the basis of the leak requirement without regard to load effects. These dimensions can then be employed to predict the leakage of other fluids under a variety of conditions, providing that the path remains constant. Experimental confirmation of this hypothesis has been demonstrated for gases (Ref. 1, 8, and 12), but attempts at liquid leakage correlation have suffered from nonrepeatable leak geometry and other experimental errors. Notable are the tests performed by Marr (Ref. 8) with water and Boeing (Ref. 12) in leakage correlation of various fluids, including storable propellants, with helium gas. In the latter case, single path leaks produced by scribing an AN fitting and drawn glass tubing experienced contamination and/or chemical reaction blockage of the leak path. Other leak paths, such as crushed tubing, had similar problems and could not be duplicated.

The Boeing program unfortunately failed to conclusively correlate the measured leakages because of nonrepeatable data, simply because the most important parameter of the test effort (the leak path geometry) could not be repeated or measured. Moreover the leak path selected to represent typical seal leakage, a single circular hole, is almost never the cause of leakage in the test range of interest (i.e., 1.0 to 1000 scc/hr). Suffice to say, if precision, separable, measurable, inspectable, and cleanable leaks been produced for the noted effort, a considerably higher degree of repeatability and correlation would have been achieved, especially in view of the technical competence demonstrated by the report.

The results performed for the many tests nevertheless strongly support the theoretical flow equations and it is recommended in Ref. 12 that they be used in prediction of probable maximum gaseous and liquid propellant leakage based on measured helium leakage. This conclusion is supported herein with the reservation that seal loading must be comparable for the different conditions examined. Because virtually all seals experience load and thus gap change with pressure variation, correlation can only be obtained at comparable pressures or pressure drops. The check valve is a prime example of a load sensitive seal closure.

Seal Model

The seal model chosen for analysis is based on the prototype check valve with a flat poppet and seat. The mean seat diameter is 1.02 inch. Parametric leakage data are generated for several hypothetical test conditions. Three leak paths are established for a given model by constant leakages of 0.001-, 0.01-, and 0.1-scim helium obtained for inlet pressures from 0.1 to 1000 psig, with discharge to atmospheric pressure of 14.7 psia. Data are given for two land widths to show the effect of this parameter on leakage. These leak models are graphically displayed in Fig. 2-3. Although it is improbable that an actual check valve would leak exactly as envisioned, tests herein have demonstrated that the usual trend is for leakage to vary within an order of magnitude of the assumed model, with reduction at higher pressure drops. Nevertheless, the model is useful in defining a limit condition and provides a sound basis for evaluation of other fluid leakages.

Analytical Model

Helium leakage in the range of 0.001 to 1.0 scim occurs in the molecular-laminar transition region. The equivalent seat gap (h_e) is computed from the equations of Table 2-2; the reduced equation for laminar plus molecular flow is

$$Q = \frac{1.50227 W h_e^3 (P_1^2 - P_2^2)}{\mu L T} + 4.5220 \times 10^4 \sqrt{\frac{R}{T}} \frac{W h_e^2}{L} (P_1 - P_2)$$

Fluid properties data are given in Table 2-7.

Seat gap data for land widths of 0.0002 and 0.006 inch are shown in Fig. 2-4 and 2-5. The predominant flow for the narrow land is molecular, whereas the wider land permits a greater gap for the same helium leakage and thus provides for laminar flows comparable with molecular at the larger gaps.

Propellant leakage through the check valve seal is hypothesized to occur in two mechanisms of flow as follows:

1. Propellant liquid migrates to the seal, or vapor condenses at the seal to form a liquid meniscus at the sealing land crack. Thermally induced pressure drop provides the driving force to produce reverse flow leakage.
2. Propellant vapor present at the valve is driven upstream through the seal gap by the vapor pressure differential across the seal. Leakage will be a function of the gap resulting from seat loads which vary from zero to that which might be obtained by thermally induced pressure drops. The influence on helium flow downstream is neglected based upon the premise that the predominant flow is molecular. Consequently, molecules can migrate in opposite directions without influencing each other.

Propellant liquid leakage will be in the laminar regime. It is assumed that the liquid completely wets the seal, and surface tension effects are negligible. Also, the path remains unblocked from contaminants or chemical reactions. The defining equation is given in Table 2-3. For comparison with helium leakage, the mass flow leakages are converted to hypothetical gas flow in scim. For the assumed

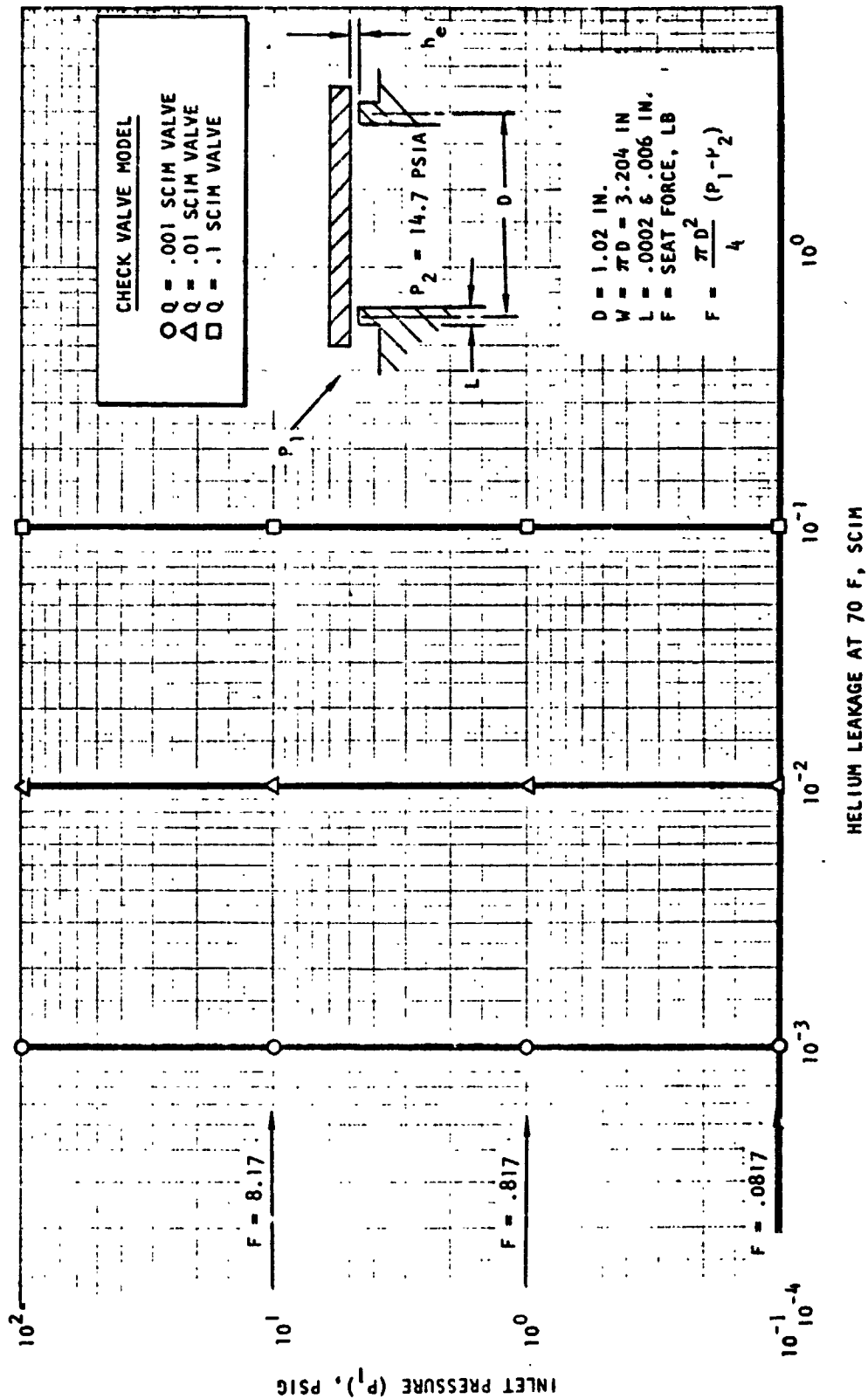


Figure 2-3. Check Valve Leakage Model

TABLE 2-7. FLUID PROPERTIES AT STANDARD TEMPERATURE AND PRESSURE
(14.7 psia and 70 F)

| Fluid (formula) | Molecular Weight | Vapor Pressure (P), psia | Density (ρ), lb/in. ³ | Gas Constant* (R), in./R | Viscosity (μ), lb-min/in. ² |
|---|---------------------|-----------------------------|--|-----------------------------|---|
| Helium (He) | 4.003 | -- | 5.9832×10^{-6} | 4635.6 | 4.7135×10^{-11} |
| Nitrogen Dioxide (NO ₂ vapor) | 46.01 | 14.8 | 1.227×10^{-4} ** | 228.0 | 3.204×10^{-11} (77 F) |
| Nitrogen Tetroxide (N ₂ O ₄) | 92.016 | 14.8 | 0.0521 | Liquid | 99.8×10^{-11} |
| MMH (CH ₃ N ₂ H ₃) | 46.075 | 0.760 | 0.0317 | Liquid*** | 206.0×10^{-11} |
| Water (H ₂ O) | 18.016 | 0.3631 | 0.0361 | Liquid | 230.0×10^{-11} |
| Water Vapor (H ₂ O) | 18.016 | 0.3631 | 6.67×10^{-7} ** | 1027.0 | 2.32×10^{-11} |
| Nitrogen (N ₂) | 28.01 | -- | 4.1917×10^{-5} | 661.7 | 4.2742×10^{-11} |
| *Computed from $R = P/\rho T$ **at P _v *** R for vapor $\approx \frac{1545 \times 12}{46.075} \approx 402 \text{ in./R}$ | | | | | |

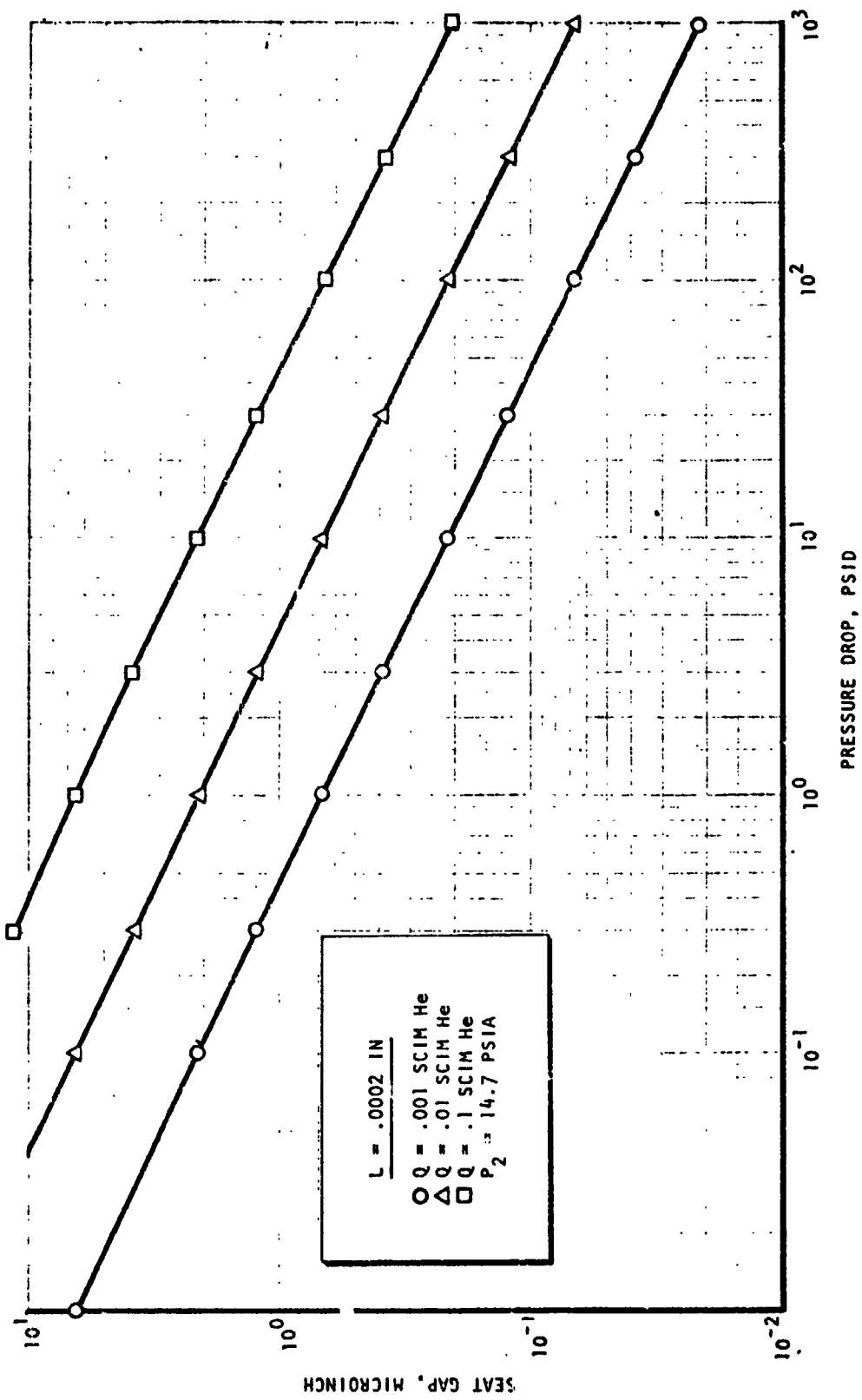


Figure 2-4. Model Gap for Narrow Land (0.0002 inch)

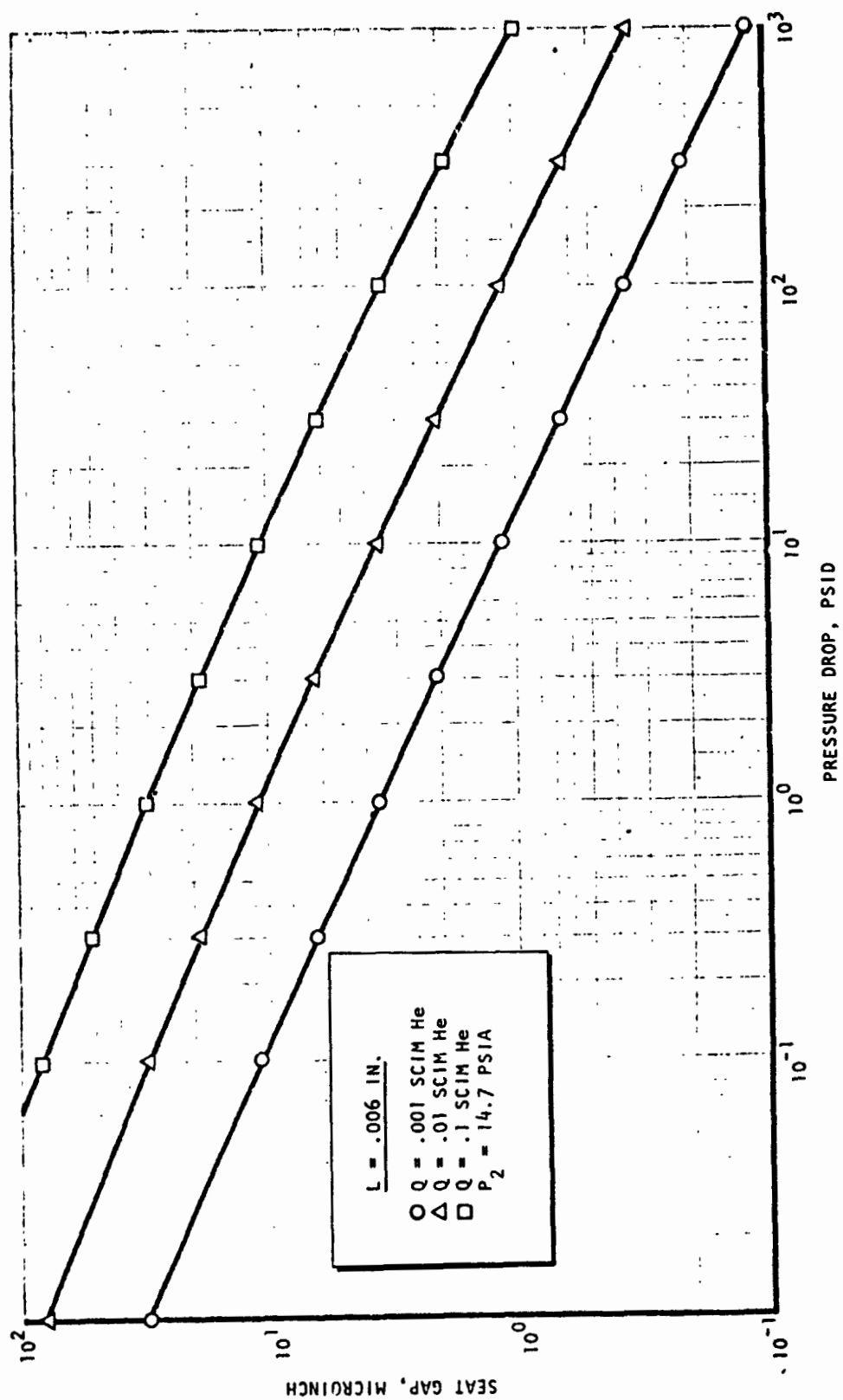


Figure 2-5. Model Gap for Wide Land (0.0006 inch)

temperature of 70 F, the N_2O_4 vapor (NO_2) will exist as a gas at STP. However, MMH and H_2O vapor would be condensed at 14.7 psia, but are nonetheless presented in terms of scim flows based on the gas constants shown in Table 2-7. Deining equations are as follows:

$$\dot{w}_L = \frac{\rho_L w h_e^3 \Delta P}{12 \mu L} = \rho_L Q_L = \rho_{SG} Q_G$$

$$\rho_{SG} = \frac{P_S}{RT_S}$$

These equations show that mass and volumetric leak rates differ by only a constant. Thus, all data presented in scim units are readily converted to mass or equivalent liquid volume, as applicable.

Propellant Leakage

Computed liquid leakage data for N_2O_4 , MMH, and water are presented in Fig. 2-6 through 2-8. The basic correlating factor is pressure drop which relates to computed seat gap (Fig. 2-4 and 2-5) based on the assumed model leak (Fig. 2-3). The slope of these curves results from the predominance of molecular helium flow defining the effective gap where flow is proportional to h_e^2 as opposed to laminar flow proportional to h_e^3 .

These curves show a heretofore unknown advantage of a narrow land width for a low leakage check valve. The narrow land seat must obtain a smaller effective gap than the wide land seat for the same helium leakage. Because the pressure is low at low pressure drop and the gap is significantly reduced at high pressure drop (Fig. 2-4 and 2-5) the helium flow for both land widths is predominantly molecular. The wider seat land leaks more liquid than the narrow land for the same reason the leak curves slope, i.e., h_e^2 vs h_e^3 . The theoretical maximum leak ratio for this effect is

$$\frac{Q \text{ (wide land)}}{Q \text{ (narrow land)}} = \sqrt{\frac{h_{\text{wide}}}{h_{\text{narrow}}}}$$

For the subject model, this ratio is about 5.5:1. For a larger land of 0.03 inch and a narrow land of 0.0002 inch the leak ratio would be about 12:1.

Propellant leak data of Fig. 2-6 through 2-8 indicate rates somewhat greater than the respective helium rates at low pressure drops. It would appear that the 0.01 scim helium requirement will restrict propellant leakage to values less than the helium requirement with a narrow land model.

The vapor leakage data are presented somewhat differently than the preceding liquid data. As previously noted, propellant vapor leakage is driven across the seal by the partial pressure of the vapor. To show the effect of variable seat load (and thus gap) on the vapor leak rate it has been hypothesized that seat force corresponds solely to pressure drop times effective area. The results,

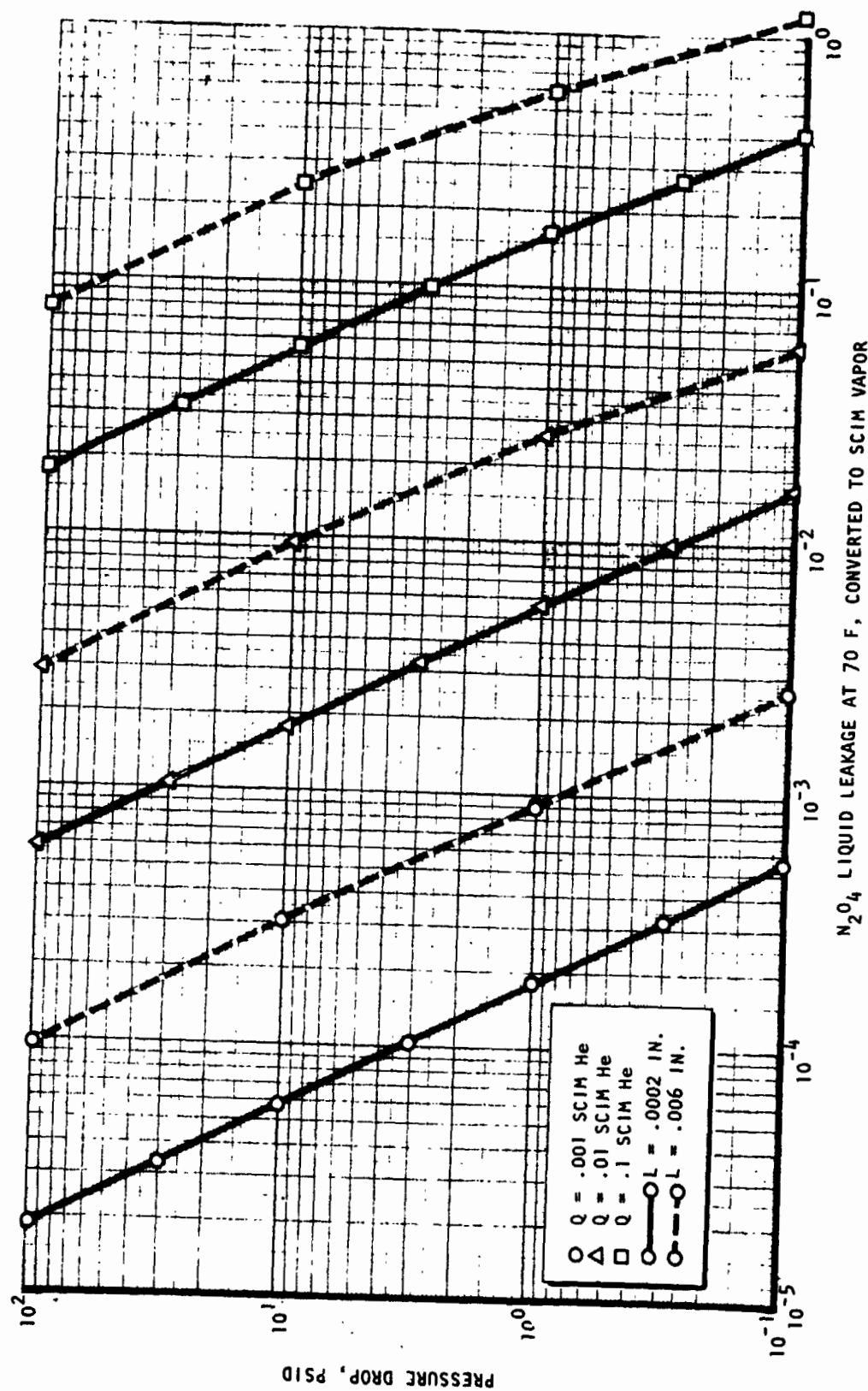


Figure 2-6. N_2O_4 Liquid Leakage Correlation

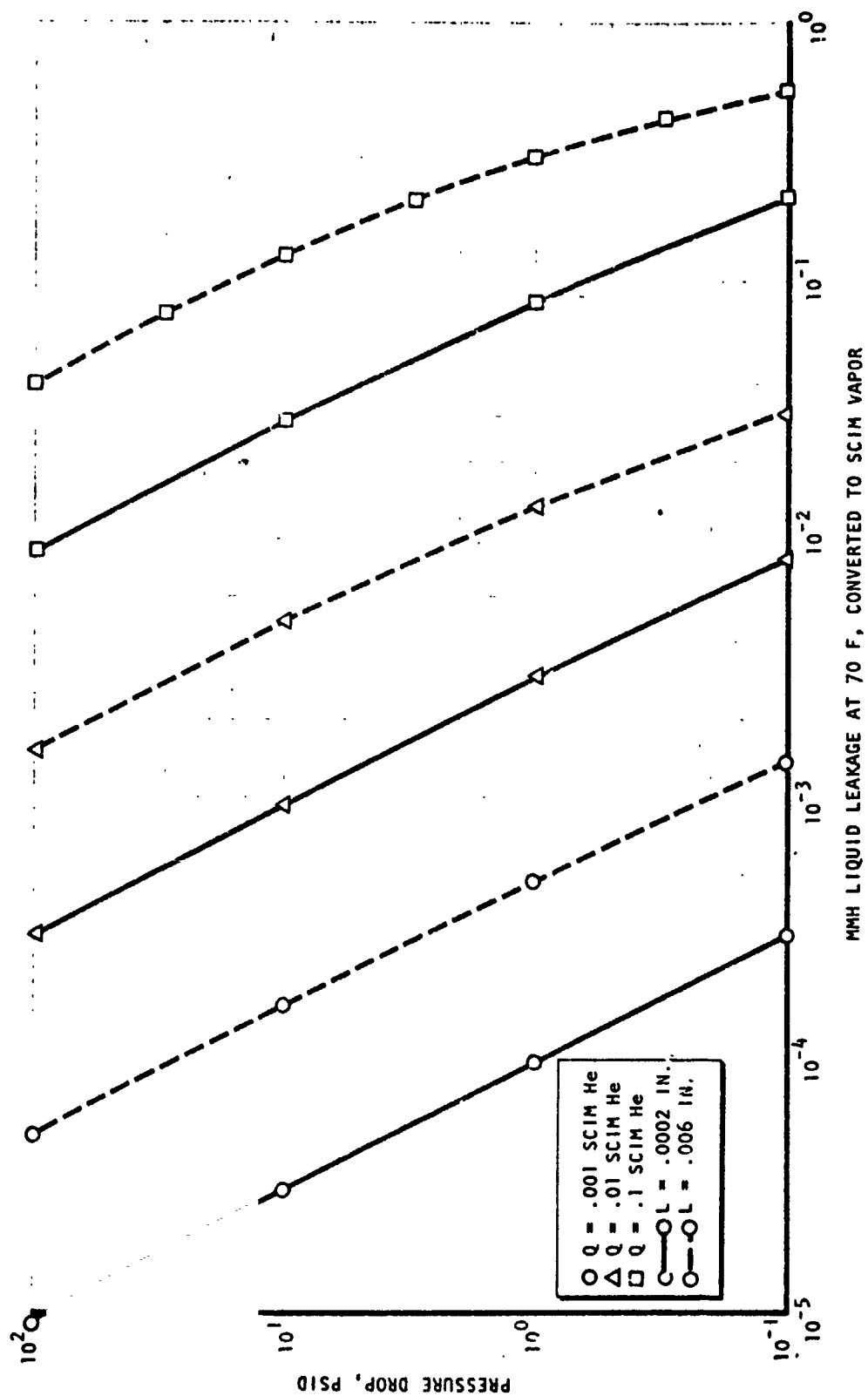


Figure 2-7. MMH Liquid Leakage Correlation

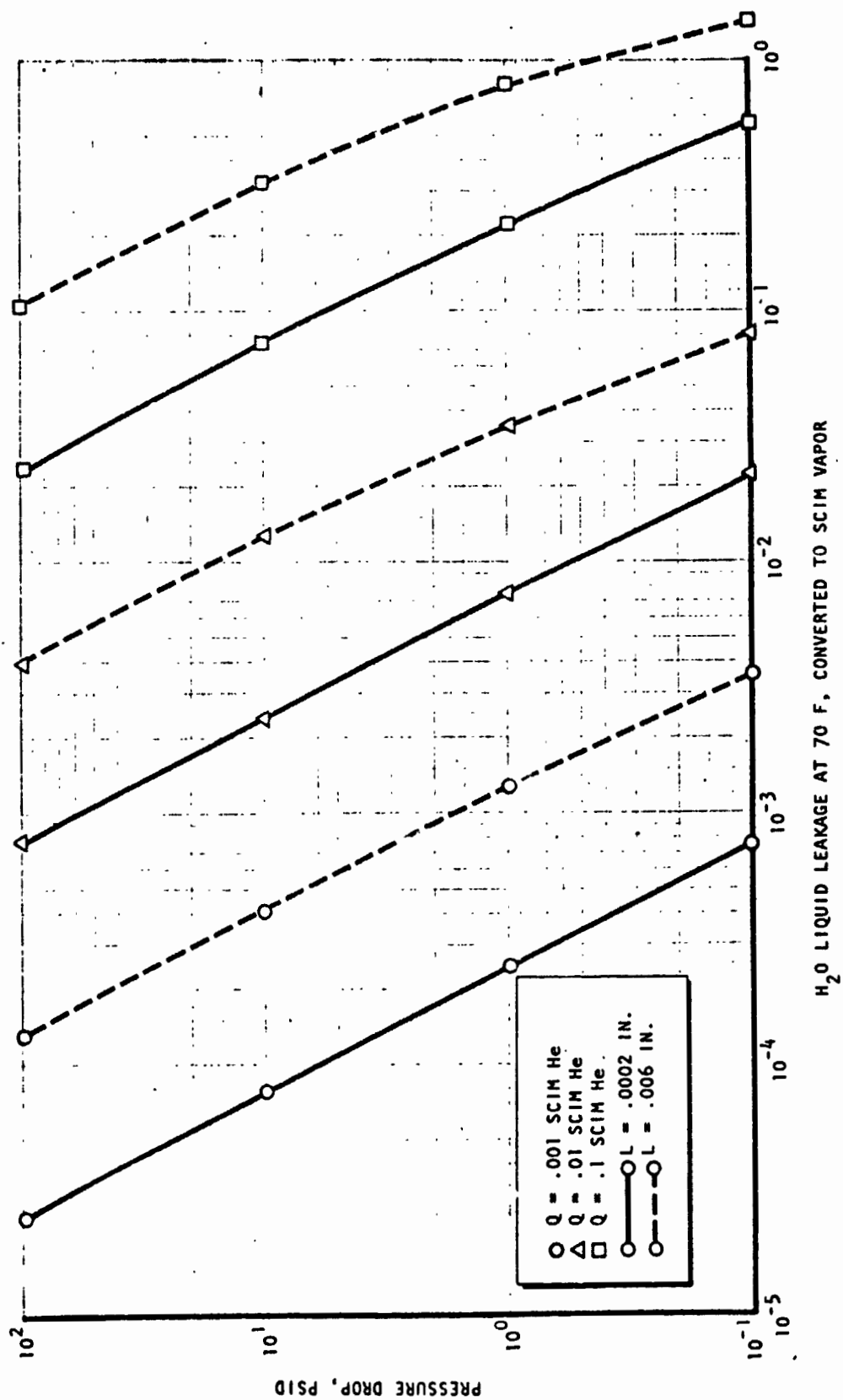


Figure 2-8. H_2O Liquid Leakage Correlation

plotted in Fig. 2-9 are simply used to relate the leak and pressure-drop-defined gaps (Fig. 2-4 and 2-5) to a realistic load parameter.

Computed vapor leakage for NO_2 and water are presented in Fig. 2-10 and 2-11. The water data have been included for comparison with MMH and because of a lack of data on MMH vapor. These curves indicate little difference between wide and narrow land leakage because all leaks are predominantly molecular. Data for loads less than the cracking force (1 to 2 pounds) result from forward pressure drop tending to open the seal. The concept of constant specification leakage under this condition is more or less realistic for flat lapped metal seals, particularly the cutter seal, because of the extremely flat, smooth, sealing surfaces attendant with these closures. (leakage on the order of 10^{-3} scim helium has been obtained with the prototype check valve with seat loading resulting from poppet weight of 0.02 pound and pressure drop from 0.1 to 500 psid.) However, polymeric seals of substantially rougher surface would require a minimum positive load to seal and thus, for the hypothesis of seal inloading to the levels indicated, the leakage would probably be substantially in excess of that shown.

Review of the data indicate that for the assumed model, the 14.8 psid driving force from the N_2O_4 vapor causes a high leak rate at the lower loads. Even with a 1.5 pound spring load the vapor leak rate exceeds the helium requirement. On the other hand, the water vapor, having little driving force, leaks substantially less; and, MMH leakage would probably be even less because of greater molecular weight.

This analysis shows that vapor leakage constitutes a worst condition. However, an analysis of the time to diffuse and fill upstream volumes under a range of thermal conditions would be necessary to define the probable impact on the system of these initially high leak rates. It would appear that, based on the helium leak requirements, without frequent intermittent helium purging, some NO_2 vapor will be present upstream of the check valve.

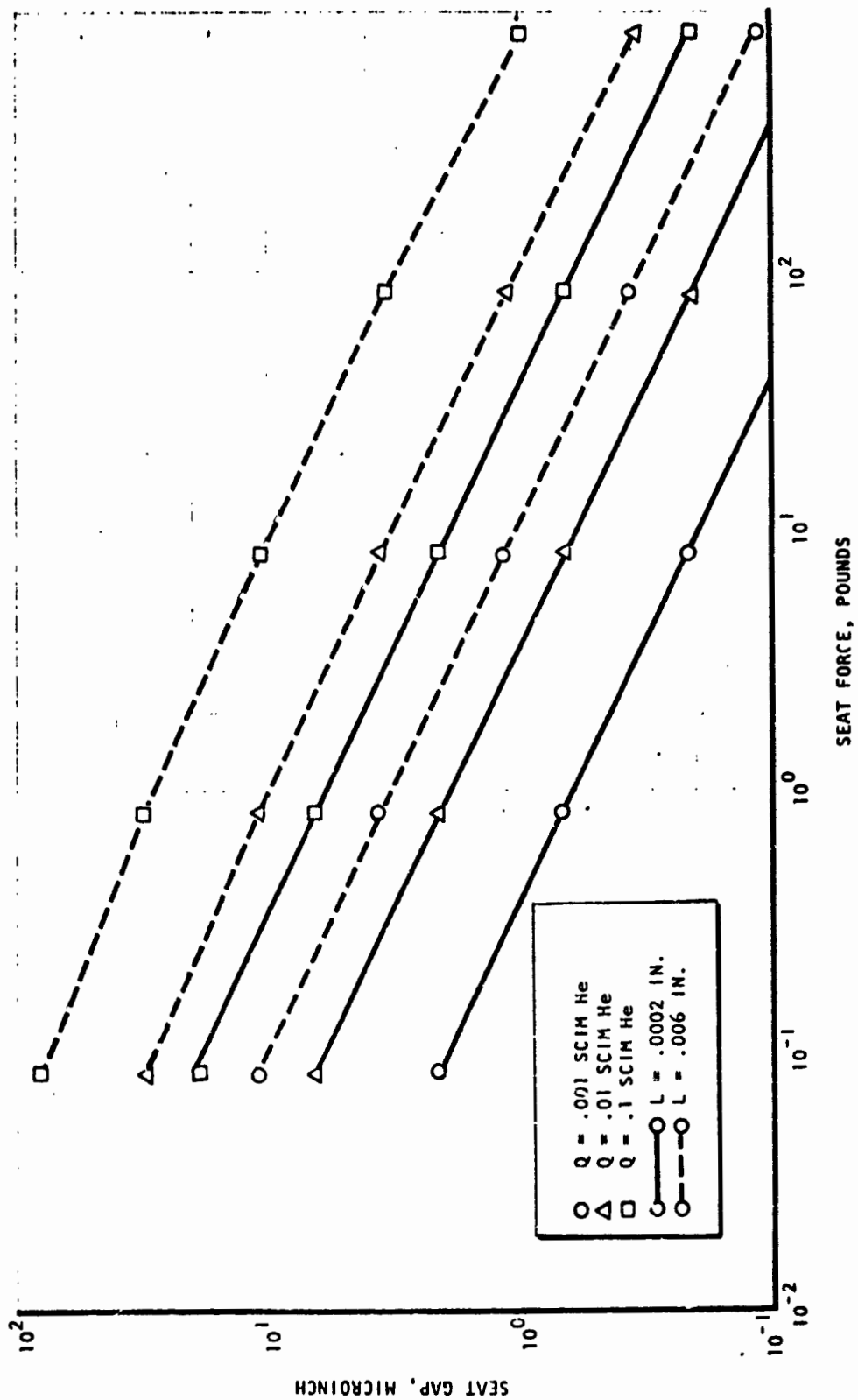


Figure 2-9. Seat Gap Versus Force Hypothesis

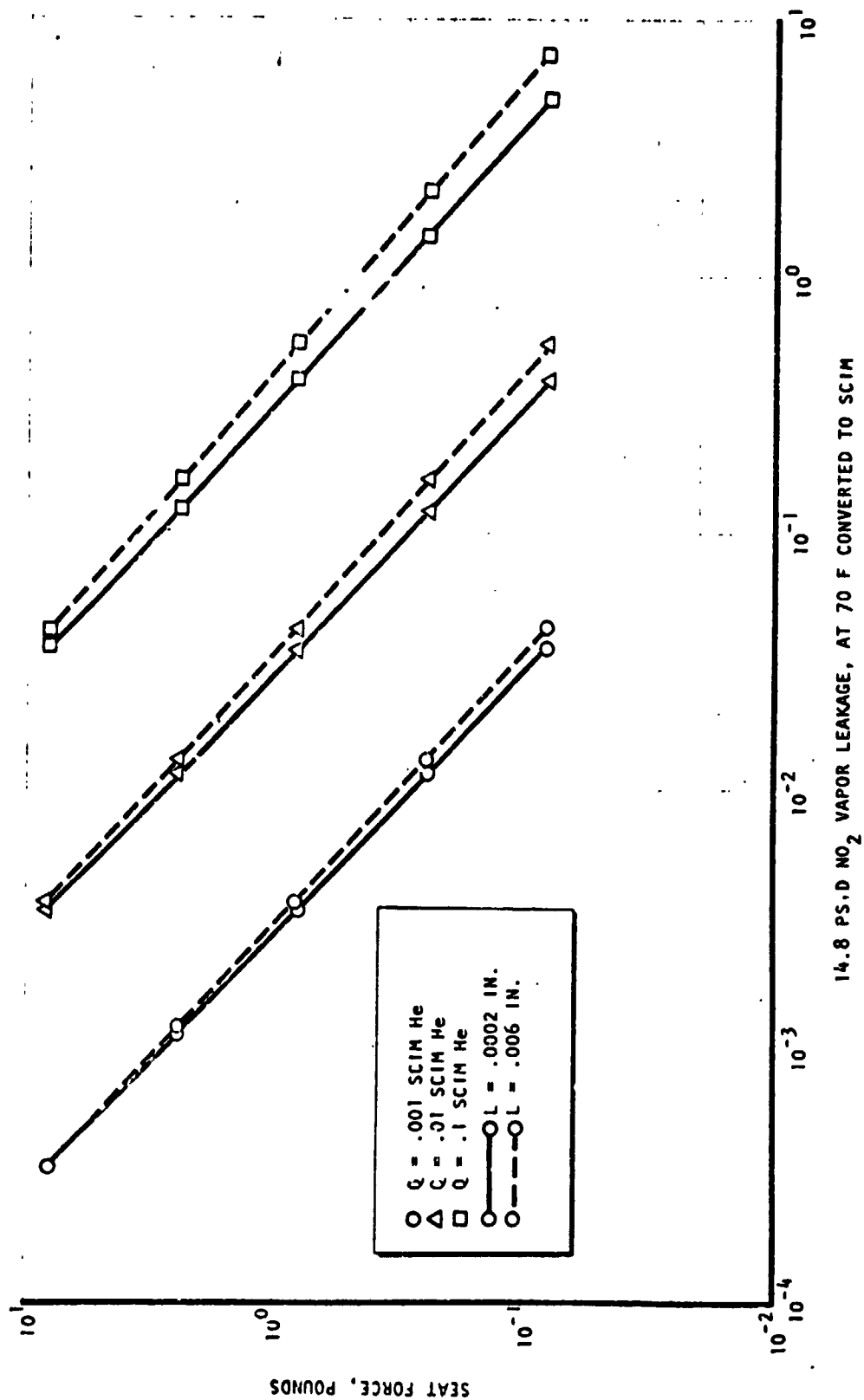


Figure 2-10. NO₂ vapor Leakage Correlation

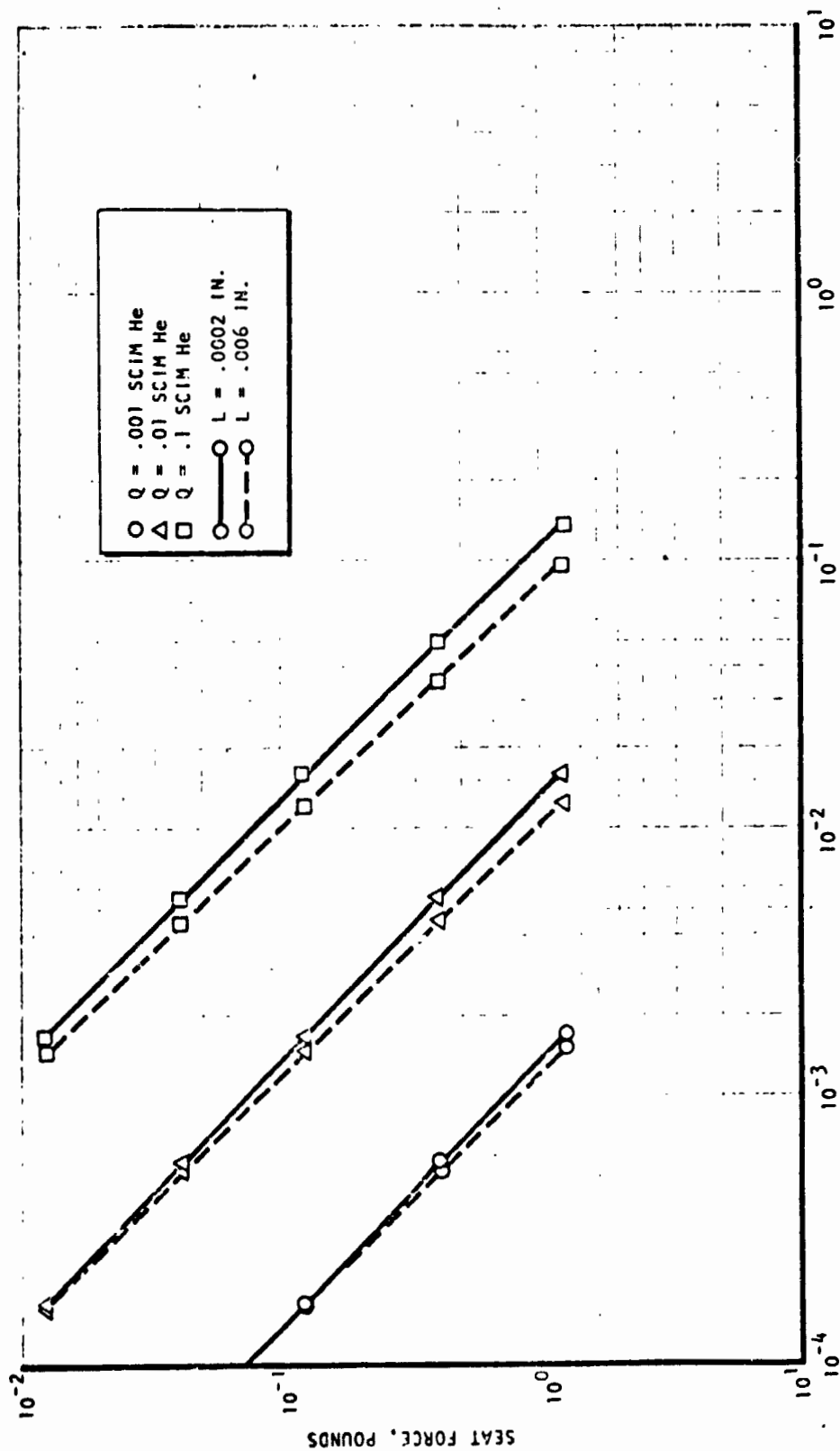


Figure 2-11. H_2O Vapor Leakage Correlation

TEST MODELS

Seal test models in precision test fixtures were used for evaluation of critical sealing parameters. This approach provided ready access to the poppet and seat for inspection and correlation of observed leakage, and also allowed precision control and measurement of the closure gap, sealing loads and leakage.

The test model designs used in the program evolved from previous research programs and further tradeoffs and analysis performed in this work. This effort is described, along with the test models, in the following paragraphs. Seal concept sketches and details of fabricated models are presented in Appendix B. Discussion of test fixtures and seal test methods is covered in Appendix D.

CONCEPT DESIGN AND TRADE STUDY

Four basic types of poppet seal closures were studied in arriving at the selected designs: (1) ceramic cutter seals, (2) AF-E-124D elastomer seals, (3) fully encapsulated Teflon, and (4) partially encapsulated or "trapped" Teflon that uses a combination of mechanical and fluid pressure retention.

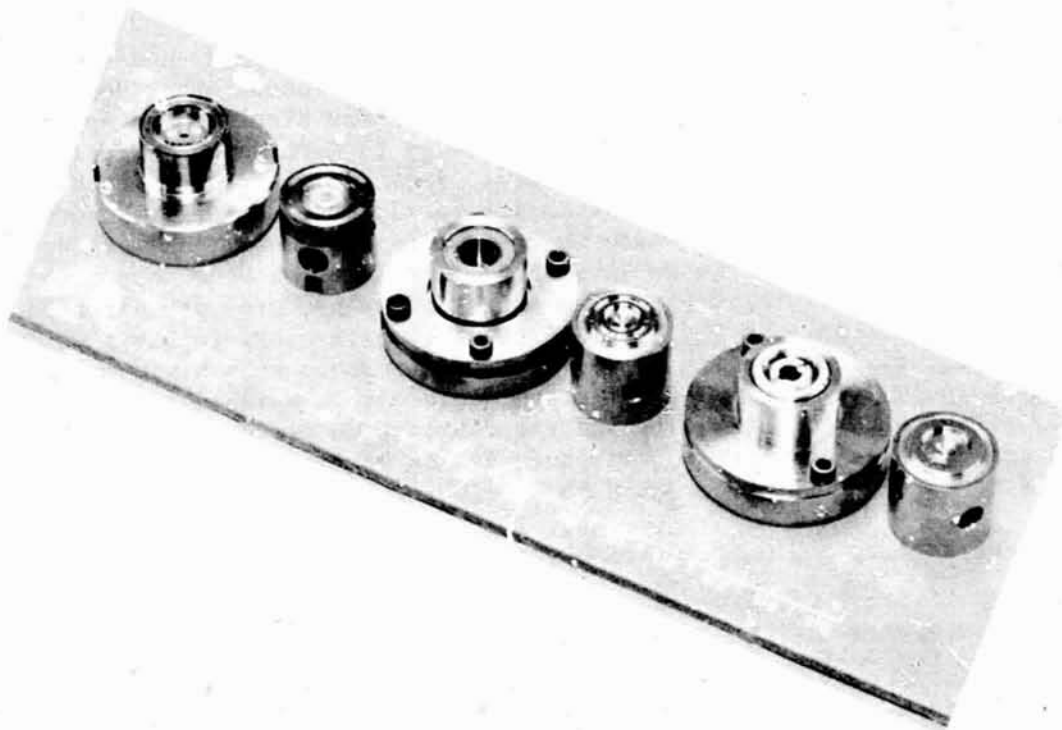
For each seal type, conceptual designs were developed, analyzed, and traded off with respect to the design goals and potential application in other Space Shuttle components. Concepts generated in this trade study are displayed in Appendix B. These sketches represent sealing concepts intended to have superior resistance to contamination effects with minimum seat load. Included with each sketch are advantages and disadvantages, some of which are fairly obvious, other determined by test in past programs, and some based on engineering judgment. As will be seen, features of various designs can be interchanged or inverted from poppet to seat depending upon such factors as the valve actuation means, pressure direction, etc. Of prime importance is the combination of complimentary features which have the maximum potential of meeting the sealing requirements with minimum complexity, particularly in fabrication. These factors could not be weighed properly until the facts relative to compatibility and the fabrication process were assessed and a design analysis was completed. Consequently, an investigation of these factors was initiated early in the program in the following areas:

1. Availability and usage of fine grain carbides, cermets, and ceramics
2. Compatibility of carbides, cermets, and ceramics with storables (literature)
3. Exposure tests to evaluate sharp-edge degradation of cutter seal materials in storable propellant and corrosive byproducts (RFNA)
4. Chemical or mechanical fusion or retention of AF-E-124D and Teflon to metal
5. Molding and curing AF-E-124D elastomer
6. Machining AF-E-124D elastomer

Initial studies in the materials investigation helped in formulating the design approach and final configuration used in the model test program. Very little information was gained from the literature in evaluating compatibility of cutter seal materials. Consequently, the test models fabricated for the S3/APS program (Ref. 4) were modified to perform initial wire cutting tests. Characterization data from TRW (Ref. 5) indicated a high degree of propellant compatibility for AF-E-124D elastomer and Teflon so there was no immediate need for further tests of these materials, and design criteria in Ref. 5 were employed in the trade study and design of the polymer seals. The materials investigation proved to be a major task in the program and extended throughout the entire effort. Detail results are presented in a subsequent section.

MODEL DESCRIPTION

The trade study and early phases of the materials investigation resulted in selection of three basic seal concepts for the seal test program. These were the carbide cutter seal, the flat polymer seal, and the captive polymer seal, as shown from left to right below.



The cutter seal model was an outgrowth of previous Air Force seal contamination programs (Ref. 2 and 3) and was developed and tested in the SS/APS valve program (Ref. 4). The flat polymer seal model was a "workhorse" configuration designed to allow evaluation of a variety of polymer seal insert materials. The captive

polymer seal model was patterned somewhat after the captive plastic closure of the SS/APS program; it too, was designed to utilize a variety of polymer seal insert materials.

To provide control and identification of test models, three-digit basic numerical designations were applied to each model configuration, and individual models were sequentially numbered. Each model assembly is described in the following paragraphs. Detail drawings are presented in Appendix B.

Cutter Model (100 Series)

The cutter model was developed from the hard-sharp carbide seal of the SS/APS valve program which had two sharp crests in contact with the mating flat carbide poppet. The inner of these two lands was the sealing land, while the outer land was a bumper land designed to absorb initial closure impact and to align the sealing interfaces prior to final closure. Because of the extremely light loads used in the program while testing in the check valve mode (i.e., load is only produced as a function of inlet pressure acting over the unbalanced seating area), the outer land was removed so that a precise assessment of the closure and seating forces could be made.

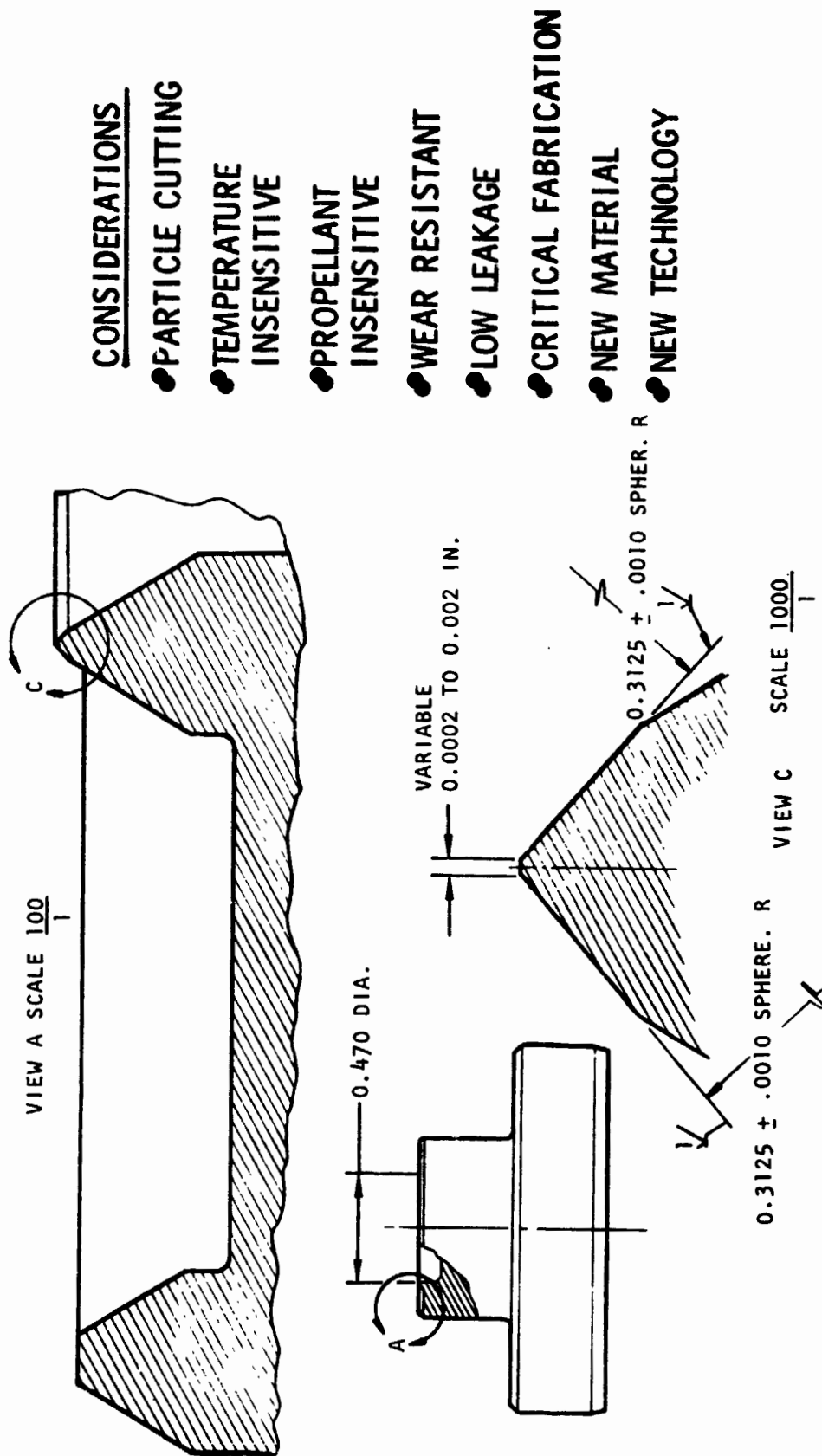
Figure 3-1 illustrates the cutter model used for this program. Two of the hard-sharp carbide seats were available from the SS/APS program; these were modified for use in the model investigation. A large body of performance data from SS/APS was also available along with the detailed fabrication technique and experience. Individually numbered models were produced by combinations of ball and cup lapping, and then flat lapping to produce different seal crest land widths.

Flat Polymer Model (200 Series)

For parametric evaluation of various polymer seal materials with numerous repeat tests, both clean and contaminated, a "workhorse" sealing concept was required for baseline control. A design was prepared which allowed fabrication of relatively inexpensive polymer seals as a separable part of a metal holder suitable for use in available test fixtures. With this approach, a new seal was used for each surface evaluation test series as required. This concept was considered to have the lowest risk factor of the polymer concepts, and is the most widely accepted sealing approach used for soft seating valves.

The detailed design is illustrated in Fig. 3-2. A flat "washer" of the polymer material to be tested is appropriately finished and then placed on the model base. The clamp is then installed with sufficient shims and springs to fill the void volume between the retention teeth, as shown in Fig. 3-2. This not only retains the seal material against pressure forces and thermally induced seal shrinkage, but affects a seal between the base and the seal washer; thus, significant leakage is across only one surface, i.e., the poppet-seal interface. Each different polymer seal washer tested produced an individually numbered model.

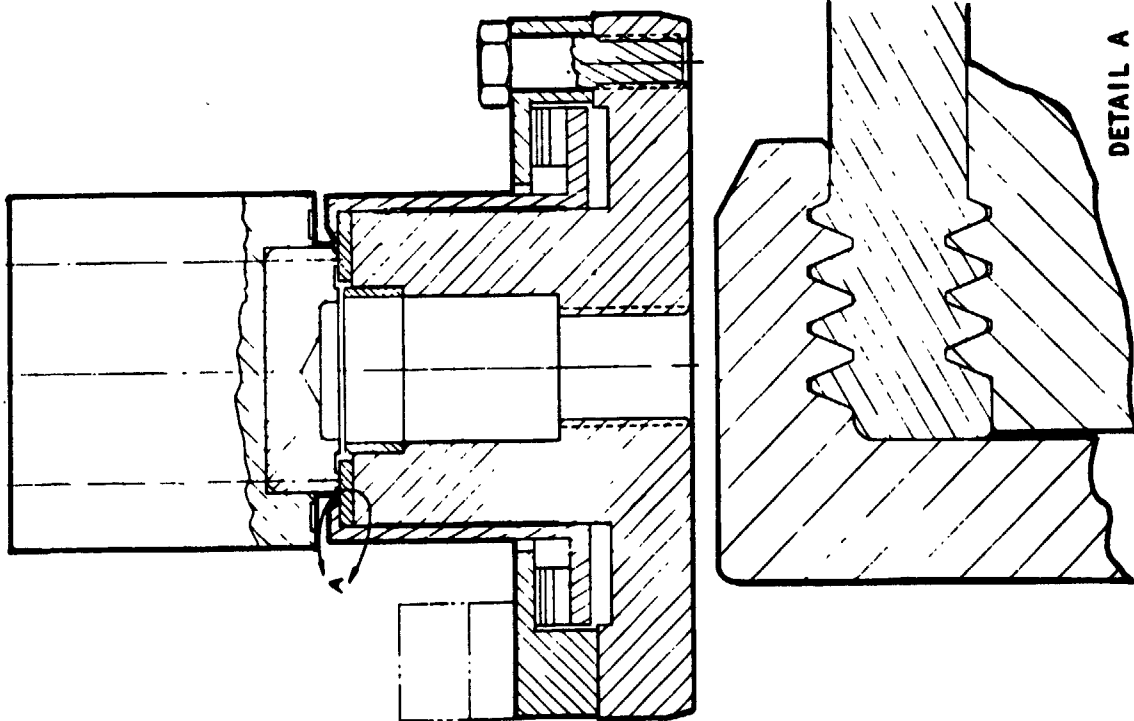
ORIGINAL PAGE IS
OF POOR QUALITY



CONSIDERATIONS

- PARTICLE CUTTING
- TEMPERATURE INSENSITIVE
- PROPELLANT INSENSITIVE
- WEAR RESISTANT
- LOW LEAKAGE
- CRITICAL FABRICATION
- NEW MATERIAL
- NEW TECHNOLOGY

Figure 3-1. Cutter Seal Model



DETAIL A

Figure 3-2. Flat Polymer Seal Model

CONSIDERATIONS

- SIMPLISTIC DESIGN
- ONE SEAL SURFACE
- POTENTIAL FOR VERY LOW LEAKAGE
- CONSTANT-RETENTION LOAD
- EXTREME SEAL PRECISION REQUIRED FOR LOW LOAD
- SEAL PROPERTIES NOT CONSTANT
- CANNOT TOLERATE FIBER

Captive Polymer Model (300 Series)

During the previously referenced SS/APS program, a captive plastic sealing concept utilizing Teflon was developed for use as a poppet-type seat where the seating impact and static seating loads were quite high. The excellent sealing performance for long-life service encouraged the use of the concept for this program for not only Teflon, but other polymers as well. The captive polymer model was based somewhat on the SS/APS design in that it had inner and outer retainers which, along with the seat ram and the poppet face, fully capture the seal member. It did not employ seal piston rings nor did it have spring-loaded retainers.

Figure 3-3 illustrates the captive polymer model. The polymer seal member is contained by an inner and outer retainer ring, and sits upon the base ram. Upon closure, the poppet face completes the capture of the seal and as seating load increases, the seal is, in effect, pressurized much as a fluid entrapped within a hydraulic cylinder. It should be noted that both the poppet-seal and seat-ram interfaces are sealing surfaces; this results in two leakage paths, one separable and one static. The flat and captive models included provisions for the center spring assembly (shown in the right half section of Fig. 3-3) so that tests could be run at constant inlet pressure. However, these parts were not used in the test program. As in the other models, different polymer seal inserts produced individually numbered models.

MODEL PREPARATION

Cutter Seal

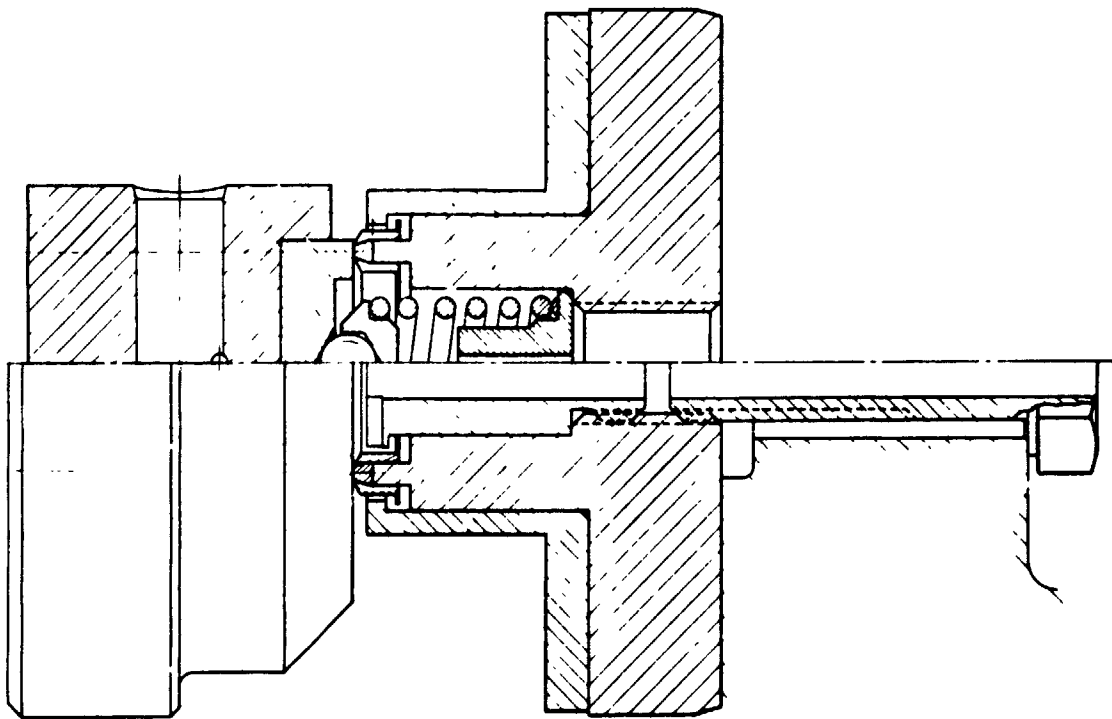
The cutter model poppets and seats were finished utilizing specialized lapping processes to achieve flatness and surface roughness commensurate with the leakage requirement. As noted in the analysis section for the prototype check valve, the gap resulting from unloaded contact between the poppet and seat is indicated as being on the order of 1 to 10 microinches.

The cutter land widths were modified by a combination of spherical and flat lapping using hardened tool steel laps and diamond compounds ranging from 3 to 0.1 micron. Circular flatness was probably well within 1.0 microinch on each part and surface roughness was between 0.3 and 0.6 microinch AA. Overall flatness across the poppet was within 5.0 microinches. Photographs of typical cutter lands are shown in the Seal Test section.

Polymer Seals

The captive and flat seal holders were fabricated using conventional machine shop tools. All turning was done in Hardinge lathes with critical features produced in one setup. Seal preparation involved specialized processes developed in the materials investigations. Seal molding and fly cutting experiments are summarized in the Materials Investigation section. Methods developed for holding, flycutting and cutting test seals out of flycut sheet material are described in Appendix C.

ORIGINAL PAGE IS
OF POOR QUALITY



CONSIDERATIONS

- CAPTIVE SEAL
- FLOATING SEAL
RETAINERS
- HIGH LOAD CAPACITY
- EXTREME SEAL
PRECISION REQUIRED
FOR LOW LOAD
- SEAL PROPERTIES
NOT CONSTANT
- CANNOT TOLERATE
FIBER

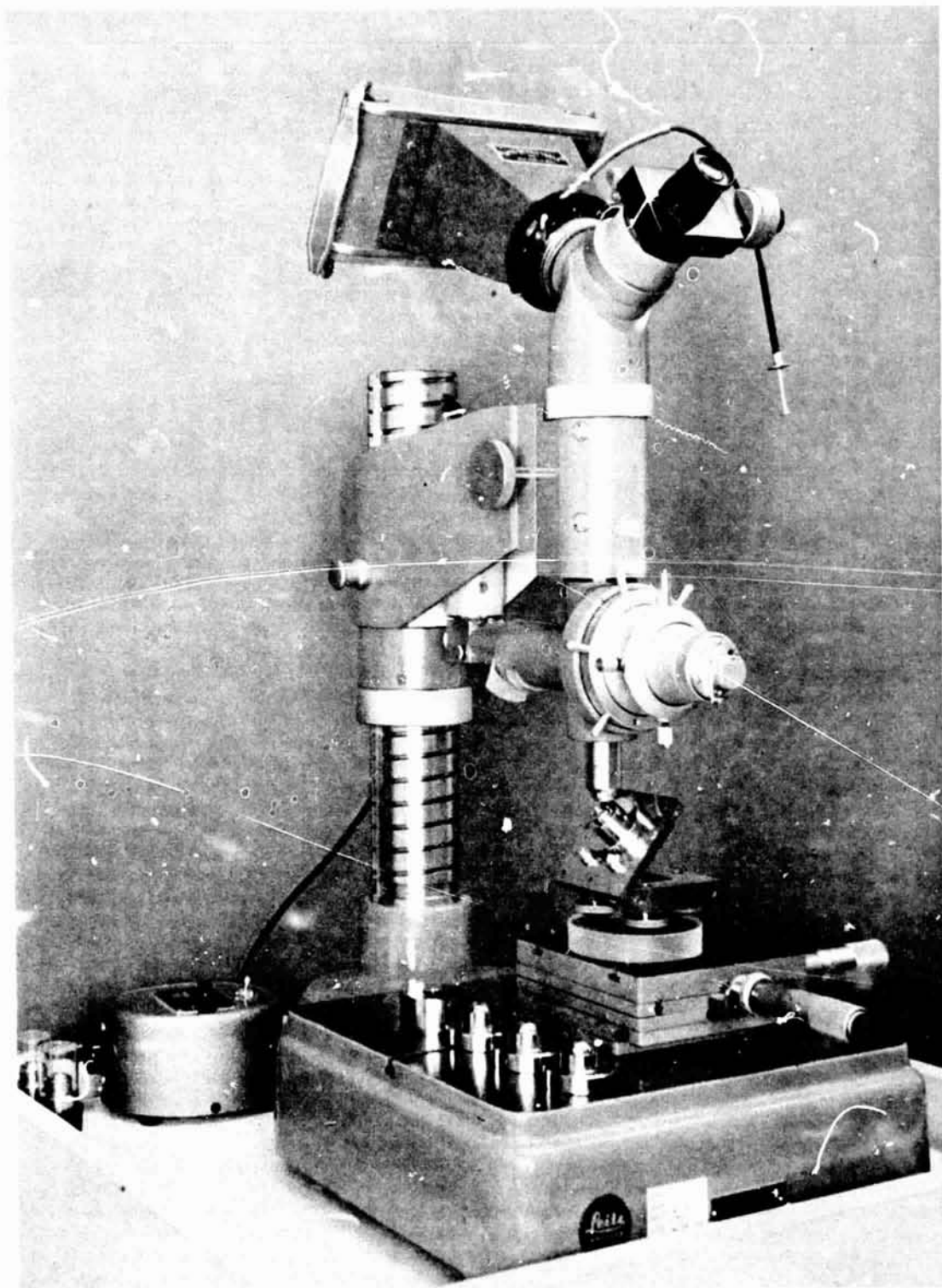
Figure 3-3. Captive Polymer Seal Model

Poppets used with the polymer seal models were modified from existing APS program 440 C poppets. A 0.03-inch-wide land was turned as shown in the Appendix B detail drawings. Poppet models with somewhat wider lands were also prepared in anticipation of fabricating grooved poppets for test; however, these parts were not used. Poppet sealing surfaces were lapped to produce flatness within 5 micro-inches and surface roughness of about 1.0 microinch AA. The captive model seat base was similarly lapped. All measured leakage from the polymer models was therefore attributable to seal geometry.

MODEL INSPECTION

Deduction of model seating geometry and surface characteristics was accomplished primarily with a Leitz interference microscope and techniques described in Ref. 1. The microscope, shown in Fig. 3-4, was the basic inspection tool used for all model surface and damage assessments. Supplementary equipment, such as the Johansson Mikrokator comparator (for parallelism measurements) or the Bendix electronic gauges (surface height variations), were used as required; operation and capabilities of these and other auxiliary equipment is reviewed in Ref. 1.

Information regarding inspection of certain polymer seals is contained in Appendix C. Specific posttest inspection techniques and procedures unique to certain models and requirements are discussed in applicable test sections.



CAD41-3/16/66-C11

Figure 3-4. Leitz Interference Microscope

ORIGINAL PAGE IS
OF POOR QUALITY

3-9/3-10

MATERIALS INVESTIGATION

Investigation of new materials for the cutter seal, and fabrication process development of polymer seals were major parts of the seal test program. In particular, the accelerated corrosion work on cutter seal materials have provided a unique microscopic view of sharp edge breakdown. Attempts with polymers to mold and machine supersmooth surfaces also led to new methods of seal fabrication. These data of a general nature are presented in this separation section. Additional data for specific seals and designs are presented in the Seal Test section.

CUTTER SEAL MATERIALS

Investigation of materials for the cutter and polymer seals covered specific areas of interest. For the cutter seal, long-term propellant compatibility with properties commensurate with tungsten carbide were paramount. Usual definitions of compatibility were not acceptable because even a few millionths inch attack by propellant corrosive byproducts would cause excessive leakage and could lead to intergranular corrosion resulting in catastrophic failure. Moreover, the literature had very little significant compatibility data on the carbide and ceramic materials. Success of the cutter concept therefore hinged on finding and verifying a carbide-like material that was literally impervious to the most corrosive constituents in the propellant environment.

Test Rationale

In the course of selecting candidate cutter materials, numerous chemists and metallurgists and those associated with the carbide and ceramics industry were contacted and questioned with regard to means for rapidly determining basic compatibility. The most conservative recommended testing in the propellant; however, this would not provide confidence for a 10-year mission. From these conversations and the literature it was concluded that the hydrazine-base fuels did not pose any serious problem with cutter materials. General consensus was that the water contamination product of nitrogen tetroxide, i.e., nitric acid, was the most severe service exposure medium. Because the exposure time, concentration, and other effects in a real system acid/ NO_2 vapor environment could not be determined, it was reasoned that a suitable material that would be impervious to concentrated acid would be a first choice. If no material survived the acid exposure, the alternative was long-term propellant testing. The exposure medium selected, therefore, was concentrated red fuming nitric acid (RFNA).^{*} Material acceptability criteria were based on examination and hardness tests of material samples with razor-sharp edges using plain, interference, and scanning electron microscope (SEM).

Sample Selection and Preparation

Following the conclusion that nitric acid was the worst test medium, manufacturers of carbides and ceramics were contacted, and small samples of candidate materials resistant to the acid were obtained. For comparison purposes, samples of carbides currently in use, but known to be incompatible, were also included. Listing of the

^{*}Red fuming nitric acid reagent, 1.59-1.60 specific gravity, approximately 20-percent dissolved oxides as NO_2 , Allied Chemicals.

material samples and other pertinent data are presented in Table 4-1. These materials are well known, with the exception of specimen 7, CM-500 by Chemetal Corporation, Pacoima, California. Unlike other sintered carbides and ceramics in which small particles are fused together and/or strengthened by a metal binder (e.g., cobalt, nickel), CM-500 is a chemically vapor-deposited alloy of tungsten and carbon, forming a fine dispersion of tungsten carbide in tungsten. The material has variable hardness depending on the deposition process variables which affect the percentage of tungsten carbide in the tungsten and degree of hardness produced by the dispersion. Hardness from 700 to 2900 Vickers can be produced. For the typical 1700 Vickers material, analysis has indicated a composition of approximately 16-percent WC and the remainder tungsten. Grain size of the WC is about 100 angstroms in tungsten having a nominal grain size of about 0.1 micron.

Selection of candidate materials for test proved considerably easier than devising means for evaluating and screening the samples. Early test efforts indicated that it was vitally important to define specific features for identification of acid exposure effects and comparison with exact locations before exposure. The right-angle sharp edge was a natural choice for test and examination because it was both simple to fabricate and similar to the cutter seal. It also provided an easily identifiable feature. Furthermore, any attack by the acid would be initiated at the edge, which amounted to a reverse stress concentration.

Final samples were prepared by grinding small specimens into rectangular blocks. Sharp edges were obtained by lapping two intersecting right-angle faces with diamond compounds down to 0.1 micron on a hard lap. Most material on the lapped faces was relieved to minimize lap area and thus lapping forces. Final lap strokes were performed pushing the blocks edge-first along the lap to minimize edge fractures. Lapped faces were not polished to preserve maximum flatness and edge sharpness. Final roughness was largely a function of the materials capability to be lapped in the manner employed and its own internal homogeneity. Up to 0.003 inch was removed from the ceramics by lapping to remove grinding pits and cracks. Edge continuity for most samples was on the order of 10 μ in. and roughness less than 1.0 μ in.

Preliminary Evaluations and Tests

Sample preparation and microscopic examination of the effects of a diamond scribe on sample surfaces and edges provided valuable subjective data on the ability of each material to be fabricated and to function as a cutter seal. The only material reported in the literature to be impervious to the acid was aluminum oxide. It was fairly certain that metal-bound carbides would not hold up; therefore, serious thought was given to synthetic sapphire or alumina as a viable material. Several special sapphire samples were therefore prepared and tested.

One sapphire sample consisted of a right angle prepared with a 0.0002-inch-wide flat approximately 0.10-inch long. The piece was held in a copper-jawed vise so that the cutting edge was vertical. Stainless-steel wires of 0.003-inch diameter, and glass rods from 0.003 to 0.01 inch were repeatedly cut by pressing them onto the edge with a flat carbide poppet; there was no visible effect at 500x on the sapphire edge. The process was repeated with 0.01-inch-diameter music wire, requiring a blow from the carbide poppet; again no significant effect. It appeared

TABLE 4-1. CUTTER MATERIAL SAMPLES

| No. | Material | Source/Designation | Composition Data |
|-----|---------------------------|---------------------------|--|
| 1 | Sapphire | Union Carbide/-- | 99.99% Al_2O_3 Clear Single Crystal |
| 2 | Ruby | Industrial Tectonics/-- | 99.99% Al_2O_3 Red Single Crystal |
| 3 | Chromium Carbide | Carmet/CA815 | Sintered 85% CrC + 15% Nickel |
| 4 | Silicon Nitride | Ceradyne/-- | Sintered Si_3N_4 , Hot Pressed |
| 5 | Tungsten Carbide | Carmet/CA315 | Sintered 85% WC + 15% Cobalt |
| 6 | Tungsten Carbide | Kennametal/K2801 | Sintered 94% WC + 6% Nickel, Hot Pressed |
| - | Tungsten Carbide | Kennametal/K801 | Sintered 94% WC + 6% Nickel |
| 7 | Tungsten Carbide "Alloy" | Chemetal/CM-500 | Vapor Deposited W + WC Over a Mo Wire |
| 8 | Tungsten Carbide | G.E./883 | Sintered 94% WC + 6% Cobalt |
| 9 | Alumina | Western Gold/Super Wearox | Sintered 99.9% Al_2O_3 , White |
| 10 | Tantalum-Tungsten Carbide | Kennametal/K602 | Sintered 10% Ta + 88% WC + 1.5% Cobalt |
| 11 | Boron Carbide | Ceradyne/-- | Sintered B_4C , Hot Pressed |
| - | Silicon Carbide | Ceradyne/-- | Sintered SiC, Hot Pressed |
| - | Alumina | Avco/-- | Sintered Pure Al_2O_3 , Black |
| - | Silicon Carbide | Amercom/-- | Vapor Deposited SiC, Over Graphite |

that sapphire was indeed an exceedingly strong material. That is until the smooth-ground shank of a 0.025-inch-diameter carbide drill was very lightly drawn across the 0.002-inch edge resulting in its total destruction. This experience, combined with the aforementioned tests with a diamond scribe emphasized the fundamental nature of brittle, single-crystal materials. That is, once fractured there is little internal force to resist major damage.

Although somewhat set back by the tests with the sapphire, it was still believed that sapphire might be the only material capable of sustaining months in RFNA. Therefore, in addition to the right-angle sapphire specimen, a ruby crystal was prepared with one lapped edge at 45 degrees to the horizontal face. With the preceding experiences in hand, a sequence of examinations and tests were devised to carefully screen and provide quantitative data for each material that would allow an optimum selection for the cutter seal. These evaluations are summarized in the data of Table 4-2. The first evaluation of grind and lapability is somewhat subjective and depends on the specific process used. All materials ground easily except for the Chemetal CM-500 which proved exceedingly tough and required a high wheel pressure and coarse diamond. The harder ceramic materials were more difficult to lap simply because more material had to be removed to eliminate grinding cracks and removal rate was slower because of high hardness.

Edge fabricability was somewhat more quantitative because the entire lapped edge (normally 0.5 inch) could be examined to estimate an overall average for the degree of edge breakdown. As shown, the tougher carbides are better than the brittle ceramics.

Edge fracturability was the most significant of the tests. A Lietz microhardness tester (utilizing a Vickers 7/1 pyramidal-shaped diamond indenter with 100-gram load) was used to produce a series of indentations along the specific edge. The indentations were made to approach closer and closer to the sharp edge until fracture occurred, or the diamond cut its way off the edge. Typical examples of this test are shown in the interference photos of Fig. 4-1 for specimens 4, 5, 7, and 10.

The strongest materials were the vapor-deposited carbide (CM-500) followed closely by the micrograin tungsten carbide (CA315) and other metal-bound carbides. The ceramics and binderless carbides indicated significantly greater edge fracturability. Edge strength is not directly related to hardness because the ceramics were generally harder but more brittle.

The remaining tests were visual evaluations of pit size and general surface. As indicated, the ceramics appeared to be somewhat more pitted and rougher in finish.

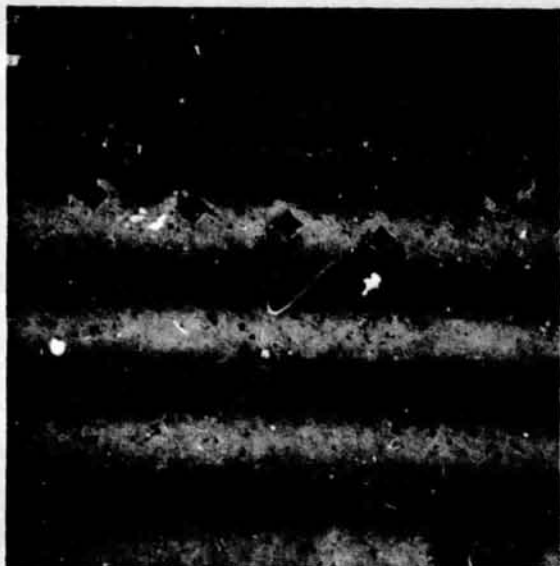
RFNA Immersion Tests

Based on the tests of Table 4-2, material samples numbered 1 through 11 were selected for RFNA immersion tests. The general test sequence consisted of four immersions in RFNA for intervals of 1 hour, 1 day, 15 days, and 169 days for a total of 185 days (~6 months). Each sample was placed in individual capped 20 cu³ sample jars filled with RFNA and maintained at about 70 F.

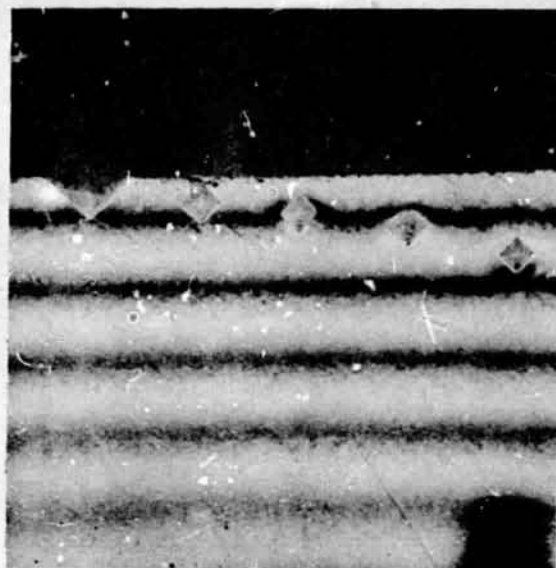
TABLE 4-2. PRELIMINARY CUTTER MATERIAL TESTS

| Specimen Number | 1 | 2 | 3 | 4 | 5 | 6 | 7 | 8 | 9 | 10 | 11 | - | - | - |
|---|------------------------------|----------------------|---------------------------|--------------------------|--------------------------|-----------------------------|----------------------------|--------------------|---------------------|---------------------------------------|----------------------------|------------------------|--------------------------|-------------------------------------|
| Material Specimen | U.C. Single Crystal Sapphire | I.T.I. Ruby Sapphire | Carmet CA815 CrC (15% Ni) | Ceradyne Silicon Nitride | Carmet CA315 WC (15% Co) | Kennametal K2801 WC (6% Ni) | Kennametal K201 WC (6% Ni) | Chemetal CM-500 WC | G.E. 893 WC (6% Co) | Wearox Al ₂ O ₃ | Kennametal K602 WC (2% Co) | Ceradyne Boron Carbide | Ceradyne Silicon Carbide | Avco Al ₂ O ₃ |
| Material Tests | | | | | | | | | | | | | | |
| 1. Grind & Lapability A - No Difficulty B - Moderate Difficulty C - Very Difficult D - Extreme Difficulty | D | D | A | B | A | A | A | C | A | D | A | C | B | D |
| 2. Edge Fabricability A - <10 microinch Break B - <20 microinch Break C - <50 microinch Break D - >100 microinch Break | D | D | B | C | A | B | B | A | A | D | B | D | C | D |
| 3. Edge Fracturability, Distance To Edge, inches, Before Edge Crumbles Or Cuts Away A - <0.0002 inch B - 0.0002-0.0003 inch C - 0.0003-0.0004 inch D - >0.0004 inch | D (0.00082) | D (0.00056) | C (0.00032) | C (0.00039) | A (0.00017) | B (0.00026) | C (0.00035) | A (0.00013) | B (0.00028) | D (0.00048) | C (0.0004) | D (0.00052) | D (0.00052) | D (0.00065) |
| 4. Hardness - Vickers, kg/mm ² (100 gram load) | 1854 | 1854 | 1290 | 1534 | 1530 | 1530 | 1530 | 1530 | 1680 | 1854 | 2055 | 3300 | 2898 | 1854 |
| Impression Diagonal, micron | 10 | 10 | 11 | 9 | 10 | 9 | 11 | 11 | 11 | 10.5 | 10 | 9.5 | 7.5 | 8 |
| 5. Pits (500x) A - <50 microinch B - <100 microinch C - <200 microinch D - >500 microinch | A | A | B | C | A | B | B | A | A | A | A | D | D | A |
| 6. Finish (500x) A - Few Pits, Good Surface B - Moderate Pits, Good Surface C - Many Pits, Good Surface D - Many Pits, Poor Surface | A | A | B | B | A | A | A | A | A | A | A | B | C | A |

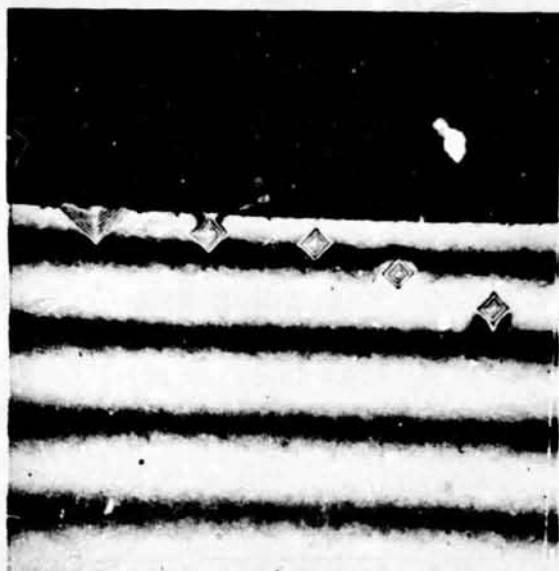
ON 12 MAR 1964
ON 1000R 100 1000



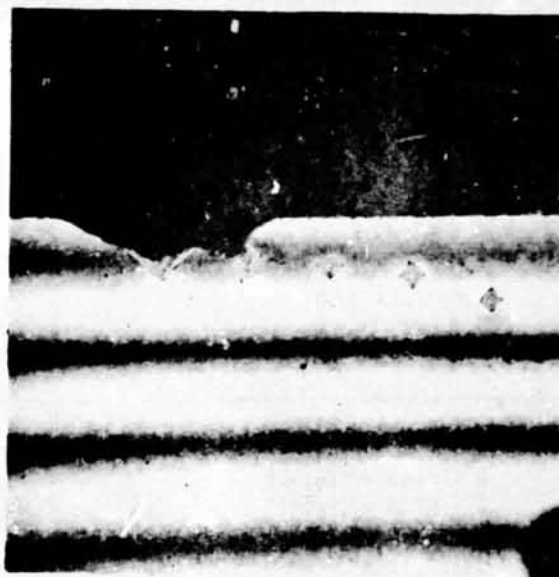
A. No. 4 Silicon Nitride



B. No. 5 Tungsten Carbide CA315



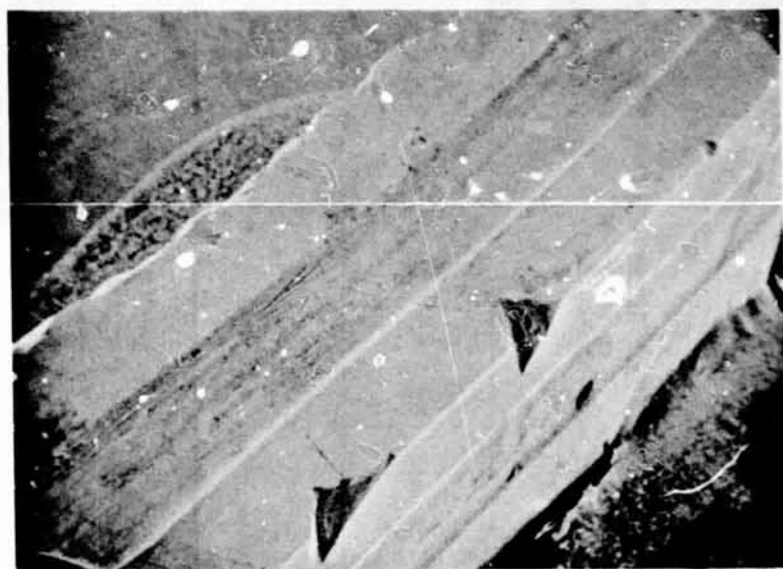
C. No. 7 Tungsten Carbide CM-500



D. No. 10 Tantalum Tungsten Carbide K602

Figure 4-1. Edge Fracturability Test of Typical Cutter Material Specimens (462X Interference Photos)

Prior to immersion, each specimen was photographed with the interference microscope in the area of the microhardness tests. This provided the baseline data for the 1 hour/day tests and subsequent inspection using the interference microscope. Primary control data were provided by the scanning electron microscope (SEM). Photographs were obtained with the SEM in the same location as with the interference scope at magnifications of approximately 500x and 5000x. These photos were taken at a nominal oblique angle of 45 degrees to the intersecting lapped surfaces, looking along the edge. A coating of 200 to 300 angstrom of aluminum was vacuum deposited on the nonconducting ceramic specimens to enhance their surface visibility. This was removed prior to RFNA immersion using a 10-percent hydrochloric acid solution. Setup of the CM-500 specimen in the SEM is typically shown below, taken at 16x.



After the 15-day exposure, the remaining specimens were cleaned, hardness tested as before, and rephotographed with interference and scanning electron microscopes. (Analysis of these data led to selection of the Chemetal CM-500 vapor-deposited tungsten carbide for the cutter seal poppet and seat.) The preceding process was repeated following the 169-day period to conclude the investigation.

RFNA Exposure Data

Results of the four exposure periods in RFNA are summarized in the following paragraphs. The majority of the information comprises visual examinations and direct comparison of plain and electron-microscope photos taken before and after exposure. Microhardness tests after 15- and 169-day periods also allowed quantitative assessment of corrosion effects and edge strength. These data are summarized in Table 4-3 for the entire test.

TABLE 4-3. CUTTER MATERIALS HARDNESS TEST DATA

| No. | Specimen Designation | Hardness - Vickers kg/mm ² (100-gram Load) | | | Edge Fracturability, Distance to Edge, inches, Before Edge Cuts Away | | |
|-----|----------------------|--|---------------------|----------------------|--|---------------------|----------------------|
| | | Pretest | Post-15 Day Test | Post-169 Day Test | Pretest | Post-15 Day Test | Post-169 Day Test |
| 1 | Sapphire | 1854 | 1854 | 1854 | 0.00082 | 0.00063 | 0.00063 |
| 2 | Ruby | 1854 | 2290 | 2510 | 0.00056 | 0.00040 | 0.00012 |
| 4 | Silicon Nitride | 1534 | 1534 | 1534 | 0.00039 | 0.00039 | 0.00039 |
| 7 | CM-500 WC | 1530 | 1530 | 1530 | 0.00013 | 0.00020 | 0.00024 |
| 9 | Wearox | 1854 | 1854 | 1854 | 0.00048 | 0.00048 | 0.00048 |
| 10 | K602 WC | 2055 | 2055 | 2055 | 0.00040 | 0.00040 | 0.00043 |
| 11 | Boron Carbide | 3300 | 3300 | 3300 | 0.00052 | 0.00052 | 0.00057 |
| 3 | CA815 CrC | 1290 | -- | -- | 0.00032 | -- | -- |
| 5 | CA315 WC | 1530 | 1530 | -- | 0.00017 | 0.00053 | -- |
| 6 | KZ801 WC | 1530 | 800 | -- | 0.00026 | 0.00060 | -- |
| 8 | 883 WC | 1680 | 1680 | -- | 0.00028 | 0.00060 | -- |

The electron-microscope work was performed at Hi Rel Laboratories (San Marino, California) using a Cambridge model SF-10 (10KV) stereoscan scanning electron microscope. The instrument is designed to provide high-resolution topographical images from about 16X to 100,000X, with an ultimate resolution of 100 angstroms. Magnifications selected for cutter seal material evaluation of approximately 500X and 5000X allowed comparison with the 462X interference scope photos and evaluation of edge degradation at a dimension of about one millionth of an inch. Higher magnifications were not warranted because of the level of roughness present in most specimens.

To provide a perspective for viewing the specimen SEM photographs, Hi Rel has photographed the head of a common house ant at 500X (Fig. 4-2). The advantage of the SEM is evident from the combination of fine detail resolution and large depth of focus. However, even more closely related to the cutter seal in size and finish, photos of Fig. 4-3, showing the edge of a new double-edge razor (with platinum), provide insight into the question of "how sharp is sharp?" The rounded, ragged edge ranges from 5 to 15 millionths of an inch in width thus providing a saw tooth cutting effect. As might be expected, the 0.0002-inch width of the cutter seal does not cut readily because of smooth edges, and relatively wide angle (90 degrees) and land width (nominally 20X the razor blade).

Photographs for material specimens 1 through 11 are displayed in Fig. 4-4 through 4-15. If there was no visible difference between the 15-day and 6-month exposure photos, only the latter are shown.

Specimen No. 1: Sapphire. This material was unaffected by all exposure tests. The sample differed from other specimens in that the top surface was lapped; whereas, the normal face (right side of photos) resulted from fracture of a ring specimen. The sharpness of the edge and brittleness of the material is revealed by the SEM photos of Fig. 4-4. Note the fractures surrounding the microhardness indentations and loss of edge material in Fig. 4-4C. These photos vividly display the catastrophic potential of a cracked brittle material. On the other hand, the sharp edge was unaffected by exposure and there was no significant change in microhardness. Material usage should be limited to applications where all stress concentrations can be avoided.

Specimen No. 2: Ruby. This sample was quite similar to the sapphire, microhardness cracks also producing cracks and material loss (Fig. 4-5A and C). An interesting increase in hardness and edge fracturability was observed, as shown in Table 4-3. There was no change in color or any other observable reason for the hardness increase.

Specimen No. 3: Chromium Carbide. Some visible pitting was evident at 500X after the 1-hour, 1-day exposures. Results of the 16-day exposure shown in Fig. 4-6 reveal substantial loss of binder material with the chromium-carbide unaffected by the exposure. The material is clearly not suitable for use in an application where nitric acid may be present.

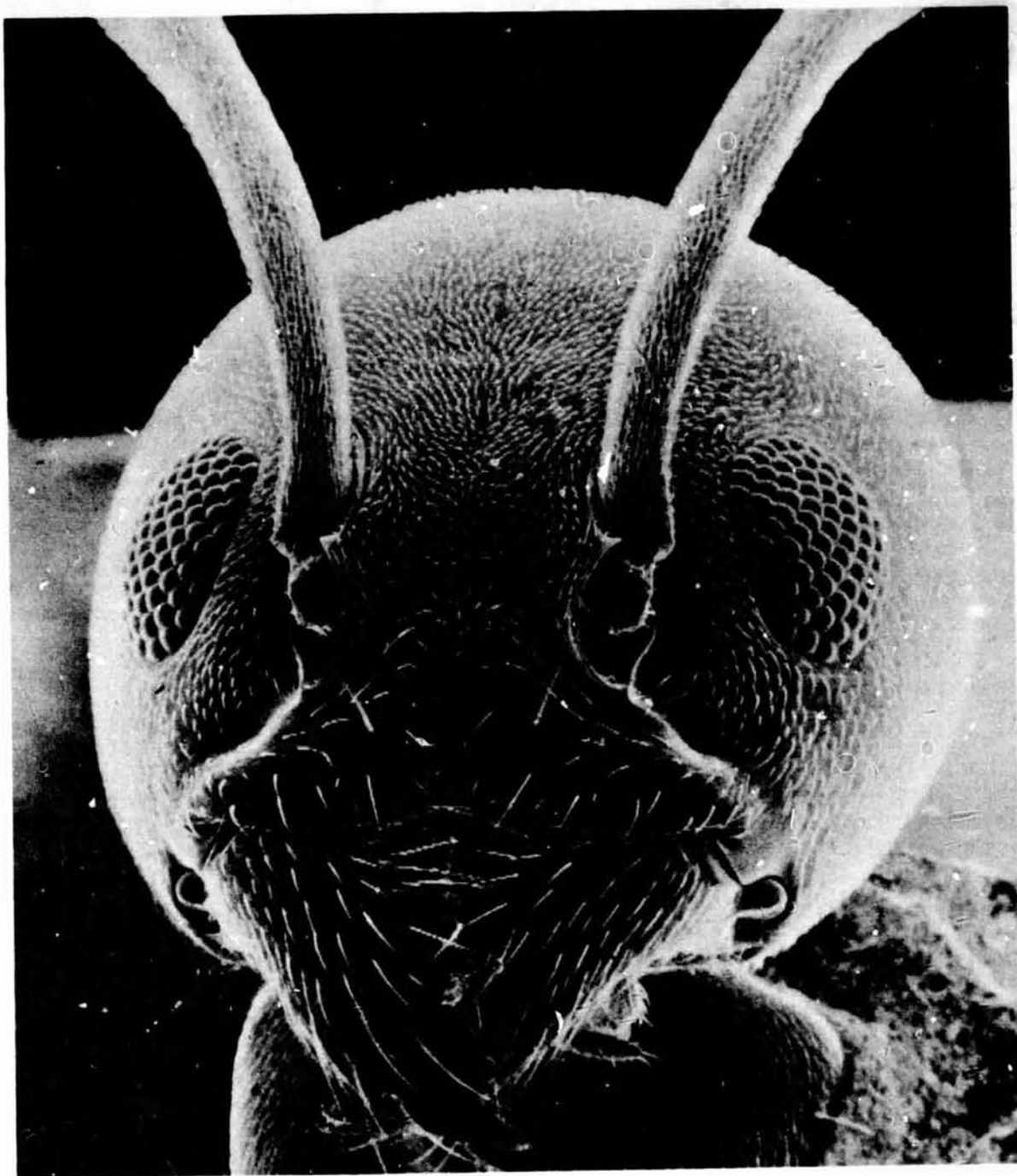
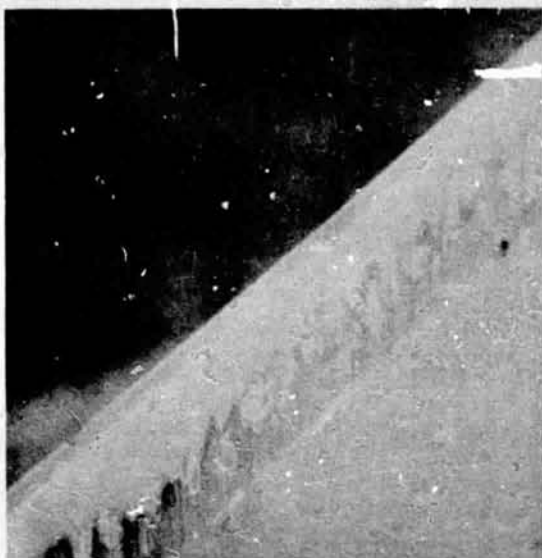


Figure 4-2. Head of Common House Ant (500X SEM Photo)

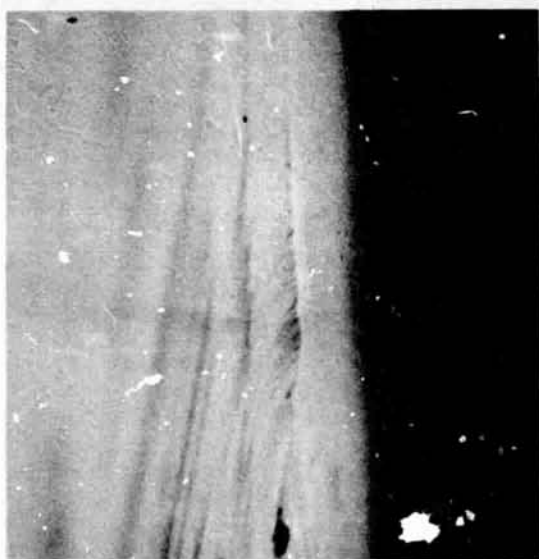
ORIGINAL PAGE IS
OF POOR QUALITY



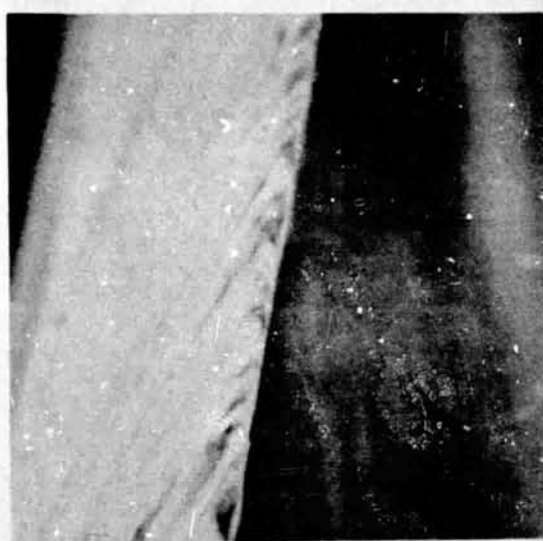
A. 70X OBLIQUE



B. 7000X LOCATION A



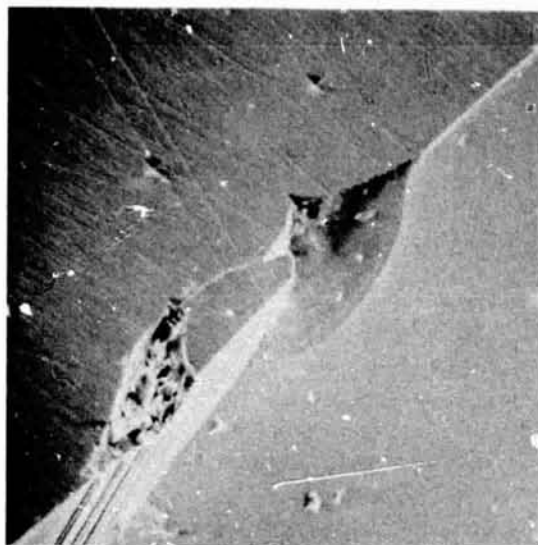
C. 650X ON EDGE



D. 6500X LOCATION C

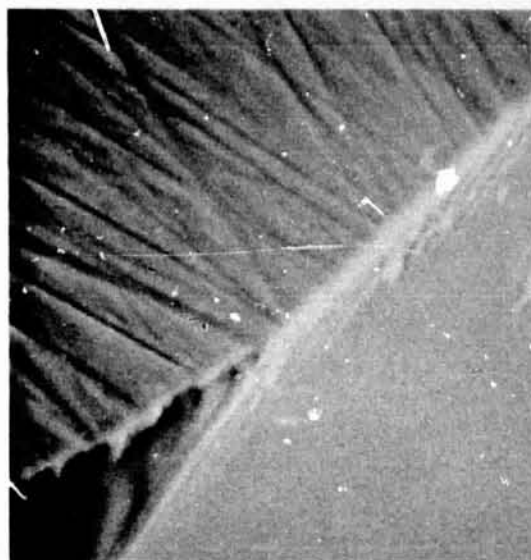
Figure 4-3. Razor Blade Edge (SEM Photos)

ORIGINAL PAGE IS
OF POOR QUALITY



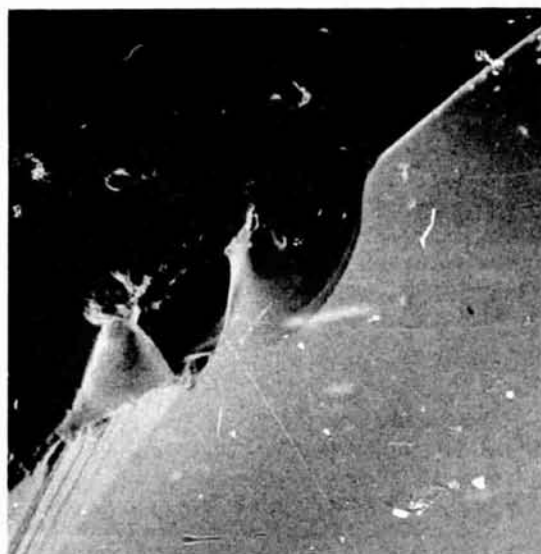
A. BEFORE EXPOSURE

475X



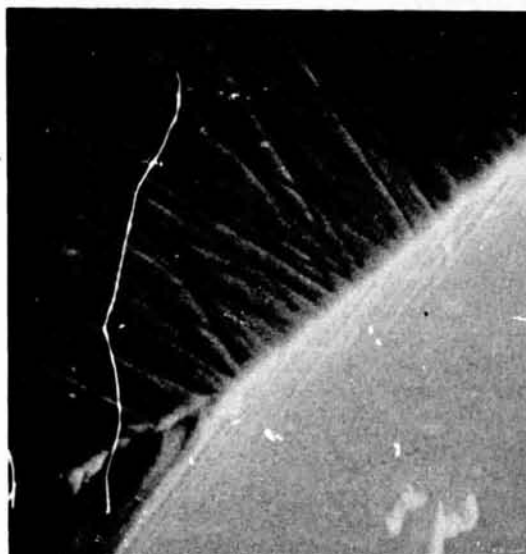
B. BEFORE EXPOSURE

470X



C. AFTER 185 DAYS

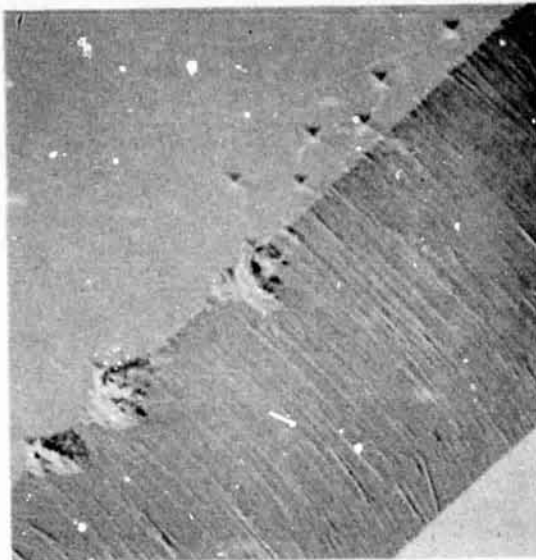
480X



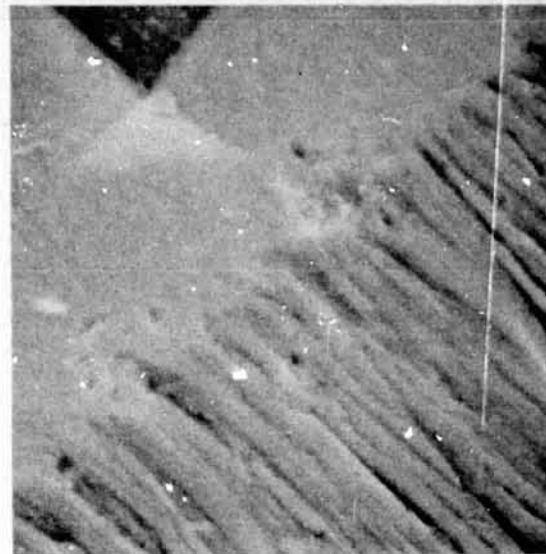
D. AFTER 185 DAYS

4800X

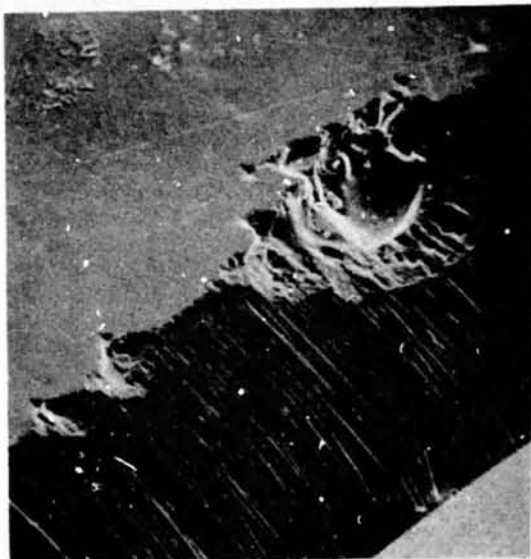
Figure 4-4. Specimen No. 1 Sapphire



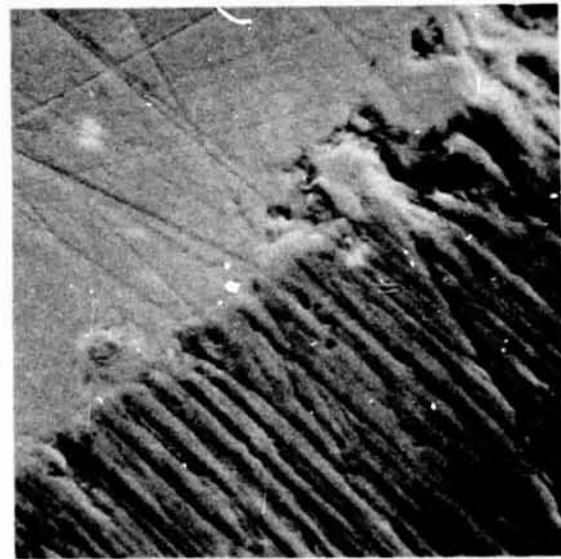
A. BEFORE EXPOSURE 510X



B. BEFORE EXPOSURE 5100X



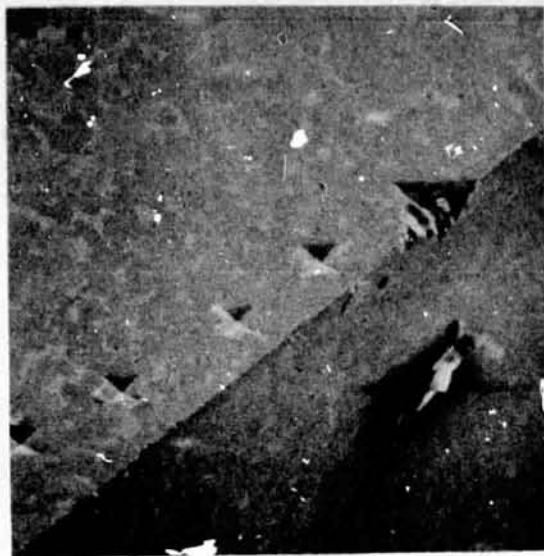
C. AFTER 16 DAYS 500X



D. AFTER 16 DAYS 5000X

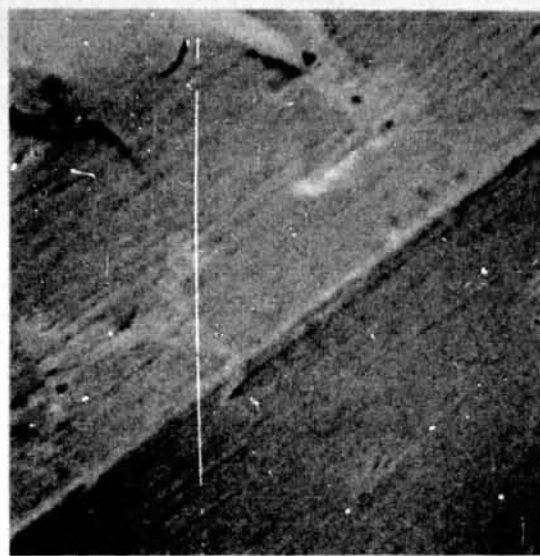
Figure 4-5. Specimen No. 2 Ruby

ORIGINAL PAGE IS
OF POOR QUALITY



A. BEFORE EXPOSURE

640X



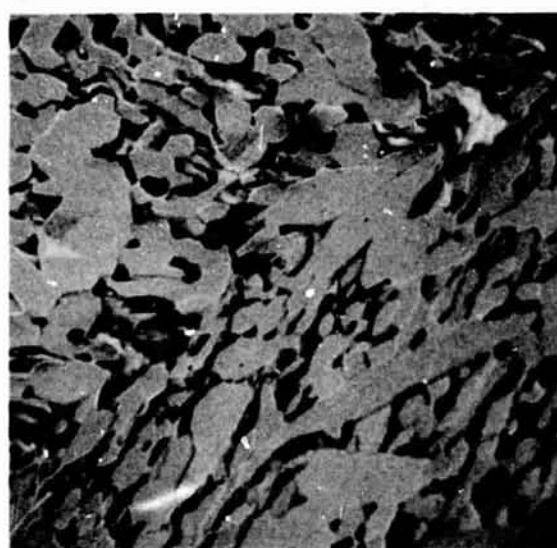
B. BEFORE EXPOSURE

6400X



C. AFTER 16 DAYS

600X



D. AFTER 16 DAYS

2400X

Figure 4-6. Specimen No. 3 Chromium Carbide, CA815 (15% Nickel)

Specimen No. 4: Silicon Nitride. Although it was decided early in the program that this material would not be used, its relative edge strength, finish, and promise of potential compatibility promoted further investigation. As shown in Fig. 4-7, the material was virtually unaffected by the RFNA exposure. The slight loss of edge material evident may possibly be due to handling and the many cleanings each material received.

Specimen No. 5: Tungsten Carbide (CA315). This material showed some pitting at 500X after 1 hour exposure, with little change noted after 1 day. Severe effects were noted after 16 days, with three corners of the specimen spalled off on the order of 0.1 inch. Another corner was easily "popped" off with pliers. This effect is visible in the loss of material around the microhardness indentations (Fig. 4-8). Increase edge fracturability was also observed (Table 4-3). The 15-percent cobalt binder is known to be attacked by nitric acid, and these results give an appreciation for the degree of attack. The material has been noted as compatible with N_2O_4 , but evidently would be a poor choice for long-term service.

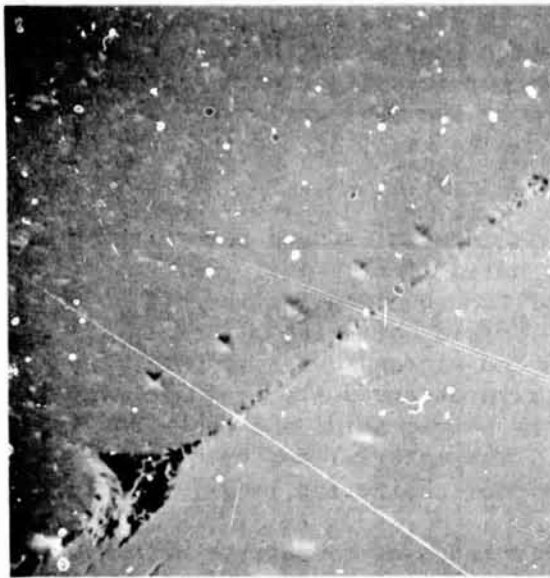
Specimen No. 6: Tungsten Carbide (KZ801). Also rated as compatible with N_2O_4 , this material did not survive even 1-day exposure. Pitting was evident at 500X after 1 day. As can be seen in Fig. 4-9, the nickel binder is deeply etched around the carbide grains. Edge strength was also degraded (Table 4-3).

Specimen No. 7: Tungsten Carbide (CM-500). This material was selected for the cutter seal. The photos of Fig. 4-10 are before exposure, except for picture D, which was included to show minor edge upset from handling. Picture C is a vertical shot to give another perspective of the edge. Six-month exposure photos are shown in Fig. 4-11 in the same areas as Fig. 4-10. As shown, the material was virtually unaffected by the RFNA. Edge strength and hardness were also unchanged.

Specimen No. 8: Tungsten Carbide (883). This 6-percent cobalt binder material was adversely affected similar to the 15-percent cobalt, CA315. The coarser grains of the 883 composition are evident in Fig. 4-12.

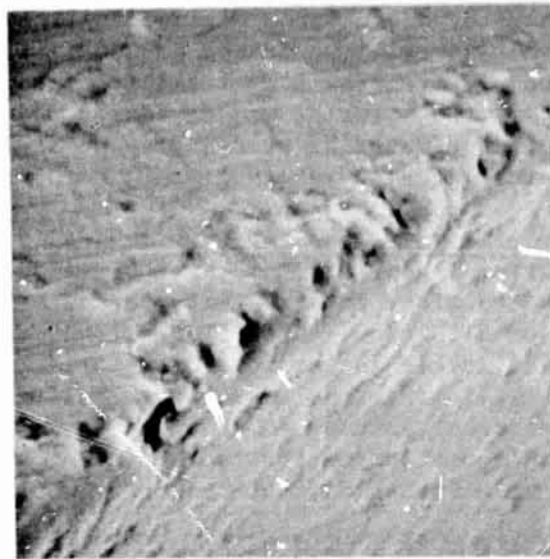
Specimen No. 9: Alumina. This material was included for comparison with the single-crystal materials. In general, the sintered material had poor fracture resistance similar to specimens 1 and 2. Although virtually unaffected by 185 days exposure, substantial loss of edge material was caused by microhardness indentation-induced cracks (Fig. 4-13). The original edge material was lost; therefore, the 16-day exposure photos are used for control.

Specimen No. 10: Tantalum-Tungsten Carbide (K602). Visibly (5000X SEM) unaffected after 16 days exposure, this material was chosen for use as guide pins in the prototype check valve. Its resistance to acid exposure can be attributed to the almost complete absence of cobalt bonder (approximately 1.5 percent). The effects of some etching are visible, however, after 185 days exposure, although there is still good edge continuity (Fig. 4-14). More important, the edge fracturability test (Table 4-3) did not indicate any loss of edge strength, so the etching could not have penetrated to a significant depth.



A. BEFORE EXPOSURE

470X



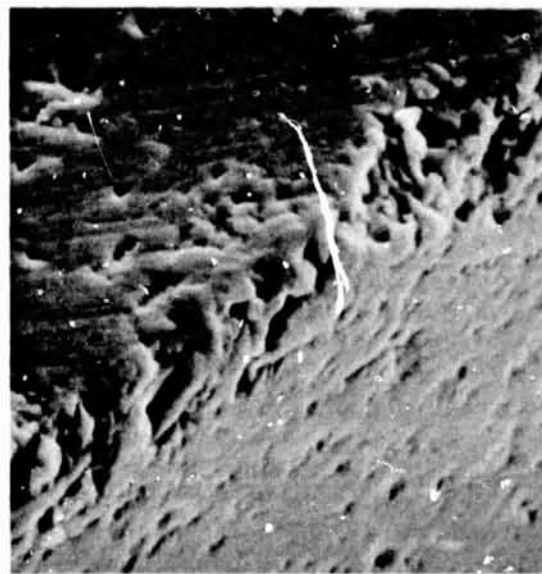
B. BEFORE EXPOSURE

4700X



C. AFTER 185 DAYS

480X

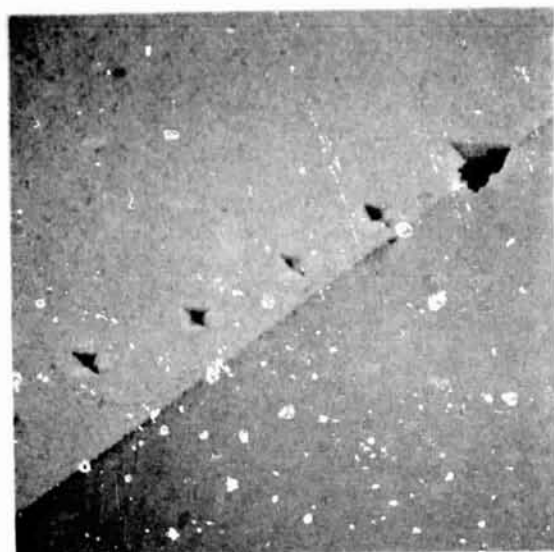


D. AFTER 185 DAYS

4800X

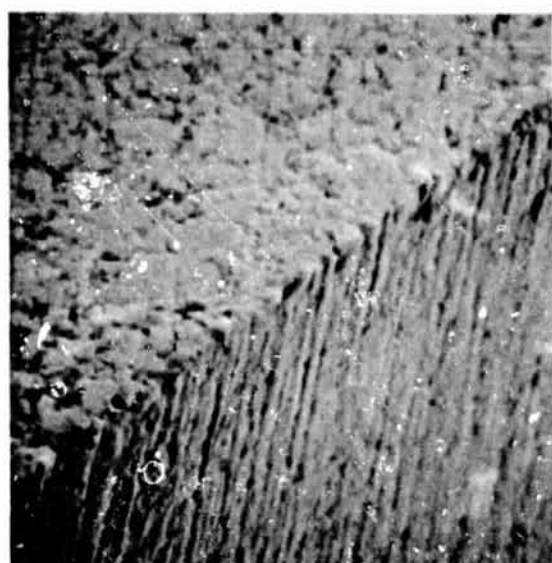
Figure 4-7. Specimen No. 4 Silicon Nitride

ORIGINAL PAGE IS
OF POOR QUALITY



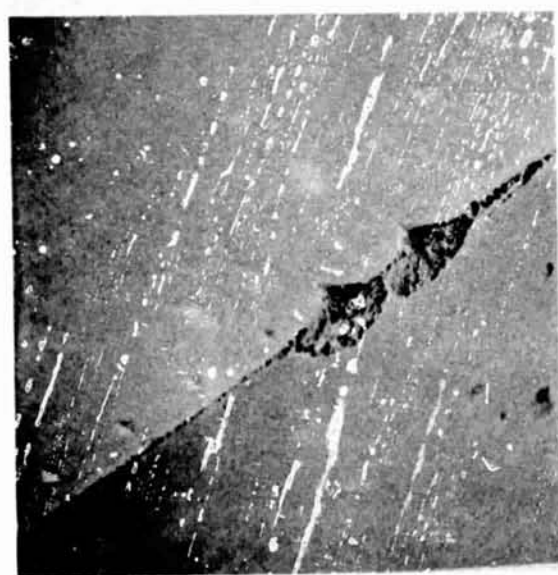
A. BEFORE EXPOSURE

570X



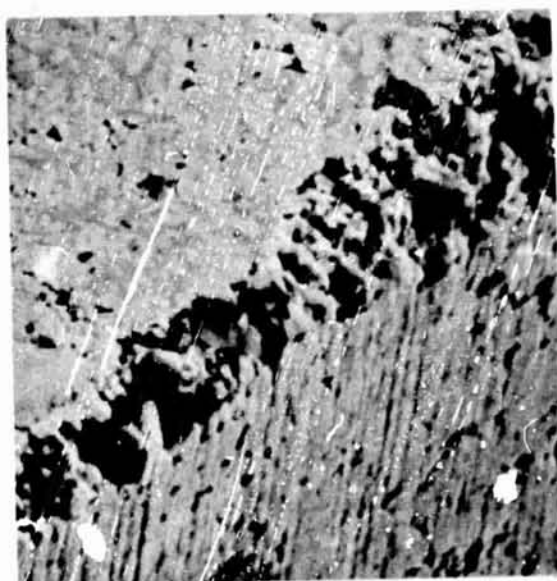
B. BEFORE EXPOSURE

5700X



C. AFTER 16 DAYS

220X

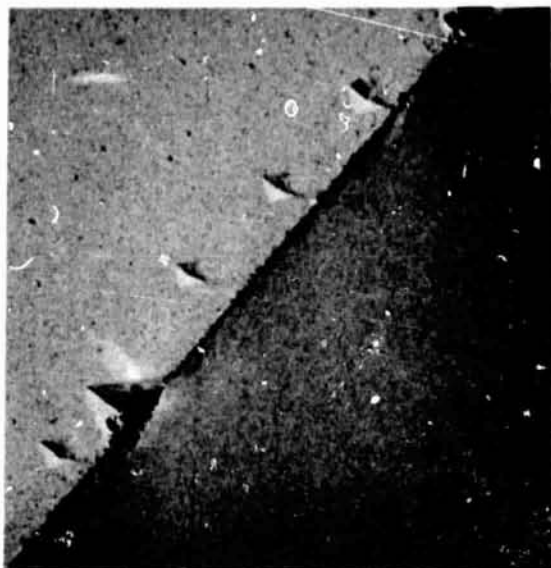


D. AFTER 16 DAYS

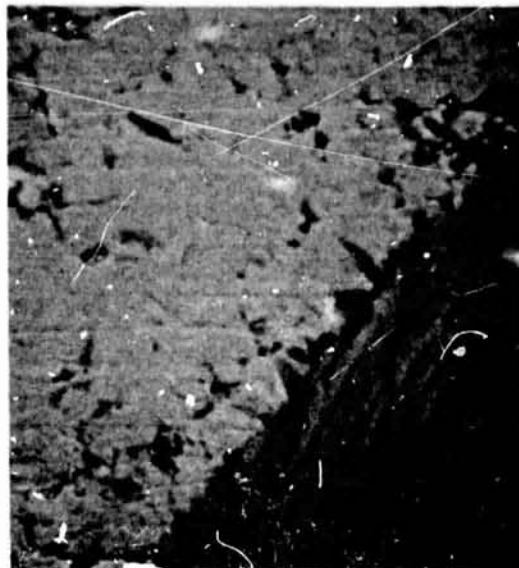
5400X

Figure 4-8. Specimen No. 5 Tungsten Carbide, CA315 (15% Cobalt)

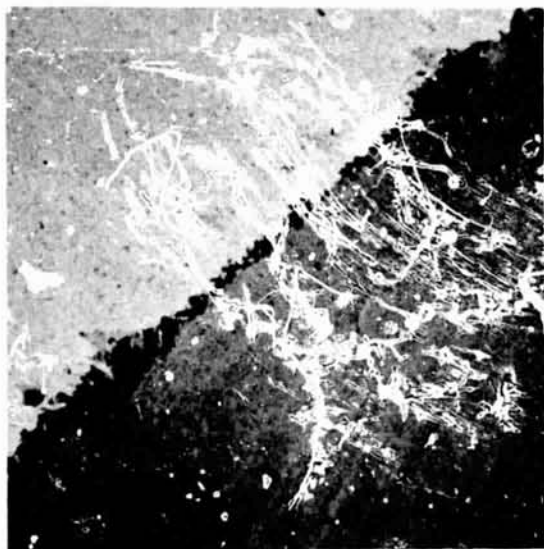
ORIGINAL PAGE IS
OF POOR QUALITY



A. BEFORE EXPOSURE 580X



B. BEFORE EXPOSURE 5800X

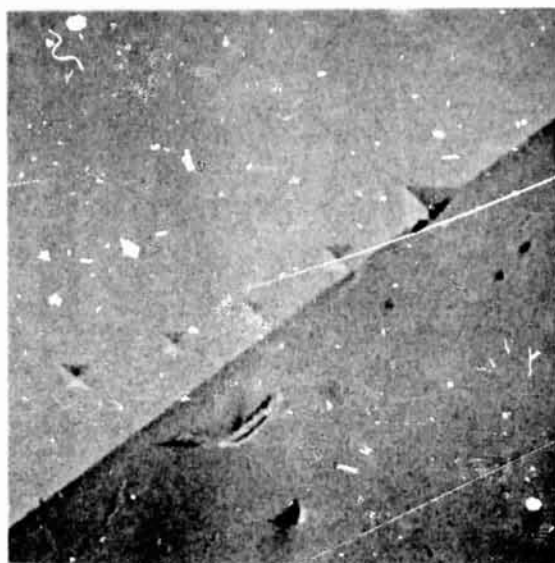


C. AFTER 2 DAYS 605X



D. AFTER 2 DAYS 6050X

Figure 4-9. Specimen No. 6 Tungsten Carbide, KZ801 (6% Nickel)



A. BEFORE EXPOSURE

550X



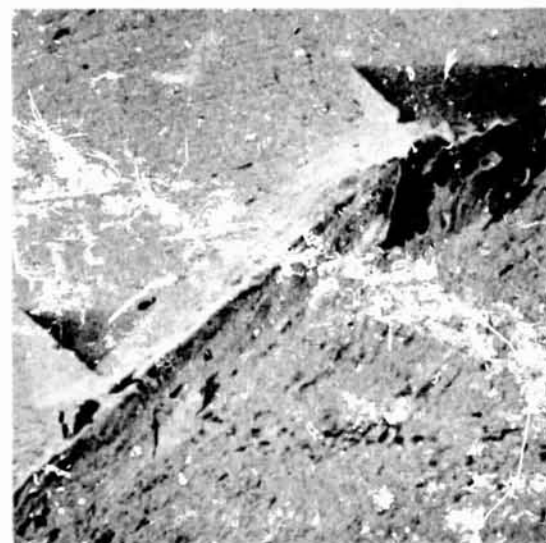
B. BEFORE EXPOSURE

5500X



C. BEFORE EXPOSURE

2100X

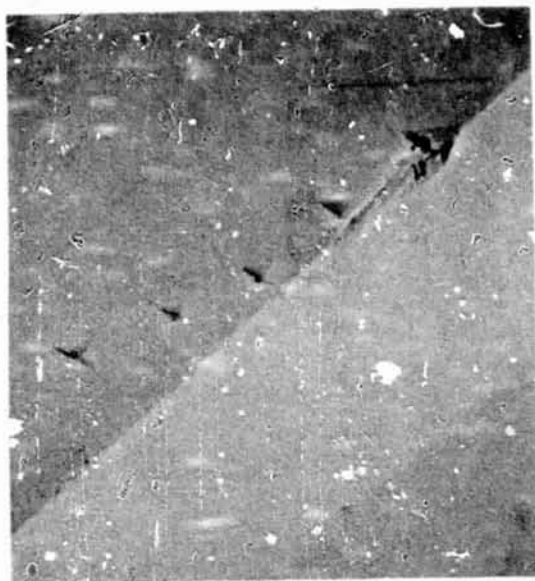


D. AFTER 16 DAYS

2200X

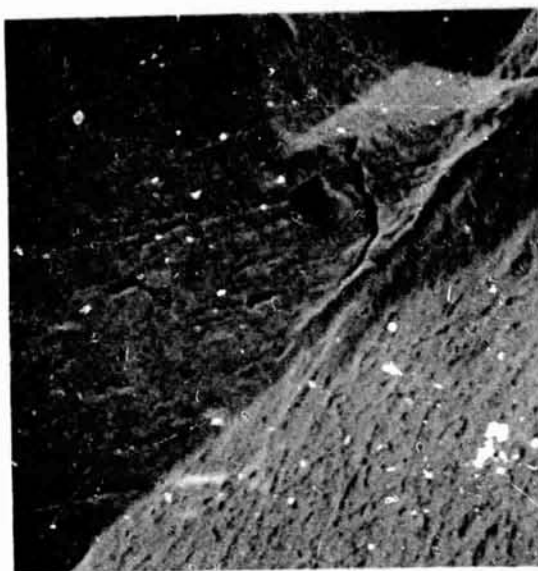
Figure 4-10. Specimen No. 7 Tungsten Carbide, CM-500 (Vapor Deposited)

ORIGINAL PAGE IS
OF POOR QUALITY



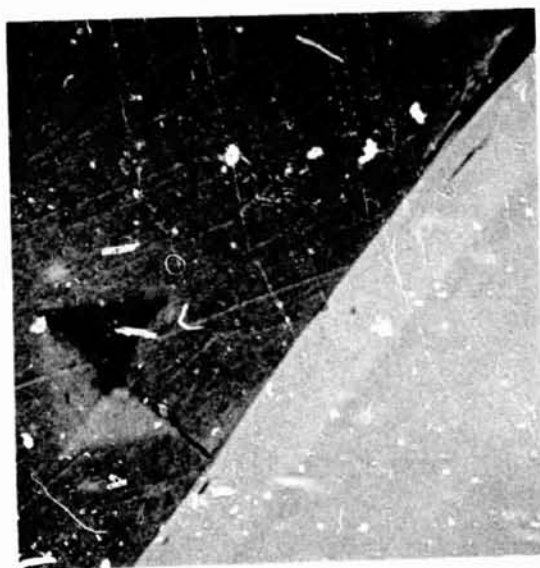
A. AFTER 185 DAYS

550X



B. AFTER 185 DAYS

5500X



C. AFTER 185 DAYS

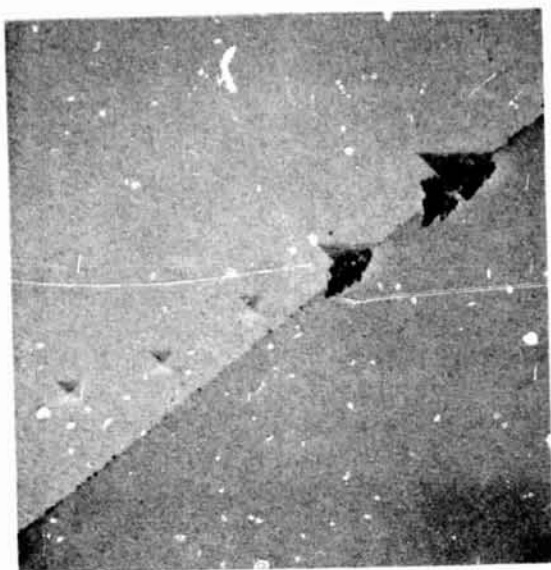
2100X



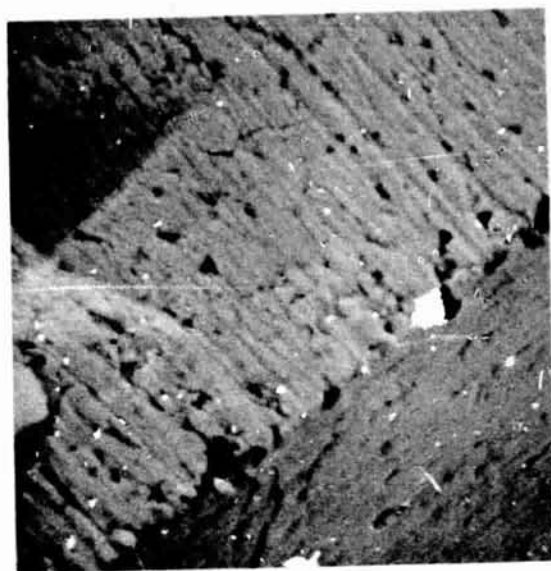
D. AFTER 185 DAYS

2200X

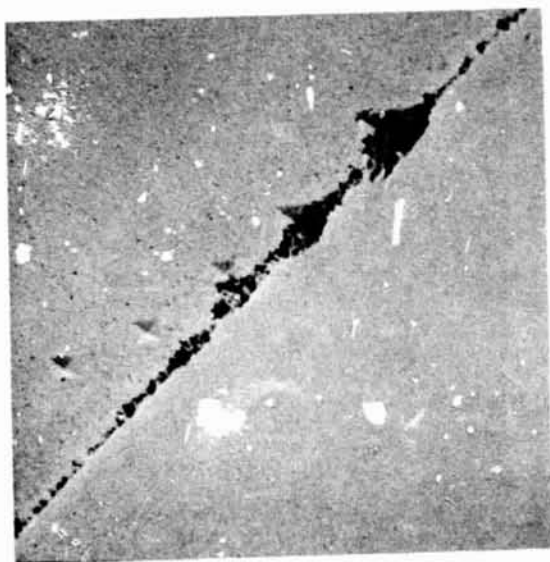
Figure 4-11. Specimen No. 7 Tungsten Carbide, CM-500 (Vapor Deposited)



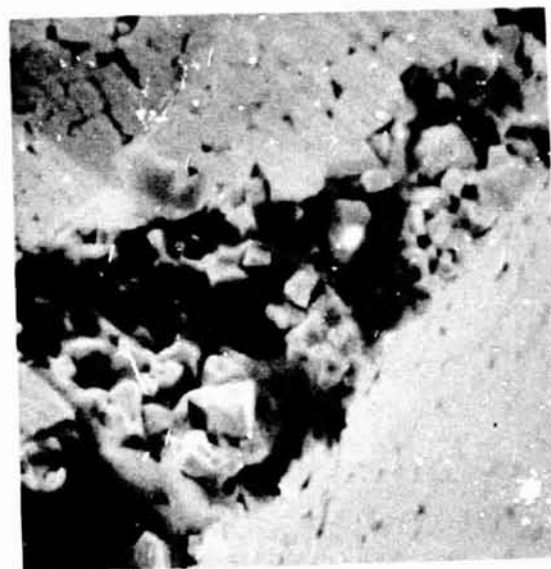
A. BEFORE EXPOSURE 580X



B. BEFORE EXPOSURE 5800X

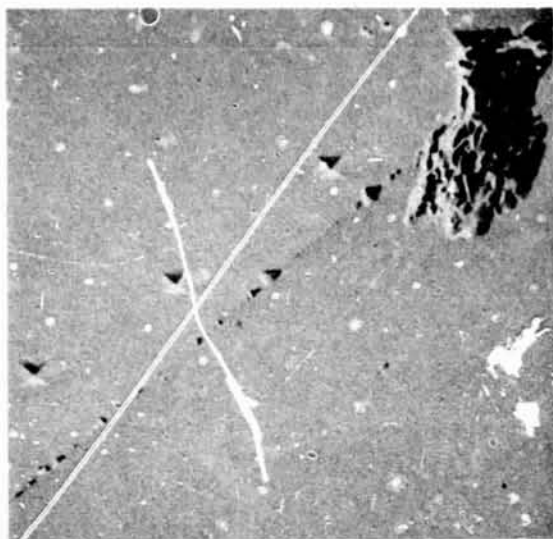


C. AFTER 16 DAYS 575X



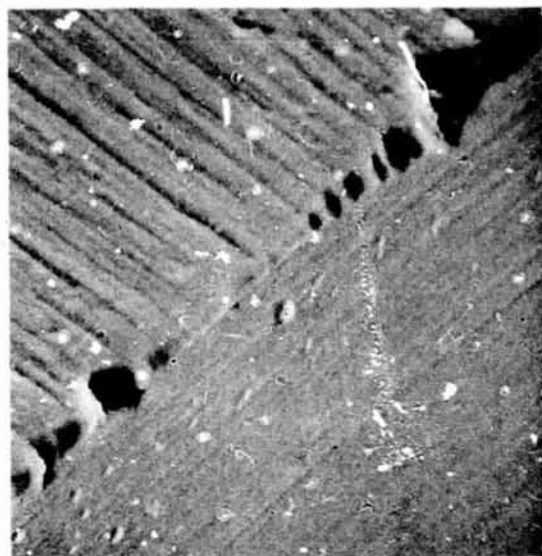
D. AFTER 16 DAYS 5750X

Figure 4-12. Specimen No. 8 Tungsten Carbide, 883 (6% Cobalt)



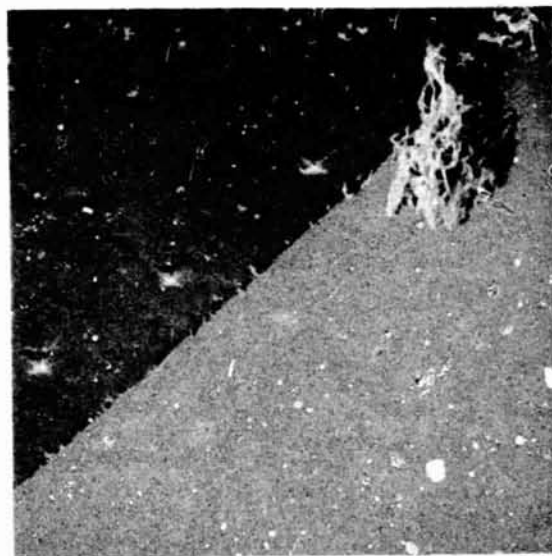
A. AFTER 16 DAYS

600X



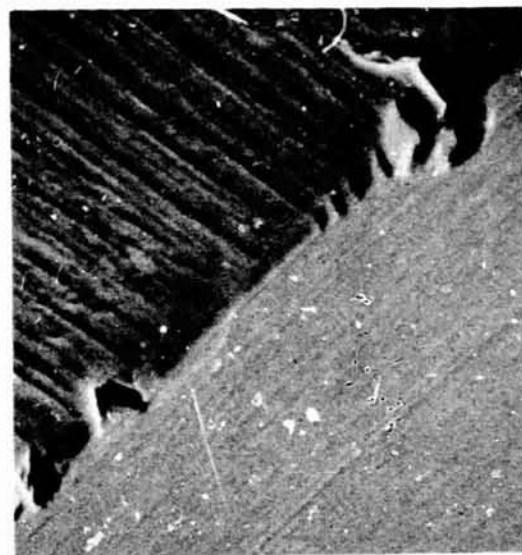
B. AFTER 16 DAYS

6000X



C. AFTER 185 DAYS

600X



D. AFTER 185 DAYS

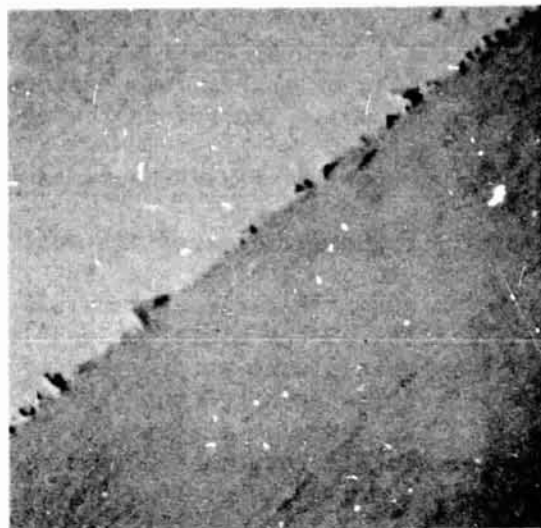
6000X

Figure 4-13. Specimen No. 9 Alumina (Superwearox)



A. BEFORE EXPOSURE

500X



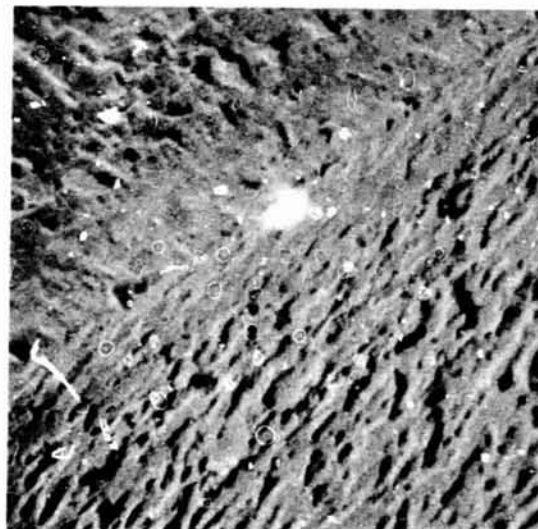
B. BEFORE EXPOSURE

5000X



C. AFTER 185 DAYS

500X



D. AFTER 185 DAYS

5000X

Figure 4-14. Specimen No. 10 Tantalum-Tungsten Carbide (K602)

ORIGINAL PAGE IS
OF POOR QUALITY

Specimen No. 11: Boron Carbide. Like the silicon nitride, boron carbide was of interest because of its extreme hardness and potential compatibility. The material proved virtually impervious to the RFNA exposure, as shown by Fig. 4-15.

Summary of Cutter Material RFNA Exposure Results

In general, the ceramic materials evaluated (sapphire, ruby, silicon nitride, alumina, and boron carbide) were not visibly (5000X) affected by the 1st-day exposure to RFNA. All sintered carbides were severely attacked because of basic incompatibility of the nickel or cobalt binders. However, the carbide crystals in these materials were not visibly affected by the acid. This also was shown by the CM-500 vapor-deposited tungsten carbide. Because of the very low cobalt binder content in the tantalum-tungsten carbide K602 material (1.5 percent), only minor surface etching of less than 20-microinch depth was evident after the 185-day exposure. Furthermore, there was no measurable loss of edge strength or hardness.

As previously noted, the RFNA exposure test is extremely severe. Materials showing degradation may be suitable for N₂O₄ service under certain conditions.

STRUCTURAL MATERIALS

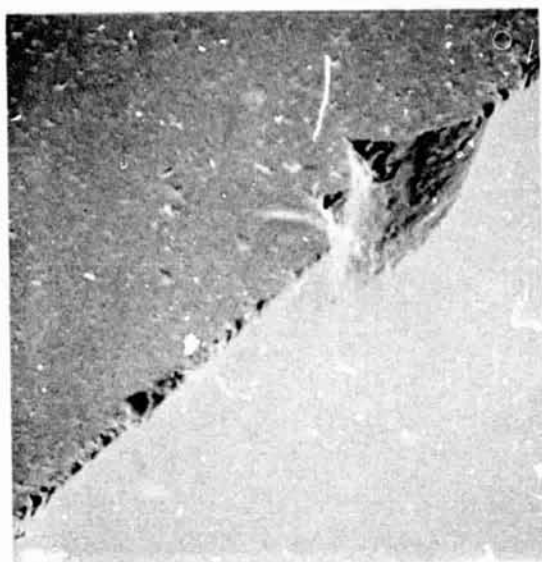
A group of materials that might be used in the prototype valve were selected for RFNA exposure. Sample preparation and testing were essentially like that employed with the cutter materials. The materials chosen were numbered sequentially to follow the eleven cutter materials.

- | | |
|--|--|
| 12. 304L CRES | 15. 17-4PH CRES |
| 13. 440C CRES | 16. Stooddy No. 2 wear-resistant alloy |
| 14. Stooddy No. 1 wear-resistant alloy | 17. Inconel 718 |

Experience during the initial 15-day period with the cutter sample RFNA testing had shown that darkening of the acid was an indication of attack. In a few days it was evident that the 440C was being attacked. After 15 days, the 440C sample was removed and the corrosion had progressed so that the original hardness indentations could not be located. After 70 days, the Stooddy No. 1 alloy was similarly attacked. Thus, each of these materials were eliminated from further consideration.

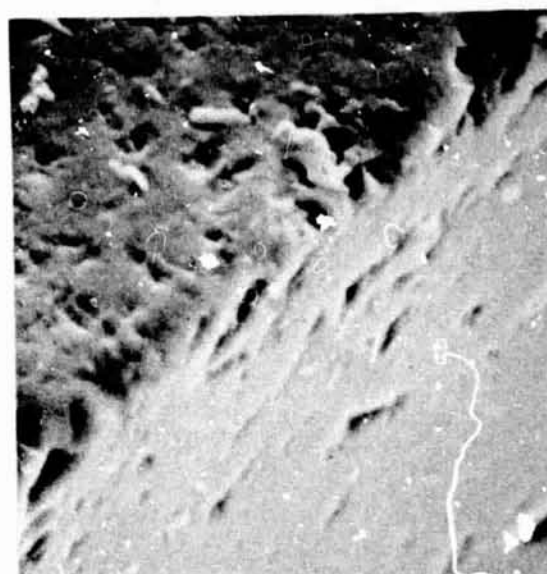
After 118 days of exposure, the remaining four samples were removed for microscopic examination. The 304L and Inconel 718 were darkened, but little attack was evident at 500X. The 17-4PH showed some edge loss, as did the Stooddy No. 2, with carbide grains accented on the surface.

To complete a 169-day period, the same four samples were re-exposed to fresh RFNA. Upon removal, their appearance was essentially unchanged from that observed after 118 days, except for additional attack of the Stooddy No. 2. The samples were then hardness tested and photographed with the SEM. Hardness test results, presented in Table 4-4, show little change on all materials except for Stooddy No. 2, which suffered a softening between carbide grains. The before and after SEM photos (Fig. 4-16 through 4-19) show that all materials suffered material loss and etching of the grain boundaries. The 304L material showed very little evidence of attack, with virtually an unchanged edge continuity (Fig. 4-16). Next choice would be



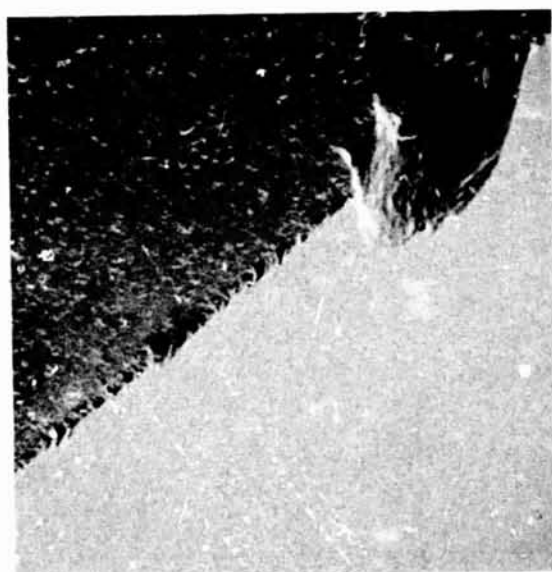
A. BEFORE EXPOSURE

535X



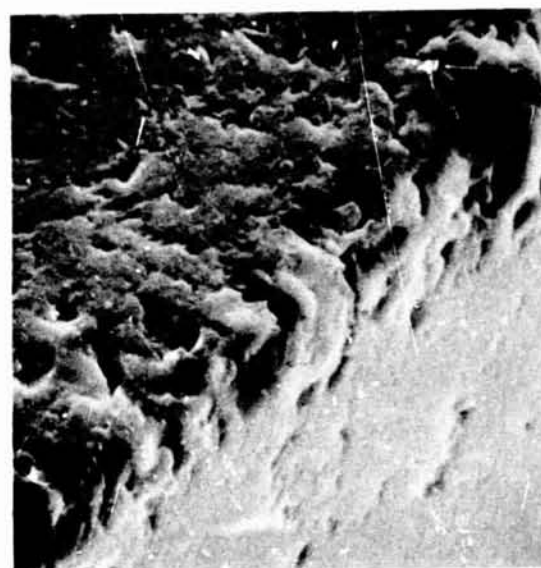
B. BEFORE EXPOSURE

5300X



C. AFTER 185 DAYS

500X



D. AFTER 185 DAYS

5100X

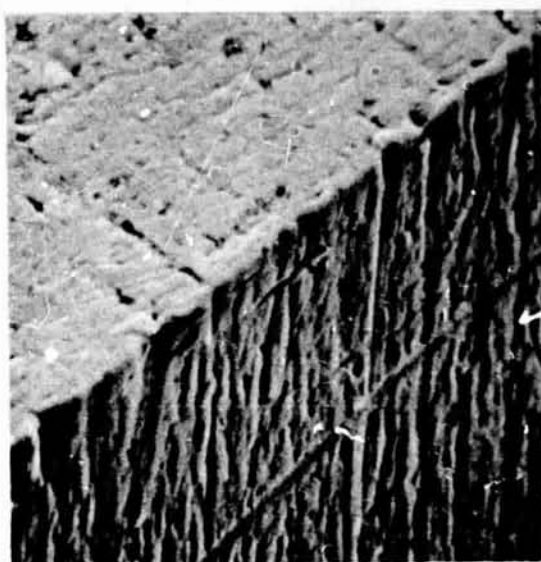
Figure 4-15. Specimen No. 11 Boron Carbide

ORIGINAL PAGE IS
OF POOR QUALITY



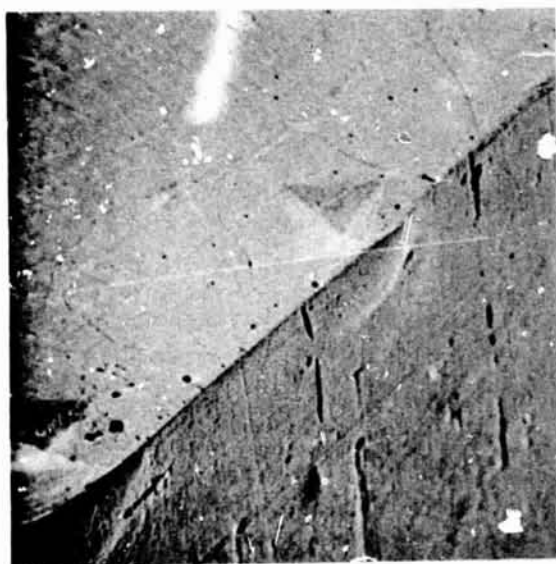
A. BEFORE EXPOSURE

650X



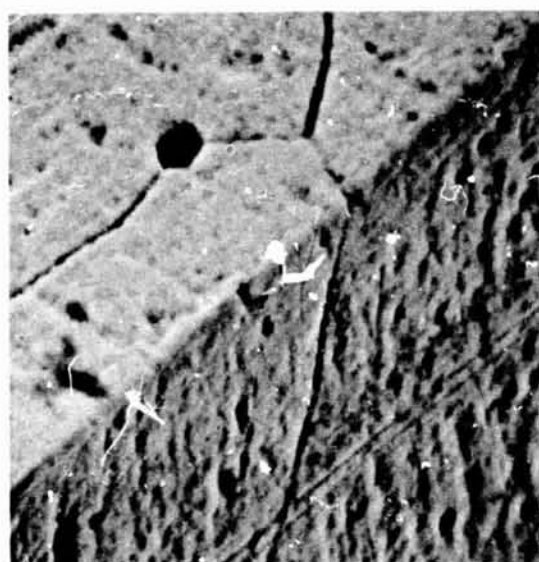
B. BEFORE EXPOSURE

6500X



C. AFTER 169 DAYS

650X



D. AFTER 169 DAYS

6500X

Figure 4-16. Specimen No. 12 304L CRES

Inconel 718 with somewhat more material loss evident by rounding of the sharp edge and softening of the hardness indentation boundaries.

TABLE 4-4. STRUCTURAL MATERIALS HARDNESS TEST DATA

| No. | Specimen Designation | Hardness - Vickers kg/mm ² (Vickers 100-gram Load) | | Edge Fracturability, Distance to Edge, inches, Before Edge Crumbles or Cuts Away | |
|------------------------|----------------------|--|-------------------|--|-------------------|
| | | Pretest | Post-169 Day Test | Pretest | Post-169 Day Test |
| 12 | 304L | 281 | 281 | 0.00041 | 0.00041 |
| 15 | 17-4PH | 464 | 464 | 0.00022 | 0.00027 |
| 16 | Stoody No. 2 | 803 | 409* | 0.00024 | 0.00024 |
| 17 | Inconel 718 | 508 | 508 | 0.00031 | 0.00031 |
| *803 on carbide grains | | | | | |

Both 17-4PH and Stoody No. 2 experienced significant material loss, although the etching shown by Fig. 4-17 and 4-18 is almost undiscernible to the naked eye.

From these photos it would appear that 304L and Inconel 718 would be best choices for use in water-contaminated N₂O₄. It should not be construed from these results that materials seriously affected by RFNA are incompatible with N₂O₄; rather their use requires more extensive testing.

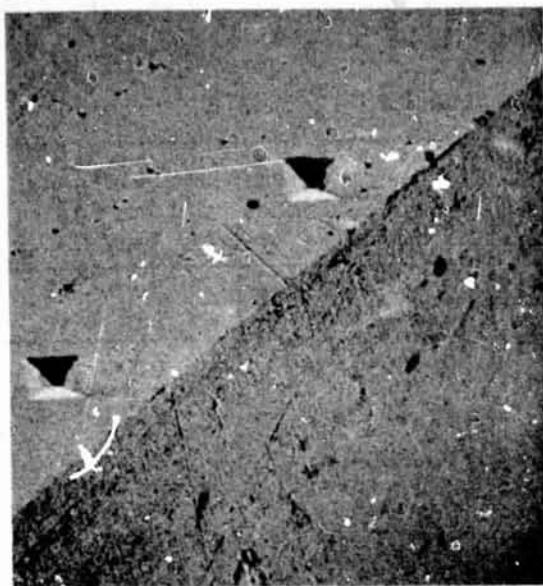
POLYMER MATERIALS

Work with polymer materials consisted of initial investigations to provide means for surface retention and definition of seal fabrication processes. Preliminary program efforts with polymers were based on the work of TRW in material and seal characterization studies (Ref. 5). Early efforts were therefore guided by their recommendation for producing seals and fine surfaces from a highly polished mold. Difficulty was experienced by TRW in molding AF-E-124D perfluoroelastomer with smooth surfaces; therefore, the Air Force Material Lab (AFMC) and DuPont were contacted and they provided interim quantities of the material. This material was not smooth but was used in machining experiments.

After many variations of the basic perfluoroelastomer were evaluated in the first half of the program, it was concluded that AF-E-124D could not be molded with a sufficiently smooth surface. This led to the use of a titanium dioxide white particulate filler* by TRW and subsequent successful molding of a single sheet of material that was flat over approximately 30 percent of the 3-inch diameter.

Details of the various attempts at obtaining material and molding and machining experiments follows.

*Titanox RA41 by N. L. Industries



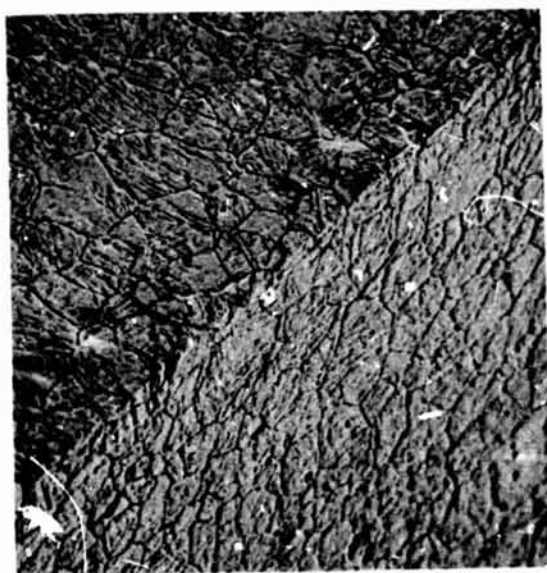
A. BEFORE EXPOSURE

590X



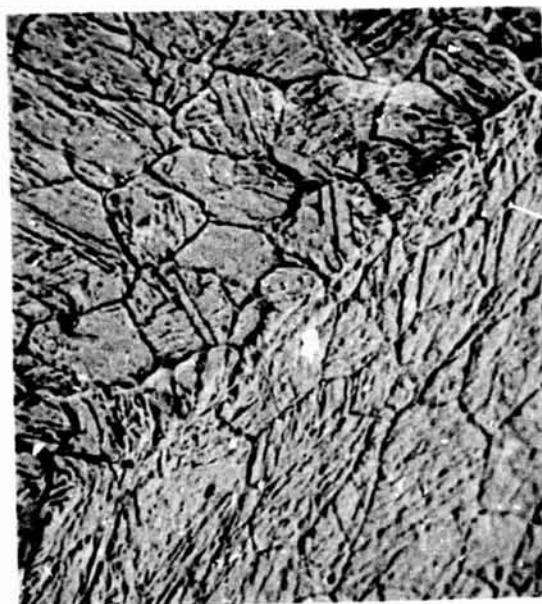
B. BEFORE EXPOSURE

5900X



C. AFTER 169 DAYS

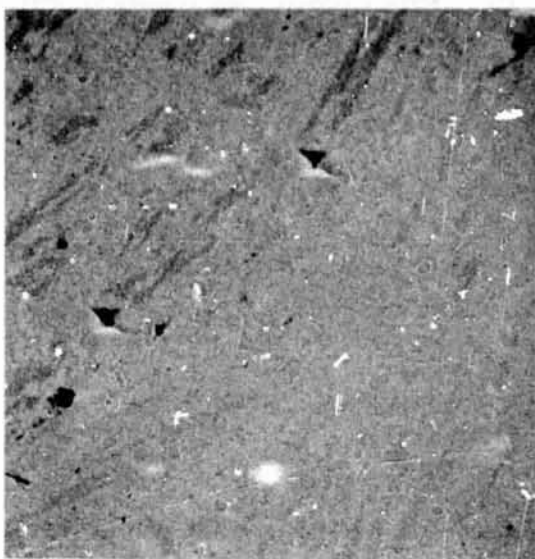
590X



D. AFTER 169 DAYS

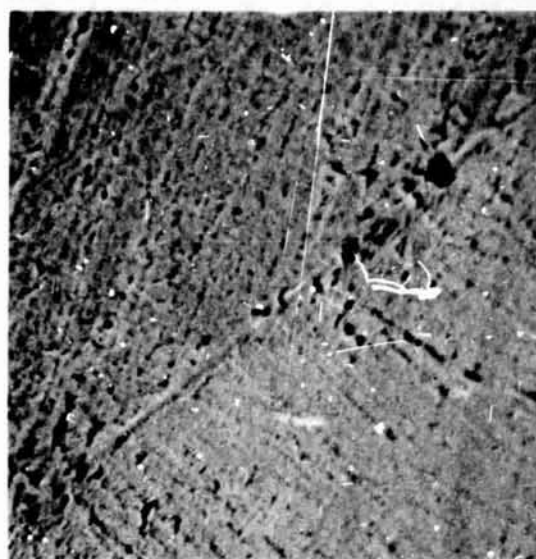
1200X

Figure 4-17. Specimen No. 15 17-4PH CRES



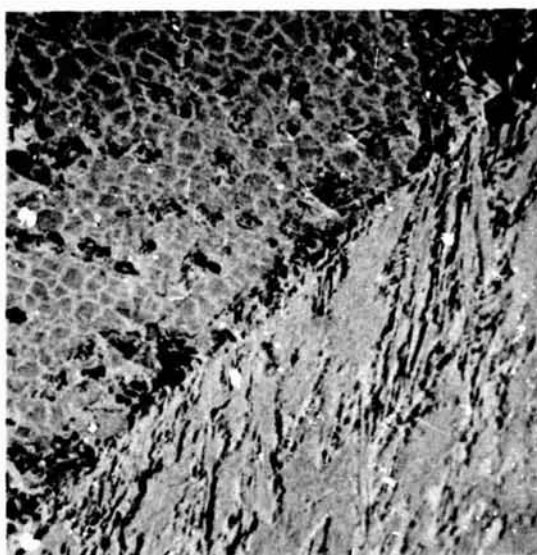
A. BEFORE EXPOSURE

500X



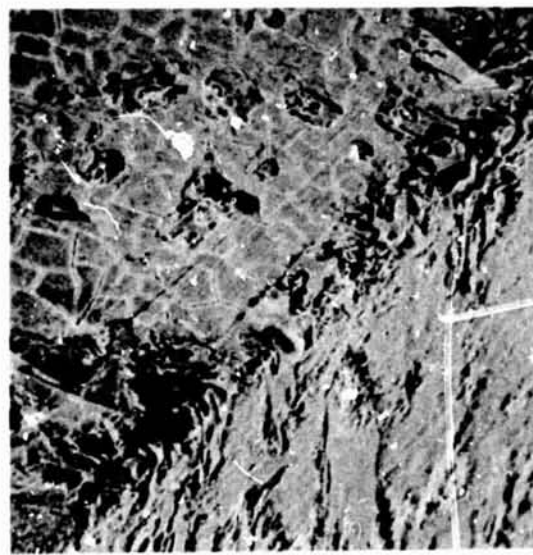
B. BEFORE EXPOSURE

5000X



C. AFTER 169 DAYS

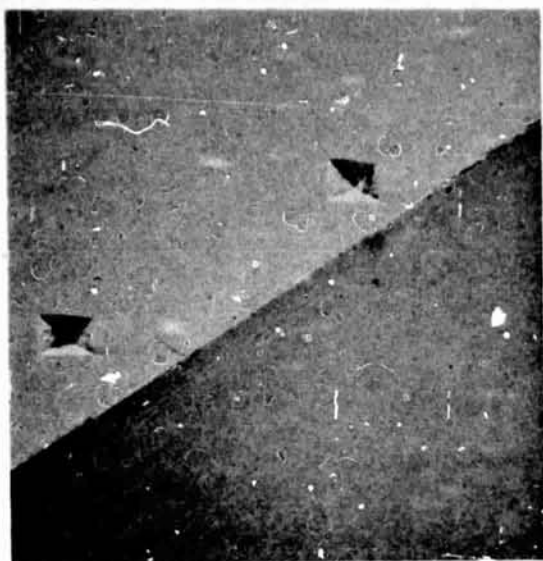
500X



D. AFTER 169 DAYS

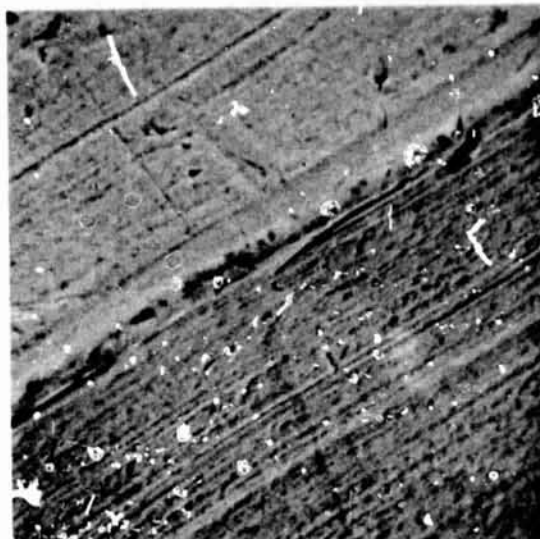
1000X

Figure 4-18. Specimen No. 16 Stoddy No. 2 Alloy



A. BEFORE EXPOSURE

550X



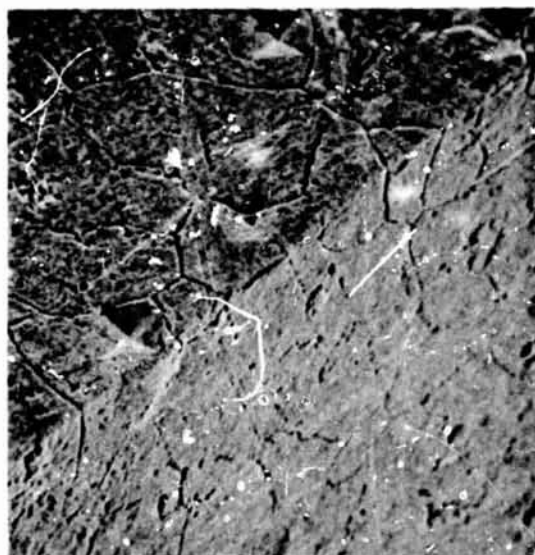
B. BEFORE EXPOSURE

5500X



C. AFTER 169 DAYS

550X



D. AFTER 169 DAYS

1000X

Figure 4-19. Specimen No. 17 Inconel 718

Seal Retention Studies

Earliest effort on the polymer materials (AF-E-124D, AF-E-124X, TFE, FEP) consisted of retention method studies. A flat piece of polymer for the "workhorse" seal concept had been projected, and a means of retaining it on the model was needed. Molding TFE to a backing of 304L sheet using several thousandths inch of FEP as a wetting agent and sealant was considered.

Additional means were evaluated for mechanical retention by creation of a 0.02-inch-deep surface structure composed of re-entrant cavities. Three means considered for this structure were (1) acid etch, (2) machining a "plowed field," and (3) diffusion bonding a 50-percent open area wire screen to the substrate. Review of polymer seal properties emphasized that major design considerations must be given to the large expansion coefficient and compression set of AF-E-124D, as well as the other polymers. Thus, the concept of molding the polymer to a metal base was not pursued in this program due to the large expansion relative to metal, and the high risk of surface disruption at low temperatures.

AF-E-124D Molding Trails

TRW was visited to discuss molding AF-E-124D and to review various sealing concepts. A 3- by 5-inch sample of AF-E-124D material (0.1-inch thick) was presented to Rocketdyne by TRW as an example of their current technology. This material was maple brown and semiopaque. The surface skin was relatively smooth, but extremely rough and wavy and contained numerous black specks which were also visible internally by viewing over a bright light. It was noted that the rough wavy condition resulted from a 5-day postcure at high temperature (Ref. 5) and was typical of the material. The black specks were contaminants carbonized in the postcure process. (This material was ultimately machined for initial seal tests in lieu of acceptable molded material.)

TRW strongly advised the use of an "as-molded" surface compared to a ground surface, and stated that surfaces essentially equal to the mold finish were possible. It was agreed, therefore, that Rocketdyne would prepare a mold die with superfinished surfaces for molding 0.04-inch-thick material. This thickness was selected on the basis that the mold could be easily reworked for a thinner material or, if the polymer surface produced was too rough, 0.01 to 0.02 inch would be available for finishing. During these discussions, TRW noted that their research had indicated that a new proprietary material, designated as AF-E-124X, had properties superior to AF-E-124D, and with better moldability. Procurement of both AF-E-124D and 'X' material was therefore initiated. A standard 4130 steel mold retainer set was obtained and modified to produce a 3.5-inch-diameter sheet. Die surfaces were chrome plated and finished to less than 1 AA. Details of the mold die preparation and finish may be found in Appendix C. The die insert was prepared with a skim for producing either 0.03- or 0.04-inch-thick material based upon TRW's estimate of a 10-percent postcure thickness shrinkage.

With delivery of the mold die, several proof sheets of various polymer materials were molded by TRW with Rocketdyne personnel present. A number of problems were evident from the days effort, which indicated process experimentation would be necessary to ever produce acceptable as-molded surfaces. The AF-E-124D material

exhibited significant OD shrinkage upon release from the hot mold (3.5 to 2.8 inch) which resulted in a 0.038- to 0.040-inch thickness rather than the 0.033-inch die gap dimension, which allowed for 10-percent postcure shrinkage. The surface texture was quite rough, and thickness varied by several thousandths inch. Several trials at molding the AF-E-124X material finally produced a continuous sheet, but the material shrank to a curled, rippled condition with a rough surface. It was apparent that the thinner material presented more problems than the previously molded thicker materials. Moreover, these were uncured sheets, and the required 5-day postcure would likely increase the rippled condition.

Several other materials more easily molded were produced from the die set: NASEAL 411, AF-E-322, and Viton E-60C. The Viton material reproduced both the die surface and thickness, and the surface appeared flawless and shiny. The other materials had flow lines and minor surface ripples.

Shortly after this preliminary work, TRW delivered six sheets of cured AF-E-124D material. All sheets contained numerous black specs and were too rippled and rough for any use. Results of this early experimentation led to the conclusion that surfaces duplicating the die could not be achieved within the schedule restraints of this program, and that some type of machine finishing would be required to produce adequate sealing surfaces.

During the ensuing 3 months, TRW experimented with molding techniques but did not produce any suitable material. Alternate sources and finish methods were investigated during this period. The USAF Material Lab (AFML) at Wright-Patterson was contacted since they served as the program monitors for TRW. The noted 3- by 5-inch sample of AF-E-124D and subsequent 'D' samples furnished by TRW were made from Lot No. 1 of the basic material. According to AFML, Lot No. 1 was quite old and not characteristic of later lots of material. AFML therefore offered to mold two 6- by 6- by 0.075-inch sheets of later "Compound 4" material. During this period, DuPont was also contacted to supply material and it was verified that Lot No. 1 was quite old and of questionable composition. DuPont noted that the basic perfluoroelastomer, ECD006-X, was available in Variants 1, 2, and 3. Variant 3 is designated AF-E-124D by the Air Force, and was chosen by them because of its superior heat resistance compared to other variants. DuPont indicated that Variant 1 would give better mold replication with little (?) loss in compatibility. Samples of ECD006-01 (Variant 1) and ECD006-03 (Variant 3, AF-E-124D) perfluoroelastomer received from DuPont were black, opaque and quite different in appearance than any other material Rocketdyne had received. The AF-E-124D was "prune-like" in finish, while the ECD006-01 was more elastic and had a better (but not usable) mold finish than the Variant 3 material. DuPont revealed that the AFML and TRW material had probably been cured in air, with oxidization taking place during cure to produce the brown color; whereas, DuPont cured its material in an inert atmosphere. Discussions with the DuPont personnel gave a greater insight into the problems associated with this material. Processing of the raw stock, heating, milling, and molding all must be carefully controlled and experimented with to produce a final-cured, good surface finish.

Some 3 months after the initial trials, TRW delivered one 3-inch-diameter, 0.040-inch-thick sheet of AF-E-124X which had a relatively smooth surface finish and was pale yellow and almost clear. Included with the 'X' material was a small, white

titanium dioxide-filled piece of AF-E-124X (0.045-inch thick) which had an excellent molded surface finish. According to TRW, this material was compatible with N_2O_4 , but did not exhibit the high-temperature resistance of AF-E-124D. It was agreed that TRW would pursue molding of the white-filled material in lieu of further efforts with AF-E-124D.

Two samples of AF-E-124D "Compound 4" material were received from AFML. One sample was grossly filled with entrapped air or gas bubbles and, therefore, was useless for any type of seal application. The other sample was somewhat better although it contained multitudinous white specks which appeared by probing (under magnification) to be minute bubble inclusions. Both samples had poor surface finish, not quite "prune like," but very rough.

Continued efforts by TRW led to delivery of a 3.5-inch-diameter, 0.045-inch-thick, molded and postcured slab of the white-filled AF-E-124X. The overall surface finish had a glassy appearance and was on the order of 1 to 2 microinch, but large areas were depressed apparently from gasses trapped in the molding die or from some postcuring action. Approximately 30 percent of the surface area was usable for as-molded seals (Fig. 4-20). At this point in the program, it was decided that to wait in hopes of getting better polymer material would cause severe schedule impact. Thus, it was decided to use the material on hand for the seal fabrication.

Near the program conclusion, TRW delivered two 3.5-inch-diameter sheets of AF-E-124E material about 0.045-inch thick to complete the original order. This material was an off-white shade of tan instead of the previous flat white. It was also notable that some change in the mold/cure cycle had resulted in degradation of the surface finish. Because the material was not used, no further consideration was given to this latest change.

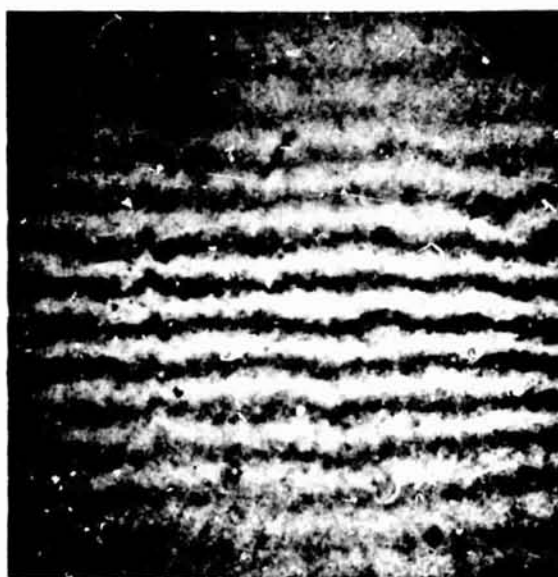


Figure 4-20. Typical Surface Texture of Molded AF-E-124X Filled Elastomer (91X Interference Photo)

Polymer Machining Experiments

The poor surfaces evident from early molding results with AF-E-124D led to investigation of various machining techniques. Rubber grinding was reviewed and it was concluded that such surfaces were too rough. Because the perfluoroelastomer polymer became hard below +20 F, it was considered necessary that seal geometry approach that expected for metal sealing. A process of lapping the AF-E-124D material was attempted using Mylar film impregnated with cutting compound similar to fine sandpaper. The material was stuck to a flat metal plate with double-back tape. The Mylar film was similarly taped to a flat plate and submerged in alcohol and dry ice. Lapping was thereby accomplished at about -20 F. The process proved to be tedious and, similar to lapping soft metals, produced a smooth surface laced with deep scratches.

Search for other methods led to utilization of a high-speed diamond fly-cutting process for producing polymer surfaces flat within 0.0001 inch over a 2.5-inch diameter and with surface finishes of about 2 to 16 AA. Although these surfaces were found to be inadequate for the OMS low-temperature sealing requirement, the process proved excellent for rapid fabrication of flat, parallel seals by flycutting only one side, leaving the opposite glassy molded side for sealing. Details of the tooling and complete seal fabrication process are described in Appendix C.

Teflon Molding Experiments

As the testing progressed, it became apparent that, if the flycut elastomer surfaces were too rough, the TFE and FEP seals would require even smoother surfaces. Attempts to form TFE in the captive seal model, as was done in the SS/APS program (Ref. 4), were unsuccessful for low-load sealing. Several experiments were therefore performed to explore the capabilities of forming flat, parallel, Teflon surfaces. A flat flycut TFE seal of 0.670-inch OD, 0.0300-inch thickness, and parallel within 0.0001 inch was placed inside of a flat-lapped metal washer of 0.0295-inch thickness with about 0.001-inch diametral clearance. Three such assemblies were placed between two polished carbide platens and loaded to 5000 pounds at 340 to 360 F for 2 hours, then allowed to cool slowly under load. High-pressure loading was evident from the Teflon flash at each seal OD. While a glossy surface was produced, the overall seal was wavy by several ten-thousandths inch. The same experiment was repeated with FEP, but at 400 F. Although somewhat better than the TFE, the surface still contained machining lines and was wavy.

A final attempt was made to replicate die surfaces by placing a 3/8-inch-diameter piece of flycut FEP between two flat-face, 3/8-inch-OD, carbide pins contained by a tool-steel cylinder with about 0.0001-inch diametral clearance. The assembly was heavily loaded using a large C-clamp and placed in an oven at 540 F for 2 hours, then allowed to cool under load. The resultant surfaces were glassy smooth and parallel but extremely fragile and easily scratched, even with a cotton swab. Photos of the three molded Teflon surfaces are shown in Fig. 4-21 through 4-23.

These experiments have led to the conclusion that proper utilization of Teflon for seals requires that there be sufficient sealing load to provide a substantial degree of plastic flow for "healing" minute flaws and surface imperfections caused by handling and contaminant entrapments.

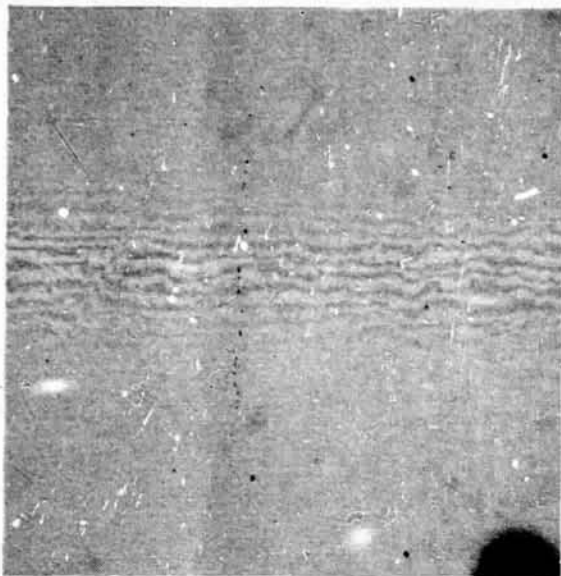


Figure 21. TFE Molded at 350F
(462X Interference
Photo)

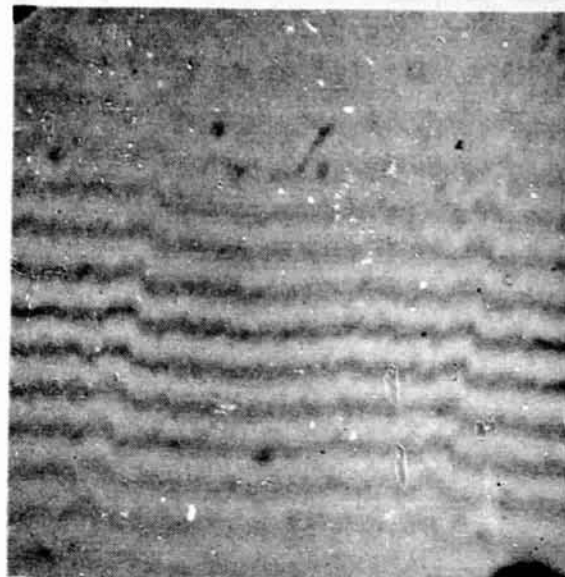


Figure 4-22. FEP Molded at 400F
(462X Interference
Photo)

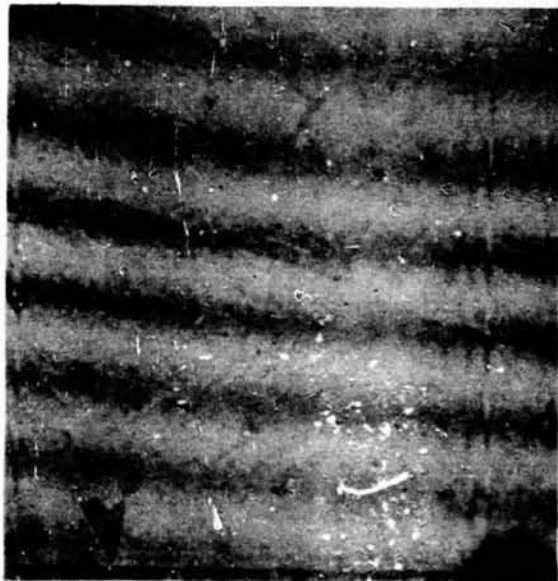


Figure 4-23. FEP Die Molded at 540F
(462X Interference
Photo)

ORIGINAL PAGE IS
OF POOR QUALITY

MODEL SEAL TESTS

The purpose of the model seal tests was to evaluate the critical performance characteristics peculiar to each of three selected model designs: flat cutter seal, flat polymer seal, and captive polymer seal. Propellant compatibility was not a part of the model tests, having been established in the Materials Investigations. Testing was limited, therefore, to static load-leakage tests to evaluate fundamental sealing capabilities, particularly at very low seal loads, on the order of 0.5 pound.

The test approach for each model was tailored to evaluate the most critical parameters that limited functional performance. Thus, the cutter seal, having demonstrated extreme cycle life and low leakage in the SS/APS program, was tested to determine contaminant particle resistance versus land width, using various wires as worst case contaminants.

Polymer seals were characterized for basic room temperature sealing and then evaluated for low-temperature (-15 F) capabilities. The ability of various polymer seals to envelope a 0.001-inch-diameter wire laid across the seal land was also determined for comparison with the cutter seal.

GENERAL APPROACH

The evaluation of each poppet and seat model involved both the test equipment and a sequence of operations and procedures that are reviewed in the following subsections. Detailed description of the SS/APS test fixture, system, and operational procedures are presented in Appendix D.

Test Models

Description and details of the three noted models are presented in the Test Models section. Each model had a mean seat diameter of 0.470 inch. Cutter seal model (100 series) land widths were varied from 0.002 to 0.0002 inch; each width constituted a different model. The perfluoroelastomer and Teflon seals were evaluated in the flat (200 series) and captive (300 series) models, with each different seal given a separate model number. Polymer seal land widths were 0.03 inch.

Test Fixture

The APS test fixture provided the functions of a precision check valve in retaining and positioning the poppet relative to the seat. The closure mode was clam-shell with repeat closures provided within 0.0001 inch. A frictionless hydrostatic piston of 1 in.² area positioned the poppet and was used to augment inlet pressure loading which acted over the nominal 0.17 in.² seat area. Initial closure was detected by a piezoelectric load cell (mounted under the seat) sensing poppet-seat contact within 0.01 pound.

ORIGINAL PAGE IS
OF POOR QUALITY

Test System

The static test system provided pressure supplies and instrumentation for the APS tester. Both inlet pressure and piston loading supplies were double regulated for a low-pressure range of 0.1 to 30 psig and a high-pressure range of 30 to 600 psig with 0.1-percent Heise gage readout. Load cell readings were obtained from an oscilloscope. With this system, on-seat loads were measured with an accuracy of 0.1 pound or 0.5 percent of reading.

All leakage was collected from small bore tubing into either a low-range flow-meter or 1.0 cm³ buret and leveling bulb apparatus. Leakage measurement range was nominally from 10⁻⁴ to 11.0 scim, with an accuracy of 10 percent of reading. The noted small bore tubing on the tester prevented higher leakage measurements because of excessive back pressure (drop) which resulted in unloading the seat.

Inlet Pressure Versus Leakage Tests

Test model performance, with or without contaminants, was determined by a check valve mode of load-leakage testing. Unlike previous programs (Ref. 1 through 4) which used a constant inlet pressure, the seat load was obtained from variable inlet pressure which acted on the poppet over the seat effective area. The position of the poppet under the seat resulted in a negative poppet weight load of 0.088 pound. Thus, a minimum inlet pressure of about 0.5 psig was required to "stick" the poppet to the seat.

The initial test of a new model was considered the control test, and provided baseline data from which sealing performance with entrapped contaminants was evaluated. If test after removal of a contaminant indicated negligible effect, this test provided the control for a subsequent test with an entrapped contaminant.

Contaminant Size and Placement

Single wires were used to simulate a worst case contaminant particle. The cutter seat was evaluated with wire diameters and materials in the following order:

- 0.0004-inch CRES
- 0.001-inch copper
- 0.003-inch copper
- 0.003-inch CRES

For comparison, the polymer seals were evaluated using only the 0.001-inch CRES wire.

For each test, a single short length of wire was placed radially across the poppet land. No adhesive was used for the cutter seals to allow cut or machined pieces to spread unhindered. Wires for the polymer seal tests were cemented to the poppet outside the sealing land.

Test Procedure

The model sealing surfaces were cleaned with benzene or alcohol and blown dry with 0.5-micron filtered helium gas. The poppet and seat then were placed in the tester, and piston control pressure (P_C) was raised to obtain the balance pressure required to just contact the seat (i.e., establish 0.01-pound load). Inlet and control pressures then were sequentially increased (inlet pressure also acted on the piston at the poppet end) until the poppet was stuck to the seat with 1.0-psig inlet pressure, and control pressure was then dropped. Inlet pressure was then raised through a logarithmic sequence of pressures (1.0, 2.0, 5.0, 10.0, 20.0, etc.) to 500 psig, then returned to 0.5 psig. Leakage was measured at each pressure level.

During the juggling of inlet and P_C pressures, the poppet and seat were loaded to somewhere between 0.5 and 0.8 pound. With some entrapped wires, this preload was sufficient to reduce the low-pressure (1.0 psig) leakage level below 1.0 scim. Subsequent increase in inlet pressure then usually resulted in less leakage because reduction of the leakage gap was of greater influence on the leakage level than the increased driving force of inlet pressure.

In cases where the noted 0.8-pound preload was insufficient to reduce 1.0-psig inlet pressure leakage below 1.0 scim, the preload was increased with piston loading (P_C), keeping inlet pressure constant at 1.0 psig. Control pressure was increased until the wire was cut, as indicated by an audible snap with reduction in leakage, or until the leakage level had been reduced to a nominal value of about 0.01 scim. The previously noted sequence of inlet pressures were then applied to obtain the characteristic data.

Cold tests were performed on selected polymer seal models by passing cold gas through the tester cap around the seat. Supplemental cooling was obtained by surrounding the cap with dry ice. All tests were performed with the poppet and seat at -15 ± 5 F, as determined by a thermocouple at the seat. During chardown the poppet was loaded onto the seat with 2.5 pounds force for the cutter seat and 1.0 pound force for the flat seal.

Following the sequence of initial control, wire cutting, or embedment (in polymer seals) and cold test, as applicable, the model was removed from the tester and examined for damage at 500x.

DATA PRESENTATION

Several forms of data presentation are employed in the ensuing discussion of test results. The following describes data format/source and interpretative procedures used in assessing the results.

Inlet Pressure Versus Leakage Plots

The characteristic leakage curves obtained with each model constitute the primary output data. Actual data points are shown and the interconnection of these points represents a best-fit plot of the information. Arrows on the curves indicate the

direction of recorded data. In the case of control data, the plot represents stabilized performance characteristics. Test variations are differentiated by appropriate test numbers, and data symbols as identified on each graph.

Correlated Data

As previously noted, all tests were performed with a negative constant load, the poppet weight. What would the leakage be if a constant positive load of, say, 1.5 pound were applied to the poppet? Of primary importance in analysis of the cutter seal, the answer to this question lies in prediction of an equivalent gap for each test point from the recorded data. Seal load may be accurately computed from the balance of forces acting on the seat (see Appendix D). The equivalent gap is obtained from the equations given in the Leakage Analysis section for laminar/molecular parallel plate flow.

The results of these analyses produce a characteristic load versus gap plot which allows prediction of leakage at other than the test pressure conditions. As will be seen, these analyses and plots are used to extrapolate the raw data for an overall correlation of cutter seal land width versus load and leakage. Verification of the analysis was demonstrated in test of a specific cutter model (105).

Model Inspection and Performance Data

Overview of the tests performed with each basic model is provided by a tabulation of tests preceding each model subsection. Listed are the model number, test number, seal data, test condition, and reduced performance data for ready comparison between models. Model inspection data are provided by plain and interference photographs of sealing surfaces and measurements of critical seal features.

Concluding each model subsection is an analysis of the test results, analytical correlations, and observations leading to design criteria.

CUTTER MODEL TESTS

A series of wire cutting tests was performed to establish the optimum land width for the cutter seal. The test models and summary of results are listed in Table 5-1

Models 101 and 102 constituted the two poppets and seats available from the APS program. Models 101 and 102 were tested first with 0.003-inch-diameter CRES wires. Poor performance with Model 102 and the resultant groove across the land indicated excessive width, so further tests were discontinued and the seal was reworked to become Model 104. Similarly, Model 101 became 103 and then correlation Model 105.

As shown in Table 5-1, Models 101, 103, and 104 were tested sequentially with a series of wire sizes which increased in size and hardness. This technique was employed so that the posttest results of a given test could be used as control for a subsequent test. With the wider lands and CRES wires, a permanent impression was made on the land which caused an increase in high-pressure leakage.

TABLE 5-1. CUTTER MODEL TESTS

| MODEL NO. (LAND WIDTH, IN.) | TEST NO. | TEST CONDITION C = CLEAN XXX = WIRE DIA, IN. S = CRES Cu = COPPER | LEAKAGE SCIM HELIUM AT 10.0 PSID, EQUIV. TO 1.65 LB INITIAL SEAT LOAD | CLOSURE LOAD (LB.) REQ'D TO REDUCE LEAKAGE TO ≤0.01 SCIM HELIUM @ 1.0 PSID | |
|-----------------------------------|-------------|--|--|--|---|
| | | | | INITIAL LOADING | AFTER PRESS. TO 500 PSID, EQUIV. TO 87 LB |
| 101 (0.00054) | 1 | C | 0.00027 | <0.1 | <0.1 |
| | 2 | 0.0004-S | 0.011 | 1.2 (1) | 0.6 (1) |
| | 3 | C | 0.00027 | <0.1 | <0.1 |
| | 4 | 0.001-Cu | 0.020 | 1.1 (1) | 0.5 (1) |
| | 5 | C | 0.00027 | <0.1 | <0.1 |
| | 6 | 0.003-Cu | 0.012 | 1.5 (2) | 0.4 (1) |
| | 7 | C | 0.00040 | <0.1 | <0.1 |
| | 8 | 0.001-S | 1.4 (1) | 2.7 (2) | <0.2 (1) |
| | 9 | C | 0.0011 | <0.1 | <0.1 |
| | 10 | 0.003-S | >10. | 4.6 (2) | ~0.1 (1) |
| | 11 | C | 0.0040 | <0.1 | <0.1 |
| 102 (0.0022) | 1 | C | 0.0020 | <0.1 | <0.1 |
| | 2 | 0.003-S | >>10. | >87. (2) | >87. |
| | 3 | C | 0.0050 | <0.1 | <0.1 |
| 103 (0.00016- 0.0002) | 1 | C | 0.0019 | <0.1 | <0.1 |
| | 2 | 0.0004-S | 0.0014 | <0.7 | <0.1 |
| | 3 | C | 0.0037 | <0.1 | <0.1 |
| | 4 | 0.001-Cu | 0.0032 | <0.7 | <0.1 |

- (1) Data obtained from correlation analysis
(2) Data obtained from preloading test with $P_1 = 1.0$ psid
(3) Noted wires cut, all others mashed

ORIGINAL PAGE IS
OF POOR QUALITY

TABLE 5-1. (Concluded)

| MODEL NO. (LAND WIDTH, IN.) | TEST NO. | TEST CONDITION | LEAKAGE SCIM HELIUM | CLOSURE LOAD (LB.) REQ'D TO REDUCE LEAKAGE TO ≤0.01 SCIM HELIUM @ 1.0 PSID | |
|--------------------------------------|-------------|-------------------|------------------------|--|---|
| | | | | INITIAL LOADING | AFTER PRESS. TO 500 PSID, EQUIV. TO 87 LB |
| 103 (Cont'd) (0.00016- 0.0002) | 5 | C | 0.0026 | <0.1 | <0.1 |
| | 6 | 0.003-Cu | 0.0032 | 1.3 (2) (3) | <0.1 |
| | 7 | C | 0.0026 | <0.1 | <0.1 |
| | 8 | 0.001-S | 0.0018 | 0.82 (2) (3) | <0.1 |
| | 9 | C | 0.0021 | <0.1 | <0.1 |
| | 10 | 0.003-S | >10. | 3.9 (2) (3) | <0.1 |
| | 11 | C | 0.00068 | <0.1 | <0.1 |
| | 1 | C | 0.0021 | <0.1 | <0.1 |
| | 2 | 0.0004-S | 0.16 | 2.3 (1) | 1.4 (1) |
| | 3 | C | 0.0040 | <0.1 | <0.1 |
| | 4 | 0.001-Cu | 1.4 | 3.9 (1) | 2.0 (1) |
| 104 (0.0012) | 5 | C | 0.0086 | <0.1 | <0.1 |
| | 6 | 0.003-Cu | 9.4 (1) | 5.0 (1) | 3.0 (1) |
| | 7 | C | 0.0018 | <0.1 | <0.1 |
| | 8 | 0.001-S | >10. | 12. (2) | --- |
| | 9 | C | 0.0035 | <0.1 | <0.1 |
| | 10 | 0.003-S | >10. | 15. (2) | --- |
| | 11 | C | 0.0030 | <0.1 | <0.1 |

This effect was, however, usually minor compared with the subsequent test with a larger wire, and thus, performance change could be assessed.

Also included in Table 5-1 are leakage and closure load data extracted from the test plots. The leakage data are taken at 10 psid, which produced a sealing load of 1.65 pounds or comparable with that expected for the OMS check valve. Similarly, the closure load required to reduce leakage to the OMS requirement at a 1.0-psid pressure drop is tabulated to show the relative difference between land widths in required sealing load.

It is notable in the cutter tests that only three wires were cleanly cut, and these only by Model 103 with 0.0002-inch-wide land. The cut wires (noted in Table 5-1) were the 0.001-inch CRES, and both 0.003-inch copper and CRES wires. Microscopic observation showed that tensile forces literally broke these wires apart before an entrapment was made. In all other cases, including the 0.0004-inch CRES and 0.001-inch copper wires with 0.0002-inch wide land, the wire was only partially cut and a mashed entrapment was produced by the test. This entrapment usually caused a significant increase in leakage except with the 0.0002-inch land.

Cutter Model 101 With 0.00054-Inch Land

Test and theoretically correlated data for cutter Model 101 with 0.00054-inch-wide land are displayed in Fig. 5-1 through 5-13. Supporting photographic data showing cut wires and sealing land depressions are covered in Fig. 5-14 through 5-21.

Initial control data and test results with a 0.0004-inch-diameter CRES wire are shown in Fig. 5-1. The characteristic shape of these curves is caused by the simultaneous changing of both gap and inlet pressure. The effect of the previously noted 0.5- to 0.8-pound preload is seen in Test 2 by an increase in leakage up to about 0.5 pound (about 3 psid). If the test had been performed without preload, leakage would have gradually decreased from a relatively high rate to intersect with the curve values shown at about 3 to 4 psid. Reversal in the leak curve above 40 psid is caused by a relative decrease in gap reduction combined with increasingly greater effective pressure driving force at higher pressure drops. This effect is better illustrated by Fig. 5-2 and 5-3, presenting computed seat gap versus seat load. As shown, the gap decreases, more or less smoothly with increasing pressure-derived seat load. The preload effect is indicated in Fig. 5-3 by the small change in seat gap at loads below 0.5 pound.

Not the 10/1 difference in gap scales in Fig. 5-2 and 5-3 which show that there is little significant gap reduction above about 5 to 10 pounds seat load with the entrapped wire, but an effective gap less than 1.0 microinch for the clean control condition.

Application of the correlated data is shown by Fig. 5-4 in which 1.0-psid helium leakage is predicted versus seat load from the seat gap data of Fig. 5-3. As initially performed (Test 2), about 10 psid, corresponding to about 1.7 pounds

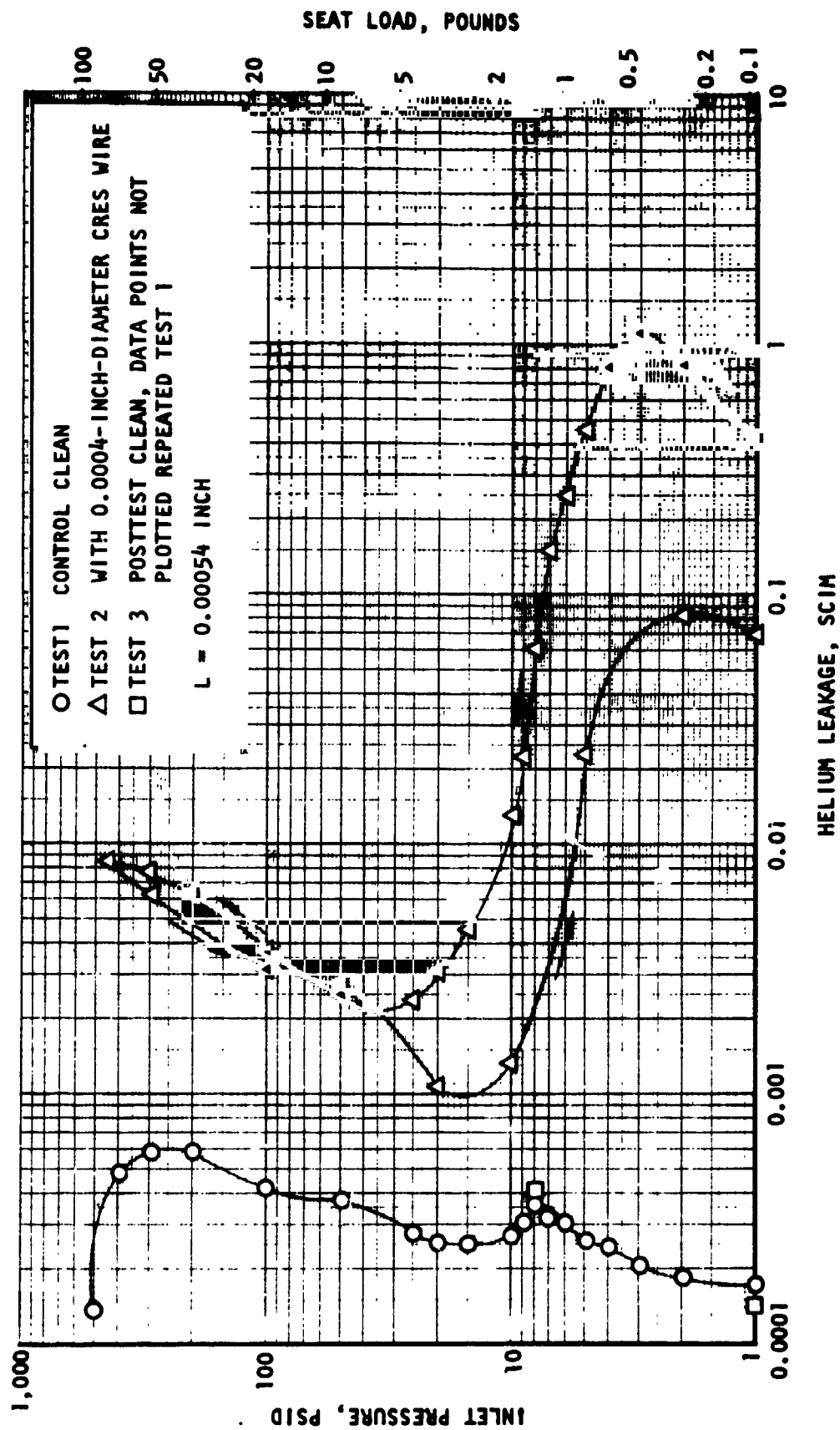


Figure 5-1. Leakage Data for Model 101, Test No. 1 Through 3

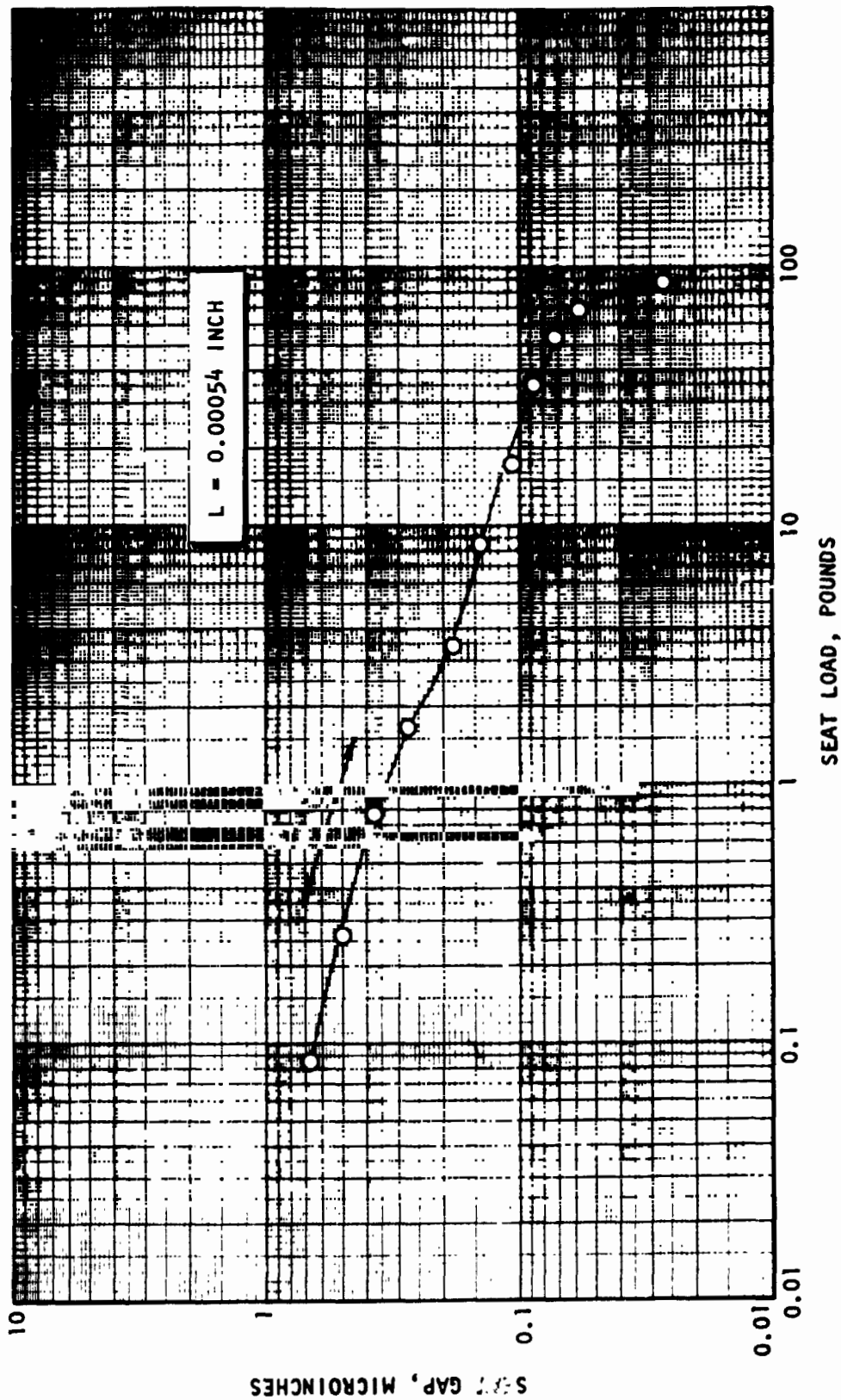


Figure 5-2. Model 101 Computed Seat Gap, Test No. 1 (Clean)

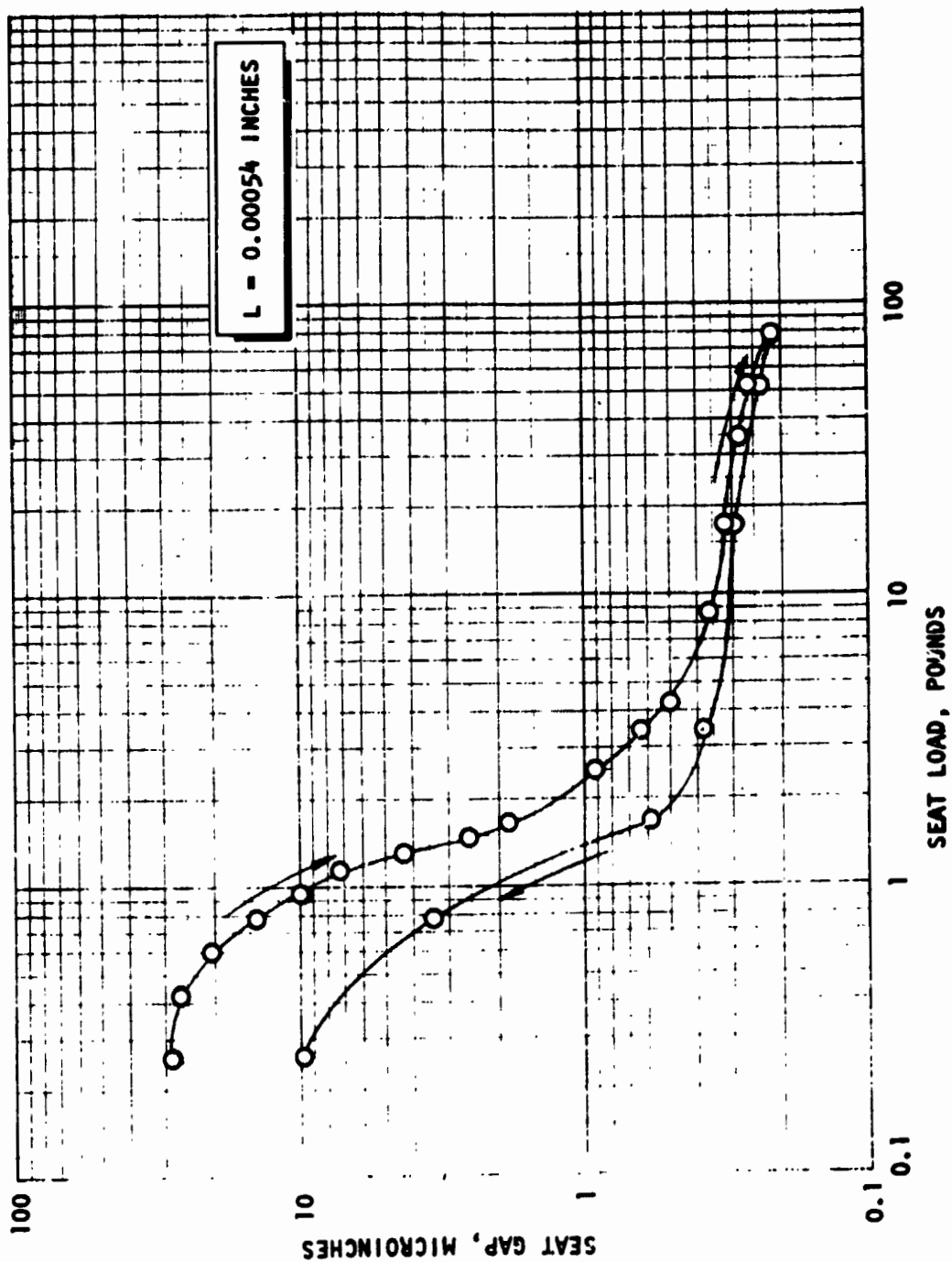


Figure 5-3. Model 101 Computed Seat Gap, Test No. 2 (0.0004 Inch CRES Wire)

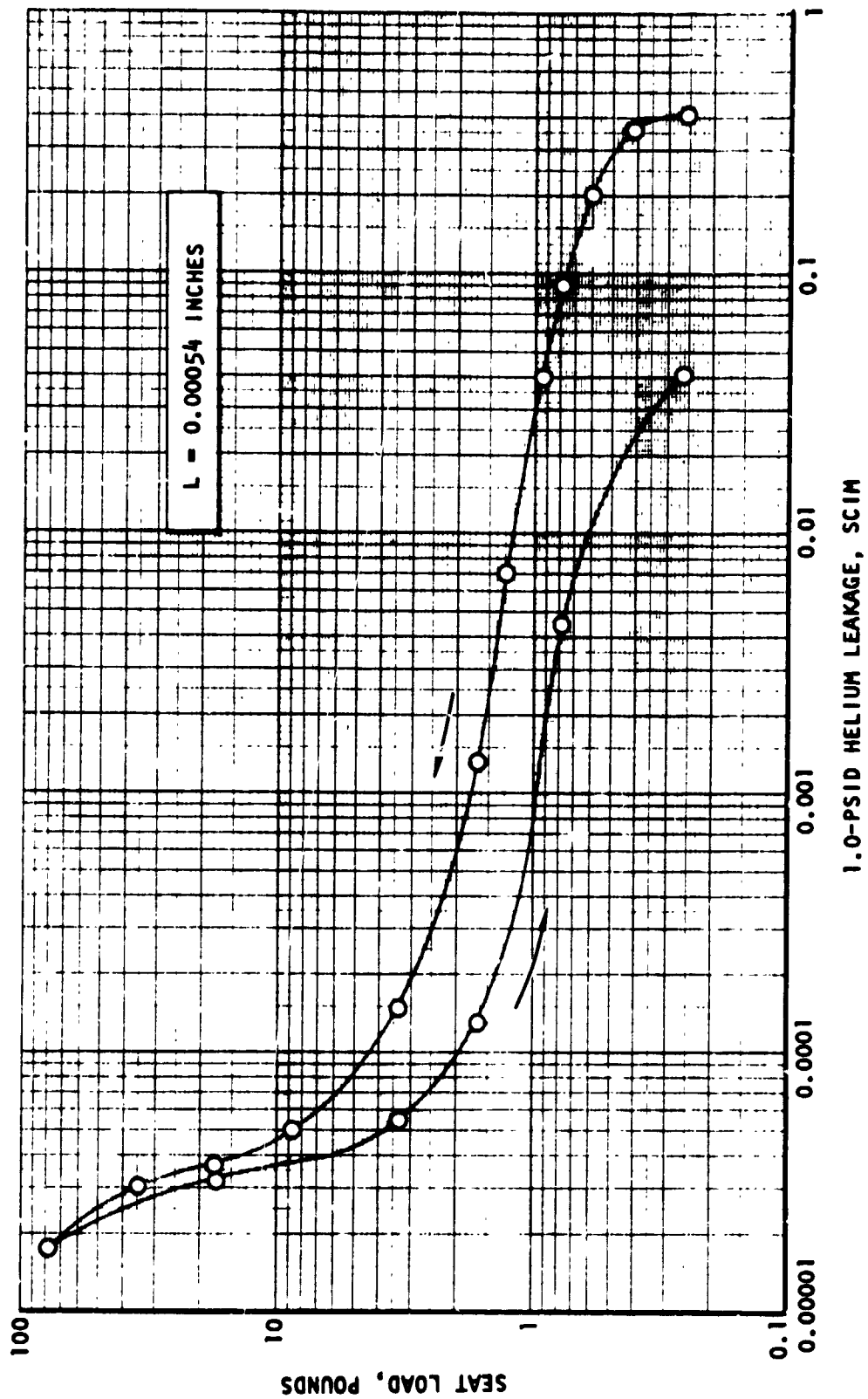


Figure 5-4. Model 101 Computed Leakage, Test No. 2 (0.0004 CRES Wire)

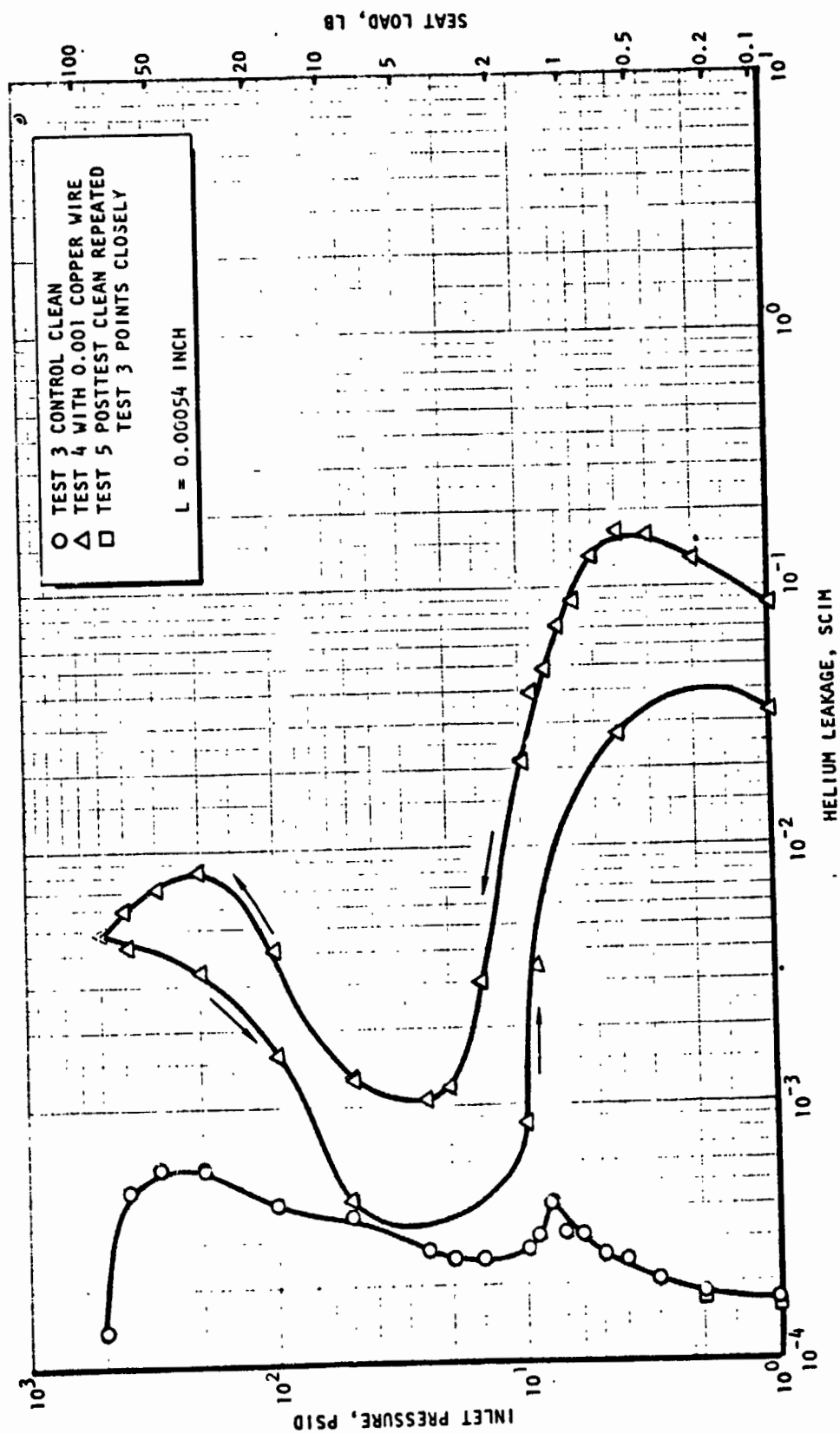


Figure 5-5. Leakage Data for Model 101, Tests 3 through 5

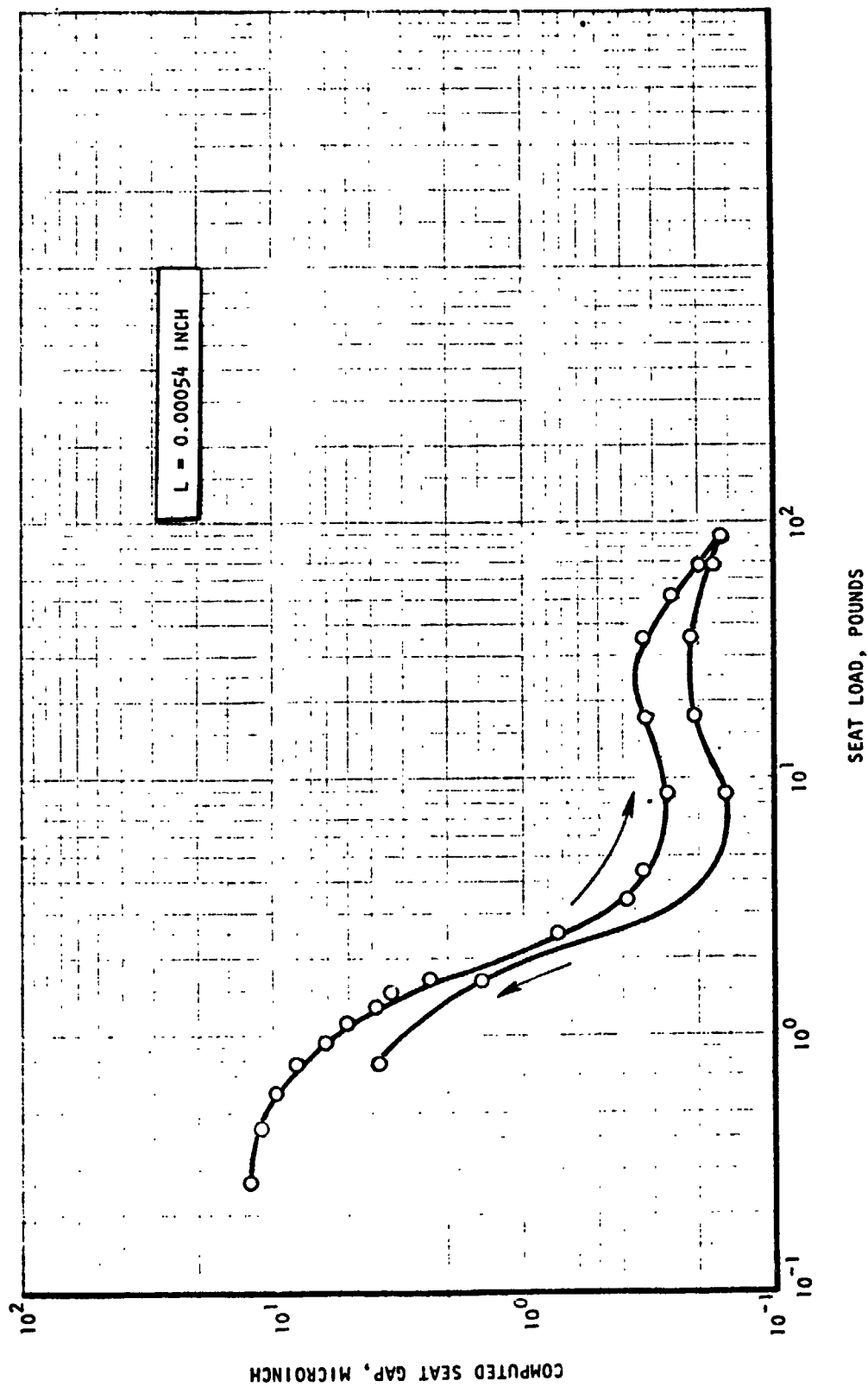


Figure 5-6. Model 101 Seat Gap, Test 4 (0.001 Copper Wire)

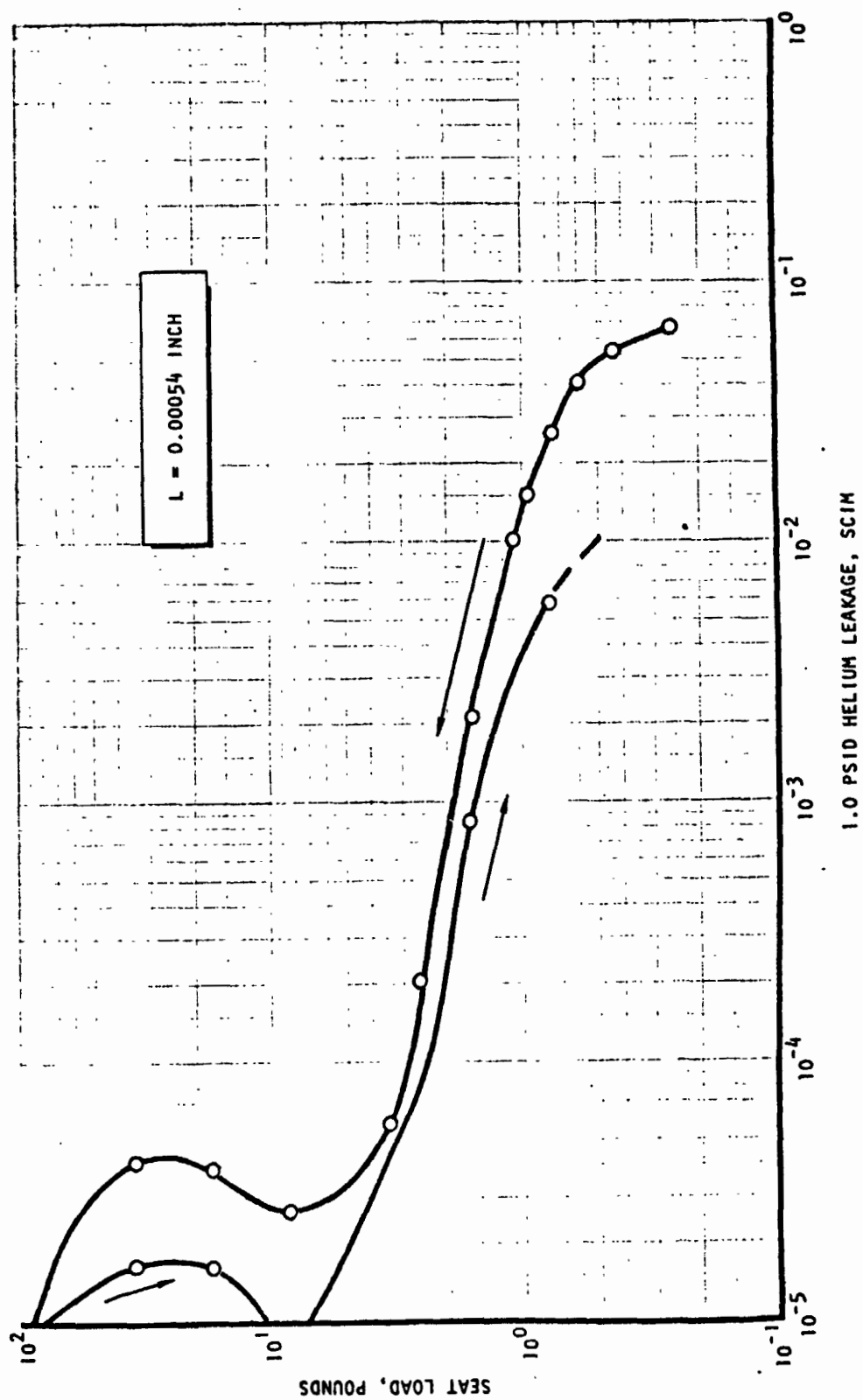


Figure 5-7. Model 101 Computed Leakage, Test 4 (0.001 Inch Copper Wire)

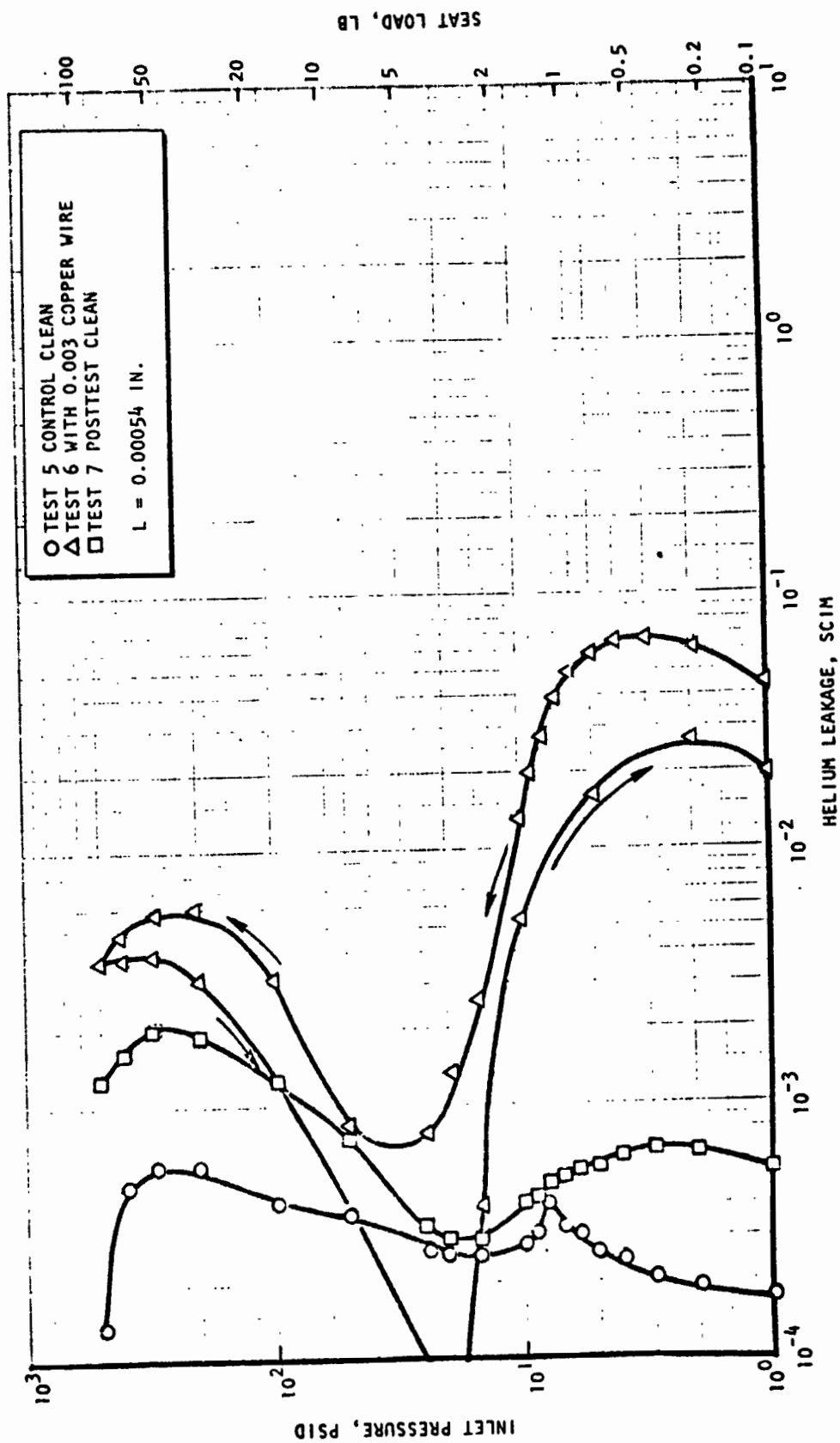


Figure 5-8. Leakage Data for Model 101, Tests 5 through 7

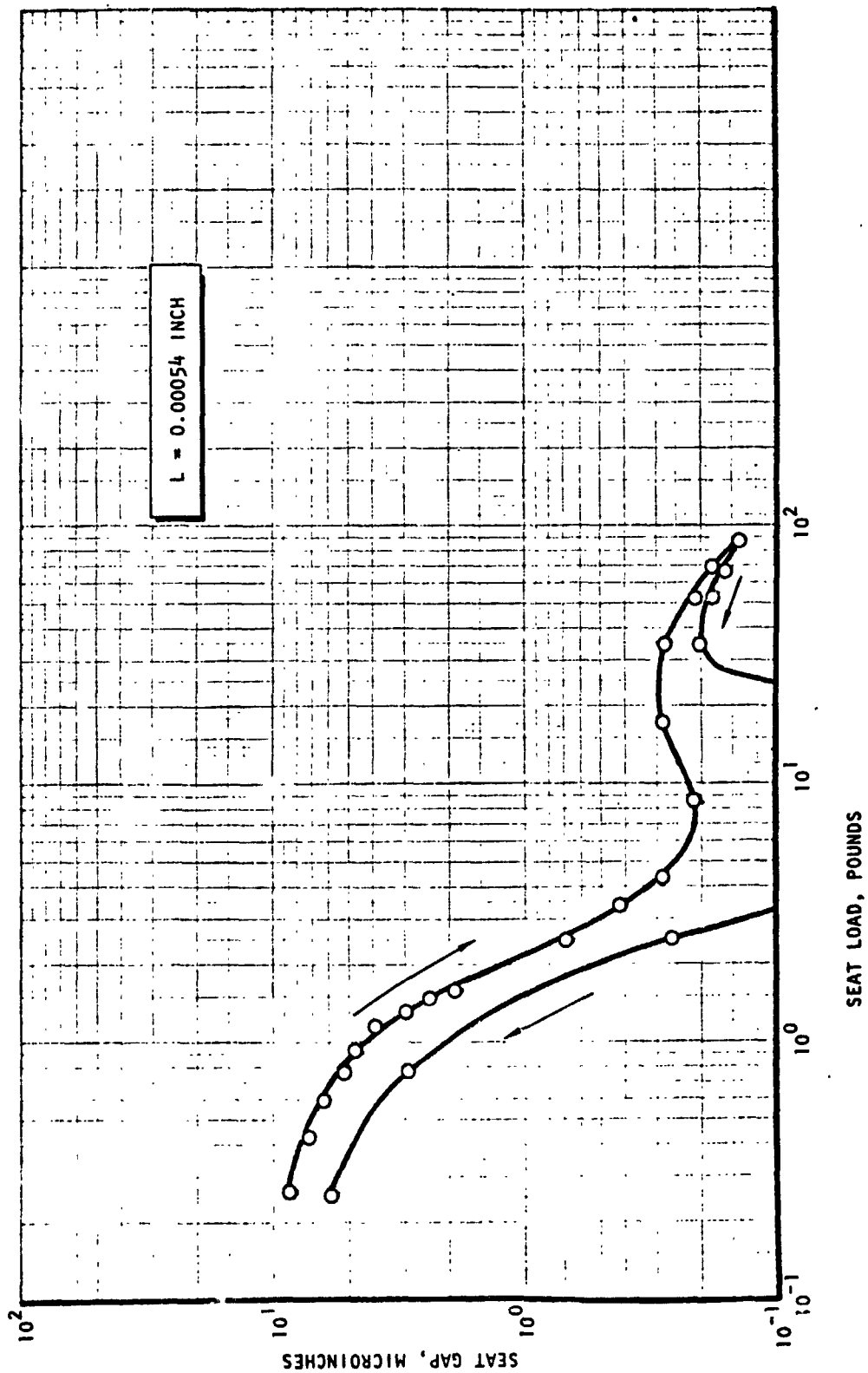


Figure 5-9. Model 101 Computed Seat Gap, Test 6 (0.003 inch copper wire)

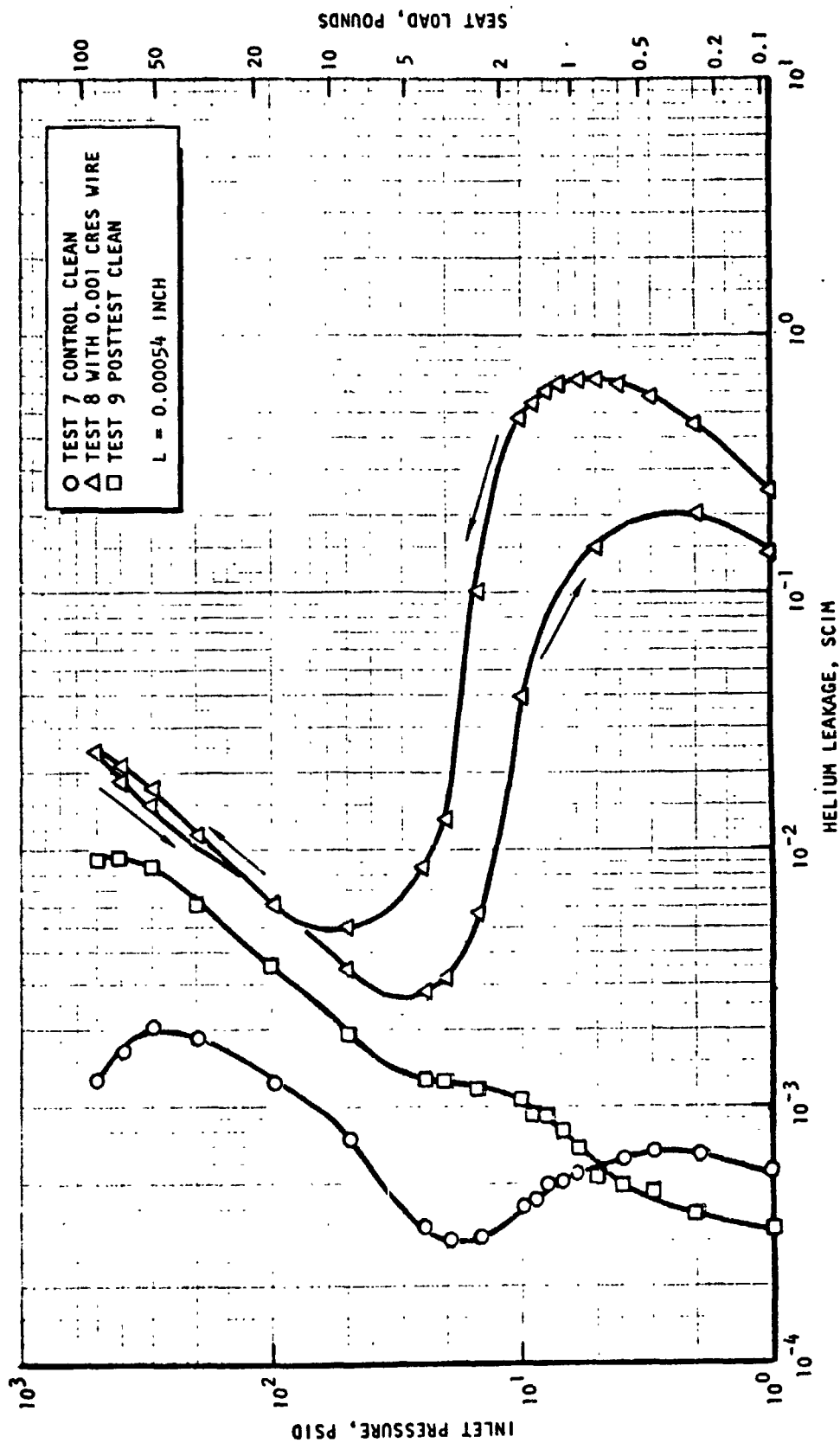


Figure 5-10. Leakage Data for Model 101, Tests 7 through 9

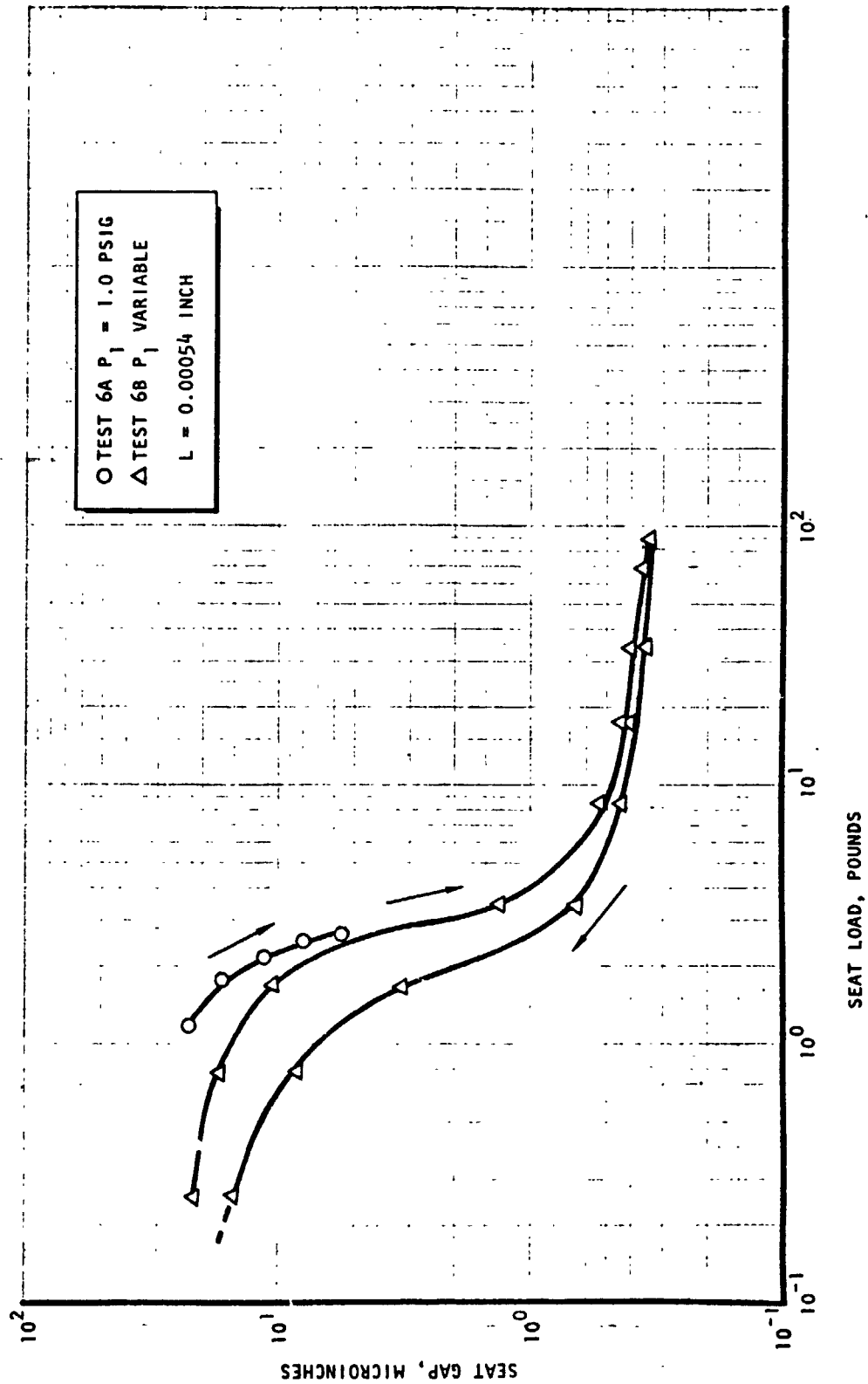


Figure 5-11. Model 101 Computed Seat Gap, Test 8 (0.001 inch CRES wire)

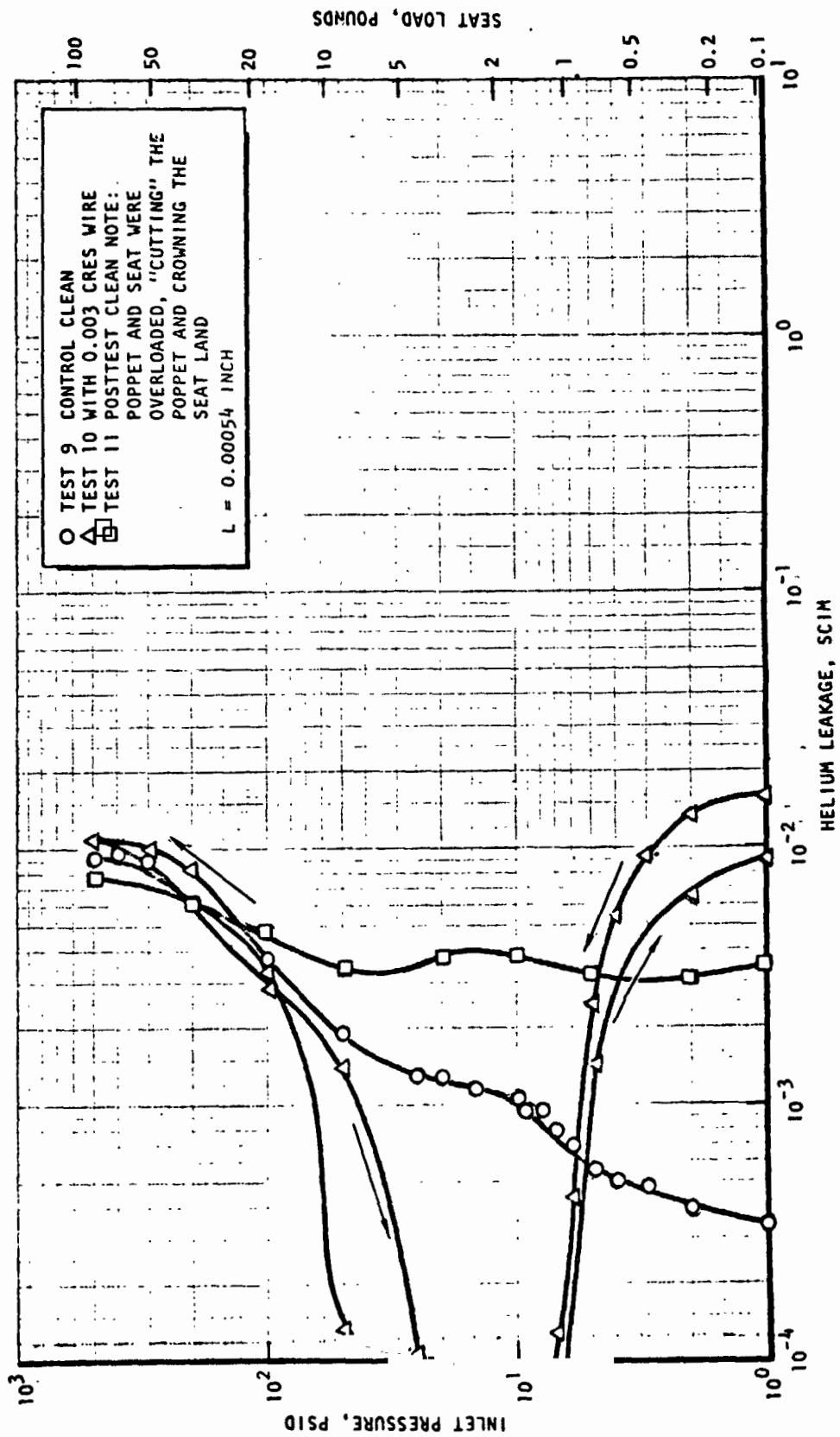


Figure 5-12. Leakage Data for Model 101, Tests 9 through 11

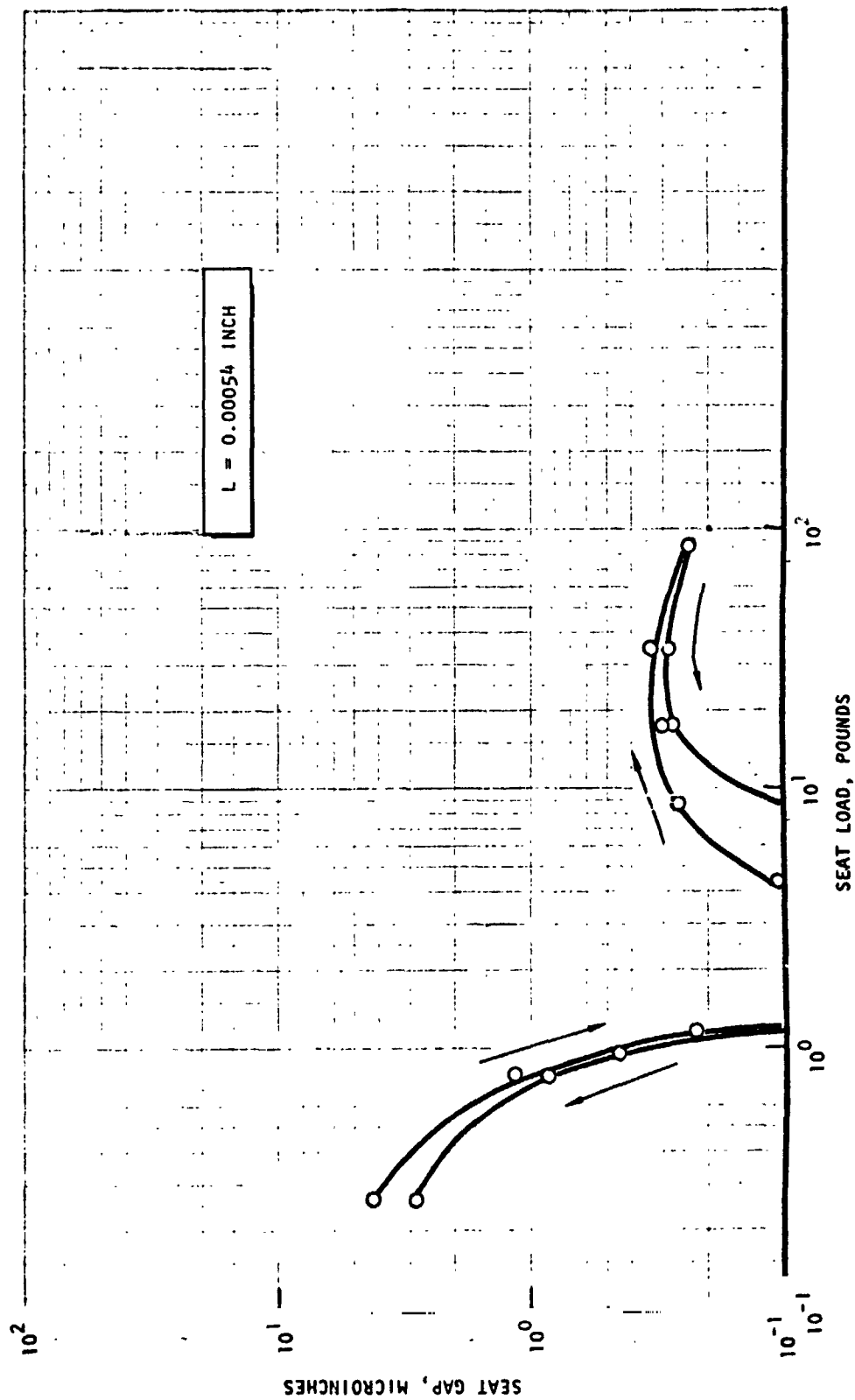


Figure 5-13. Computed Seat Gap, Test 10 (0.003 inch CRES wire)

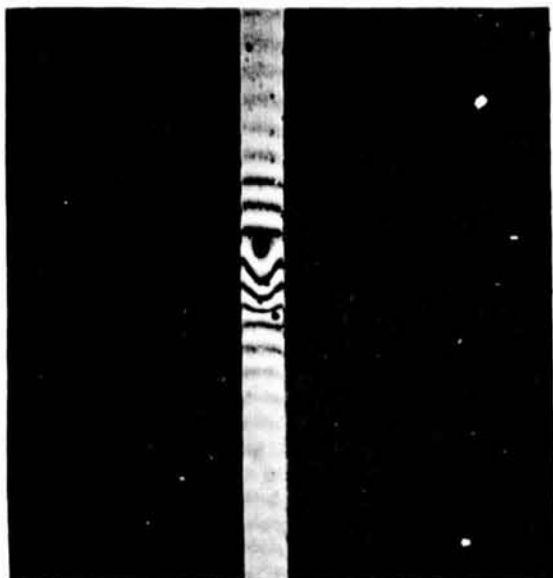


Figure 5-14. Model 101 Seat Showing Groove From 0.004 Inch CRES Wire (462X Interference Photo)



Figure 5-15. Model 101 Seat (Repeat 462X Interference Photo)

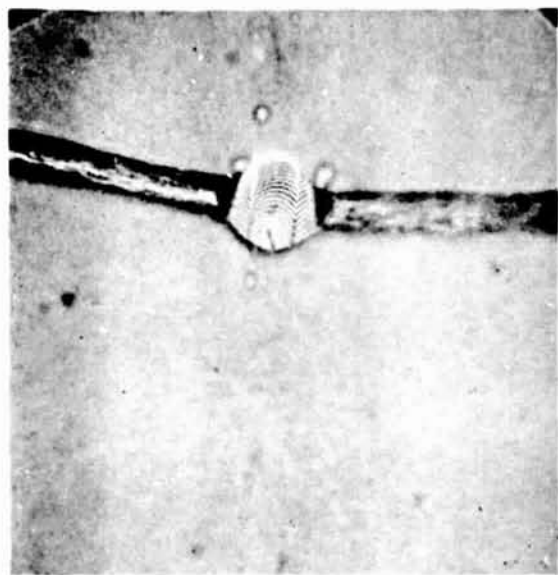


Figure 5-16. Model 101 Test 2 0.0004 Inch CRES Wire (462X Interference Photo)



Figure 5-17. Model 101 Test 6 0.003 Inch Copper Wire (462X Plain Photo)

ORIGINAL PAGE IS
OF POOR QUALITY

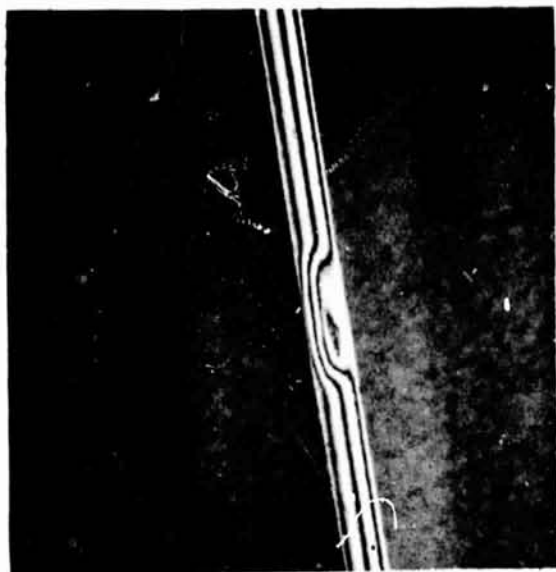


Figure 5-18. Model 101 Seat Showing Groove From 0.001 Inch CRES Wire (462X Interference Photo)

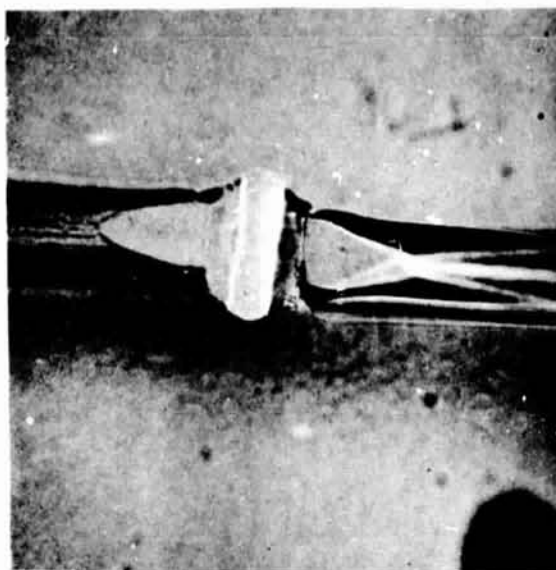


Figure 5-19. Model 101 Test 8 0.001 Inch CRES Wire (462X Interference Photo)

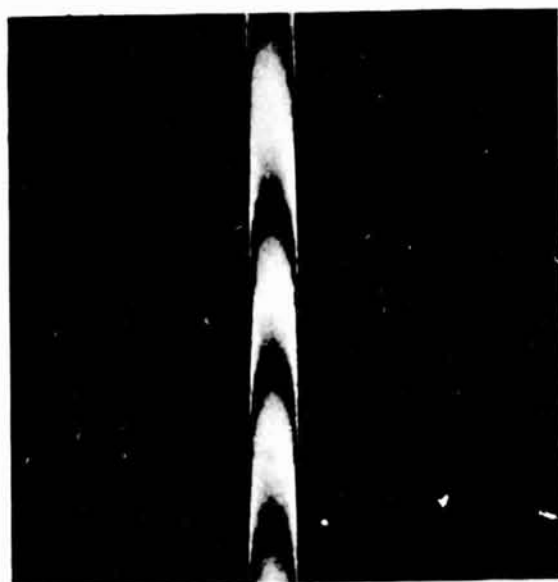


Figure 5-20. Model 101 Seat Showing Crown (462X Interference Photo)

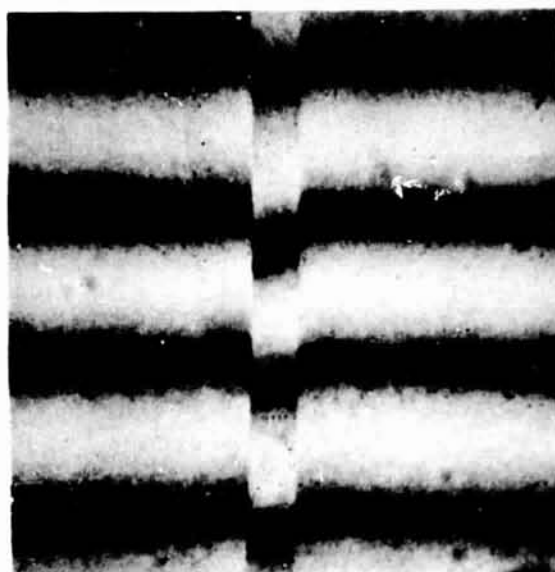


Figure 5-21. Model 101 Poppet Showing Seat Groove (462X Interference Photo)

load, was required to reduce leakage to 0.01 scim. Figure 5-4 data allow reduction of the test data to a common basis of a 1.0-psid inlet pressure for comparison between models as shown in Table 5-1.

Posttest inspection of the model following removal of the 0.0004-inch CRES wire revealed a groove across the land about 8 μ in. deep by 0.00087-inch wide (Fig. 5-14 and 5-15). At 10 psid, 0.00016-scim leakage is predicted for this groove and is in general agreement with posttest results (Fig. 5-1). The wire had been mashed, as shown in Fig. 5-16. There was no visible damage in the poppet land.

Tests 3 through 5 with a 0.001-inch copper wire (Fig. 5-5 through 5-7) produced leakage results quite similar to the 0.0004-inch wire. Posttest examination indicated that the softer wire, although not cut, did not produce a measurable seat depression.

Additional preload was required with the 0.003-inch copper wire to reduce leakage to a measurable value. Piston loading was gradually applied with 1.0-psid inlet pressure. Upon reaching 1.5-pound load, leakage abruptly reduced to 0.0034 scim, corresponding to a gap of 3.0 μ in. The subsequent check valve test (No. 6, Fig. 5-8) produced results similar to the 0.001-inch copper wire. Examination revealed the wire had been mashed (Fig. 5-17) but produced no visible seat damage.

Removal of the inlet pressure during Test 6 resulted in leakage below control at about 25 psid. This anomalous condition is evident in other tests and may be associated with the sudden closure. In any case, the equivalent gap is below the level of significance for the OMS requirement.

A preload of up to 2.7 pounds was gradually applied to the 0.001-inch CRES wire to reduce 1.0-psid leakage to 0.0126 scim. Check valve tests and correlated results displayed in Fig. 5-10 and 5-11 show the characteristic leak curves with posttest (No. 9) increased leakage indicating the effect of a permanent groove across the seat land. The groove and mashed wire are shown in Fig. 5-18 and 5-19.

Preload of the 0.003-inch CRES wire produced a sudden shutoff to 0.00018 scim (with 1.0 psid) at 4.6 pounds force. Check valve testing repeated the anomalous condition noted in Test 6 (with the 0.003-inch copper wire) of leakage less than control, as shown in the data of Fig. 5-12 and correlation plot (Fig. 5-13). Cause of this condition may have been from the impact of sudden closure, as the sealing surfaces were not separated after cutting the wire. Inspection of the model surfaces and wire after test revealed that the wire had been cleanly cut except for a minor entrapment and negligible seat groove. This particular wire cutting test had been repeated numerous times with Model 101 during preliminary testing in which wire cutting procedures were established, and it was thereby established that the cutting loads of Table 5-1 were repeatable.

Model 101 afforded an unexpected piece of data with posttest 11. Prior to recording the data shown in Fig. 5-12, the seat was loaded to 500 pounds (should have been 500-psig inlet pressure corresponding to 87 pounds). Inspection of the surfaces revealed that the seat had been plastically crowned (Fig. 5-20), and a

groove approximately 2 μ in. deep had been impressed in the poppet (Fig. 5-21). The apparent stress producing this condition was about 627,000 psi or slightly less than 1/3 of the Vickers hardness plastic flow pressure of 2.2×10^6 psi. Actual corner stress for the square-edge land was well in excess of the apparent, thus producing plastic flow in both the poppet and seat.

Cutter Model 102 With 0.002-Inch Land

Preliminary wire cutting tests were performed with this model following experiments with Model 101 using a 0.003-inch CRES wire. Control test leakage from 0.5 to 500 psig was less than 0.003-scim helium for all pressures. Attempts, however, to cut the 0.003-inch CRES wire were futile with leakage on the order of 1.0 scim from 200- to 500-psig inlet pressure. Inspection following this test showed that the center of the land was dented about 30 μ in. (Fig. 5-22) and the wire flattened (Fig. 5-23). Apparently, hydrostatic pressures were greatest at the center of the land due to containment of the CRES wire. Because of these poor results, further testing with this model was discontinued.

Cutter Model 103 With 0.0002-Inch Land

The performance of this model proved to be superior to all other models tested and verified the need for a land width less than 0.0005 inch to meet the OMS check valve load requirements. The actual land for this model varied around the circumference from 0.00016- to 0.00020-inch width. Adjacent spherical lands were 0.0038-inch wide at the OD and 0.0064 inch at the ID for a total projected width of 0.0104 inch across the 90-degree pyramid. The mean seat diameter was 0.4711 inch.

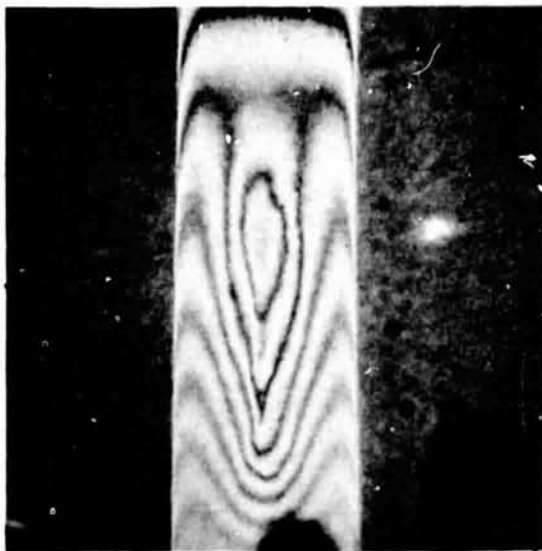


Figure 5-22. Model 102 Seat Showing Dent From 0.003 Inch CRES Wire (462X Interference Photo)



Figure 5-23. Model 102 Test 2 0.003 Inch CRES Wire (91X Plain Photo)

ORIGINAL PAGE IS
OF POOR QUALITY

Data for Model 103 are displayed in Table 5-1, graphs of Fig. 5-24 through 5-29, and photos of Fig. 5-30 through 5-34.

Check valve tests were performed with 0.0004-inch CRES and 0.001-inch copper wires; in these cases, the normal 0.5- to 0.8-pound closure preload was sufficient to submerge all effects of wire entrapment on check valve leakage performance (Fig. 5-24 through 5-26). Figures 5-31 and 5-32 show photos of the mashed wires. Seat damage from these entrapments was negligible.

Additional preload was required with the larger wire sizes; cutting loads are noted in Table 5-1. In these cases, the wires were suddenly cut with an audible snap and leakage was reduced to less than 0.001 scim at 1.0 psid (Fig. 5-33 shows a photo of the cut 0.003-inch CRES). Check valve testing then proceeded. The final posttest 11 shows that there was very little effect of the test series on seal performance.

Cutter Model 104 With 0.0012-Inch Land

Model 104 with a 0.0012 inch wide land clearly demonstrated the need for a narrow land. All wires were mashed by the land, and the larger CRES wires caused significant depressions in the land.

Test and correlated data are displayed in Table 5-1 and Fig. 5-35 through 5-46. Photos of the seat and cut wires are shown in Fig. 5-47 through 5-54. Land damage from the 0.0004-inch CRES wire and copper wires was negligible. The larger CRES wires produced substantial depressions in the land that was reflected by increased posttest leakage at higher pressures (Fig. 5-45 and 5-46), Tests 7, 9, and 11. As shown in Table 5-1, the load to reduce leakage from 10^{-2} scim was substantially higher than with the narrower lands.

Leakage Correlation Test

Cutter model 105 was created to perform leakage correlation testing. The model consisted of a flat 0.0003-inch-wide land and a flat carbide poppet with four 0.0004-inch-diameter CRES wires glued across the poppet land approximately 0.025-inch apart so that a repeatable leak path could be produced. The model was loaded 10 times to the maximum planned load to stabilize the "mashing" of the four wires for repeatability.

The data from the correlation test series is tabulated in Table 5-2. The model was first baseline tested in the check valve mode with helium up to a total seat load of 3.39 pounds, well beyond the seat load which the OMS check valve will have available. Using these baseline data, a computer program was used to predict GN₂ leakage in the pure check valve mode (no spring load), helium leakage with 2.0-pound spring load, and GN₂ leakage with 2.0-pound spring load.

Examination of the tabulated data of predicted versus actual tested leakage shows excellent correlation for all three predicted modes. In each mode, the predicted leakage is, in general, less than a factor of two greater than the actual recorded

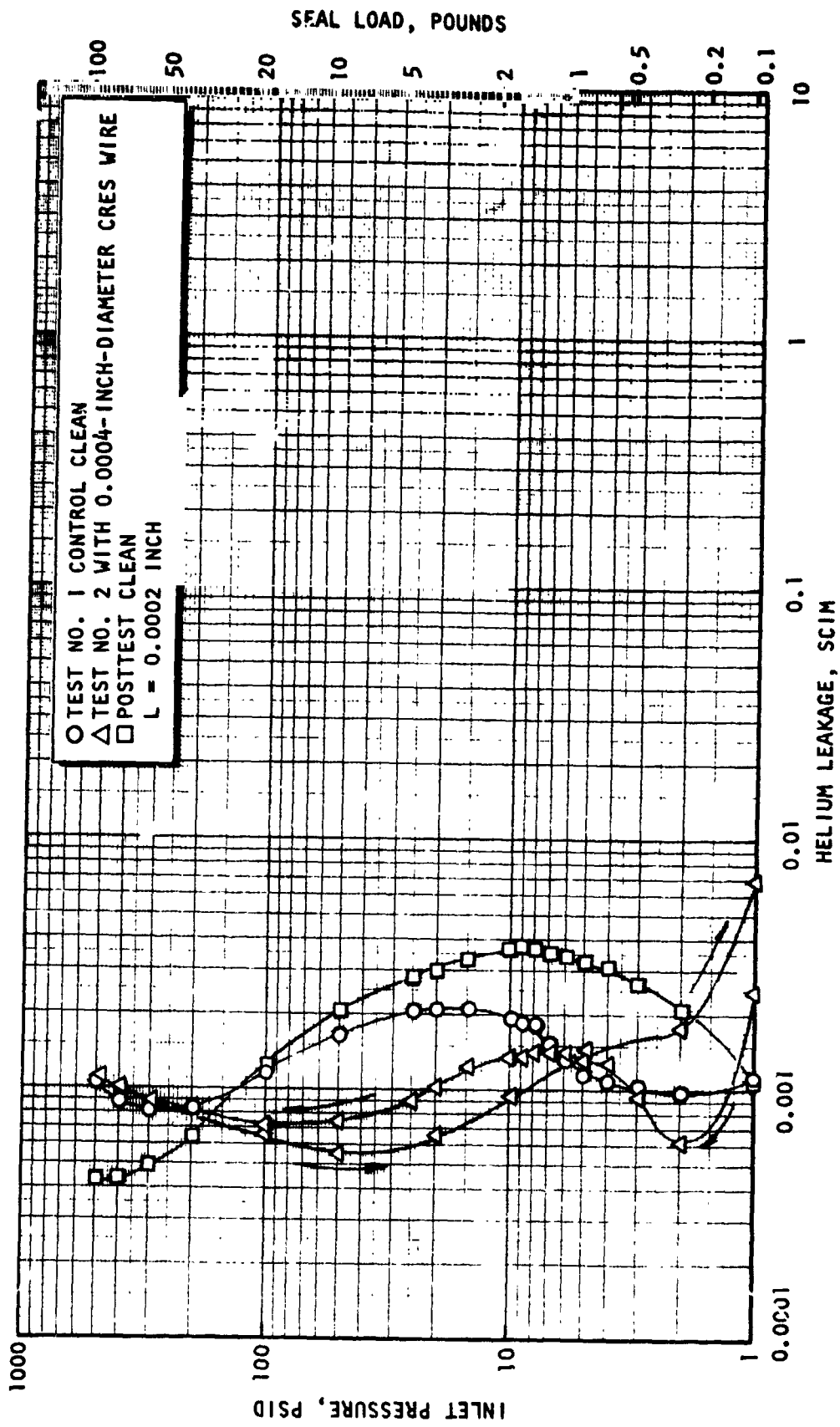


Figure 5-24. Leakage Data for Model 103, Test No. 1 Through 3

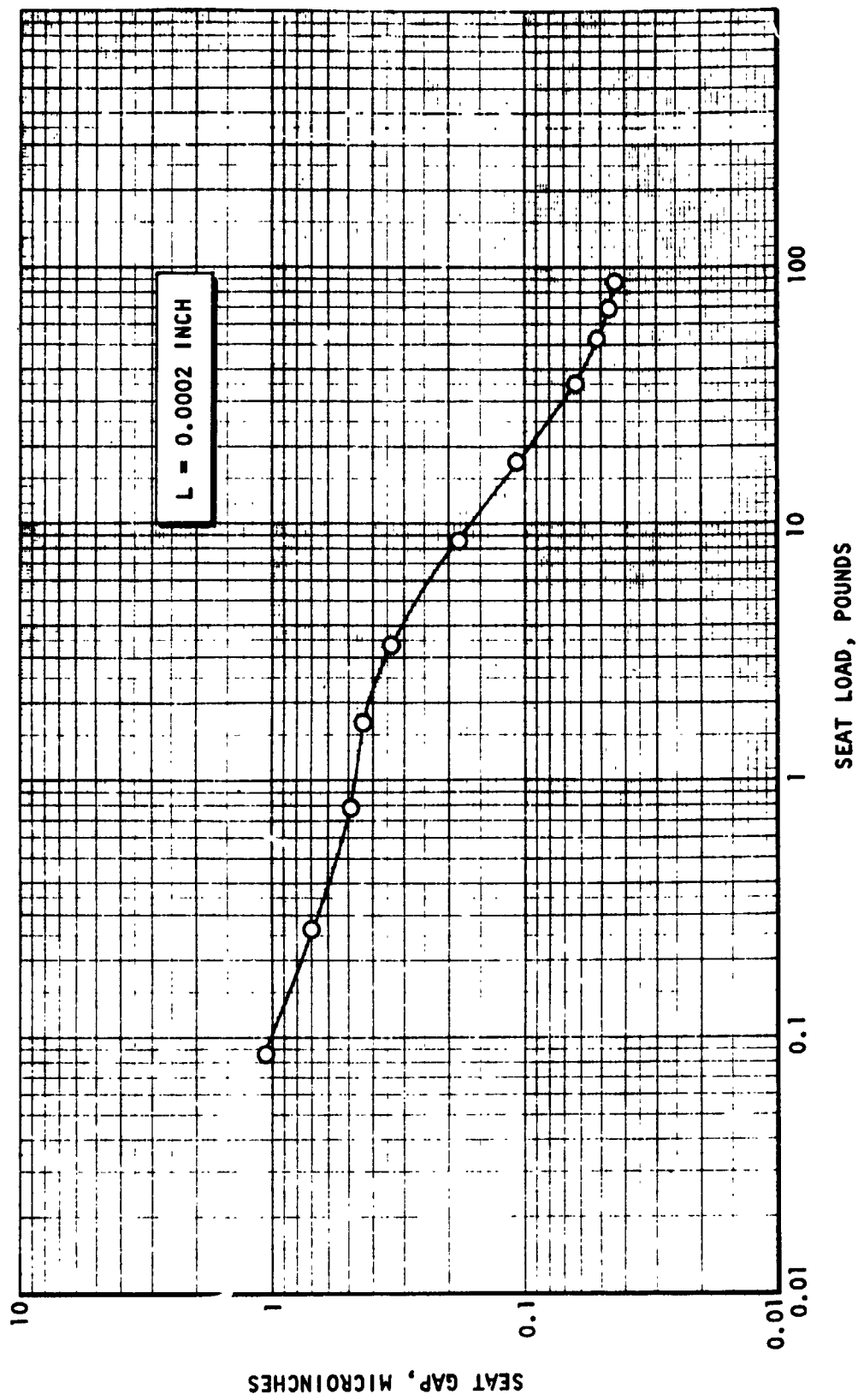


Figure 5-25. Model 103 Computed Seat Gap, Test No. 1 (Clean)

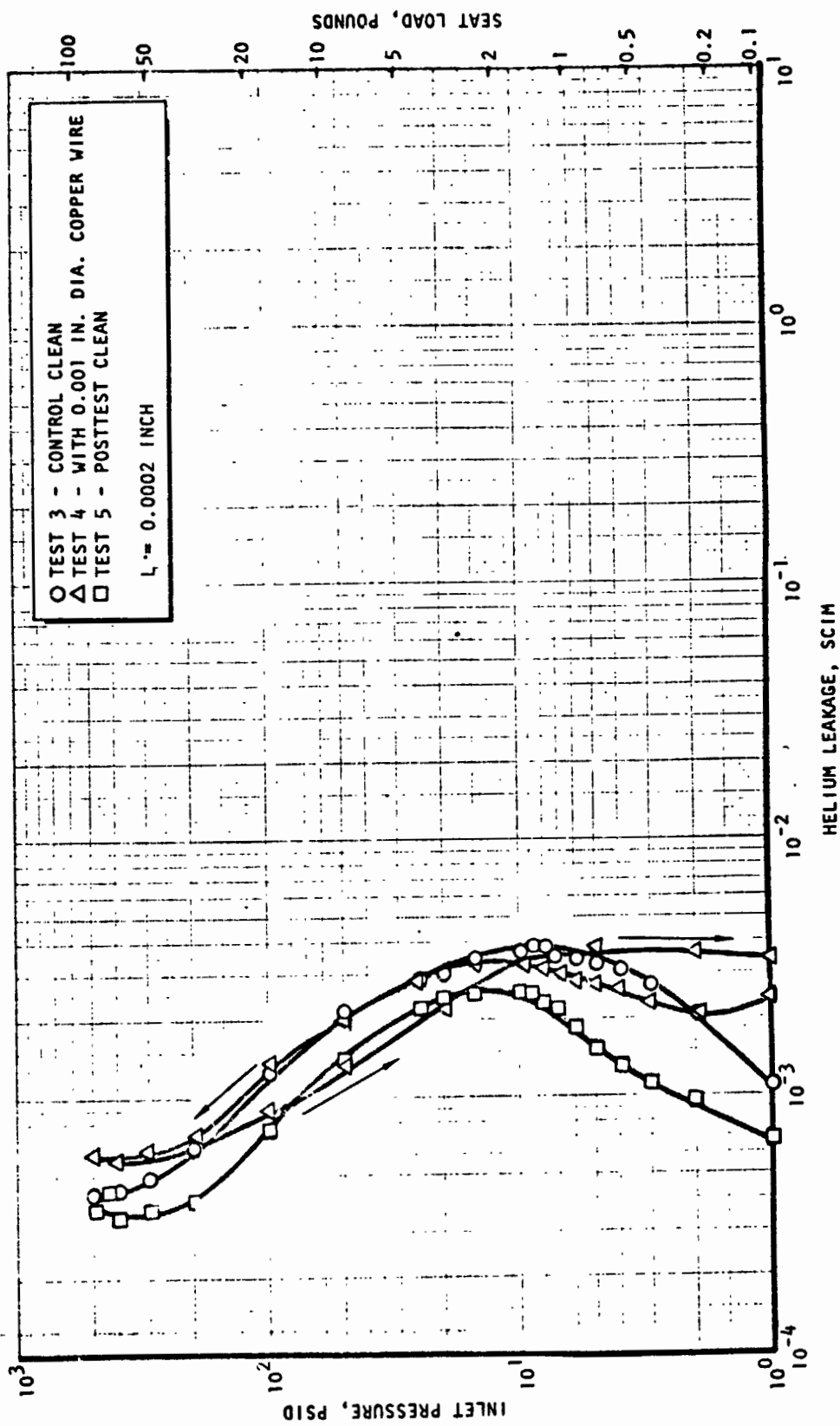


Figure 5-26. Leakage Data for Model 103, Tests 3 Through 5

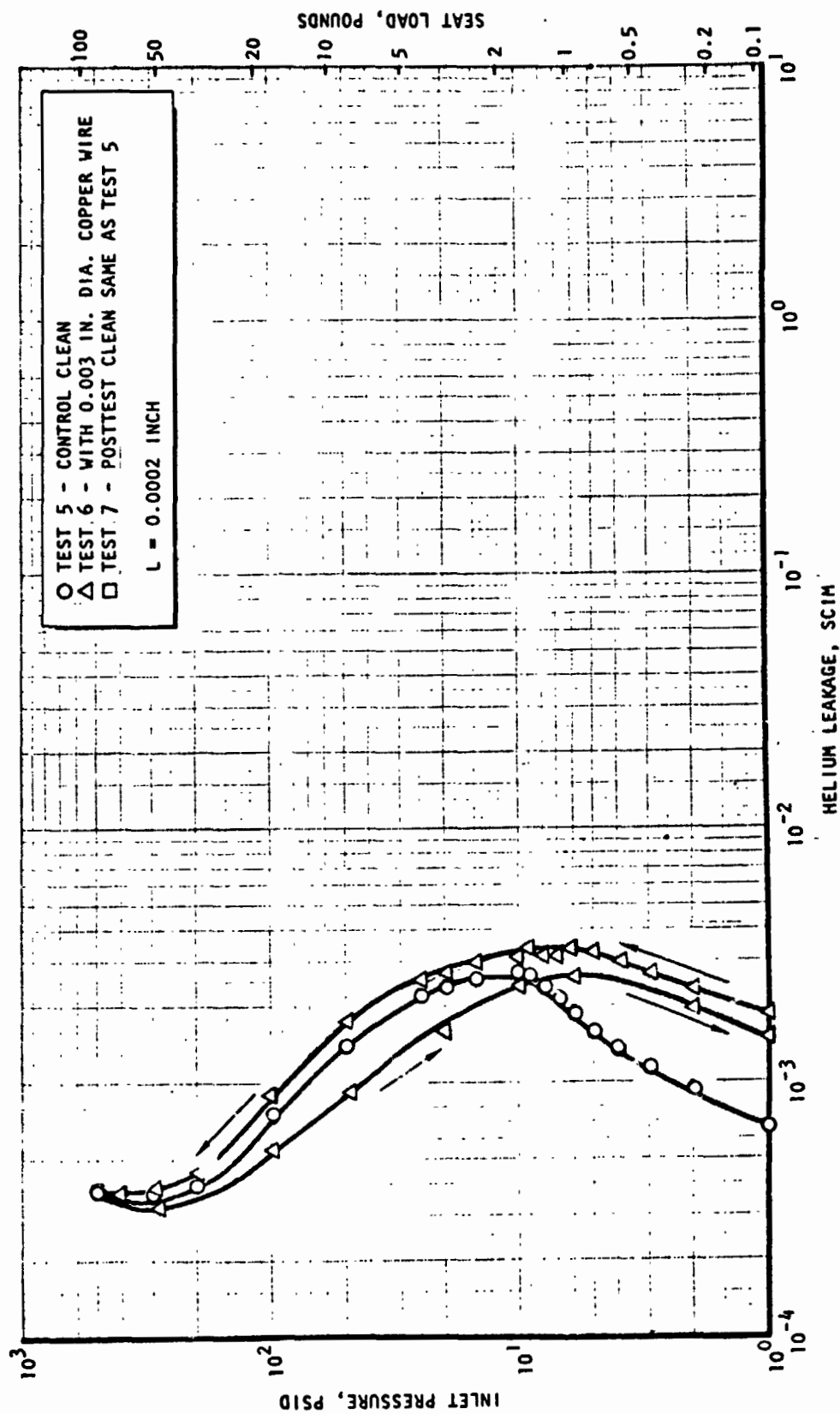


Figure 5-27. Leakage Data for Model 103, Tests 5 Through 7

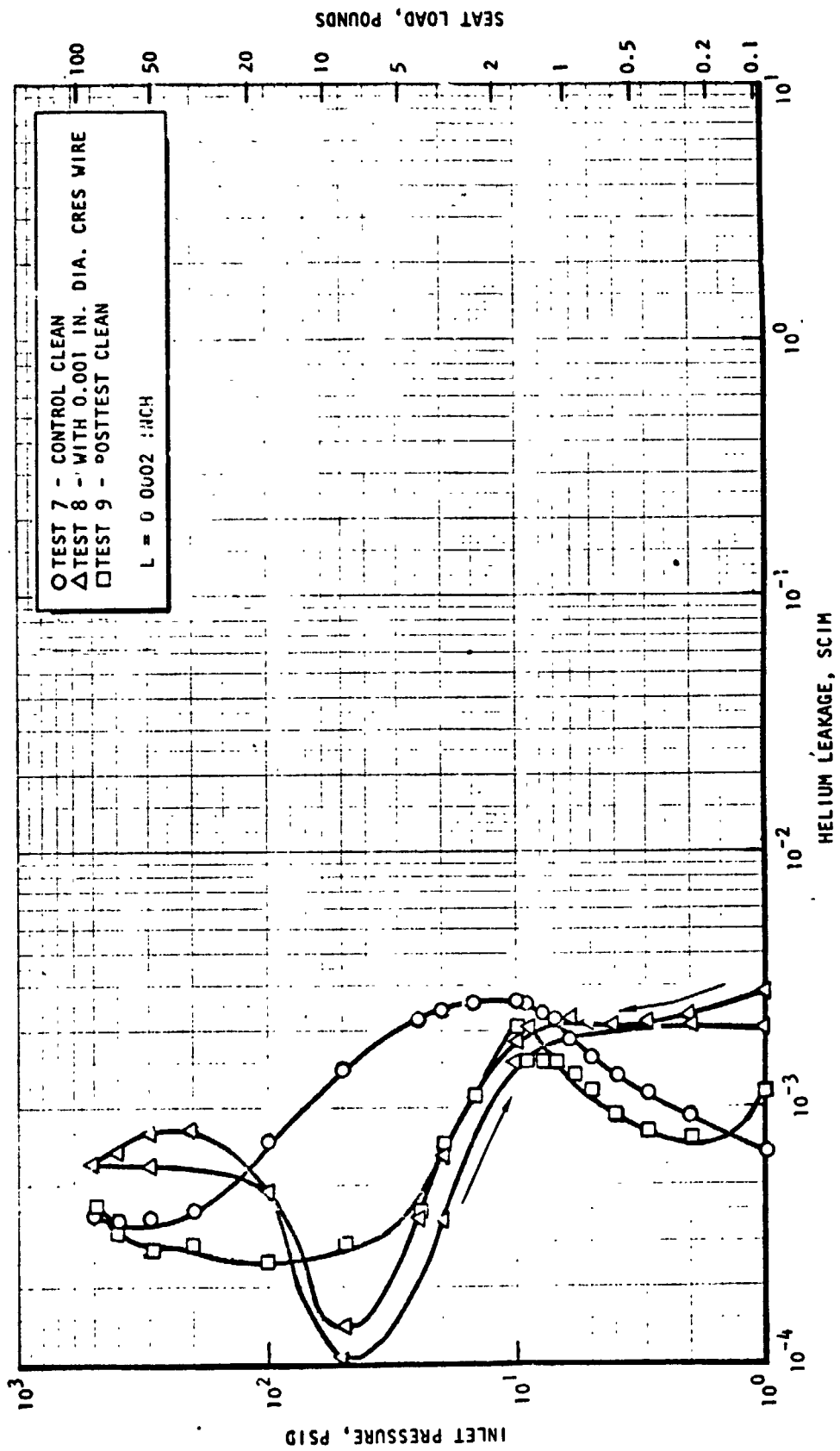


Figure 5-28. Leakage Data for Model 103, Test 7 Through 9

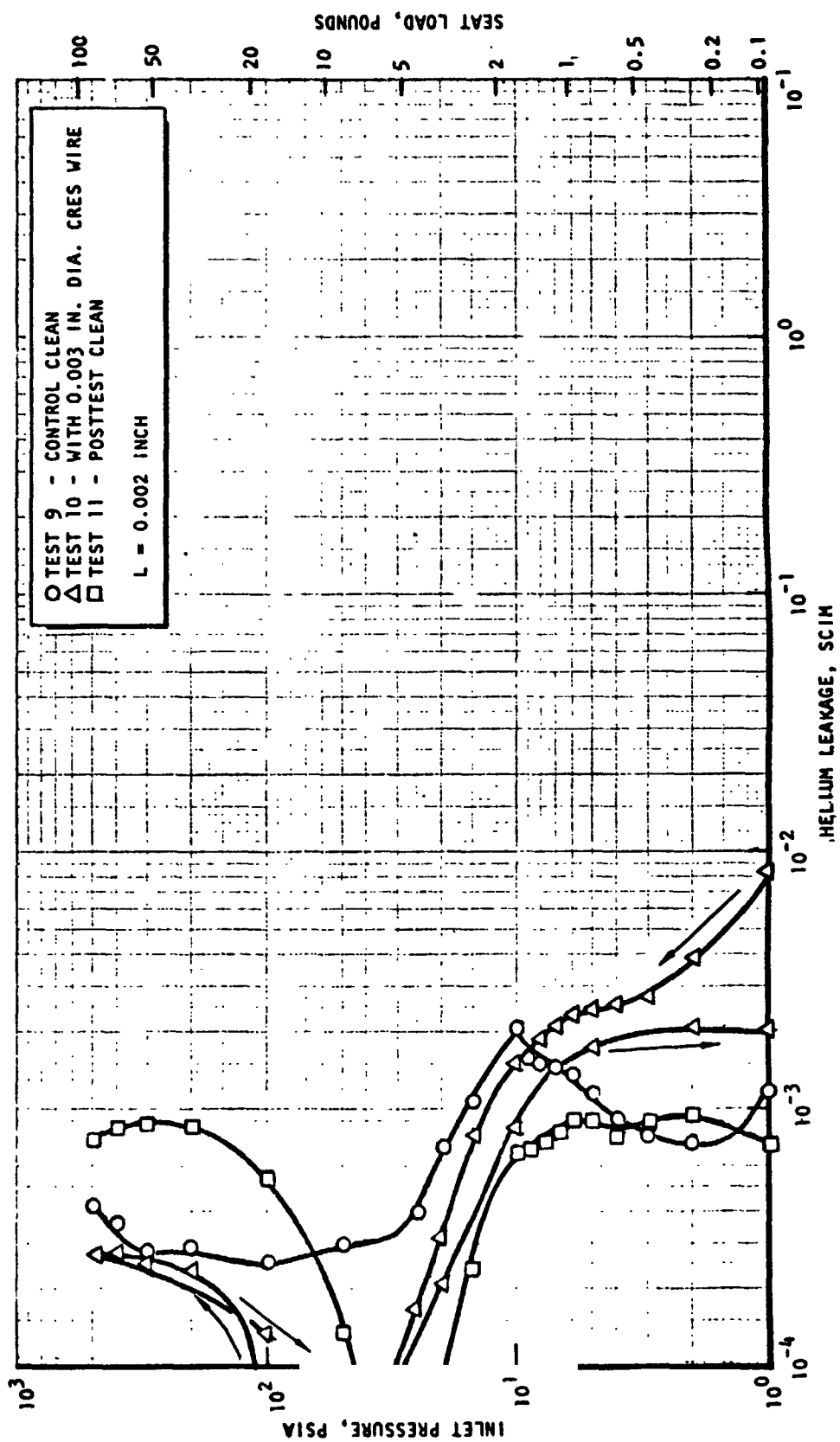


Figure 5-29. Leakage Data for Model 103, Tests 9 Through 11

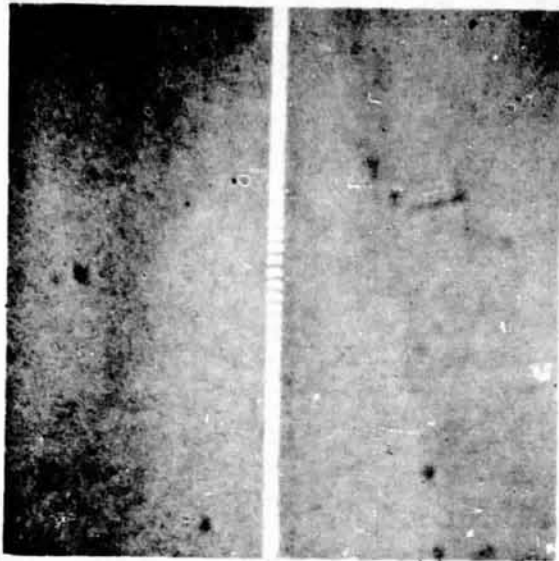


Figure 5-30. Model 103 Seat Land (462X Interference Photo)

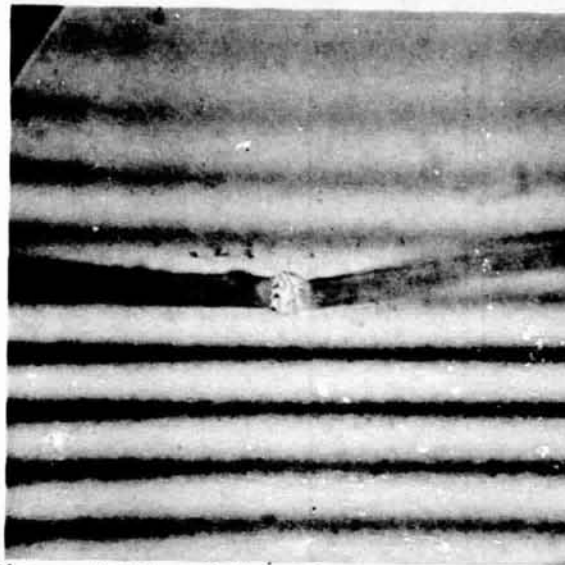


Figure 5-31. Model 103 Test 2
0.0004 Inch CRES Wire
(462X Interference Photo)



Figure 5-32. Model 103 Test 4
0.001 Inch Copper Wire
(462X Plain Photo)



Figure 5-33-34. Model 103 Test 10
0.003 Inch CRES Wire
(462X Interference Photo)

ORIGINAL PAGE IS
OF POOR QUALITY

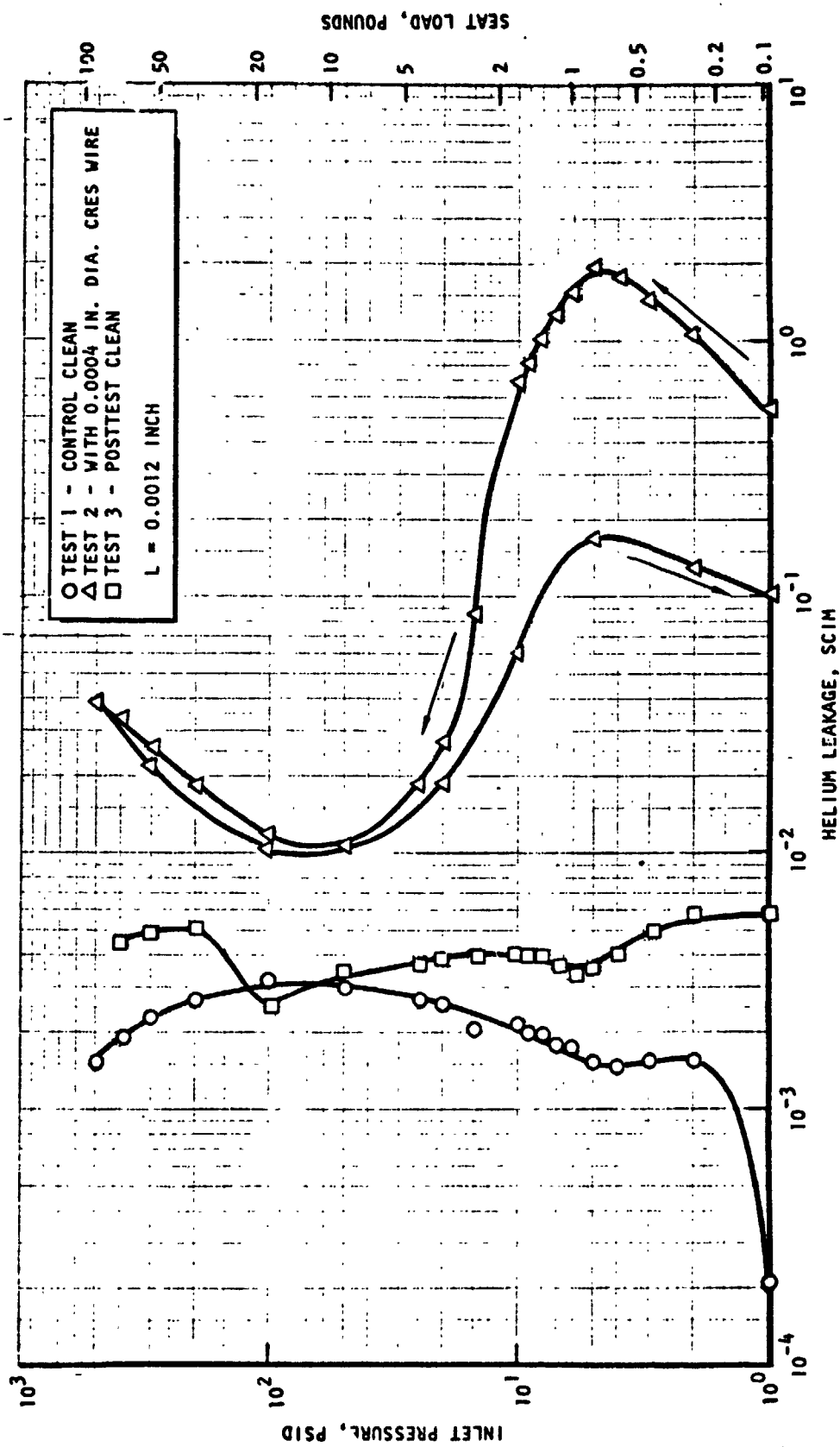


Figure 5-35. Leakage Data for Model 104, Tests 1 Through 3

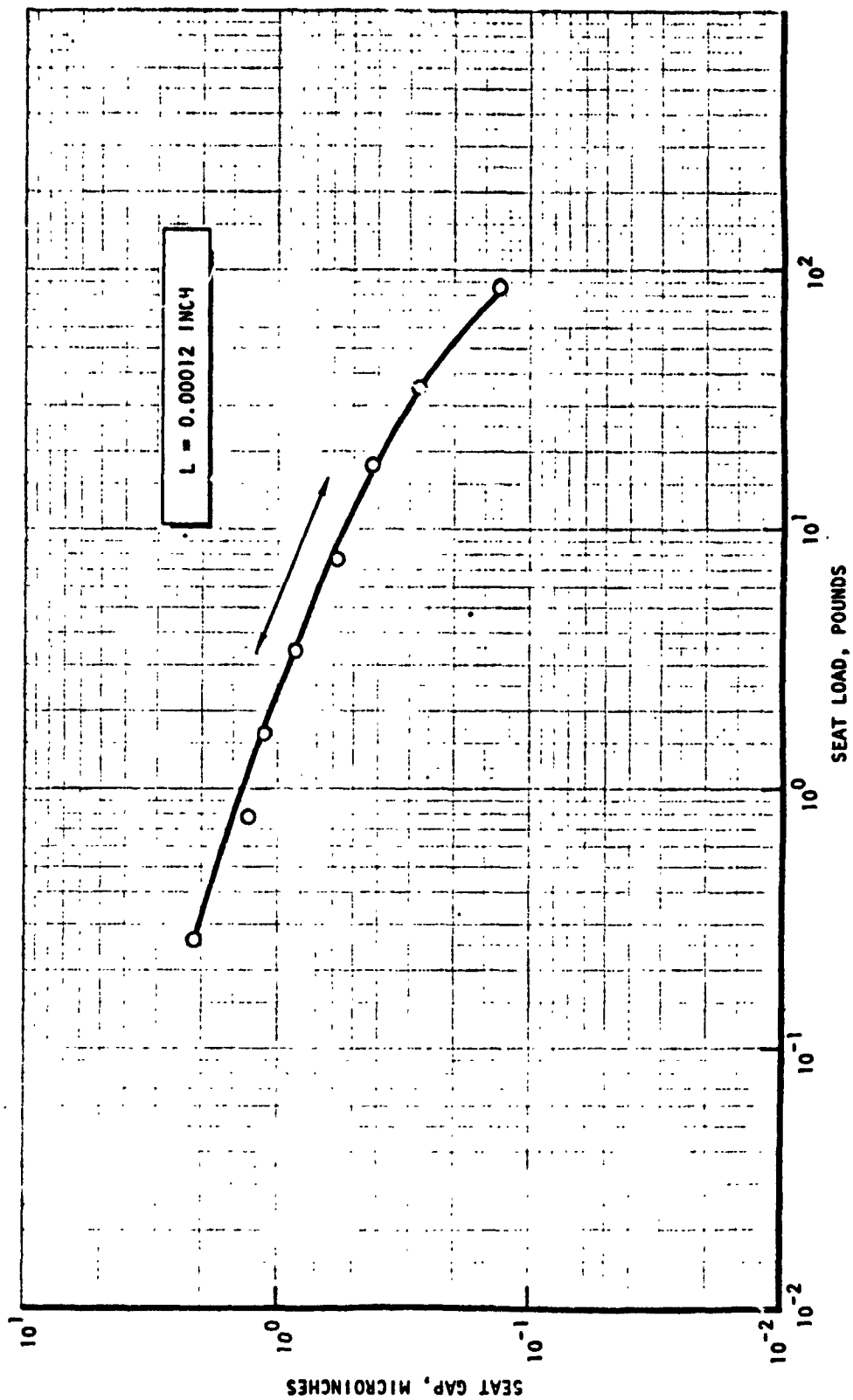


Figure 5-36. Model 104 Computed Seat Gap, Test 1 (Clean)

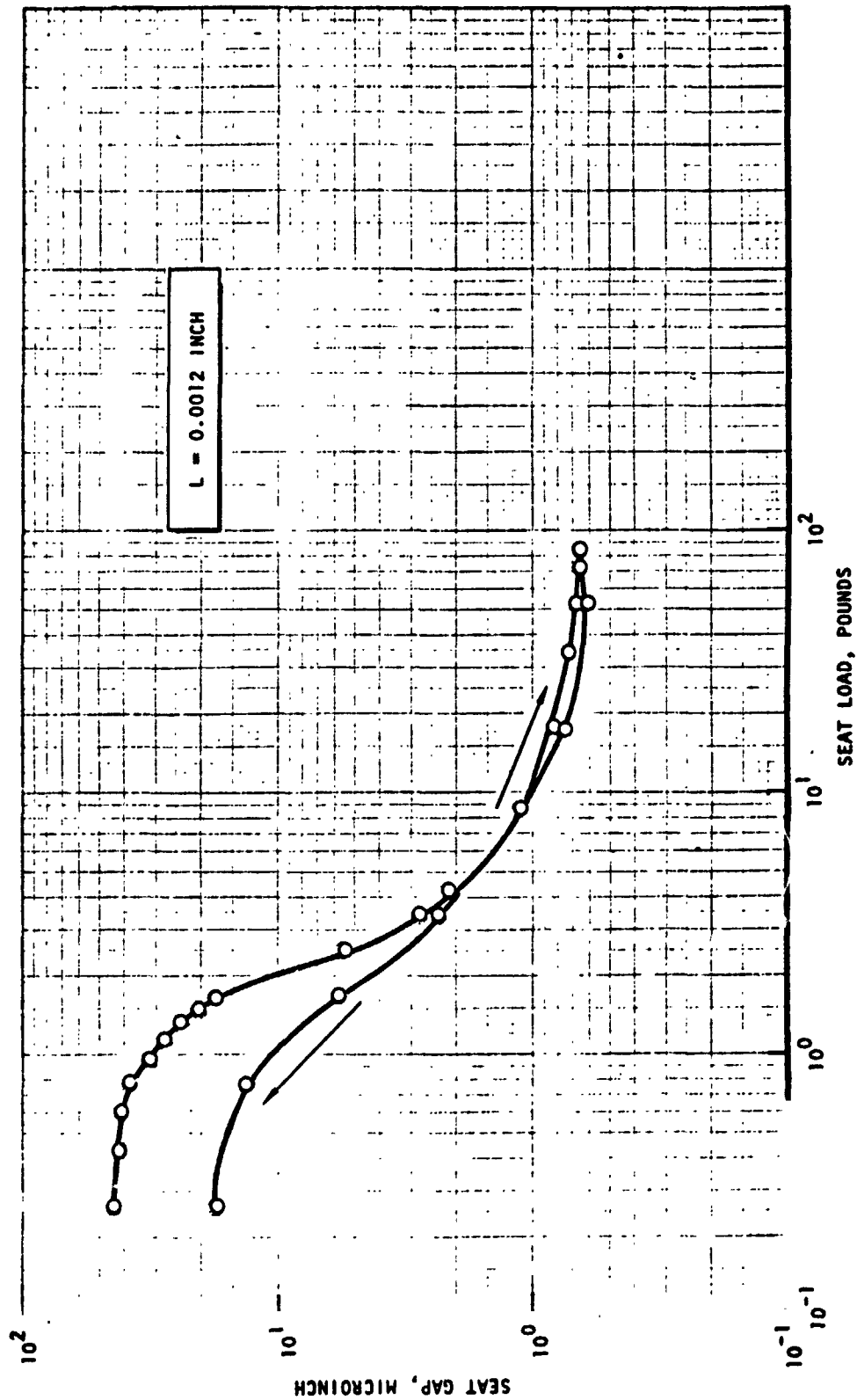


Figure 5-37. Computed Seat Gap, Test 2 (0.0004 inch CRES wire)

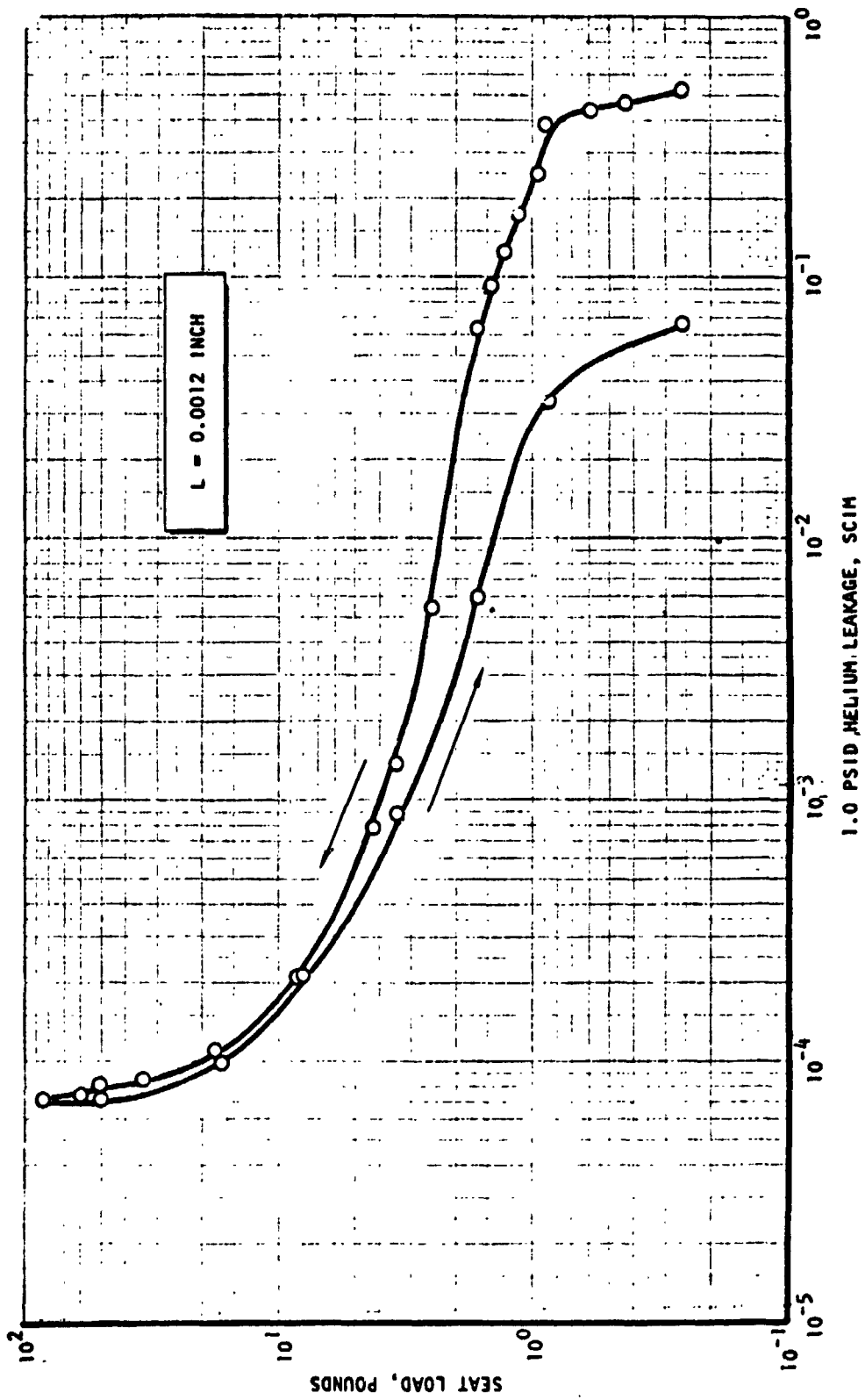


Figure 5-38. Model 104 Computed Leakage, Test 2
(0.0004 inch CRES wire)

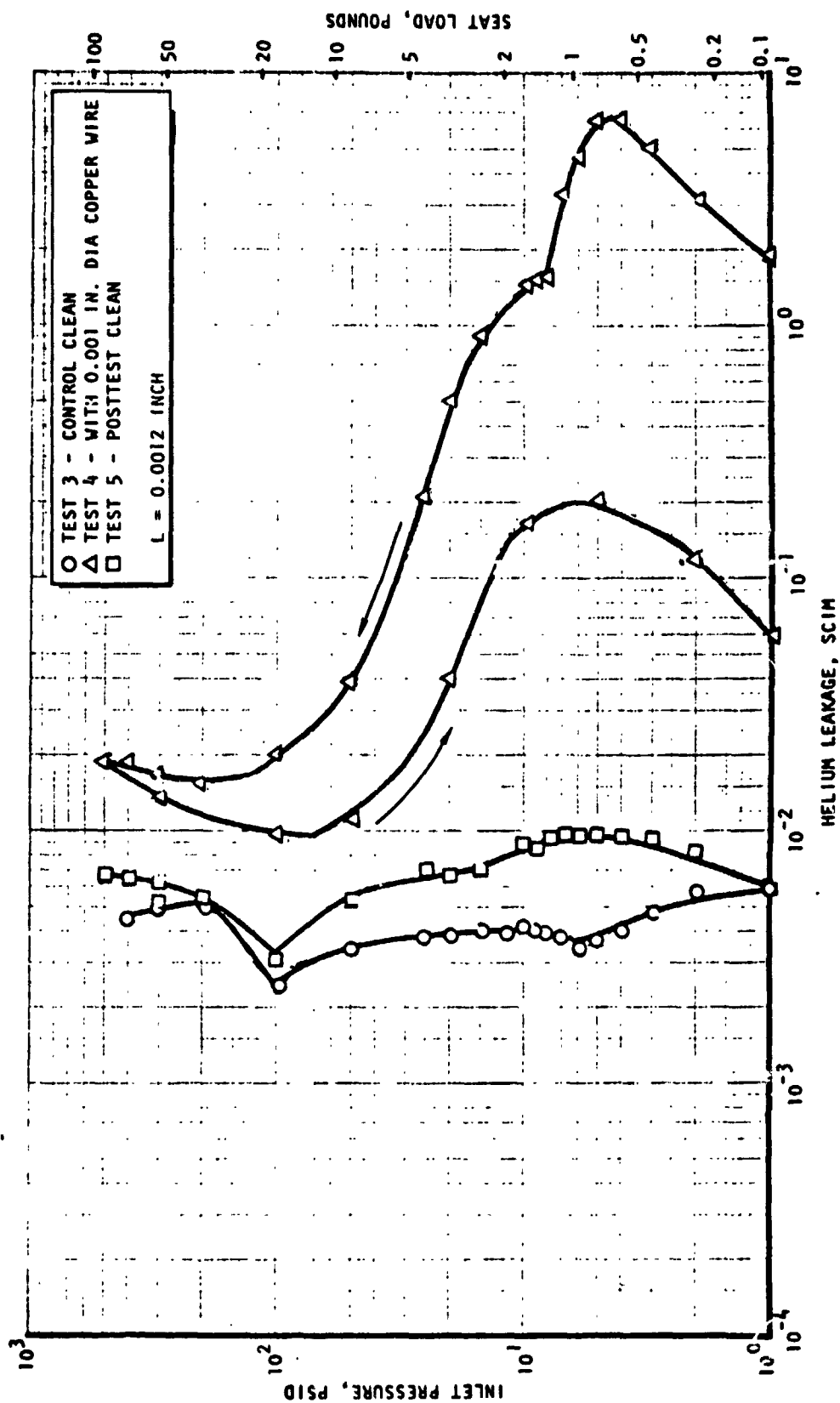


Figure 5-39. Leakage Data for Model 104, Tests 3 Through 5

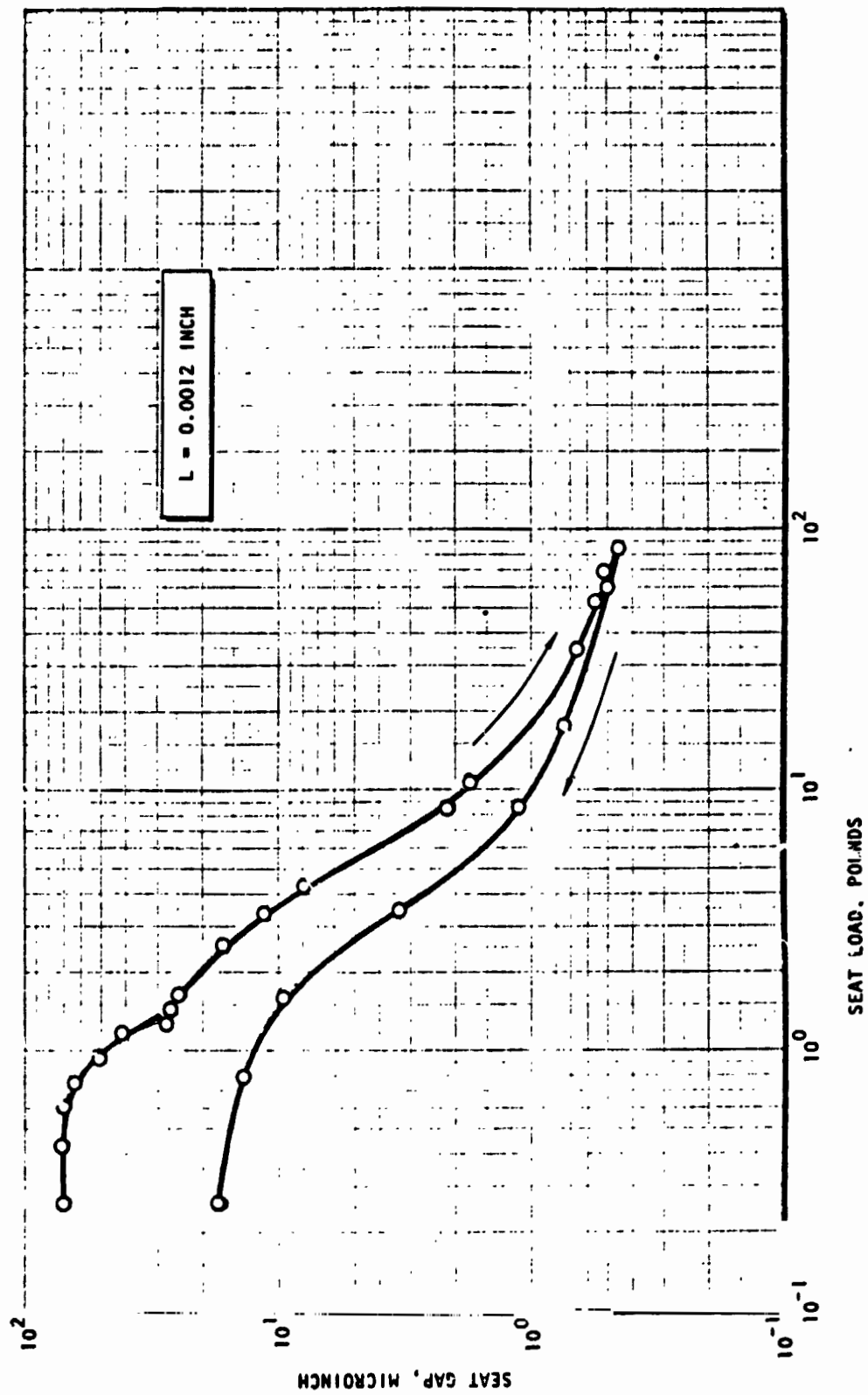


Figure 5-40. Model 104 Computed Seat Gap, Test 4
(0.001 inch copper wire)

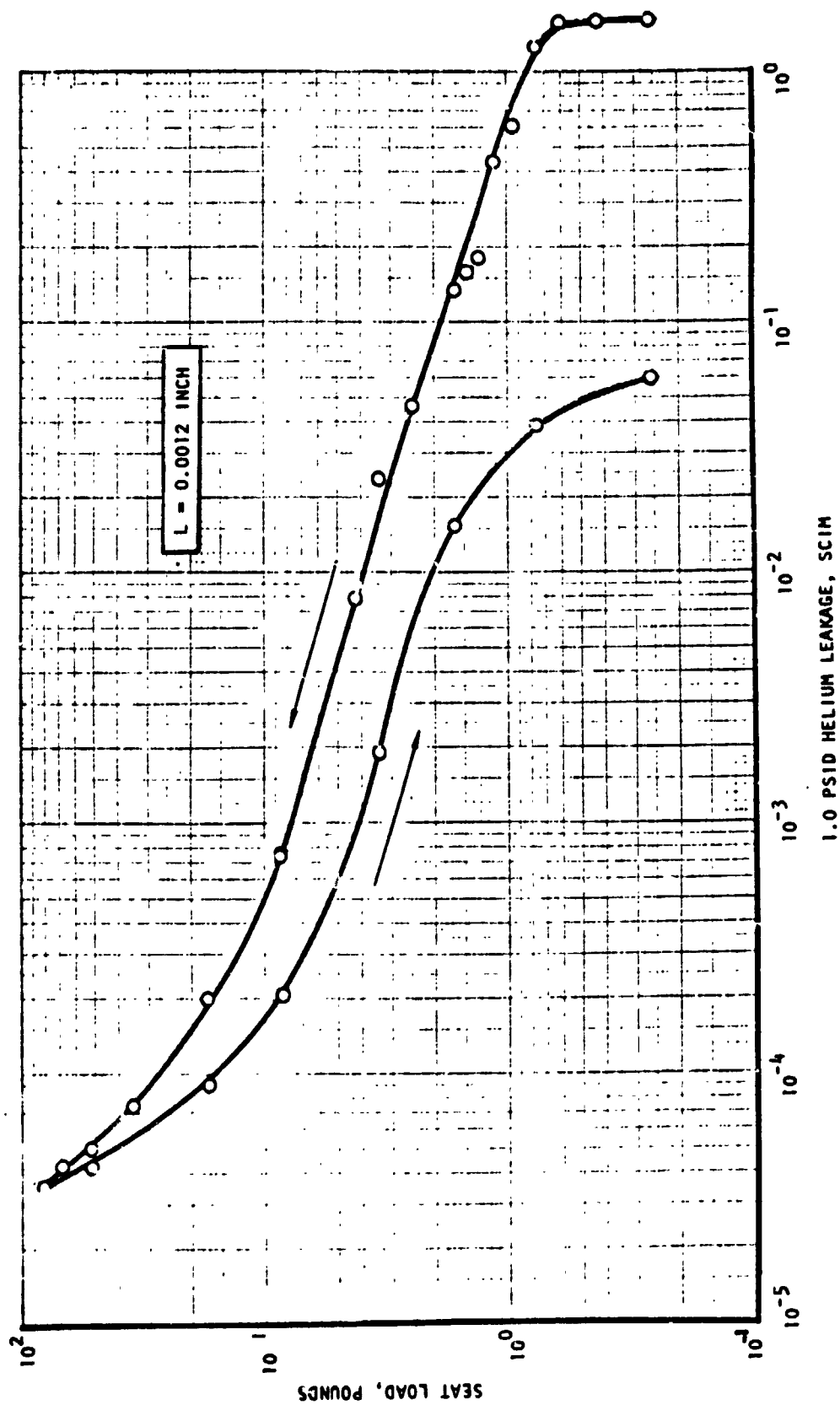


Figure 5-41. Model 104 Computed Leakage, Test 4
(0.001 inch copper wire)

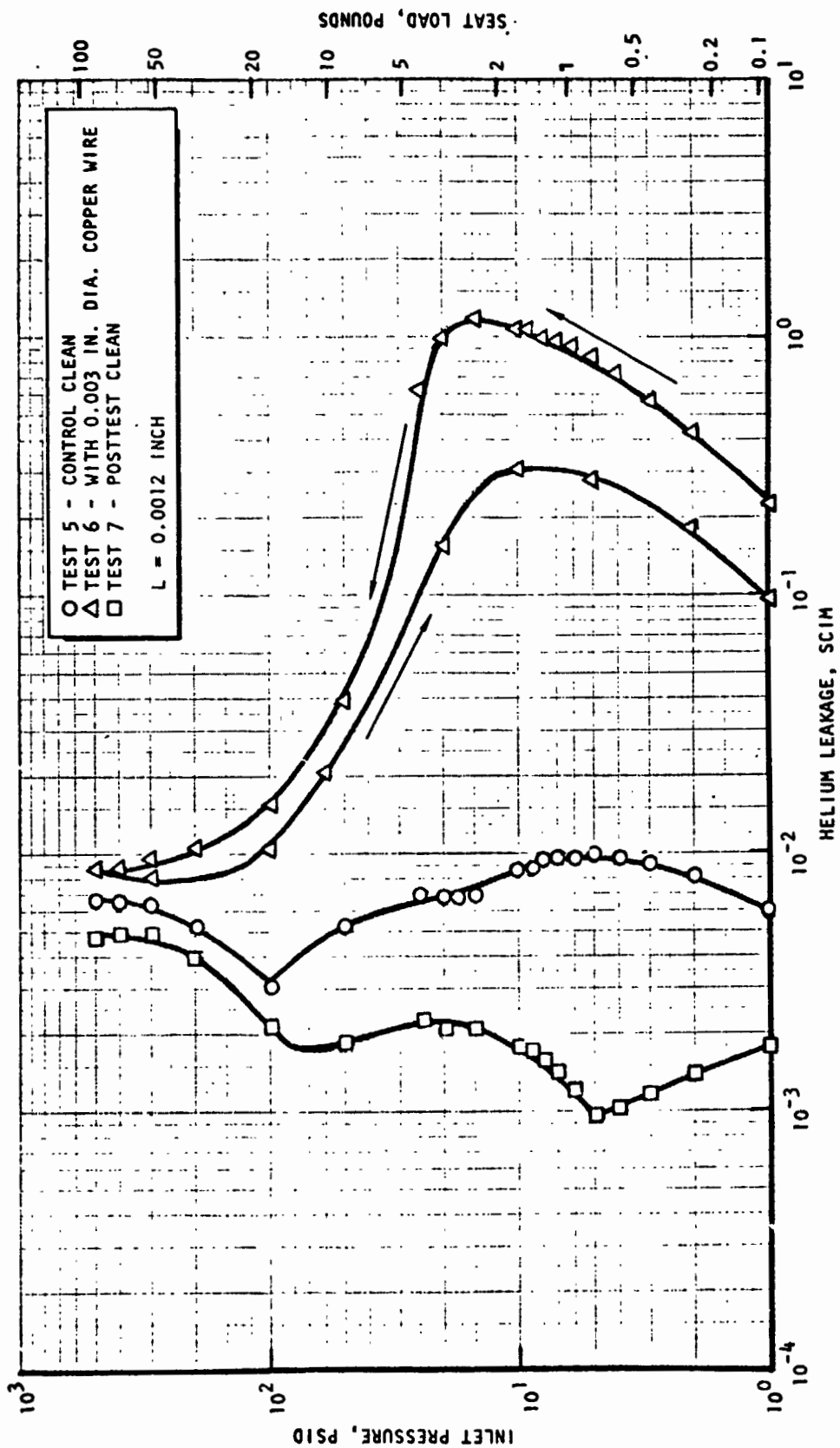


Figure 5-42. Leakage Data for Model 104, Tests 5 Through 7

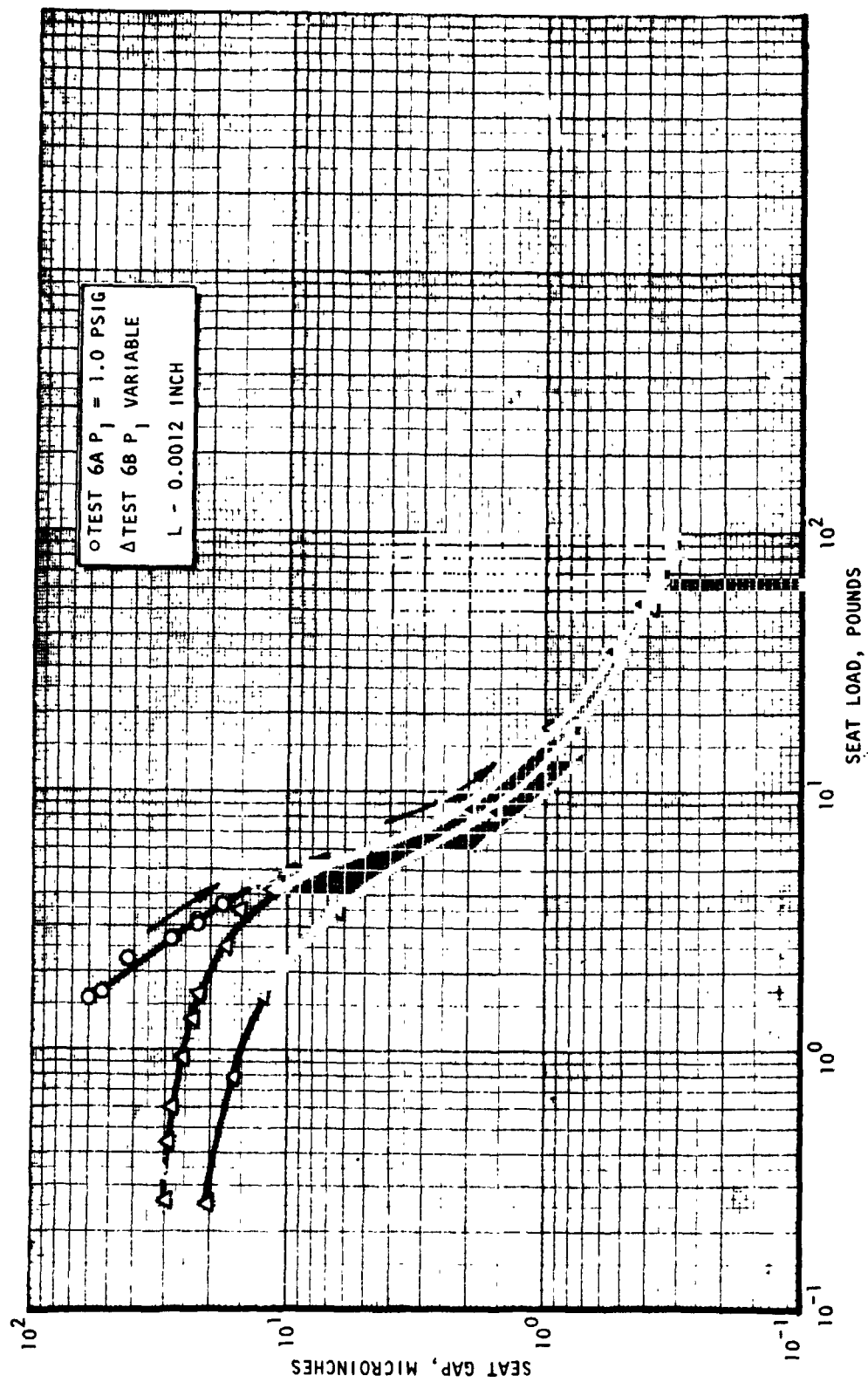


Figure 5-43. Model 104 Computed Seat Gap, Test 6
(0.003 inch copper wire)

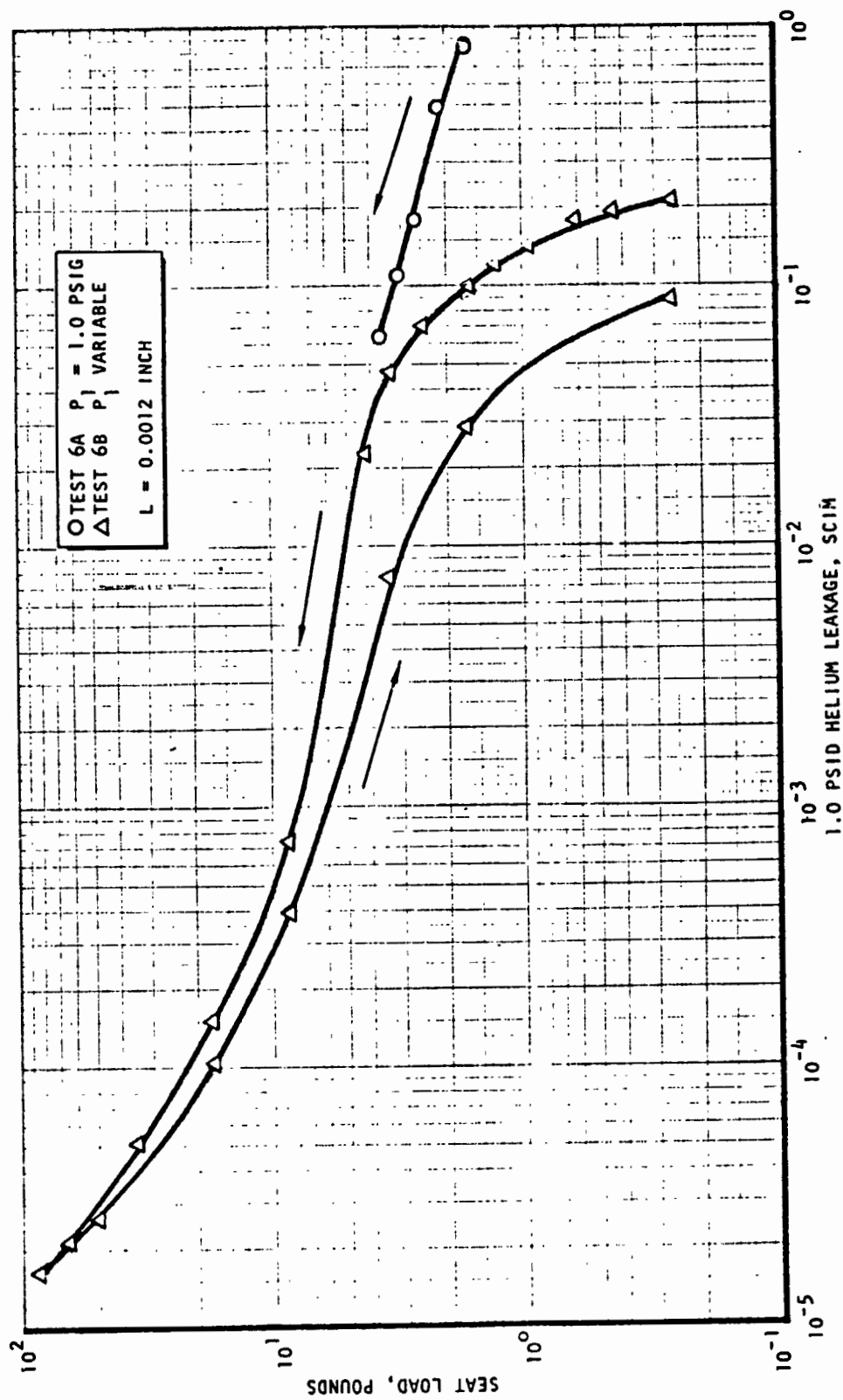


Figure 5-44. Model 104 Computed Leakage, Test 6
(0.003 inch copper wire)

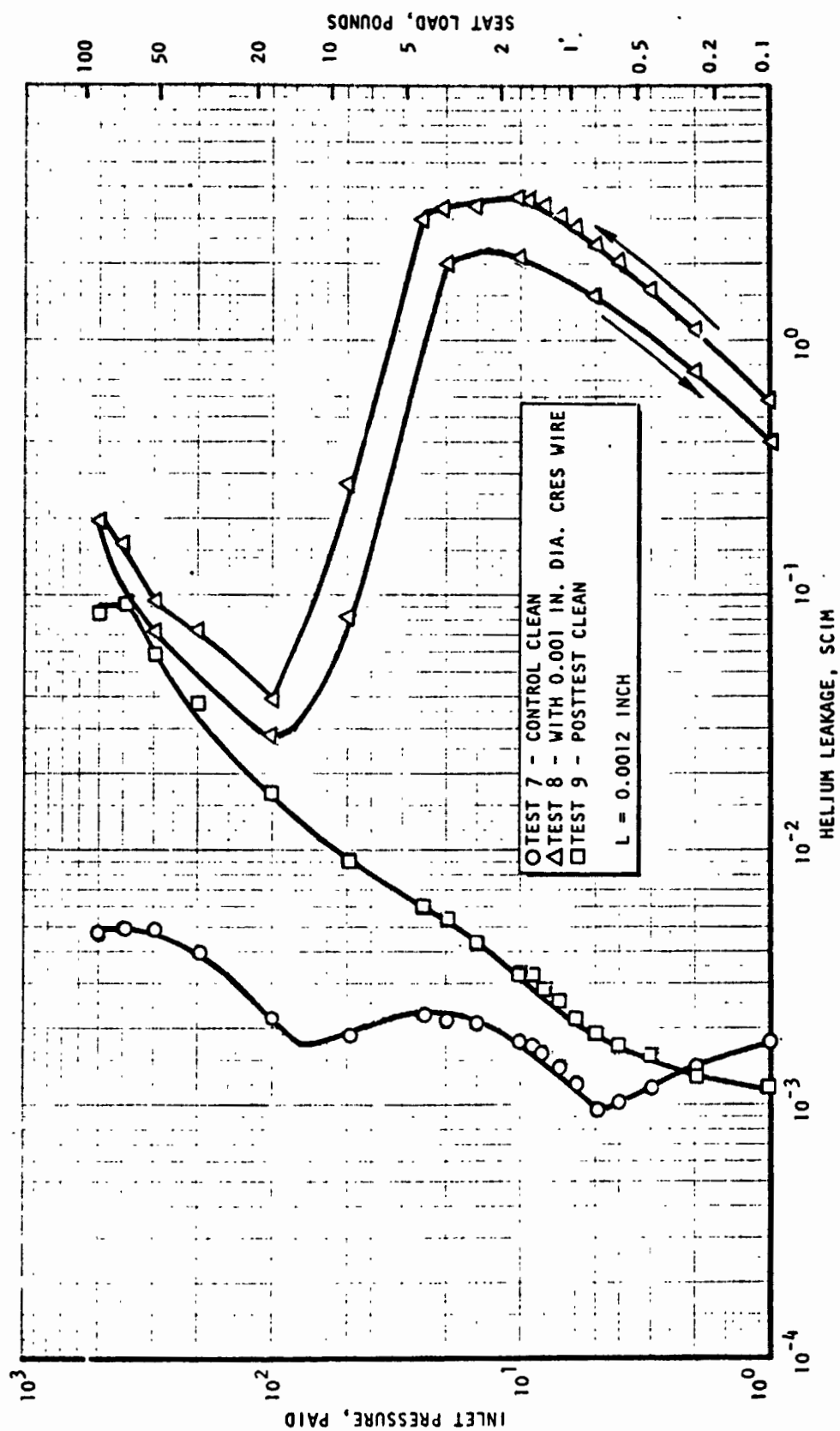


Figure 5-45. Leakage Data for Model 104, Tests 7 Through 9

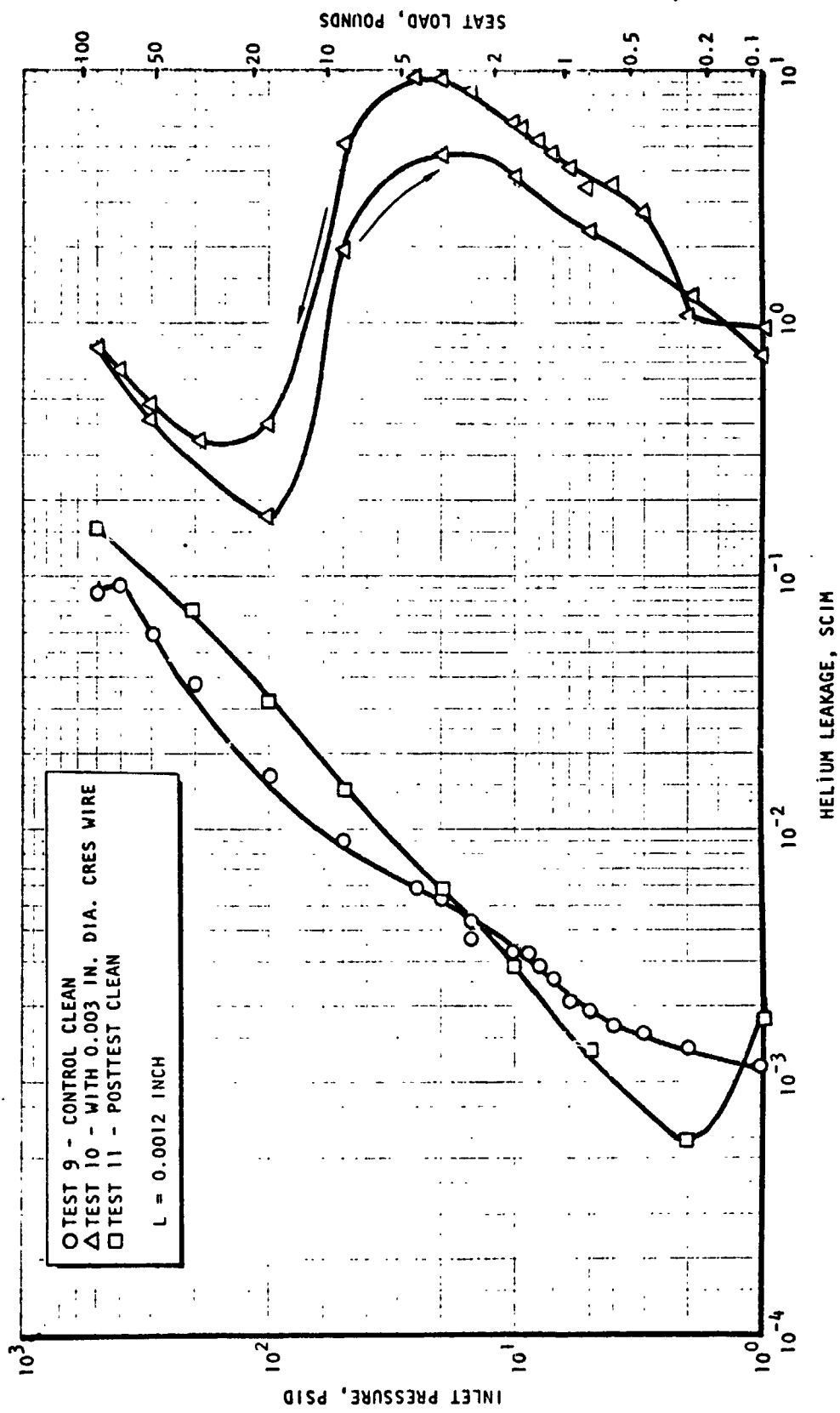


Figure 5-46. Leakage Data for Model 104, Tests 9 Through 11

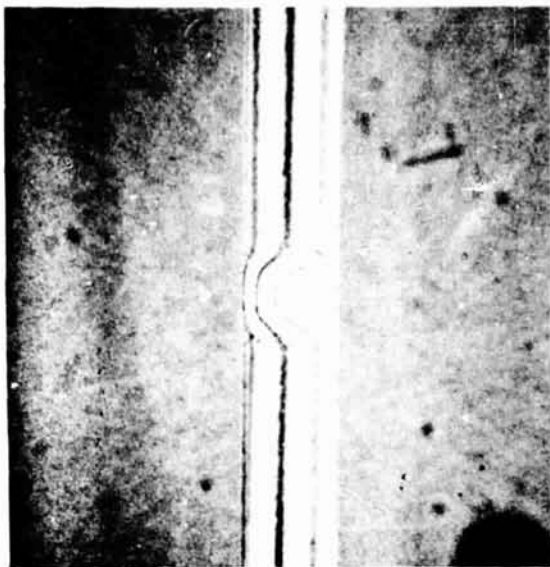


Figure 5-47. Model 104 Seat Showing Groove from 0.0004 Inch CRES Wire (462X Interference Photo)



Figure 5-48. Model 104 Test 2
0.0004 Inch CRES Wire
(462X Interference Photo)

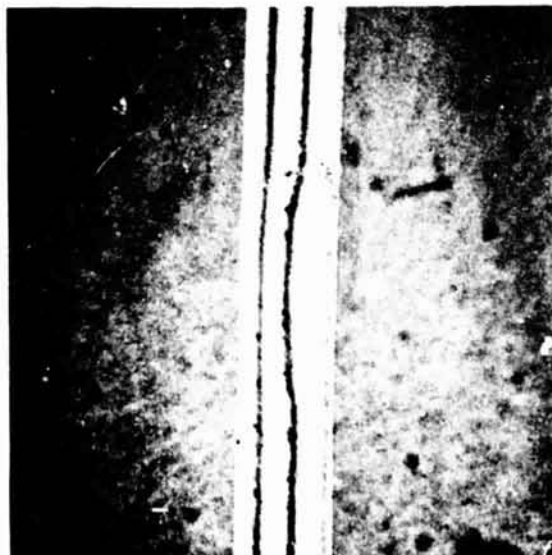


Figure 5-49. Model 104 Seat Showing Depression from 0.001 Inch Copper Wire (462X Interference Photo)

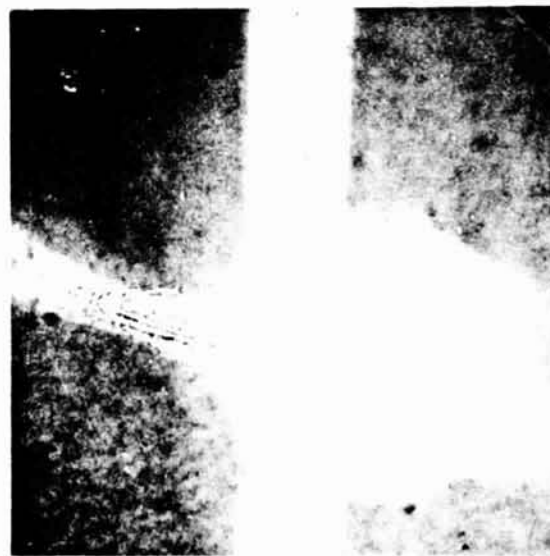


Figure 5-50. Model 104 Test 4
0.001 Inch Copper Wire
(462X Interference Photo)

ORIGINAL PAGE IS
OF POOR QUALITY

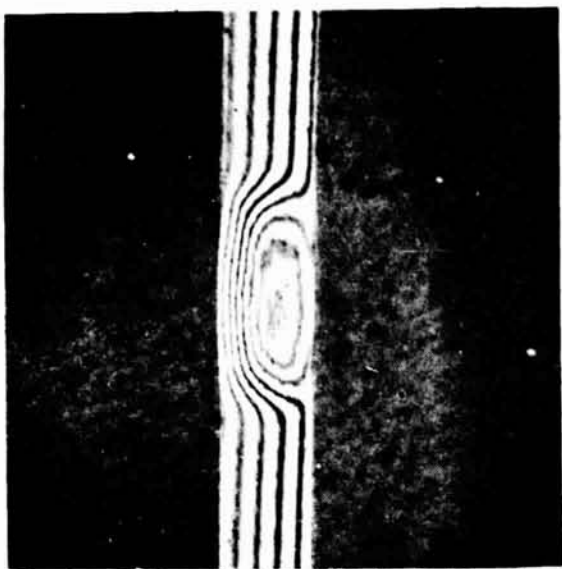


Figure 5-51. Model 104 Seat Showing Groove from 0.001 Inch CRES Wire (462X Interference Photo)

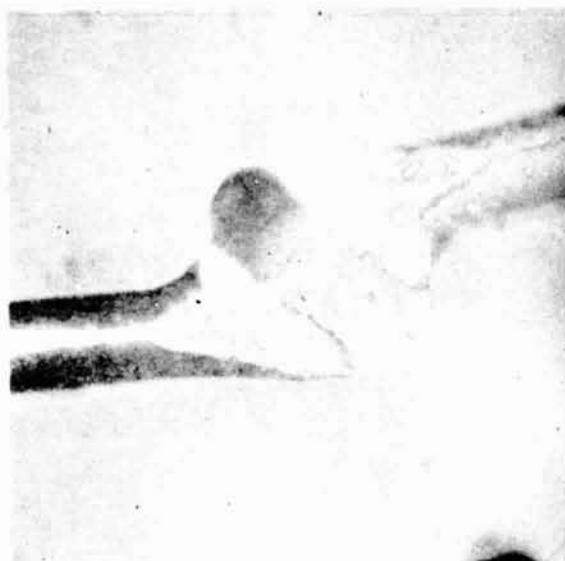


Figure 5-52. Model 104 Test 8
0.001 Inch CRES Wire
(462X Interference Photo)

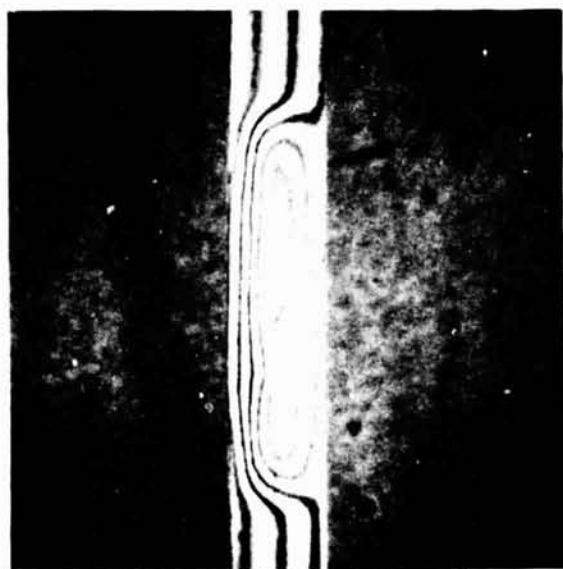


Figure 5-53. Model 104 Seat Showing Groove from 0.003 Inch CRES Wire (462X Interference Photo)



Figure 5-54. Model 104 Test 10
0.003 Inch CRES Wire
(462X Plain Photo)

TABLE 5-2. LEAKAGE CORRELATION DATA, MODEL 105

| PURE CHECK VALVE MODE TEST | | | | SPRING-LOADED CHECK VALVE MODE TEST, 2.0 LB SIMULATED SPRING LOAD | | | | FINAL REBASELINE PURE CHECK VALVE MODE TEST DATA | | | |
|----------------------------------|----------------------------|---------------------------------------|-----------------------------|--|-----------------------------|------------------------|-----------------------------|--|-----------------------------|----------------------------|-----------------------|
| BASELINE CHECK VALVE DATA, HE | | GN ₂ LEAKAGE DATA, SCIM | | INLET PRESSURE, PSIG | | HE LEAKAGE, SCIM | | GN ₂ LEAKAGE, SCIM | | INLET PRESSURE, PSIG | |
| SEAT LOAD, LB. | INLET PRESSURE, PSIG | HE LEAKAGE, SCIM | PREDICTED BY ANALYSIS | ACTUAL TEST DATA | PREDICTED BY ANALYSIS | ACTUAL TEST DATA | PREDICTED BY ANALYSIS | ACTUAL TEST DATA | PREDICTED BY ANALYSIS | INLET PRESSURE, PSIG | HE LEAKAGE SCIM |
| .084 | 1.0 | .0340 | .01493 | .00714 | - | - | - | - | - | 1.0 | .00636 |
| .258 | 2.0 | .0534 | .02335 | .0135 | - | - | - | - | - | 2.0 | .0108 |
| .780 | 5.0 | .0402 | .0166 | .00754 | - | - | - | - | - | 5.0 | .00614 |
| 1.65 | 10.0 | .0140 | .00552 | .00432 | - | - | - | - | - | 10.0 | .00323 |
| 2.084 | 12.49 | .0116 | .00453 | .00289 | 1.0 | .000919 | .000357 | .00232 | - | - | - |
| 2.52 | 15.0 | .00957 | .00371 | .00262 | 3.51 | .00221 | .000857 | .00626 | 15.0 | .00264 | .0070 |
| 2.78 | 16.49 | .00866 | .00339 | .00244 | 5.0 | .00262 | .00102 | .00725 | - | - | - |
| 3.39 | 20.0 | .0070 | .00273 | .00212 | 8.51 | .00297 | .00115 | .00935 | 20.0 | .00210 | .00540 |
| 2.78 | 16.49 | .00847 | .00272 | .00228 | 5.0 | .00256 | .000816 | .00730 | - | - | - |
| 2.52 | 15.0 | .00950 | .00369 | .00240 | 3.51 | .00219 | .000850 | .00580 | 15.0 | .00232 | .00705 |
| 2.084 | 12.49 | .0116 | .00453 | .00269 | 1.0 | .000917 | .000357 | .00216 | - | - | - |
| 1.65 | 10.0 | .0141 | .00556 | .00372 | - | - | - | - | 10.0 | .00316 | .00945 |
| .780 | 5.0 | .0384 | .01582 | .00580 | - | - | - | - | 5.0 | .00567 | .0149 |
| .258 | 2.0 | .0406 | .01729 | .00950 | - | - | - | - | 2.0 | .00875 | .0220 |
| .084 | 1.0 | .0316 | .01396 | .0060 | - | - | - | - | 1.0 | .00640 | .0155 |

ORIGINAL PAGE IS
OF POOR QUALITY

leakage value. The repeated pressure loading cycles of the model throughout the correlation test series resulted in a reduction of the leak path such that the final rebaseline helium leakage values are lower than the initial baseline leakage values. The percentage of rebaseline leakage reduction is comparable with the percentage of reduction of actual versus predicted leakages. At these levels of leakage, a factor of 2 correlations is quite good and, considering the rebaseline leakage reduction, the actual correlation is much better than a factor of 2. These data give confidence in the leakage analyses for predicting leakages for different conditions and/or different gases. A visual presentation of the correlation is presented in Fig. 5-55. It can be seen that the actual values of each test versus the predicted values are lower by the same order as the rebaseline test is lower than the initial baseline test.

Data Correlation and Observations

The cutter seal test series has demonstrated the advantage and limits for the narrow land seal with practical limits placed between 0.00015- and, say, 0.0003-inch width. Manufacturing, finish, and length resistance considerations limit the design on the low side; whereas, cutting loads and high leakage from particle entrapments provide a boundary for the upper dimension. Visual display of the leakage performance and closure load of the cutter model is shown in Fig. 5-56. Data points for these graphs were taken from Table 5-1 to show the effect of wire size and hardness versus seal land width. As might be expected, both leakage and load increase with land width for the noted parameters.

FLAT POLYMER MODEL TESTS

The flat model seal holder was designed to allow evaluation of a single flat sealing surface with minimal influence from mechanical seal retention forces. As illustrated in the Test Model section, the seal material is gripped near the OD by serrated surfaces. The volume of the serrations protruding above the seal plane is equal to the groove volume so that displaced material can be accommodated without distortion of the inner sealing face. The material is retained at the OD so that low-temperature shrinkage will tend to smooth the seal plane.

The basic seal materials evaluated were the perfluoroelastomers (AF-E-124D and 'X supplied by TRW) and Teflon polymers (TFE and FEP). Descriptions of molding and machining experiments leading to the final sealing surfaces evaluated, and photomicrographs of typical polymer material surfaces are covered in the Materials Investigation section.

The test models and summary of leakage results are listed in Table 5-3. Models 201 and 202 were used for preliminary tests with machined AF-E-124D seals which demonstrated the need for smoother surfaces. Model 203, with the seal cut from molded AF-E-124X filled material, demonstrated satisfactory sealing ability under all conditions except with a 0.001-inch wire entrapped. Models 204, 205, 207, and 208 were tests of Teflon seals to compare with the elastomer seals. A Viton elastomeric material of exceptional finish was evaluated as Model 206 to compare with Model 203.

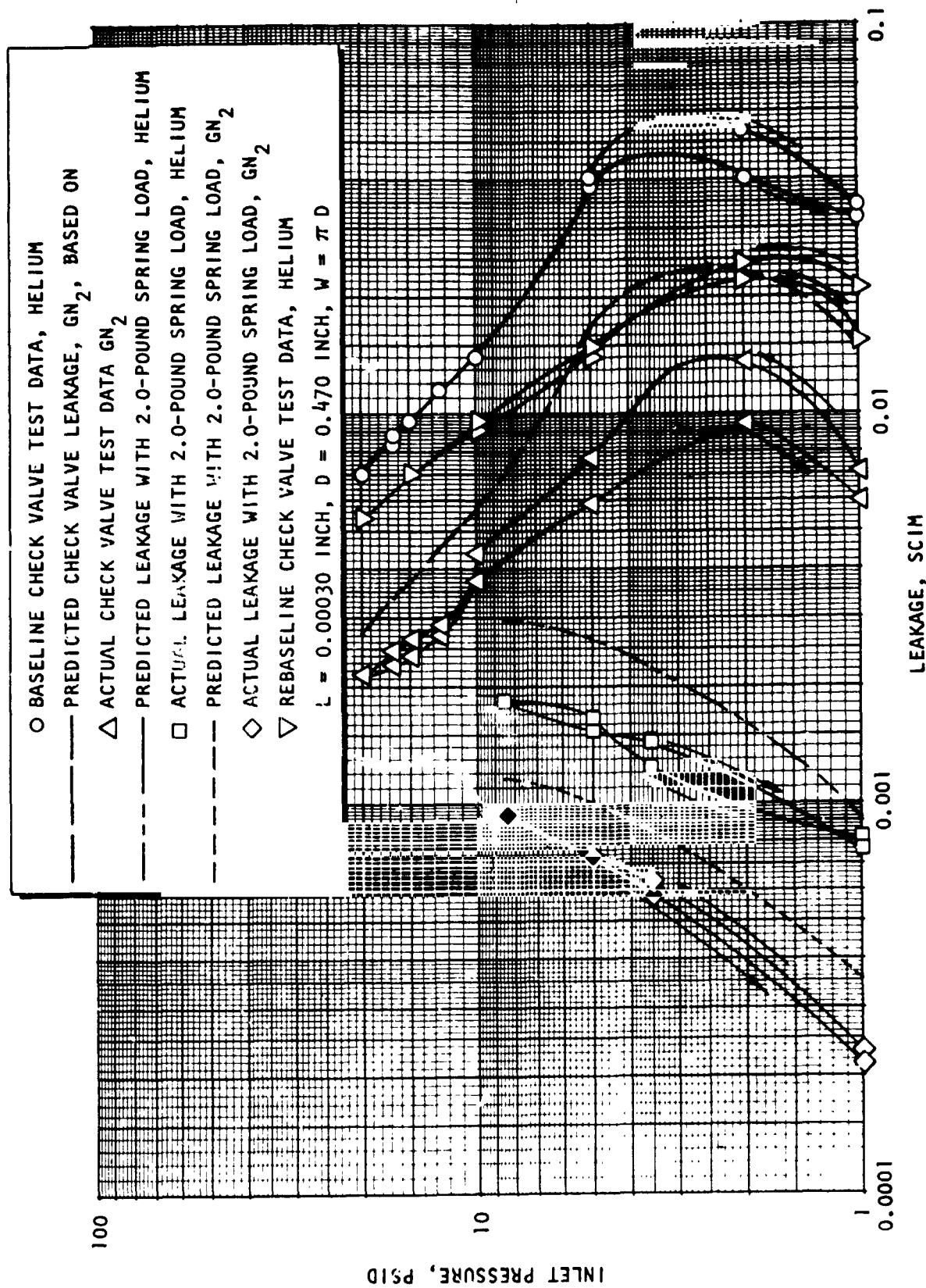


Figure 5-55. Leakage Correlation Plot, Model 105

ORIGINAL PAGE IS
OF POOR QUALITY

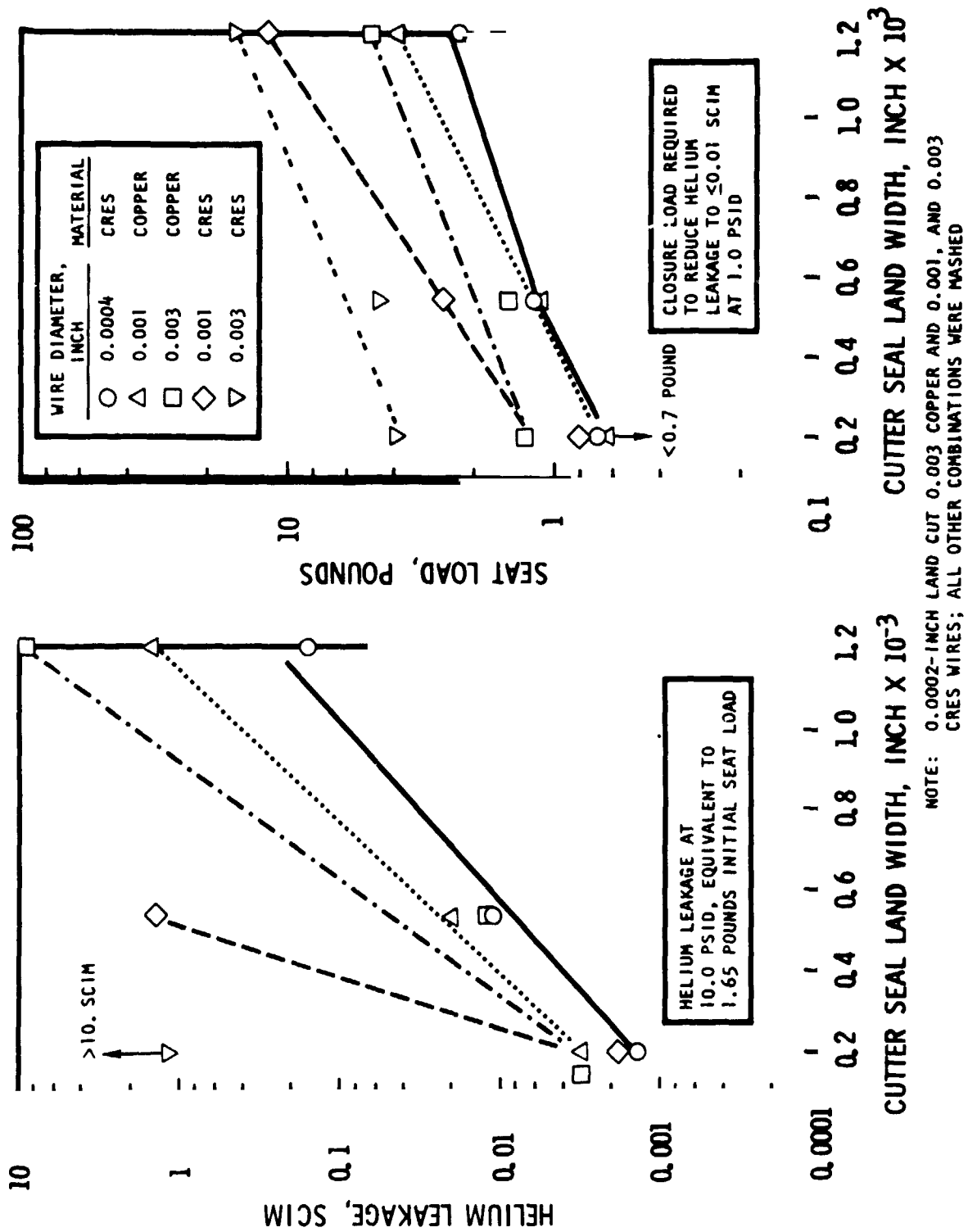


Figure 5-56. Relative Helium Leakage and Closure Load

TABLE 5-3. FLAT POLYMER MODEL TESTS

| MODEL NO. (LAND WIDTH, IN.) | TEST NO. | SEAL DATA | | TEST CONDITION | | | LEAKAGE SCIM HELIUM |
|--------------------------------|----------|--|--|-------------------|---|---|---------------------|
| | | MAT'L | SURFACE FC = FLYCUT N = MOLDDED | TEMPERATURE OF | C = CLEAN W = WITH 0.001 INCH WIRE | REMARKS | |
| 201 (0.03) | 1 | AF-E-124D Seal #2 | FC-16 AA, wavy by approx. 10. micron. per 0.10 in. | 70 | C | These tests demonstrated need for smooth surface for low load sealing | 0.00080 |
| | 2 | | | -15 | C | | 0.50 |
| | 3 | | | 70 | C | | 0.00015 |
| 202 (0.03) | 1 | AF-E-124D Seal #1 | FC-16 AA, wavy by approx. 60 micron. per 0.10 in. | 70 | C | | 0.00086 |
| | 2 | | | -15 | C | | >10. |
| | 3 | | | 70 | C | | 0.00072 |
| 203 (0.03) | 1 | AF-E-124X, White Filled Seal #4 | M-glassy surface, wavy by approx. 30 micron. per 0.10 in. | 70 | C | Chilled closed | <10 ⁻⁴ |
| | 2 | | | -15 | C | Chilled separated | <10 ⁻⁴ |
| | 3 | | | -15 | C | | <10 ⁻⁴ |
| | 4 | | | 70 | C | 4.2 lb req'd to obtain 0.009 scim @ 1.0 psid | <10 ⁻⁴ |
| | 5 | | | 70 | W | | 0.335 |
| | 6 | | | 70 | W | Cannot meet requirement with wire | 0.29 |
| | 7 | | | -15 | W | | 0.85 |
| | 8 | | | 70 | W | | 0.20 |
| | 9 | | | 70 | C | Seal surface sticky, req'd 2.5 lb to separate | <10 ⁻⁴ |
| | 10 | | | -15 | C | | 0.00021 |
| | 11 | | | -15 | C | Surfaces separated & resealed | <10 ⁻⁴ |

ORIGINAL PAGE IS
OF POOR QUALITY

TABLE 5-3. (Concluded)

| MODEL NO. (LAND WIDTH, IN.) | TEST NO. | SEAL DATA | | TEST CONDITION | | LEAKAGE SCIM HELIUM AT 10.0 PSID EQUIV. TO 1.7 LE INITIAL SEAT LOAD |
|--------------------------------|----------|-----------|--------------------------------------|-------------------|---|---|
| | | MAT'L | SURFACE FC = FLYCUT M = MOLDED | TEMPERATURE OF | C = CLEAN K = WITH 0.001 INCH WIRE | REMARKS |
| 204 (0.03) | 1 | TFE | FC-16AA | 70 | C | Leakages reduced at higher pressures, surface too rough |
| | 2 | | | -15 | C | 0.03 |
| | 3 | | | 70 | C | 0.03 |
| | 4 | | | 70 | N | ~5. lb req'd to obtain 0.007 scim @ 1.0 psid |
| | 5 | | | 70 | C | Permanent groove 0.18 |
| 205 (0.03) | 1 | TFE | FC6M @ 350F | 70 | C | Wavy surface 0.07 |
| 206 (0.03) | 1 | VITON-E | M-glassy surface | 70 | C | <10 ⁻⁴ |
| | 2 | | | 70 | N | 0.14 |
| 207 (0.03) | 1 | FEP | FC6M @ 400F | 70 | C | Not flat, sealed on poppet OD corner <10 ⁻⁴ |
| 208 (0.03) | 1 | FEP | FC6M @ 400F | 70 | C | Flat on captive model base 0.0041 |
| | 2 | | | 70 | N | 0.15 |
| | 3 | | | 70 | C | Permanent groove 0.040 |

In all tests with the perfluoroelastomer seals, it was found that a positive load was required to separate the flat-lapped poppet from the seal face. This load ranged from 1.5 to 2.5 pounds, equivalent to 34- to 56-psi seal stress (Table 5-3). This sticking effect could increase in a check valve and cause excessive cracking pressure.

Models 201 and 202 With AF-E-124D Seals

Preliminary tests were performed with Model 201 to establish load-deflection data for AF-E-124D seals in the flat model. The wave washer load required to deflect the seal at the serrations 0.005 inch at each surface was measured in the static tester (Ref. 1). The results of loading to 0.0094-inch deflection, and permanent set when left at this deflection for 11 days, are shown in Fig. 5-57. The wave spring force was set subsequently at 16.2 pounds to maintain the noted deflection, and this force was used for all succeeding tests.

The force required to deflect the same AF-E-124D flat seal in the seat area was measured using a flat poppet with 0.03-inch-wide land and 0.470-inch mean diameter. A positive stop was machined to limit seal deflection to 20 percent of the seal thickness. Data of Fig. 5-58 show that the seal is deflected on the order of 0.0005 inch with about 1.0 pound of seat load.

Test data for Models 201 and 202 are shown in Fig. 5-59 and 5-60. Each model sealed reasonably well at ambient temperature, but failed to seal adequately at -15 F. Cause of the high leakage was traced to a wavy condition in each seal and almost complete loss of elasticity of the seals at -15 F. Model 201 seal had surface thickness variation of about 0.0001 inch per 0.1 inch, while Model 202 had variations of up to 0.0006 inch per 0.1 inch. This excessive waviness was caused by recutting these two seals with the diamond flycutting tool using doubleback tape on the vacuum chuck face. The seals were initially flycut directly on the chuck face to a thickness of 0.0300 inch using a carbide cutter, but the surface was too rough; the seals were therefore recut as noted. These tests demonstrated the need for improved seal surface geometry.

Model 203 With AF-E-124X Seal

White-filled AF-E-124X material molded by TRW had a glassy surface over a portion of the 3.5-inch sheet. One surface was flycut and seals were cut from selected areas to maintain thickness variation within 30 μ in. per 0.1 inch in the glassy surface area.

Basic leakage results with the seal were excellent, as shown by the data of Table 5-3 and Fig. 5-61. Even at -15 F, the leakage was less than 10^{-4} , although an initial high leakage was recorded for Test 3 when the seal was chilled with surfaces separated. The resulting 0.8 scim leak at 1.0 psid corresponds to a theoretical gap of about 0.0002 inch. At 6.0 psid (equivalent to a net seat force of 1.0 pound), the gap was closed.

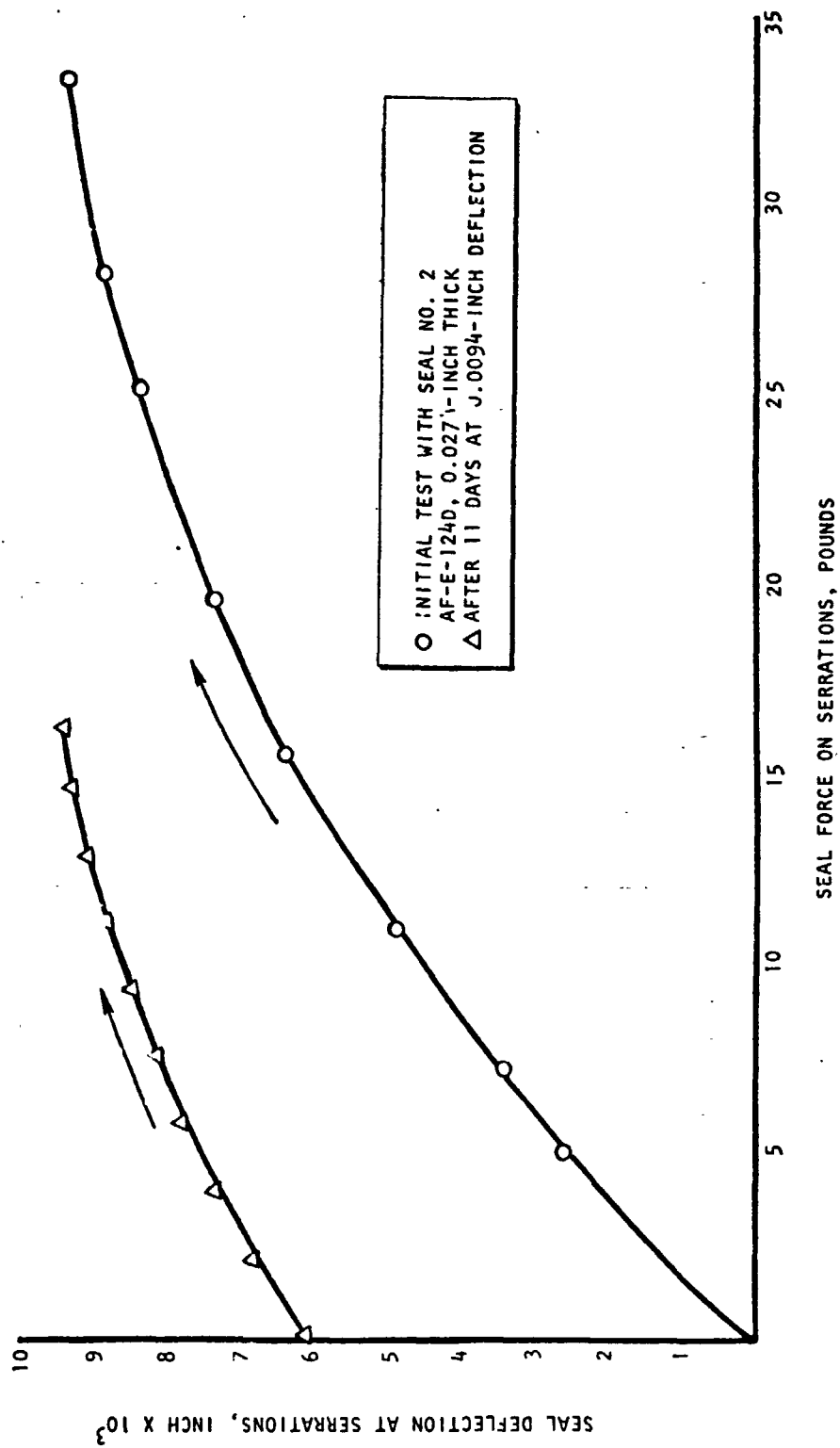


Figure 5-57. Seal Serration Force Deflection

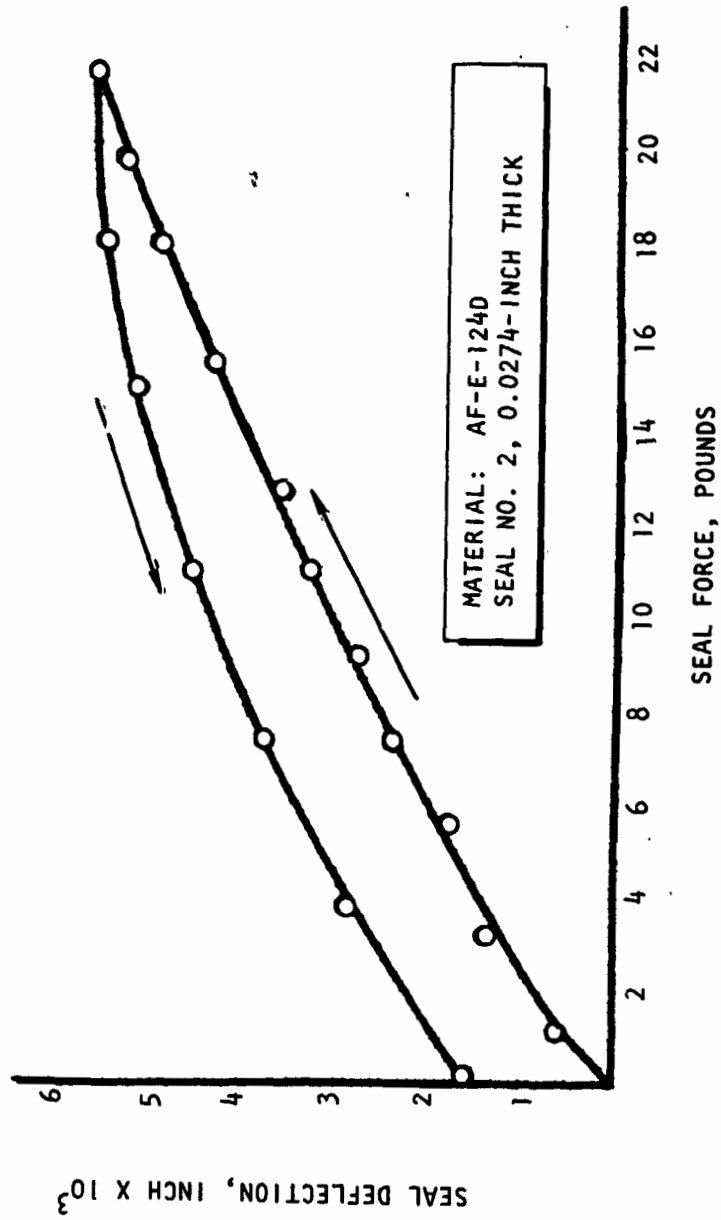


Figure 5-58. Flat Seal Force Deflection

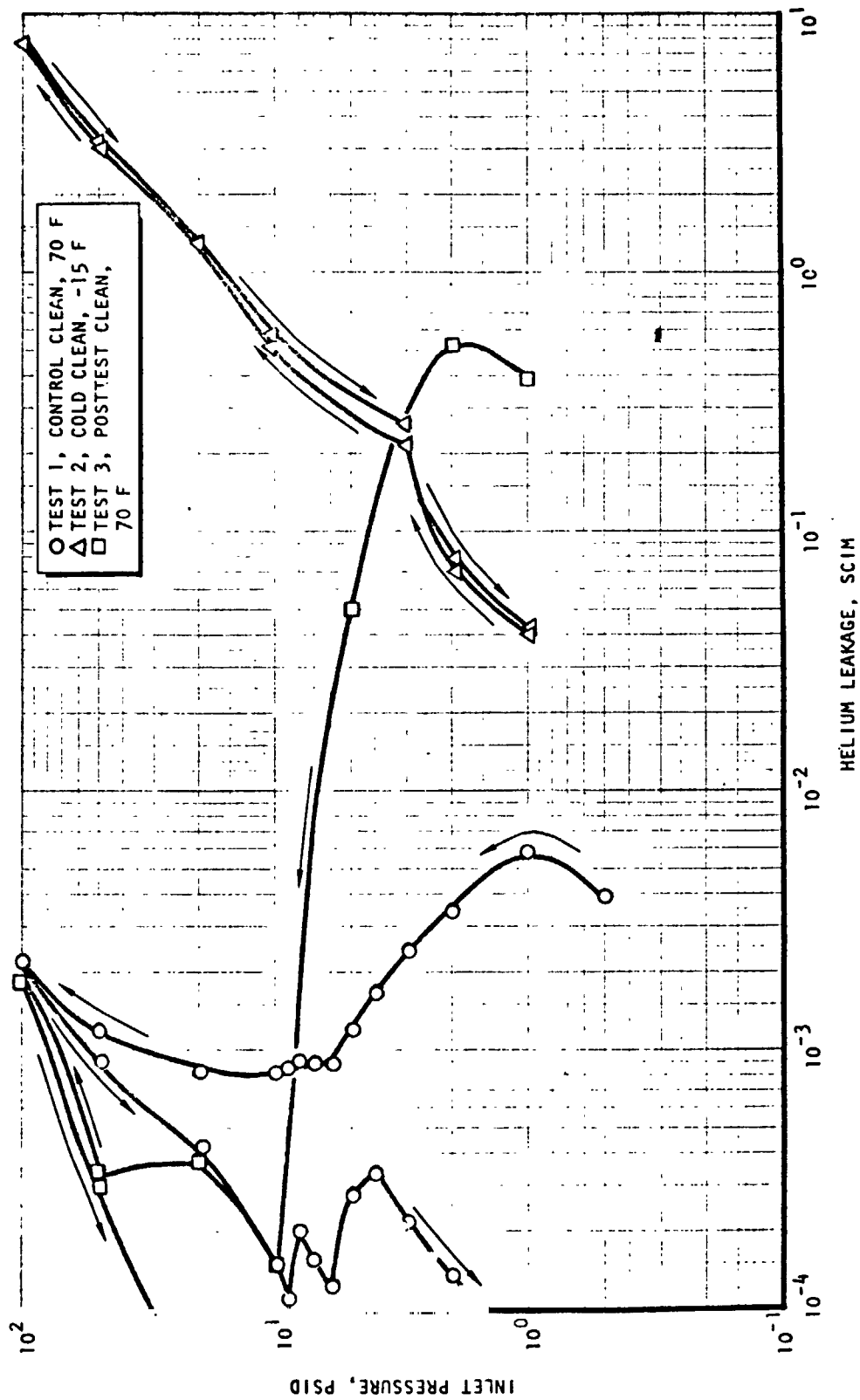


Figure 5-59. Leakage Data for Model 201, Tests 1 Through 3

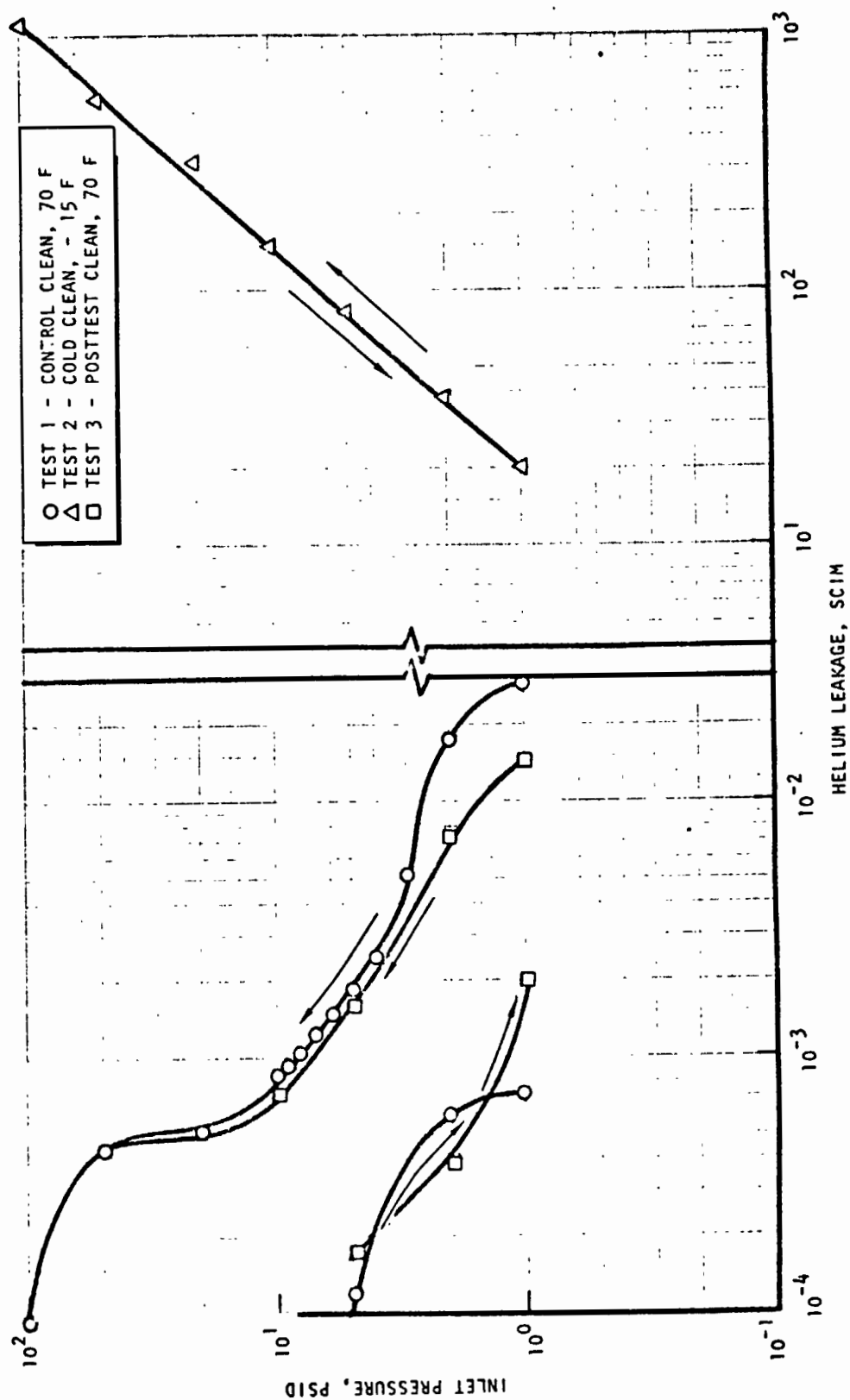


Figure 5-60. Leakage Data for Model 202, Tests 1 Through 3

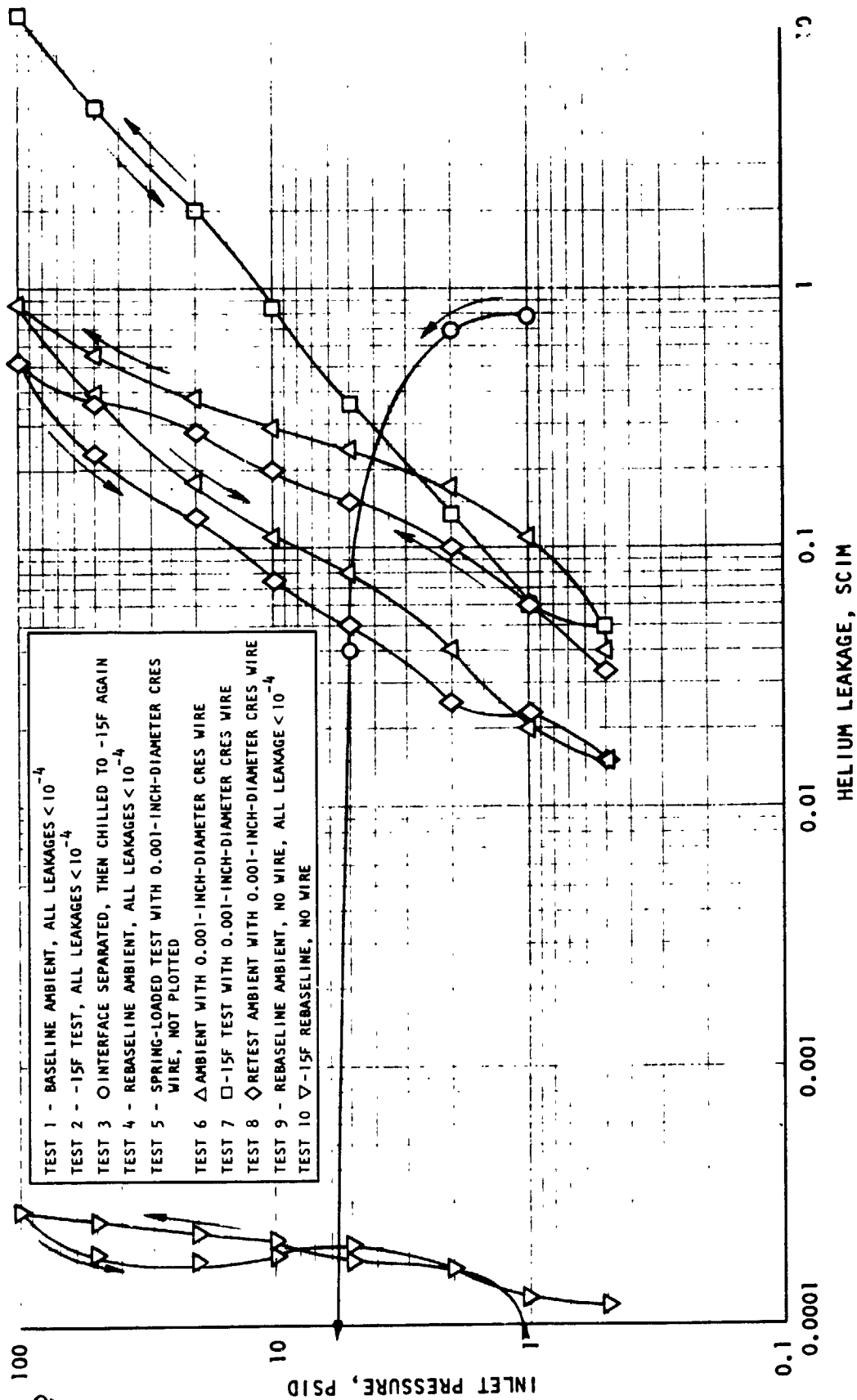


Figure 5-61. Leakage Data for Model 203, Tests 1 Through 10

ORIGINAL PAGE IS
OF POOR QUALITY

The elastomer seal was unable to seal adequately with a 0.001-inch CRES wire crossing the 0.03-inch-wide poppet land, either at ambient or -15 F temperatures. The test results (Fig. 5-61) show that increasing load of higher pressures did not close off the leak path caused by the wire. However, the seal did function satisfactorily after removal of the wire (Tests 9 and 10). The measurable leakage of Test 10 in the range of 0.0001 to 0.0002 scim below 10.0 psid shows the effects of a permanent groove in the elastomer that was measured as about 30 to 50 μ in. deep by about 0.005-inch wide. These dimensions correspond closely with predicted flow.

Models 204 and 205 With TFE Seals

Flat TFE seals were made by flycutting sheet stock using the vacuum chuck. Surfaces were parallel within 0.0001 inch, but the surfaces were too rough for light load sealing. This is shown by the data of Fig. 5-62. Leakage values were in the range of 10^{-1} to 10^{-2} scim at ambient and -15 F temperatures up to 100 psid (Tests 1 through 3). With a 0.001-inch CRES wire across the land, leakage was excessive and, with 5.0-psid inlet pressure, seal loads of 5 to 20 pounds produced leakages of from 0.03 to 0.01 scim. Test 5 showed the effect of a permanent groove in the Teflon with removal of the wire. Ambient-temperature leakage ranged from 0.5 to 3.0 scim with pressures of 1.0 to 100.0 psid.

Model 205 was used in an attempt to improve the TFE surface by molding the machined seals in steel washers at 350 F (described in the Materials Investigation section). The resultant surfaces, although improved, were excessively wavy and there was negligible improvement of the performance compared with Model 204.

Models 207 and 208 With FEP Seals

FEP Teflon is notable for its moldability; therefore, flycut seals were molded in the steel washers, similar to the TFE seals of Model 205 but at 400 F. The resultant surfaces were considerably improved but still retained machining lines and were visibly wavy.

Initial tests were performed with one seal as Model 207. It was determined, however, that the wave washer load was inadequate to impress the serrations into the seal. The seal was therefore raised up from the seat base by several thousandth inch. This caused the flat poppet corner radius to dig into the seal under load with the unrealistic results shown in Fig. 5-63.

The test was repeated with a second seal (Model 208), using the captive model base. The seal base was greased lightly to allow leakage at only the poppet/seal interface. The improved flat surface is evident from baseline ambient Test 1 (Fig. 5-64). As expected, however, the 0.001-inch CRES wire could not be tolerated by the Teflon seal (Tests 2 and 3).

Improvement in flatness and finish is required to obtain low load leakage with Teflon comparable with the elastomer seals. This can be achieved by diamond tooling with a circular lay or molding at high pressure (and temperatures) in a

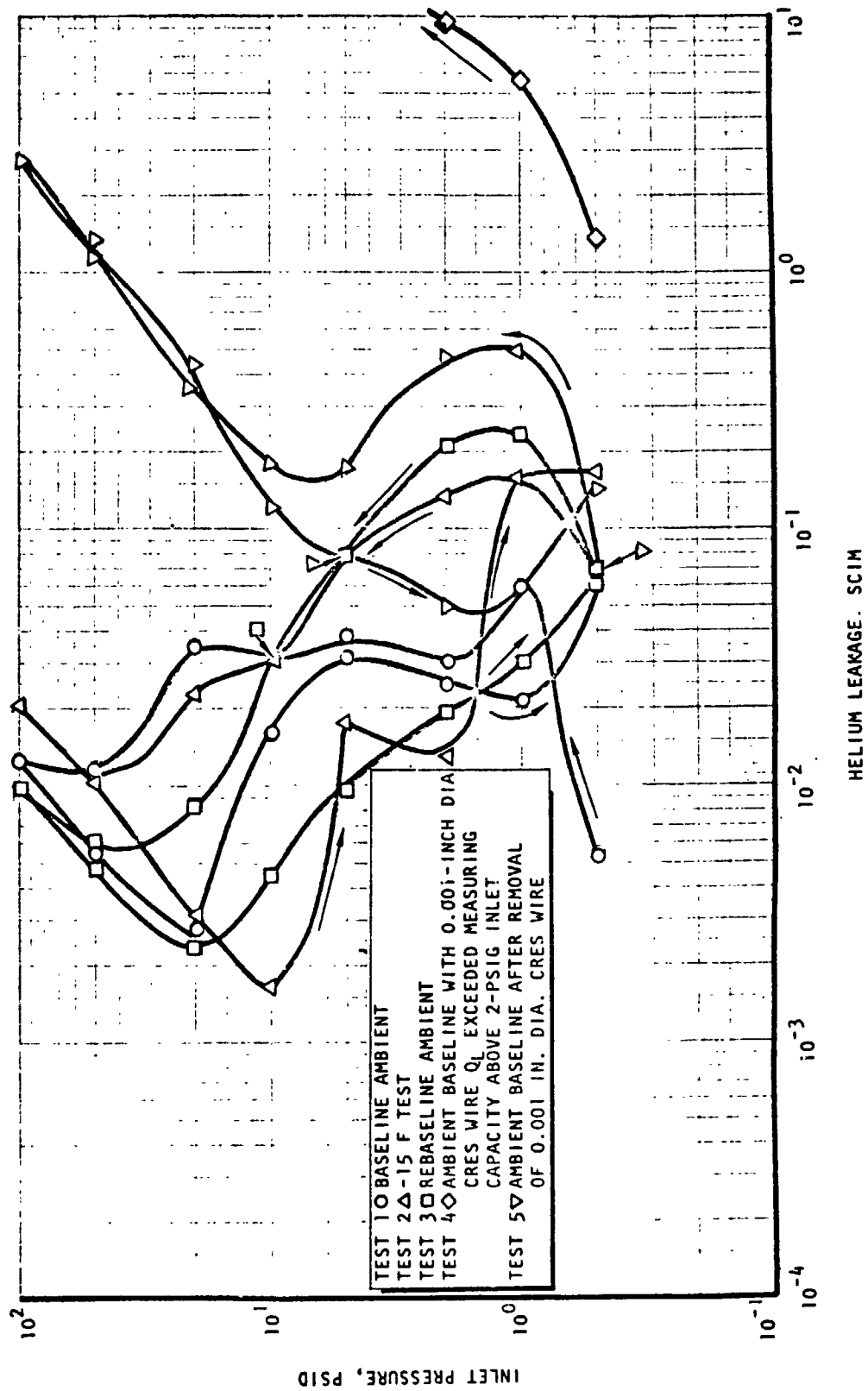


Figure 5-62. Leakage Data for Mode 204, Tests 1 Through 5

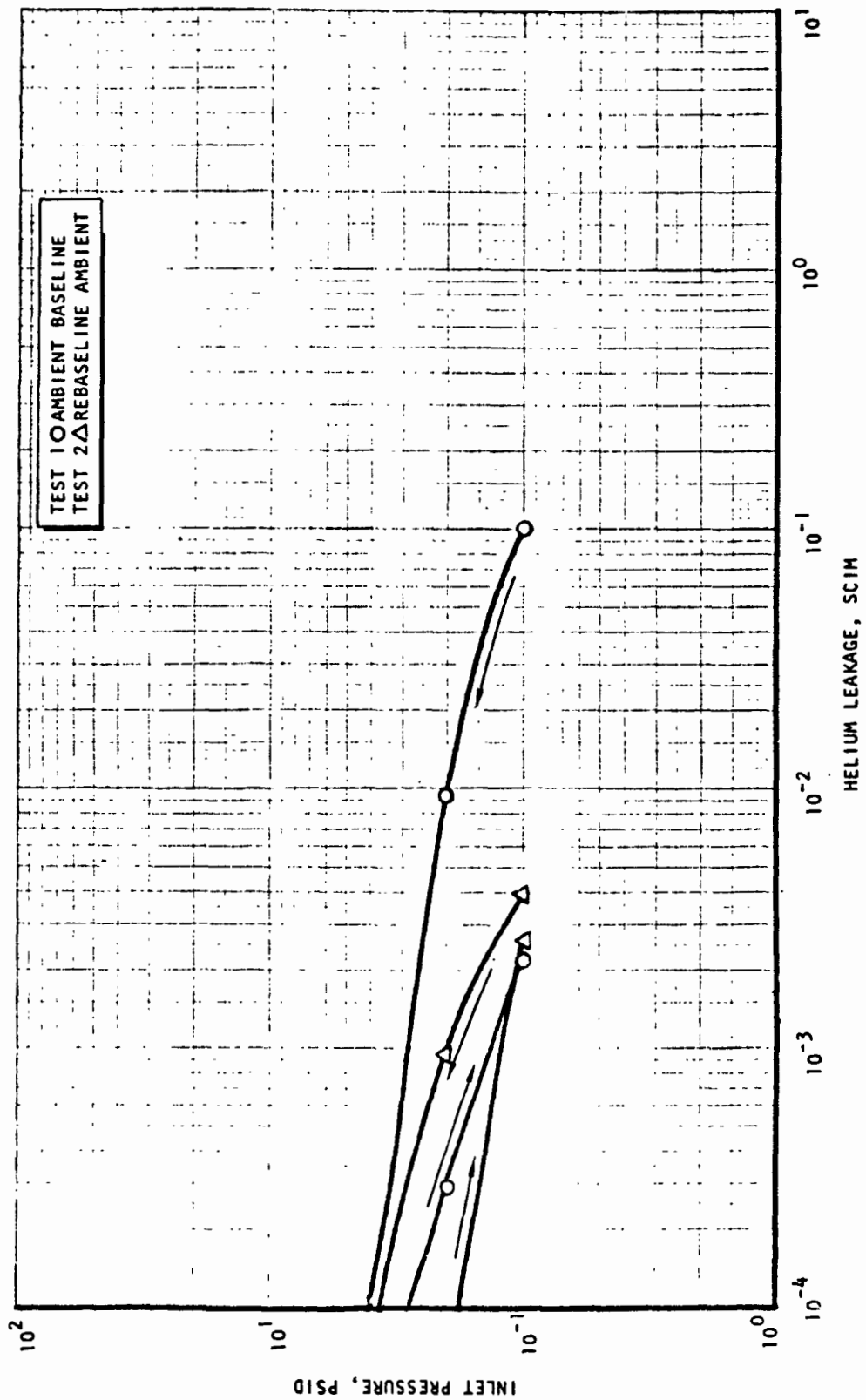


Figure 5-63. Leakage Data for Model 207, Tests 1 and 2

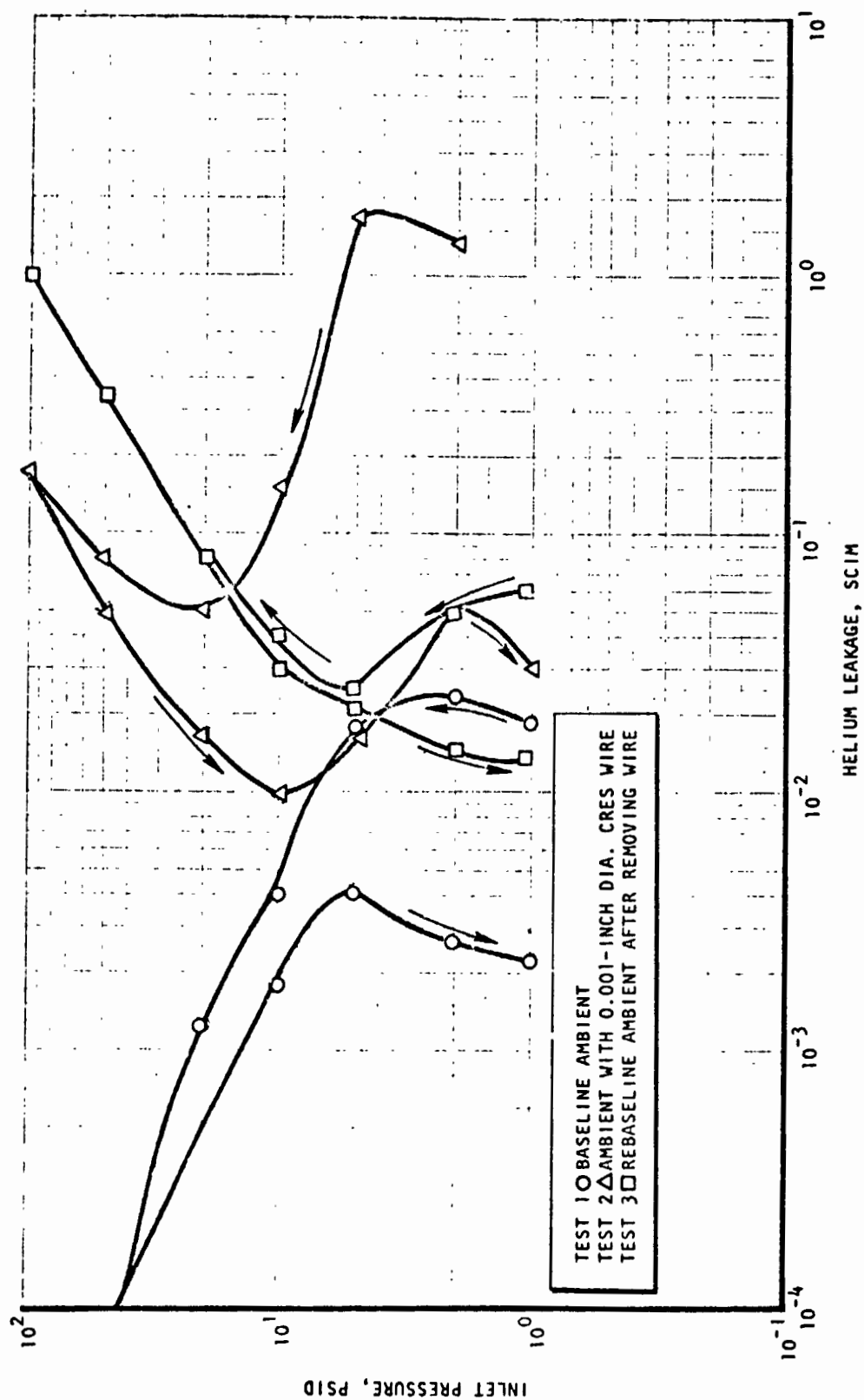


Figure 5-64. Leakage Data for Model 208, Tests 1 Through 3

totally contained die, as described in the Materials Investigation section. However, this material is subject to permanent damage from entrapped particles which may or may not become embedded in the seal.

Model 206 With Viton Seal

During the early molding experiments by TRW, a sheet of Viton elastomer was molded to proof the mold surfaces. The resultant sheet was glassy in appearance with an almost perfect reproduction of the polished chrome mold surfaces. A seal was cut from this material and tested to compare with previous models, particularly Model 203. The results, shown in Fig. 5-65, are similar to Model 203 (AF-E-124X seal, which had an equally good molded surface), but leakage was excessive with the 0.001-inch CRES wire entrapped.

Observations

Tests with the flat seals have demonstrated the sealing advantages of the elastomeric seals over Teflon and the need for flat, smooth surfaces to obtain low load sealing. A more narrow poppet land would reduce the load necessary for a given deflection but at the expense of contamination resistance. Multiple lands would improve particle resistance and, with sufficient width between grooves, could provide protection against wire-like contaminants. Furthermore, reduction of the land area would reduce the sticking characteristic of the elastomer seals, but this problem should be considered for low cracking pressure requirements.

The tests performed were limited, and additional effort is required to provide detailed static and cyclic data over a broad temperature range with contaminant particles.

CAPTIVE POLYMER MODEL TESTS

The captive polymer seal model utilizes a flat seal contained by inner and outer floating retainers (see Test Models). The flat polymer seal land is 0.03-inch wide and is overlapped by a wider flat-lapped poppet surface. The concept thus provides for seal containment with high loading. Initial assembly and tests with Models 301, 302, and 303 showed that the free position of the retainers was above the seal face by several thousandths inch. This condition may be desirable for maximum seal protection and contaminant with higher load valves, but these preliminary tests indicated that up to 2.0 pounds was required to force the poppet onto the elastomer face. The retainers were therefore reworked to locate the seal about 0.005 inch above the retainers.

Captive seal testing generally followed the flat seal tests and, therefore, benefited from the experience gained. The AF-E-124X seal evaluated was flycut on one side and had a glassy molded surface on the narrower seal side. Teflon seals were flycut on both sides and heat formed in place.

A summary of the models tested is listed in Table 5-4. As shown, the results are similar to the flat model.

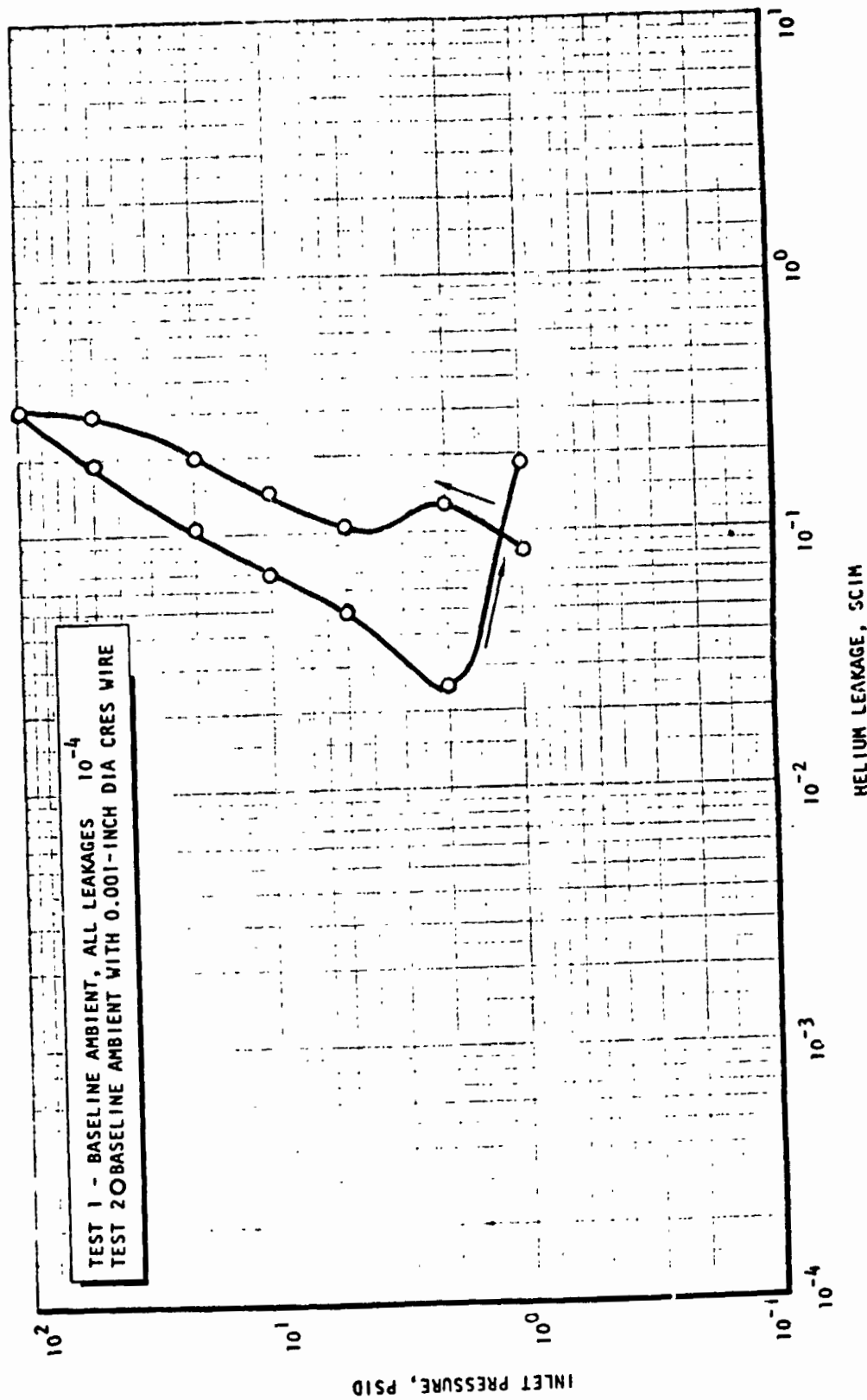


Figure 5-65. Leakage Data for Model 206, Tests 1 and 2

TABLE 5-4. CAPTIVE POLYMER MODEL TESTS

| Model No. (Land Width, in.) | Test No. | Seal Data | | Test Condition | | | Leakage SCIM Helium |
|-----------------------------------|-------------|--------------------------|--|----------------|---|--|--|
| | | Material | Surface FC = Flycut M = Molded | Temperature, F | C = Clean W = With 0.001 Inch Wire | Remarks | At 10.0 psid Equivalent to 1.7 lb Initial Seat Load |
| 304 | 1 | AF-E-124X Seal No. 10 | M-glassy surface, no retainers | 70 | C | All tests 50 psid maximum | 0.00054 |
| | 2 | | | -15 | C | Chilled closed | 0.00063 |
| | 3 | | | -15 | C | Seal separated (~1.0 lb) and resealed | 0.0017 |
| | 4 | | | 70 | C | Rebaseline | 0.00080 |
| | 5 | | | 70 | C | After 24 hours in RFNA (seal blew at 50 psid) | 0.00015 |
| 305 | 1 | AF-E-124X Seal No. 10 | M-glassy surface, ~0.005 in. above retainers | 70 | C | 1.0 lb to separate | <10 ⁻⁴ |
| | 2 | | | -15 | C | 4.9 lb to separate | <10 ⁻⁴ |
| | 3 | | | -15 | C | Seal separated and resealed | <10 ⁻⁴ |
| | 4 | | | 70 | C | Rebaseline | <10 ⁻⁴ |
| | 5 | | | 70 | W | | 0.17 |
| | 6 | | | 70 | W | ~4.0 lb to obtain 0.025 scim at 10 psid | --- |
| | 7 | | | -15 | W | 4.9 lb to separate | 0.06 |
| | 8 | | | 70 | W | | 0.08 |
| | 9 | | | 70 | C | | <10 ⁻⁴ |
| 306 | 1 | TFE Seal No. 1 | M-heat formed in place at 300F | 70 | C | Wavy surface | 0.34 |
| | 2 | | | 70 | C | After 600 lb load for 24 hours | 0.033 |
| | 3 | | | 70 | W | Leakage exceeded tester capacity | >10 |
| 307 | 1 | TFE Seal No. 1 | M-flash trimmed from base | 70 | C | Permanent groove from Model 306, Test 3 | 0.32 |

ORIGINAL PAGE IS
OF POOR QUALITY

Models 304 and 305 With AF-E-124X Seal

To demonstrate performance comparable with the flat model using the best AF-E-124X material, an initial test was performed without retainers. The test was therefore limited to 50-psid inlet pressure. Test results with the model were quite good, as shown in Table 5-4 and Fig. 5-66. Approximately 1.0 to 1.5 pounds were required to separate the poppet and interface in each test. Loss of stickiness was noted in immersion tests of this material in RFNA; therefore, the seal was exposed to the acid for 24 hours, cleaned in alcohol, and vacuum degassed for several hours. There was negligible change in the seal from the RFNA exposure (as shown by Test 5) but the poppet-to-seal separation load was decreased to less than 0.4 pound.

A complete test series was run with the same seal as Model 305, using the seal retainers (Fig. 5-67). Performance was similar to the flat Model 203 except that seal separation loads after cold Tests 2 and 7 were 4.9 pounds. For these tests, the seal was preloaded to 2.5 pounds during chardown. Once separated and re-seated cold, the separation load was negligible (Test 3). As with the flat seal, adequate sealing could not be obtained with an entrapped 0.001-inch CRES wire.

Models 306 and 307 With TFE Seal

Model 306 represented the only attempt to evaluate the captive concept with Teflon. The seal was heat formed in place (in the model) under a 350-pound load (approximately 8000-psi stress) at 300 F. The resultant surface was smooth but wavy and tapered, with the ID approximately 0.0006 inch higher than the OD. Initial sealing performance was not acceptable, as shown in Fig. 5-68. The seal, therefore, was loaded to 600 pounds at 70 F for about 20 hours, which somewhat improved performance (Test 2). The model was not capable of sealing with an entrapped 0.001-inch CRES wire, Test 3.

Posttest disassembly of Model 306 revealed that TFE had extruded into the clearance between the retainers and seal base. This flash was removed and the seal retested as Model 307. The results were substantially the same as Test 1 of Model 306.

OBSERVATIONS

The sealing investigation model tests clearly demonstrated the superiority of the cutter seal concept compared with the polymer model seal technology uncovered and developed herein for meeting the OMS check valve requirements. Insensitivity to temperature extremes, propellant degradation and contaminant entrappings are advantages for the cutter design whereas the elastomer seal suffers in these areas. On the other hand, the two tests with AF-E-124X using flat Model 203 and captive Model 305 have indicated a strong potential for this material, even though only one molded surface was obtained which performed adequately. However, much additional testing is required to fully define the capabilities and limitations of this material because of the additional factors that can affect its sealing performance.

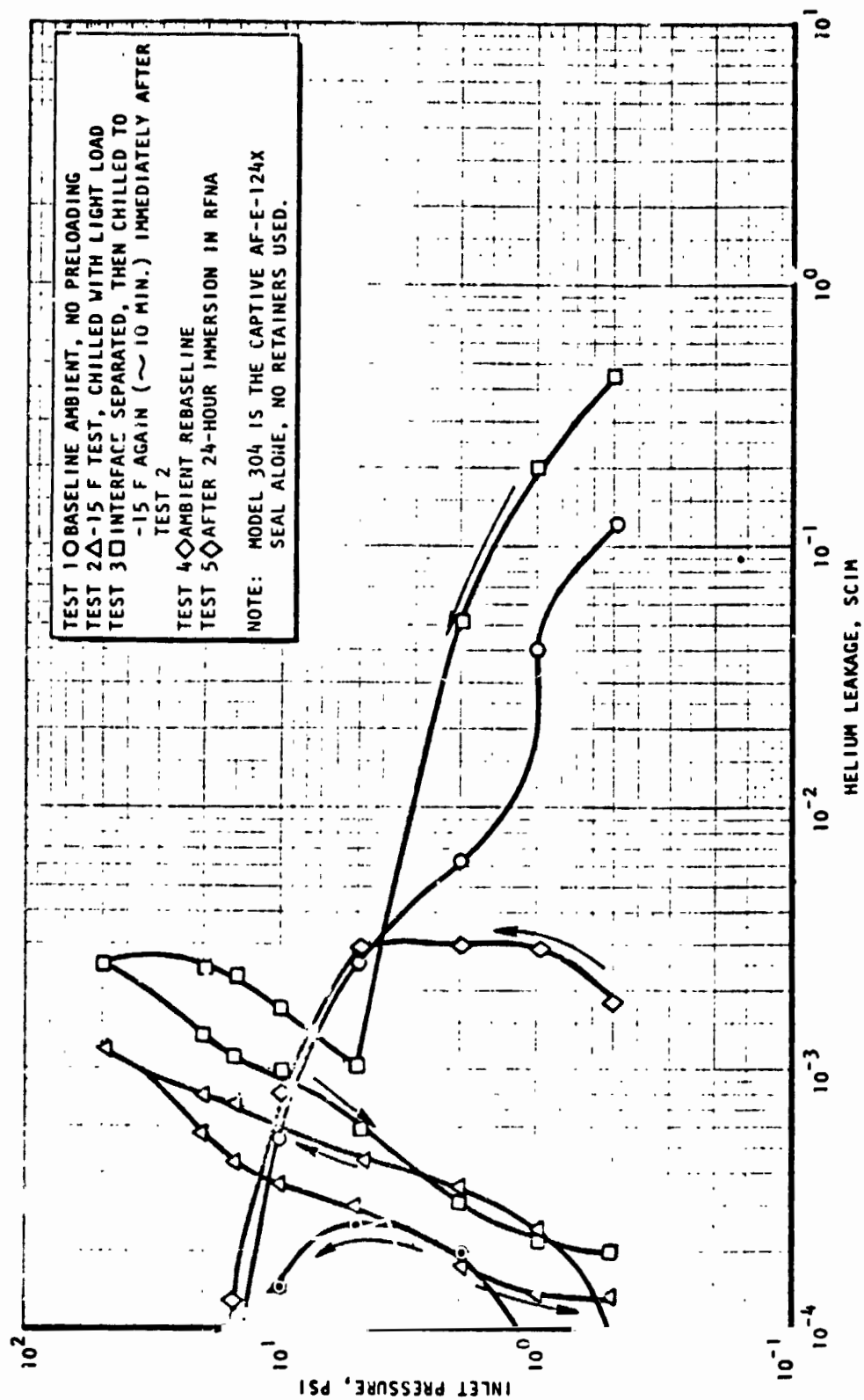


Figure 5-66. Leakage Data for Model 304, Tests 1 Through 5

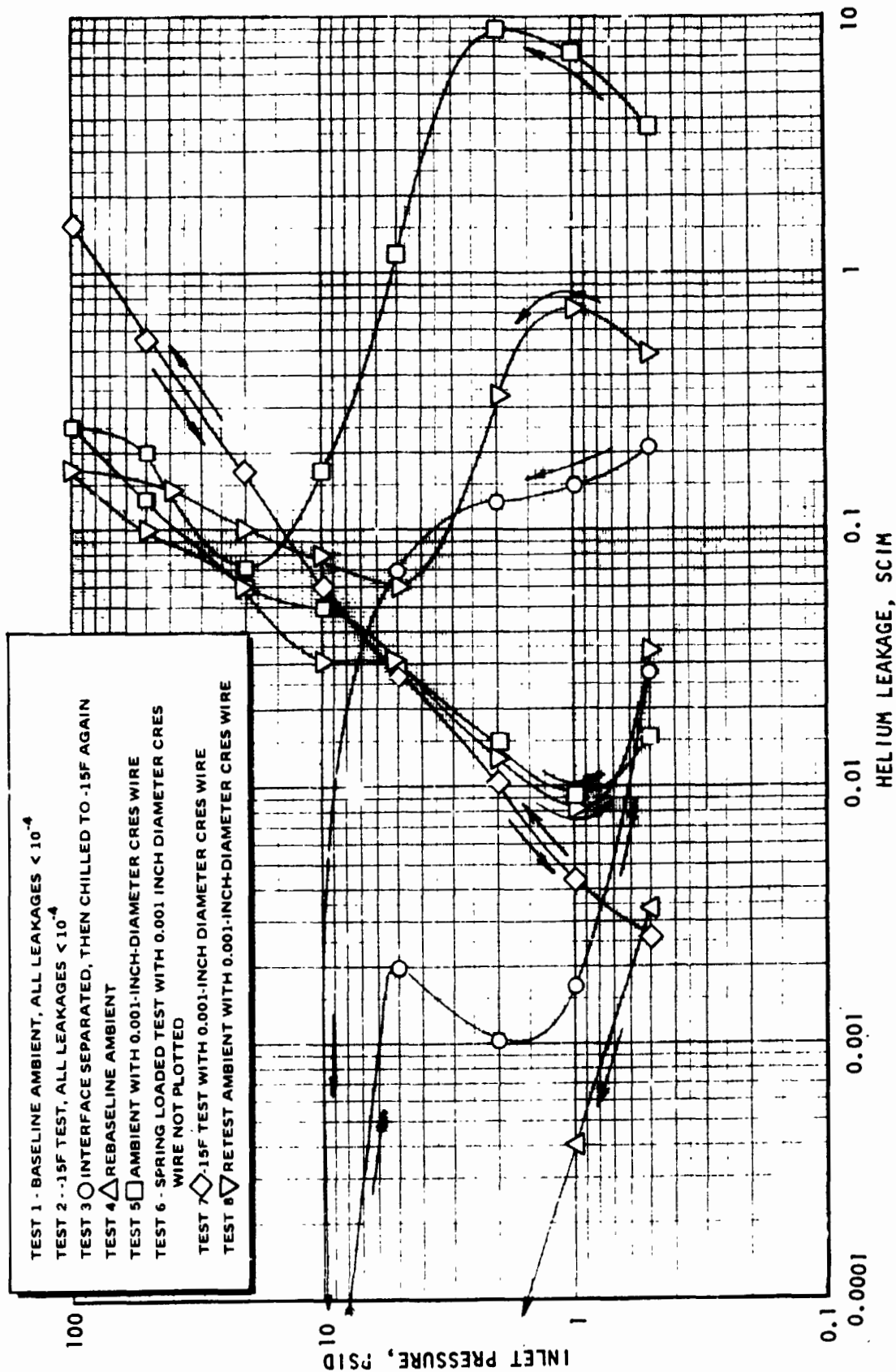


Figure 5-67. Leakage Data for Model 305, Test No. 1 Through 8

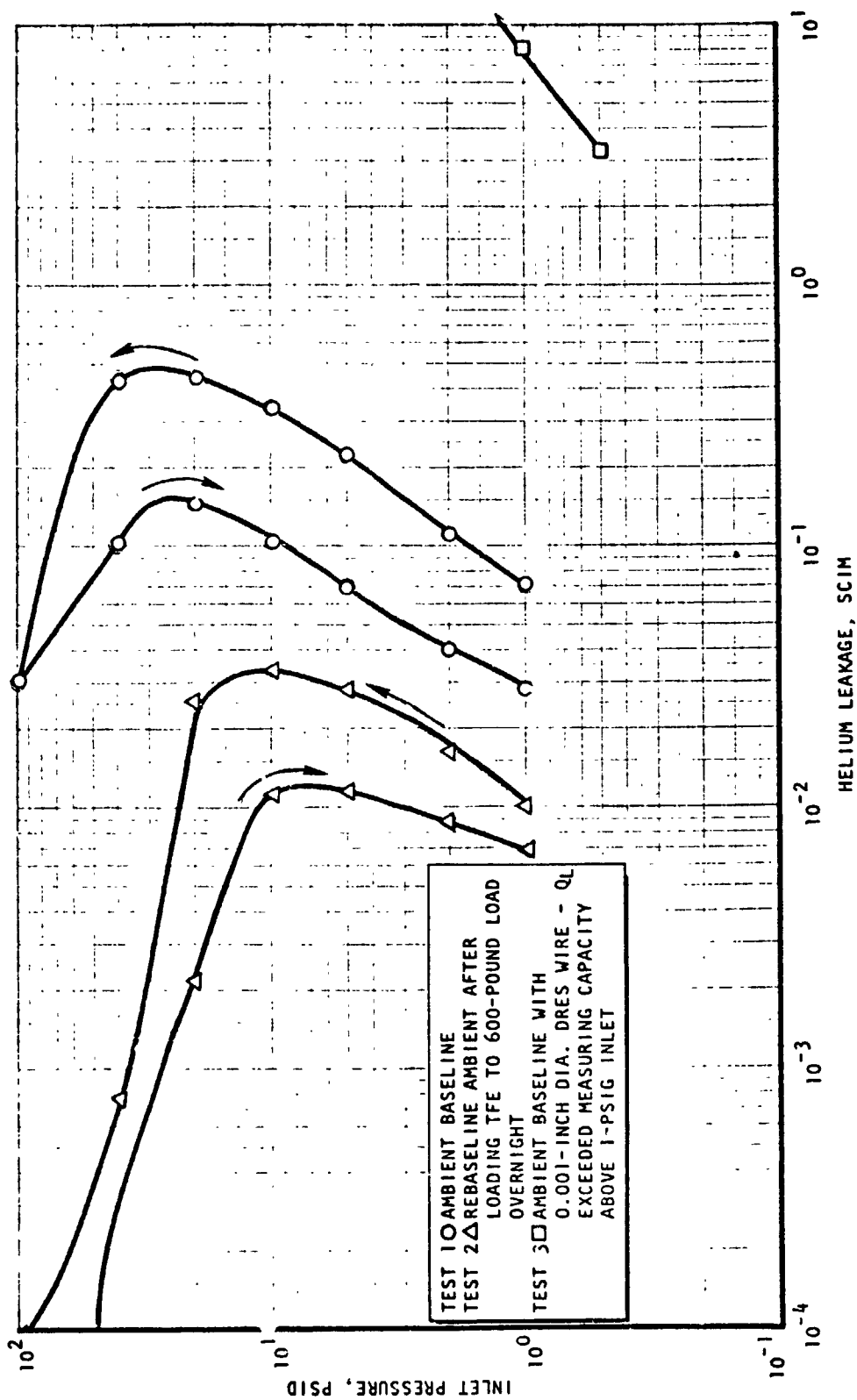


Figure 5-68. Leakage Data for Model 306, Tests 1 Through 3

CHECK VALVE DEVELOPMENT

Design and development of a prototype check valve was undertaken to provide further data toward obtaining an optimized quad propellant check valve for OMS/RCS application. Trade studies were performed in review of past state of the art, but the stringent requirements and goals set forth for the valve (Appendix A) clearly indicated need for a new approach to check valve closure and sealing.

Application of concepts developed in the sealing investigations with the trade study and subsequent design work led to a unique check valve design incorporating the cutter seal concept. Detail parts were fabricated for a single prototype check valve element with spare poppets and seats.

A series of tests was performed with the prototype valve to demonstrate basic functions and full-flow stability. Primary development effort was directed toward demonstrating satisfactory cycle life. Initial cycle tests revealed insufficient poppet hardness, which limited cycle life. An additional spare poppet and seat were fabricated having greater hardness under a separate follow-on contract. These parts were ultimately employed in a final cycle test of 100,000 cycles in which leakage throughout the test was less than 0.001 scim (1.0 scc/hr) helium.

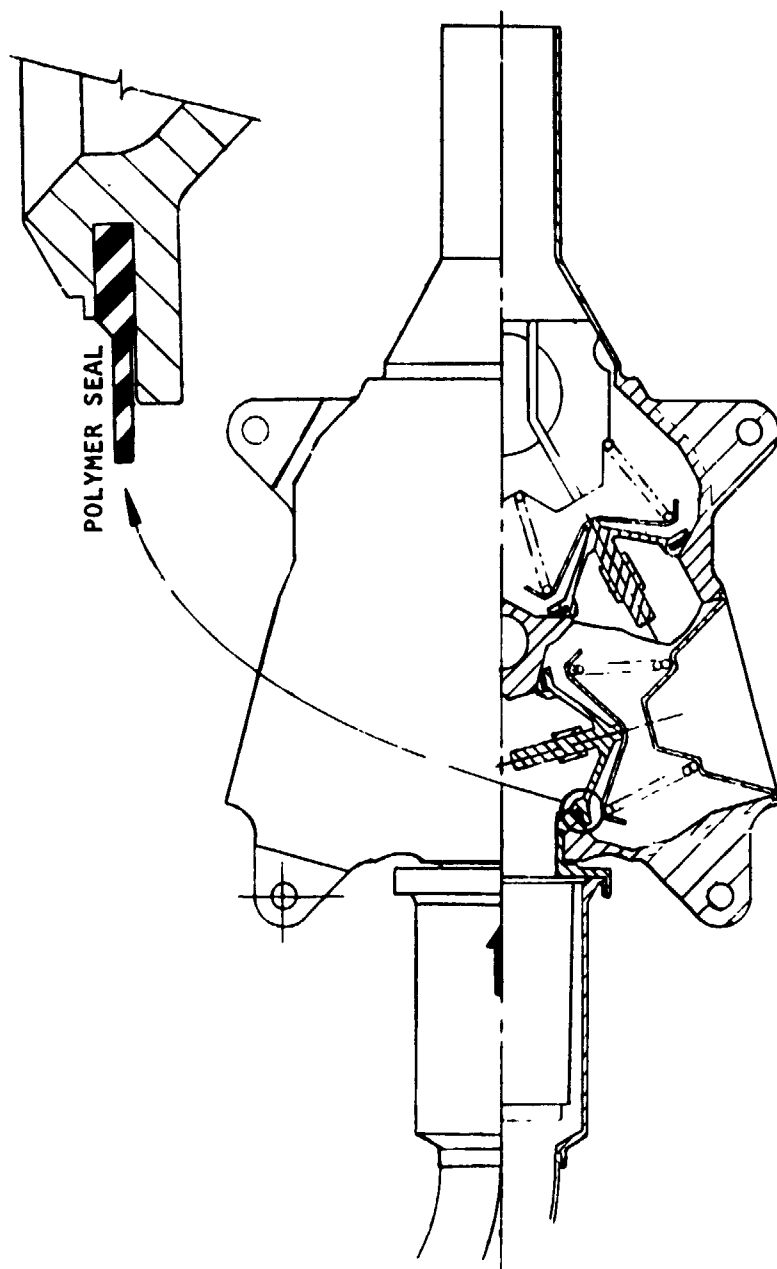
Details of the trade study, valve design, fabrication, and discussion of the test results follows.

TRADE STUDY

During the sealing investigation tasks a concurrent trade study of sealing and closure concepts was performed to identify the best approach for use in a prototype check valve capable of meeting the goals defined in Appendix A. The trade study was accomplished through a systematic evaluation of current state of the art and elemental concepts defined in the program. From past sealing studies, it was reasonably certain that sealing goals could be achieved as an individual function. Obtaining the desired performance with contaminants and propellant residues in a high vibration, extreme temperature environment for thousands of cycles with light sealing load attendant with 1-psig cracking pressure was yet to be achieved in any check valve.

The Apollo valves, utilizing TFE and nitroso rubber, had numerous sealing and function problems; these are summarized in Fig. 6-1. The inability of nitroso rubber to tolerate extreme low temperature, its incompatibility with MMH, and the relative stiffness of TFE eliminated these materials for the seat seal. Tests in the sealing investigations uncovered major disadvantages with AF-E-124D and other perfluoro-elastomers as follows:

1. Material becomes hard below +20 F
2. Contamination sensitivity at low temperature
3. Composition and molding technology was in a state of flux throughout the program; reproducibility was, therefore, questionable.



| PROBLEMS | | |
|---|---|---|
| LEAKAGE <ul style="list-style-type: none"> • SEAL COMPRESSION SET • SOLID PARTICLE ENTRAPMENT • PROPELLANT RESIDUE • SEAL INCOMPATIBILITY TO FLUIDS • LOW TEMPERATURE DEGRADATION | POPPET STICKING <ul style="list-style-type: none"> • CYLINDRICAL GUIDES • SELF GENERATED CONTAMINANTS • PROPELLANT/FLUSH RESIDUE • FOULING | POPPET INSTABILITY (BUZZING) <ul style="list-style-type: none"> • PARTIAL OPEN FLOW • LOW DAMPING • EXCESSIVE STROKE-AREA CHANGE • VIBRATION |

Figure 6-1. Apollo Technology (GPS Oxidizer Quad Check Valve)

In addition, polymer seals change shape and physical properties as a function of temperature, chemical exposure and time. As a consequence, the functional performance of a given polymer seal design is virtually unpredictable and must be verified through an extensive combination of many tests and environmental conditions.

Results from the sealing investigations showed that the cutter concept could meet the OMS sealing requirements. However, conventional sintered carbides were not sufficiently compatible with the corrosive byproducts of nitrogen tetroxide (e.g., nitric acid), and compatible ceramics were simply too brittle for the narrow land concept. As shown in the materials investigations, a form of chemically vapor deposited tungsten carbide proved to be not only the strongest available carbide, but virtually unaffected by 6 months exposure to concentrated red fuming nitric acid. Furthermore, when applied as a thin coating (~0.001 inch) over a carbide base, the material demonstrated sufficient adherence to sustain complete shattering of a test specimen without interfacial separation. The preceding considerations led to selection of the cutter concept and CM-500 vapor deposited tungsten carbide for use in a prototype check valve.

A wide variety of closure designs and valve concepts were sketched and traded off in arriving at the selected configuration. Utilization of tungsten carbide for sealing posed a serious poppet weight problem because of the light closure spring force allowed by low cracking pressure (2.0 psid maximum) and relatively high vibration (2.0 g²/Hz random). Furthermore, hard seating requires that the poppet be able to self-align so that the seat load is more or less uniformly distributed around the seal diameter. General valve concepts evaluated incorporated flexure springs for poppet guidance and force reference, zero clearance bearings for precise closure, and negative rate reference spring concepts (belleville washer, toggle, magnet, etc.) to provide increased on-seat load. Damping devices included coulomb friction, magnetic hysteresis and a stepped flow area approach. More-complex designs, such as pilot and diaphragm operations, were simply too complex for the application and suffered from excessive moving parts weight and thus vibration sensitivity. These studies led to the conclusion that coulomb friction was the most simple approach to obtain low flow stability, the disadvantage being a hysteresis band between crack and reseal pressures.

A unique bearing concept was employed in the valve trade study to overcome problems experienced with the Apollo check valves. Valve poppets that are guided by a piston-in-cylinder approach are easily stuck from contaminants or galling because once the clearance space is filled with debris, binding forces become very large. This problem is overcome by greatly reducing the guide bearing area (giving room for contaminants) and replacing at least one-half the diameter with a low rate spring. The result is a "zero-clearance bearing" poppet, which can move over or around contaminants. The low rate spring provides force to hold the poppet in its guide and also a controlled level of coulomb friction to ensure low-flow dynamic stability and freedom from all chatter.

Sketches of conventional stem guided check valves incorporating the zero-clearance bearing and carbide poppet with a ball joint were made and analyzed. In all cases, not only was weight excessive for the vibration environment, but detail parts were overly complex because of the alignment requirements of a metal-to-metal seal.

To alleviate the problem, several sketches were made of single, flat-plate-type closures without a stem guide. The concept called for a relatively large-diameter poppet and corresponding short stroke to minimize angular contacts. Breakthrough to the final concept was an offshoot of a flat plate poppet fabricated of graphite and entirely vapor deposit coated with CM-500 tungsten carbide. Although the box section was strong, weight reduction was still marginal. The next step was elimination of the graphite in favor of a free-standing shell.

Semifinal sketches incorporating the preceding concepts are shown in Fig. 6-2. On the right are two designs employing stem guides (the bearing is upstream in one case and downstream in the other). These designs do not allow the hard seat poppet to self-align and are much too heavy. The alignment problem is overcome by eliminating the stem and guiding on a carbide poppet ring (left sketch of Fig. 6-2). As shown, one of the knife-like guides is a cantilever spring that holds the poppet against the other solid guides. The poppet is reduced to a single flat disk in which the stroke is minimized by a large seat diameter that also provides for a relatively larger closure spring. The center sketch of Fig. 6-2 is the final version in the trade study incorporating three carbide guides and a machined carbide seal ring snapped into a steel plate. The complexities of this poppet design with its required static seals, and overall excessive weight, led to the finally selected configuration.

PROTOTYPE DESIGN

Layout and assembly of the prototype check valve is shown in Fig. 6-3. The poppet is fabricated by vapor depositing tungsten carbide over a molybdenum mandrel to provide a nominal 0.03-inch thickness. The poppet is machined and lapped using the mandrel as a holding fixture and datum to obtain the required outside diameter, seal land flat and edge height. The mandrel is dissolved in acid to produce the free-standing shell poppet.

Guiding the poppet are three carbide pins, one of which is a cantilever spring providing a nominal 1-pound side load on the poppet rim. Each of these guide pins is retained and angularly located by CRES pins locked by a set screw and Teflon plug, which also provides an external seal. This arrangement allows each pin to be easily removed and interchanged for evaluation purposes.

The cutter seat detail is comprised of two lands separated by a nominal 0.03 inch. The inner land is the primary seal and the outer land serves to align the poppet during closure and also provides a secondary seal. The seat is retained in the body by a metal K-seal, which provides an external seal and secondary seal around the seat base. Leakage past the K-seal is vented through the body-base interface. A Teflon gasket at the seat base further isolates the upstream side of the closure from downstream.

Details of the prototype valve are shown in Fig. 6-4 through 6-12. Fabricated parts are shown in Fig. 6-13, which also includes a Teflon plug and B-nut used to reduce downstream volume and collect leakage. A closeup of the seat is shown in Fig. 6-14. Specialized fabrication processes are discussed following the performance analysis.

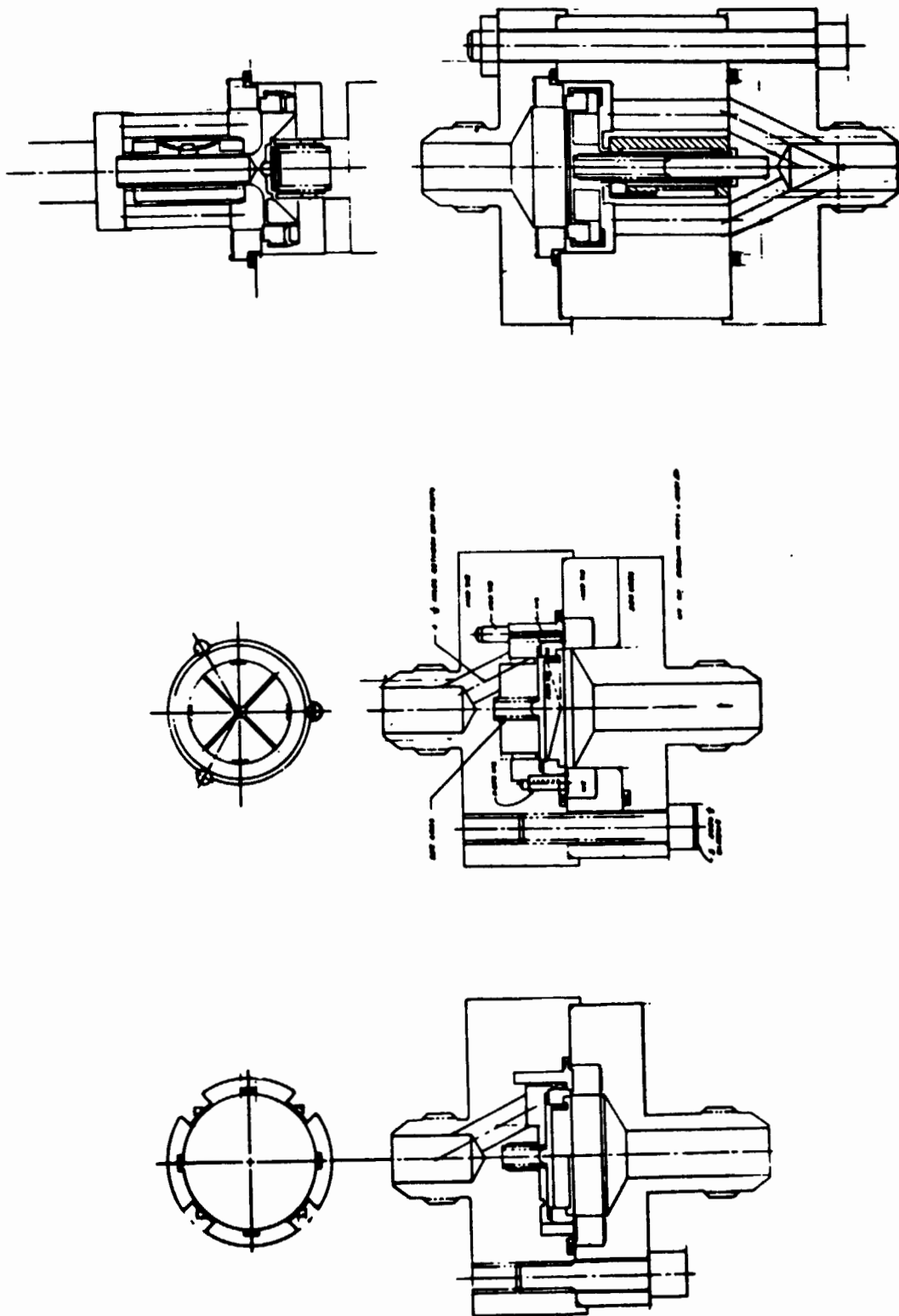
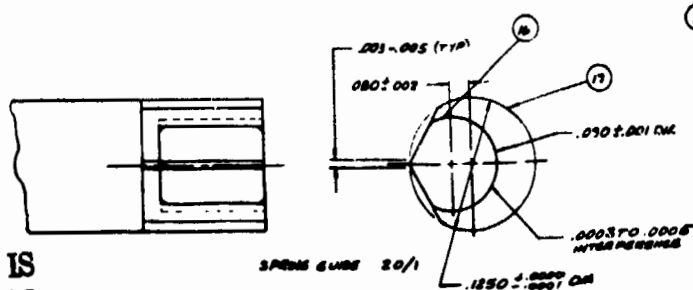
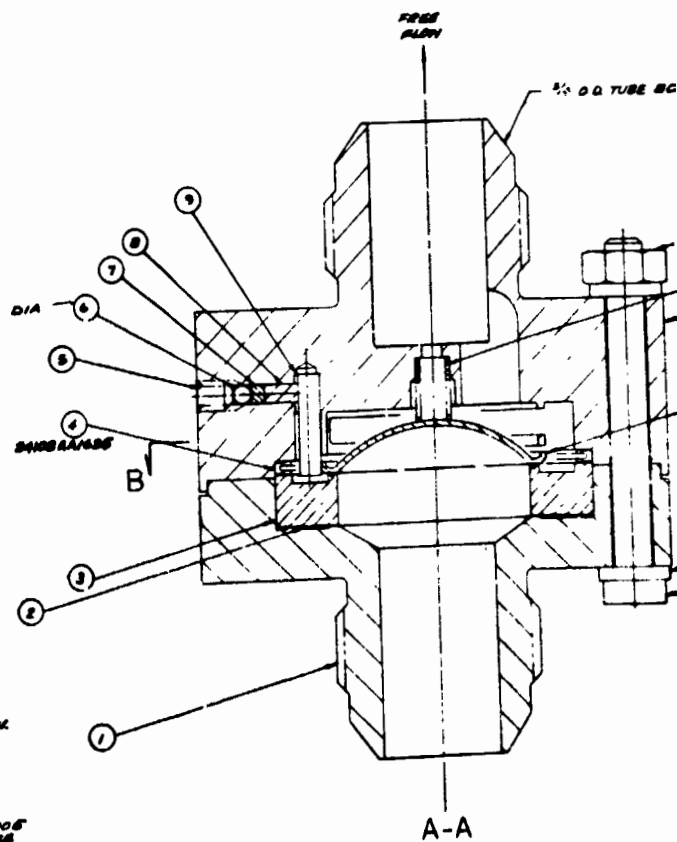
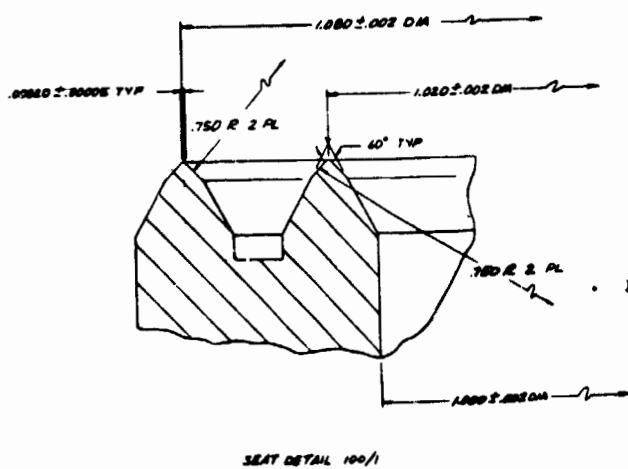
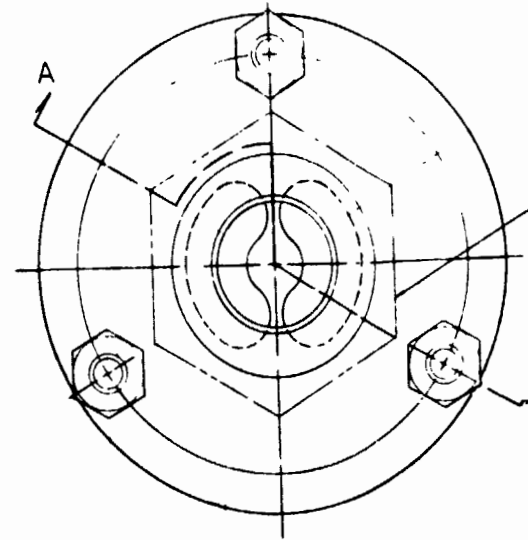
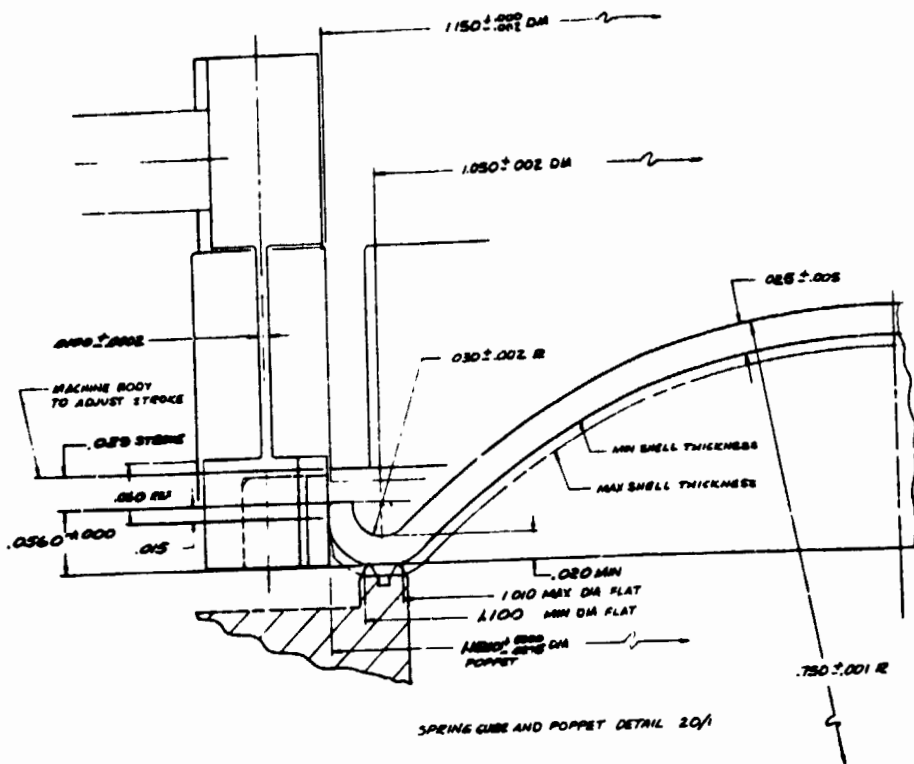


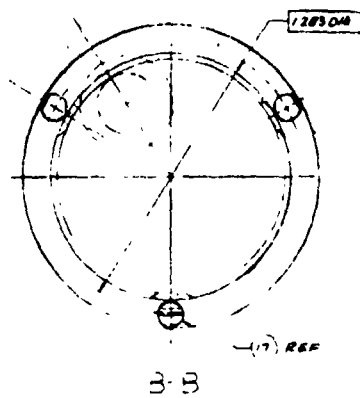
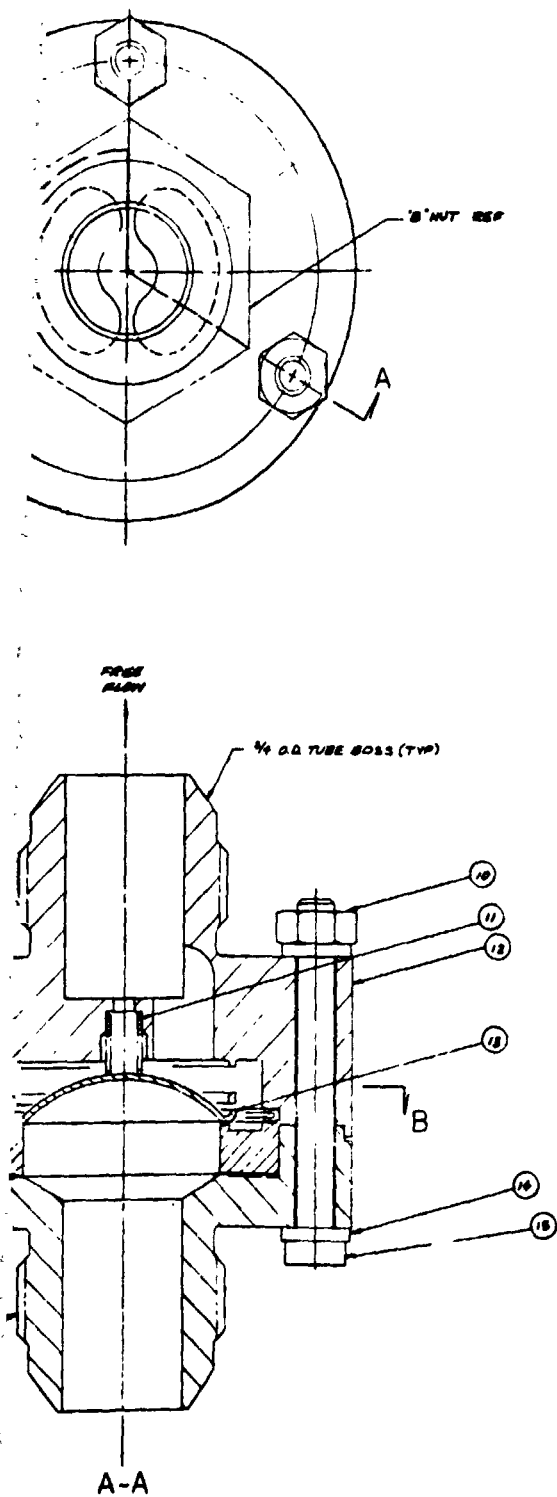
Figure 6-2. Check Valve Conceptual Design and Selection

ORIGINAL PAGE IS
OF POOR QUALITY



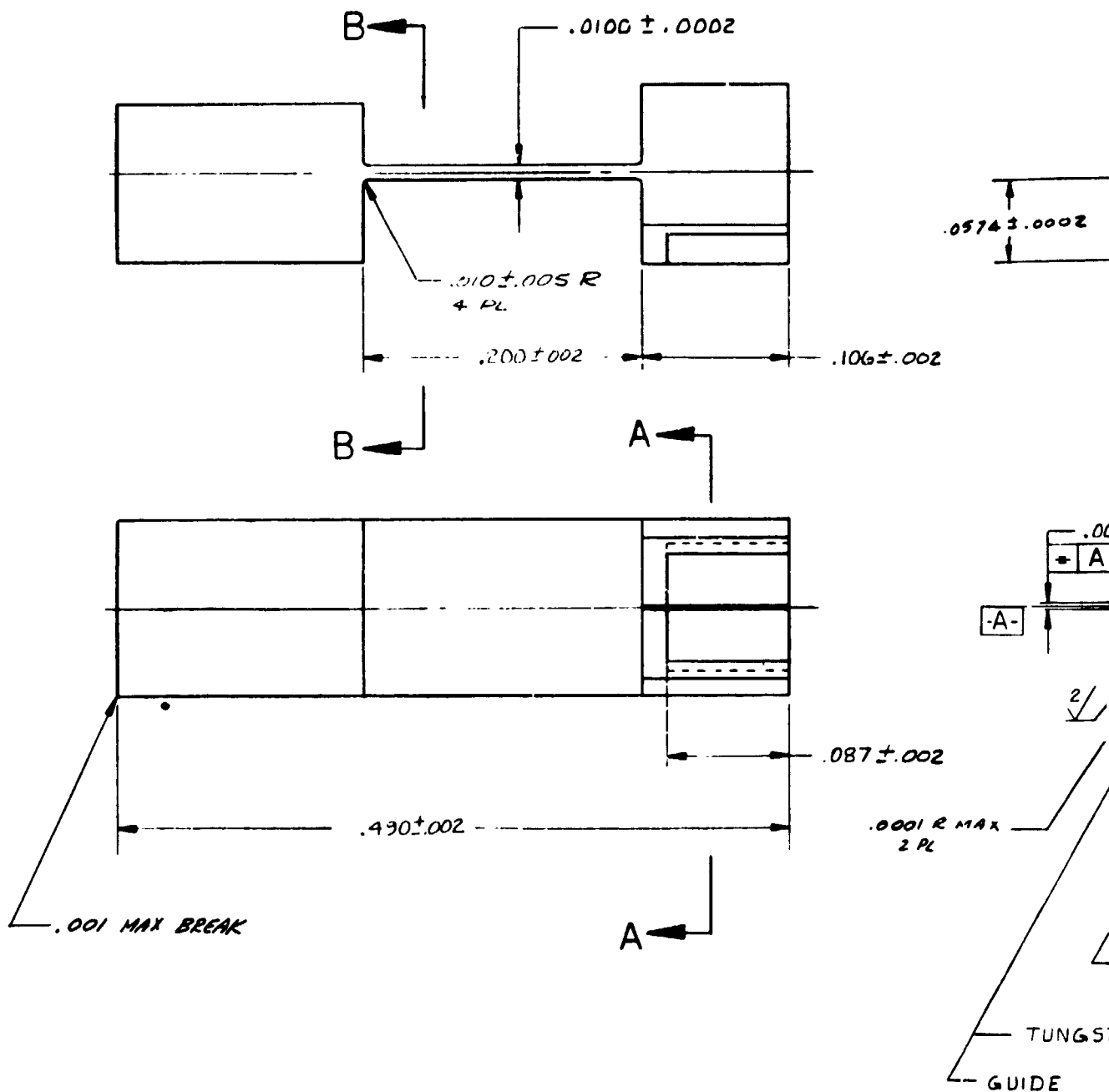
ORIGINAL PAGE IS
OF POOR QUALITY

FOLDOUT FRAME /



| NO. | DESCRIPTION | MATERIAL | FINISH | SUPPLER | QTY |
|-----|--------------|----------|--------|-----------|-----|
| 17 | CAPL EVER LP | 304 SS | NO 8 | PASSIVATE | 1 |
| 16 | 1/4" DIA | 304 SS | NO 8 | PASSIVATE | 1 |
| 6 | 5/8" DIA | 304 SS | NO 8 | PASSIVATE | 1 |
| 15 | WASHER | 304 SS | NO 8 | PASSIVATE | 1 |
| 18 | POCKET | 304 SS | NO 8 | PASSIVATE | 1 |
| 12 | 1/4" DIA | 304 SS | NO 8 | PASSIVATE | 1 |
| 11 | 1/4" DIA | 304 SS | NO 8 | PASSIVATE | 1 |
| 10 | 1/4" DIA | 304 SS | NO 8 | PASSIVATE | 1 |
| 9 | 1/4" DIA | 304 SS | NO 8 | PASSIVATE | 1 |
| 8 | 1/4" DIA | 304 SS | NO 8 | PASSIVATE | 1 |
| 7 | 1/4" DIA | 304 SS | NO 8 | PASSIVATE | 1 |
| 6 | 1/4" DIA | 304 SS | NO 8 | PASSIVATE | 1 |
| 5 | 1/4" DIA | 304 SS | NO 8 | PASSIVATE | 1 |
| 4 | 1/4" DIA | 304 SS | NO 8 | PASSIVATE | 1 |
| 3 | 1/4" DIA | 304 SS | NO 8 | PASSIVATE | 1 |
| 2 | 1/4" DIA | 304 SS | NO 8 | PASSIVATE | 1 |
| 1 | 1/4" DIA | 304 SS | NO 8 | PASSIVATE | 1 |

Figure 6-3. Prototype Check Valve

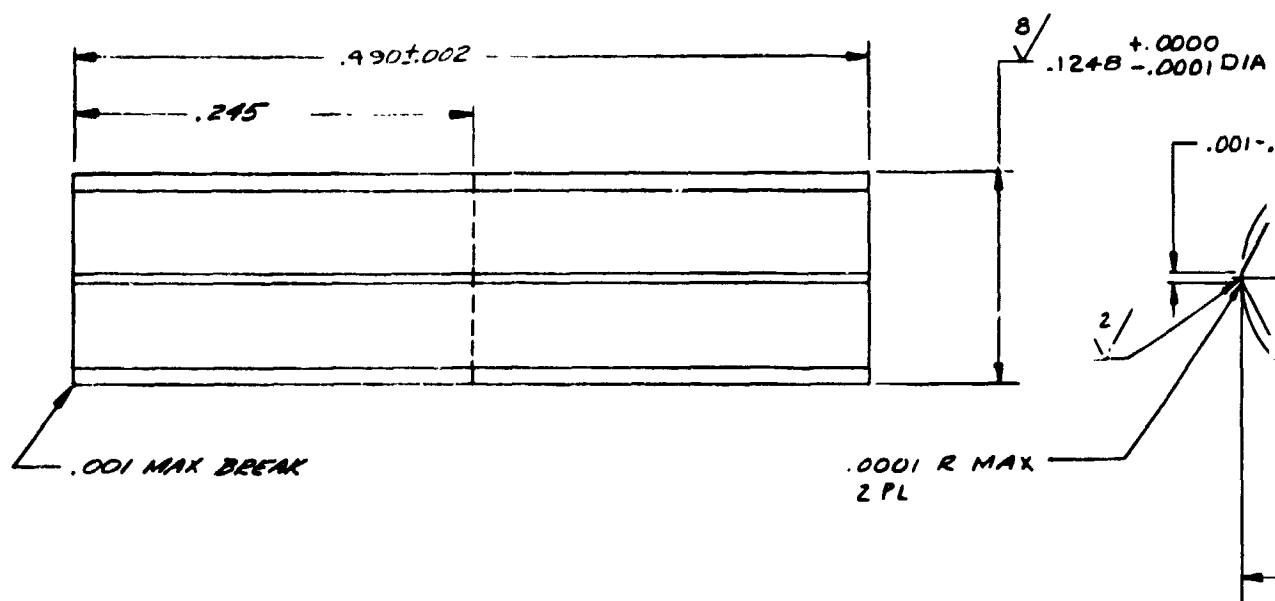


ORIGINAL PAGE IS
OF POOR QUALITY

FOLDOUT FRAME /

5. $\frac{32}{\sqrt{}} ALL MACHINED SURFACES$
4. FILLETS $.003 R MAX$
3. BREAK CORNERS $.001 \pm .000$
2. CLEAN 302 CRES SPRING PER RA0103-002
1. MACHINE PER RA0103-002

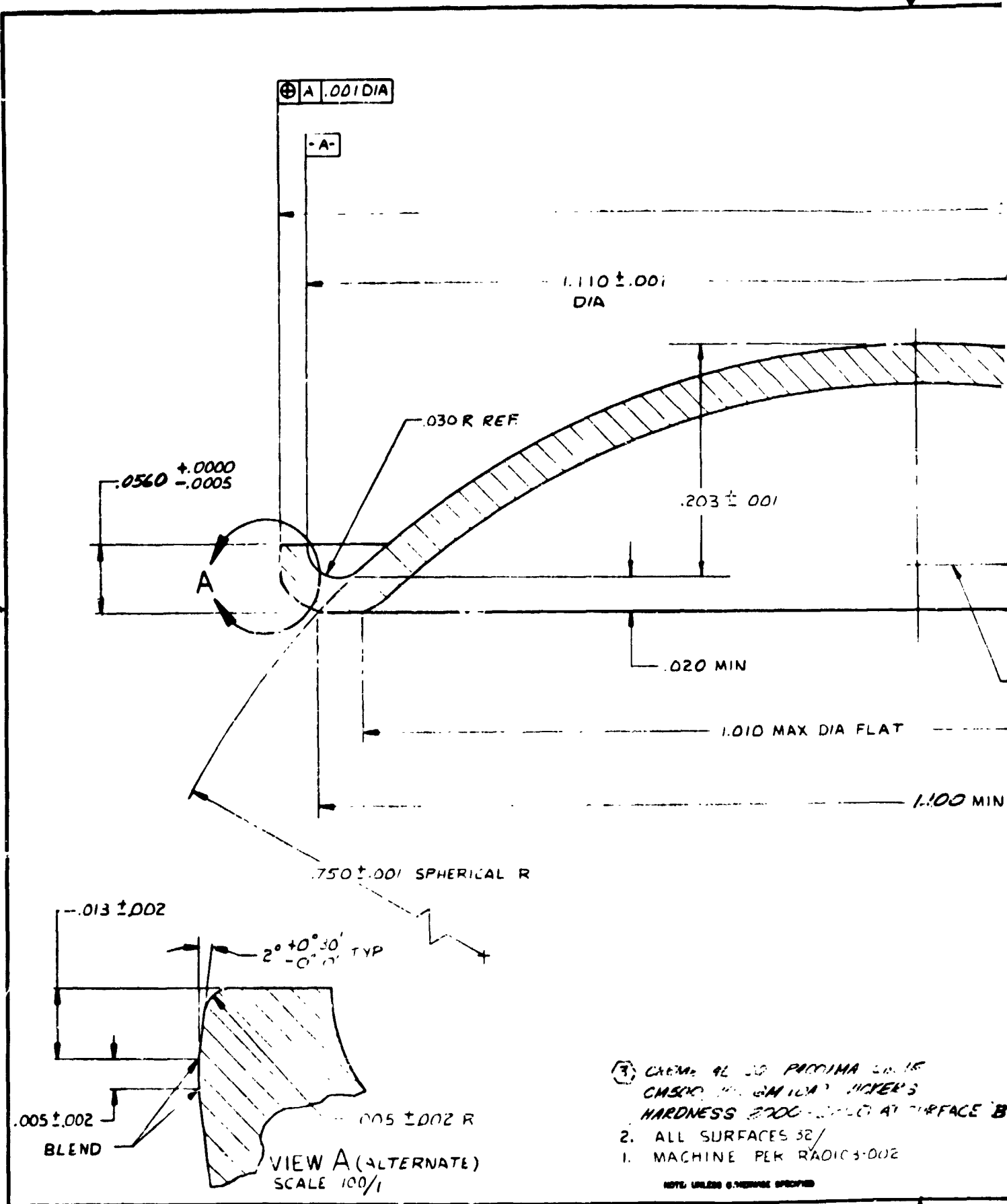
NOTE: UNLESS OTHERWISE SPECIFIED



- 3 $\sqrt{32}$ ALL MACHINED SURFACES
- 2 BREAK EDGES $.001 \pm .002$
1. MACHINE PER RA0103-002

NOTE: UNLESS OTHERWISE SPECIFIED

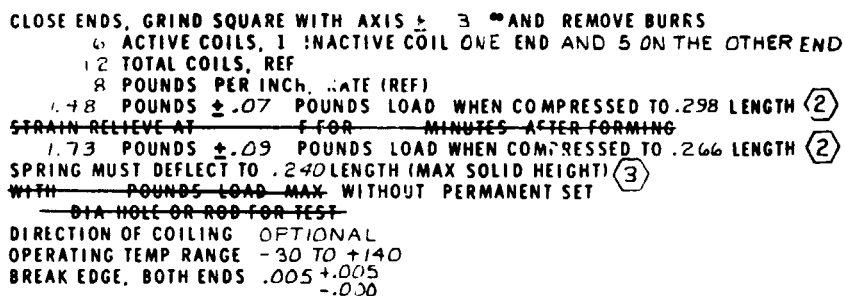
FOLDOUT FRAME /



- ③ CHEM: 92.50 PPMIMA 20.15
 CHSIC 10.04 10.1 10.1 10.1
 HARDNESS 2700-2800 AT SURFACE B
- ALL SURFACES 32/
 - MACHINE PER RADIOS-002
- NOTE: UNLESS OTHERWISE SPECIFIED

ORIGINAL PAGE 1

ORIGINAL PAGE 15
 OF POOR QUALITY



6-10

- NOTE: UNLESS OTHERWISE SPECIFIED:**

FOLDOUT FRAME /

IMRESSED TO .298 LENGTH (2)
 AFTER FORMING
 IMRESSED TO .266 LENGTH (2)
 HEIGHT) (3)
 IT SET

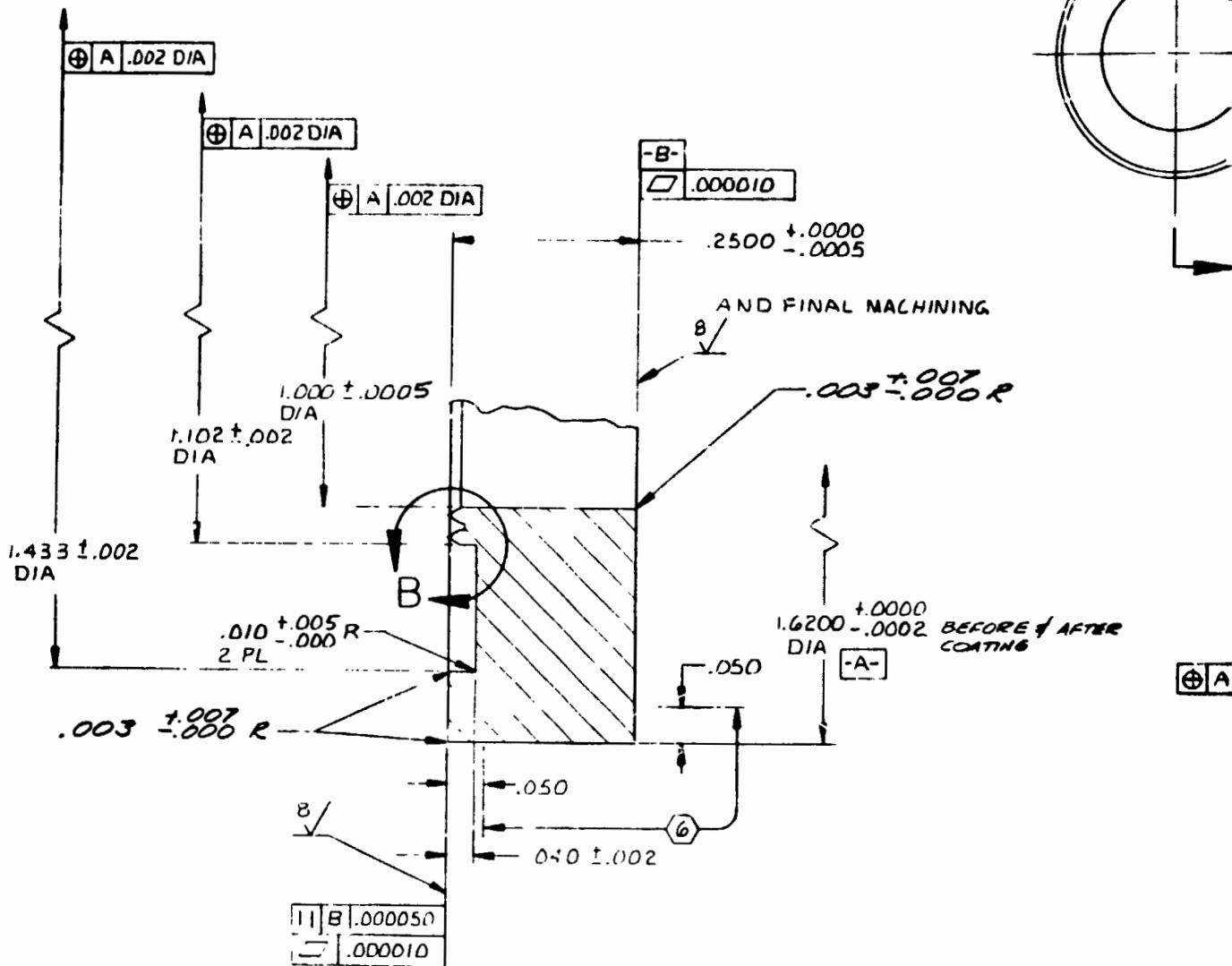
| REVISIONS | | | DATE | APPROVED |
|-----------|-----------------------|----------------------|--------|----------|
| LTR | DESCRIPTION | | | |
| | 1. MAY BE REMORKED | 3. RECONJ CHANGE | DISP N | |
| | 2. CANNOT BE REMORKED | 4. NOW SHOP PRACTICE | | |
| | B. PARTS MADE OK | | | |

Figure 6-7. Check Valve Spring

6-10

| | | | | | |
|---|---|---|--|--|--|
| HWT TREAT <div style="text-align: center;">NONE</div> | UNLESS OTHERWISE SPECIFIED: DIMENSIONS ARE IN INCHES AND APPLY PER TO FINISH SURF. MAINT. SURF. ROUGHNESS | DIM <div style="text-align: center;">D. Cecil</div> DATE <div style="text-align: center;">10-2-74</div> | Rockwell International Corporation Rocketdyne Division Canoga Park, California | | |
| | | | SPRING, CHECK VALVE | | |
| FINISH <div style="text-align: center;">NONE</div> | TOLERANCES ON PARTS ± 0° 30' DECIMALS .XX ± .01 .XXX ± .005 HOLES NOTED "DRILL" OVER THRU TOLERANCE .0000 .0000 + .0015 - .0000 .0000 .0000 + .0020 - .0000 .0000 .0000 + .0040 - .0010 .0000 .0000 + .0060 - .0010 .0000 .0000 + .0070 - .0010 .0000 .0000 + .0090 - .0010 .0000 .0000 + .0120 - .0010 | DIM <div style="text-align: center;">B. J. Jones</div> DATE <div style="text-align: center;">10-2-74</div> | | | |
| | | | SCALE NONE | | |
| MATL. 302 CRES .020 DIA 10000003 CONGR B | DO NOT SCALE PRINT | DESIGN ACTIVITY APVD <div style="text-align: center;">B. J. Jones</div> DATE <div style="text-align: center;">10-2-74</div> | SIZE <div style="text-align: center;">D</div> | CODE IDENT NO. <div style="text-align: center;">02602</div> | DRAWING NO. <div style="text-align: center;">XEOR94230604</div> |
| | | | SHEET | | |

FOLDOUT FRAME 2



SECTION A-A
SCALE 10/1

ORIGINAL PAGE IS
OF POOR QUALITY

- 6 DO NOT COAT THIS AREA
3 VAPOR DEPOSIT .0010 ± .0006 THICK PU
TUNGSTEN CARBIDE (CHEMETAL CO., CM
EXCEPT AREA CODED A THICKNESS TO
.0010 ± .0002 . 100GM LOAD VICKERS
HARDNESS 1600-1800 IN AREA
CODED A MIN. COAT THICKNESS AFTER
FINISH .0003
- 4 BREAK CORNERS .004
3 CARMET CO., PITTSBURGH, PA.
2 ALL MACHINE SURFACES 32/AFTER COATING
1. MACHINE PER RA0103-002

NOTE: UNLESS OTHERWISE SPECIFIED



ORIGINAL PAGE IS
OF POOR QUALITY

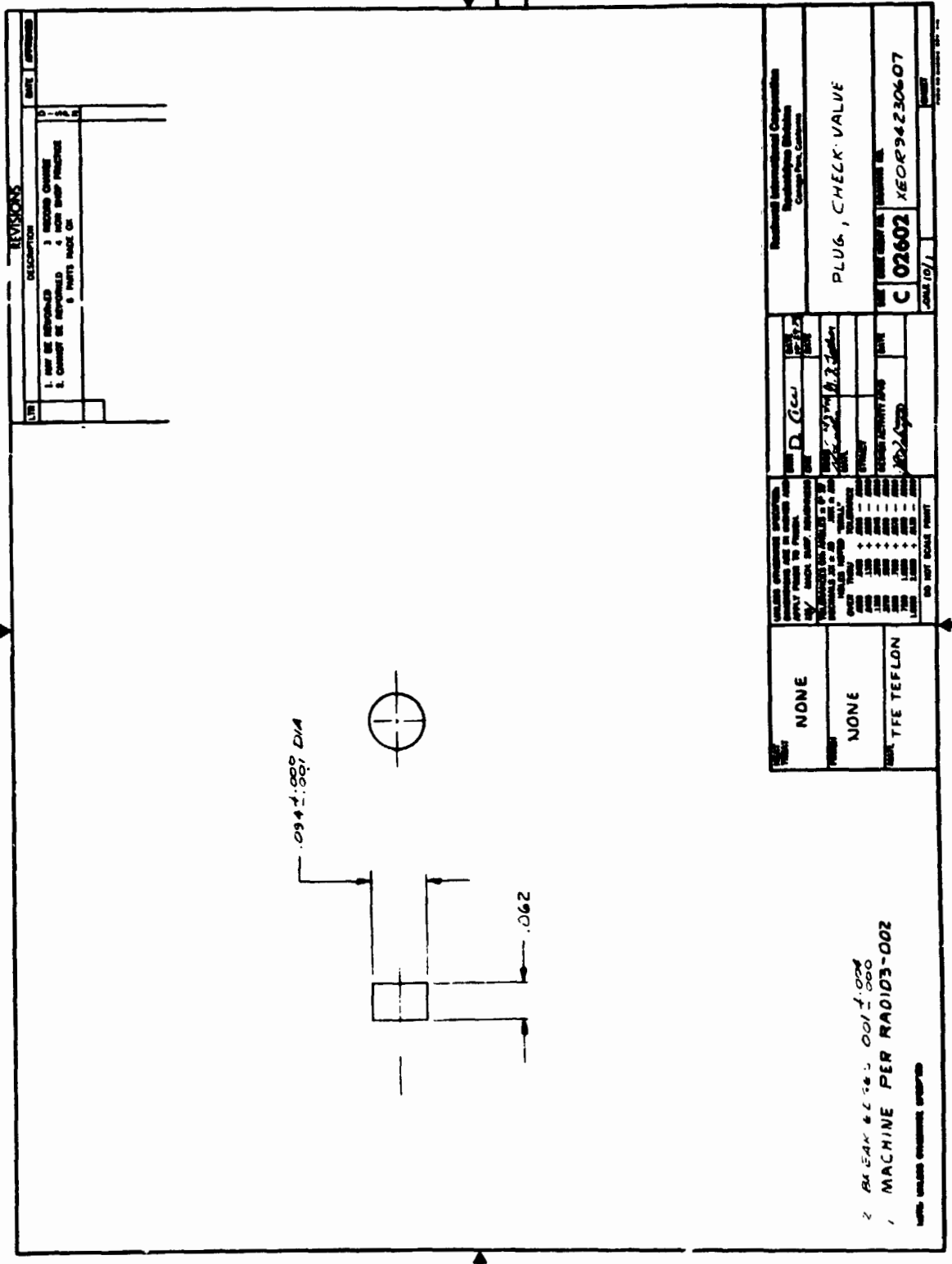
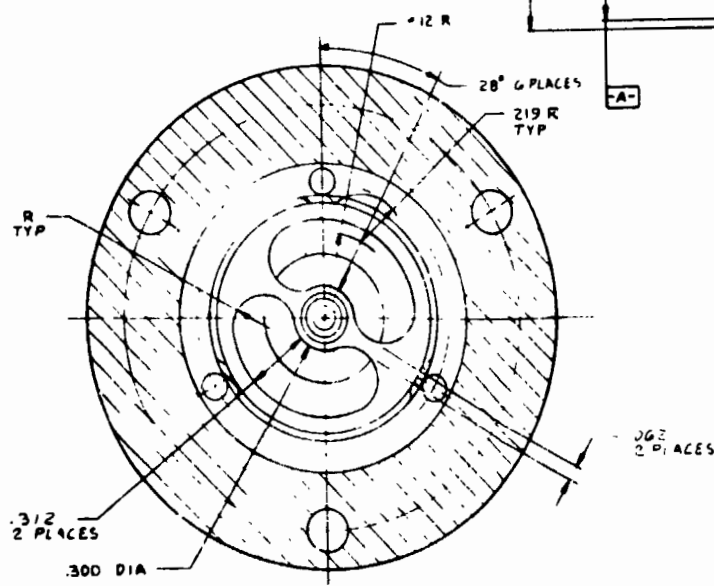
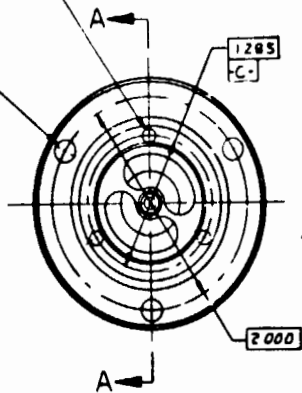


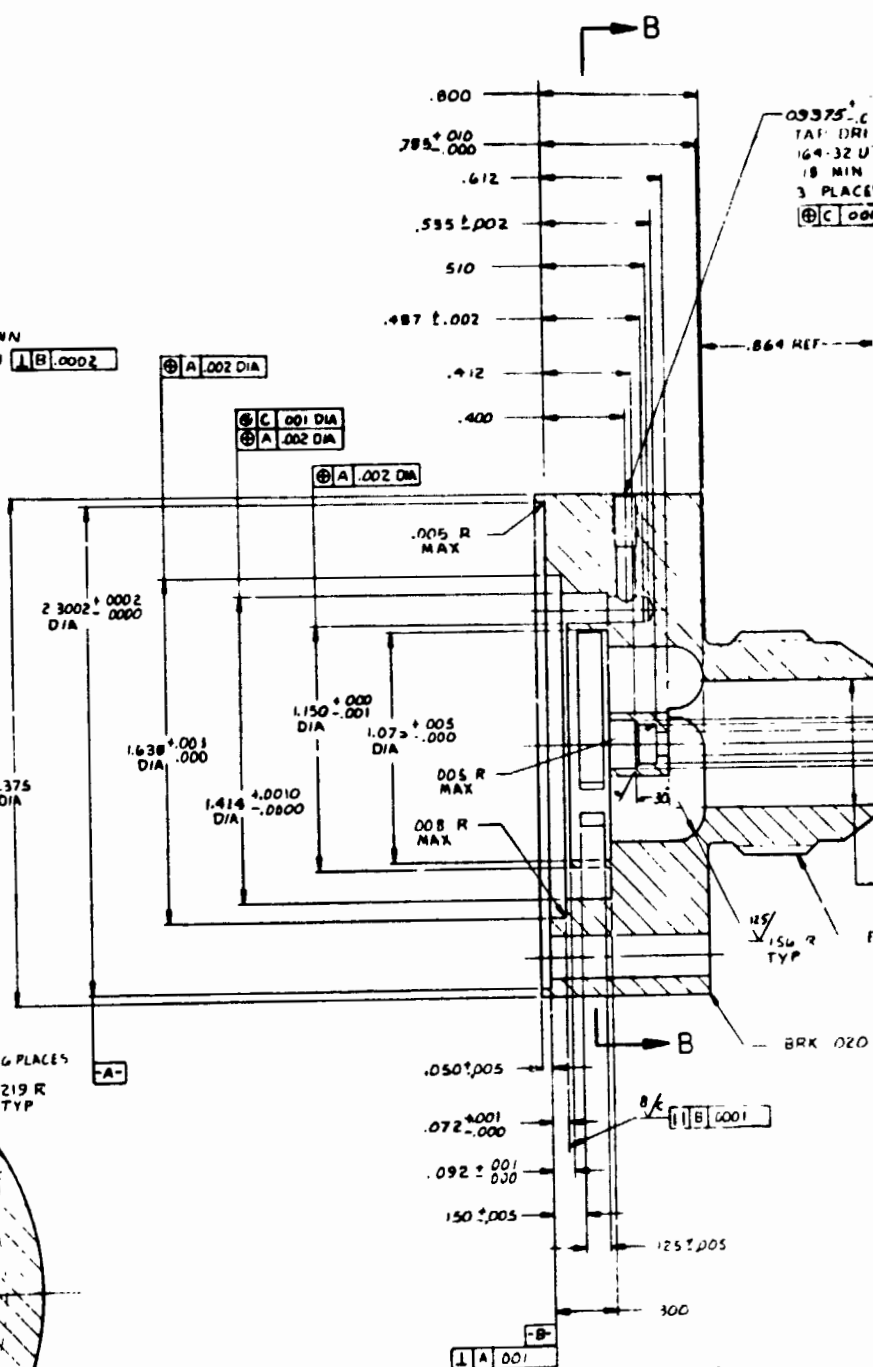
Figure 6-10. Check Valve Plug

REAM .250 THRU
3 HOLES EQ SP
MACH MACHINE WITH
TEOR 94230629

DRILL NO 31 (.120) DEPTH SHOWN
.1250 +.0003 DIA DEPTH SHOWN
.003 MAX FILLET R
3 HOLES EQ SP



SECTION B-B
SCALE 4/1



SECTION A-A
SCALE 4/1

ORIGINAL PAGE IS
OF POOR QUALITY

- 5. FILLETS .010 R MAX
- 4. 63° ALL MACH SURF
- 3. BREAK CORNERS .001-.002
- 2. MACHINE PER RADIOS .002
- 1. CLEAN PER RADIO .018

| |
|---------|
| NOI |
| NON |
| 3CAL |
| 80% 781 |
| COLD A |

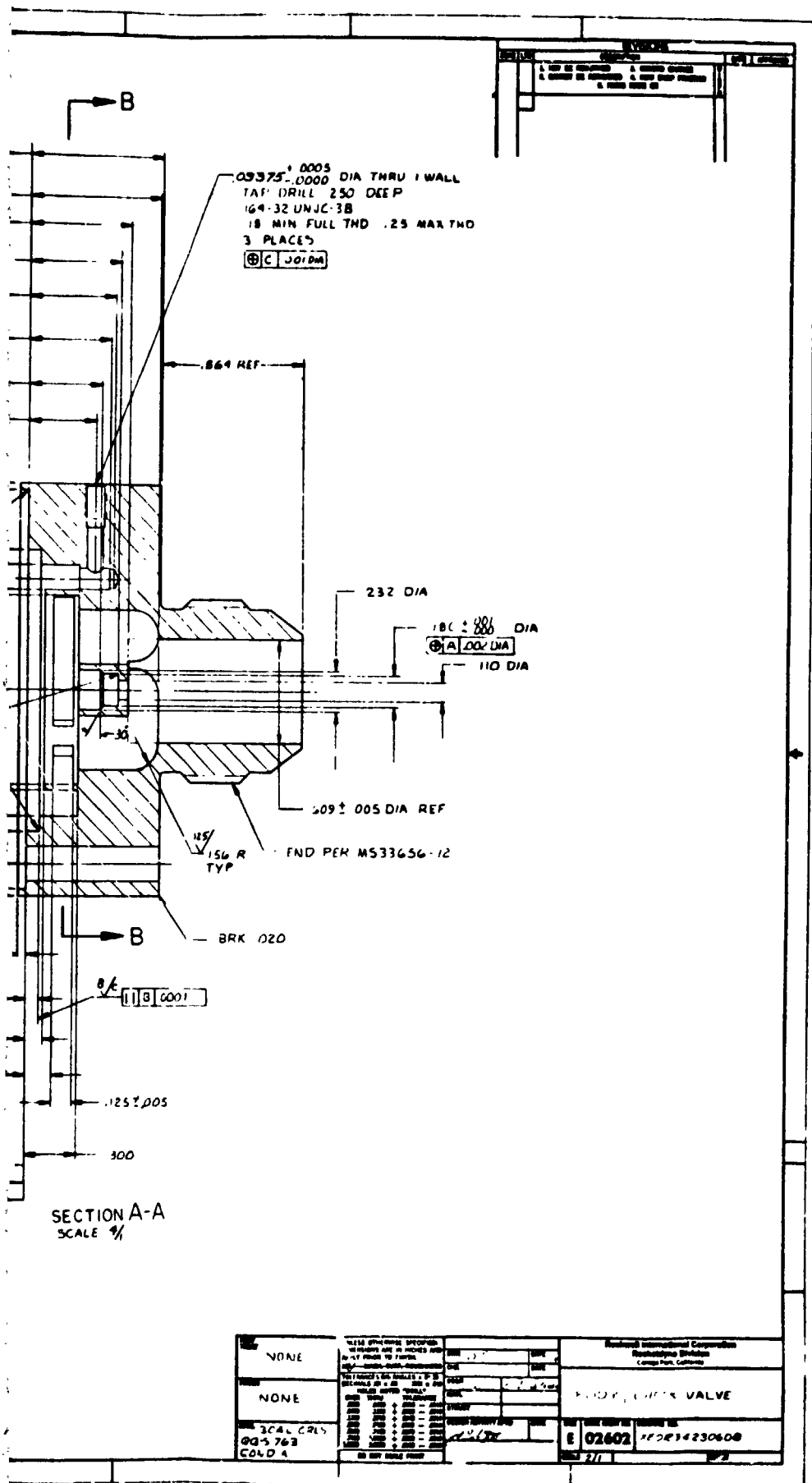
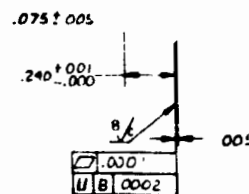
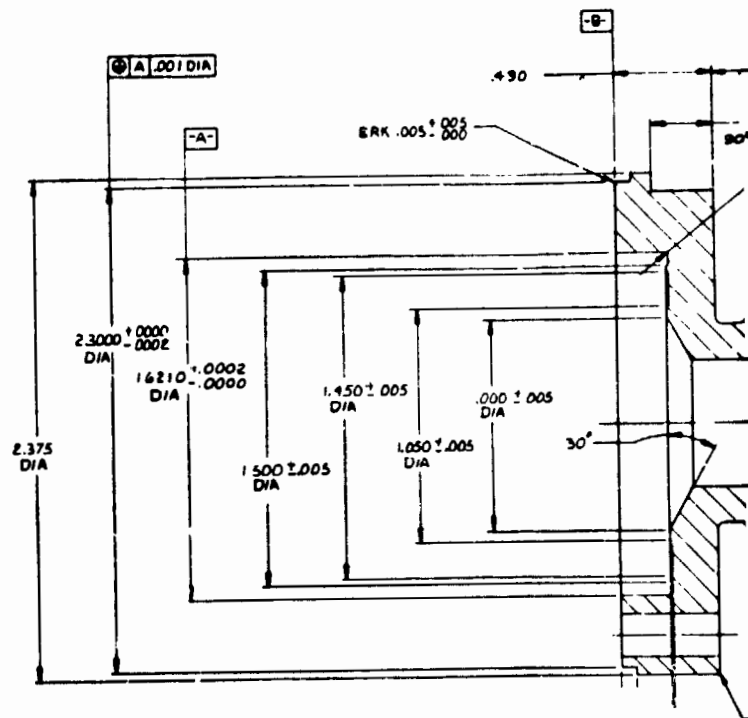
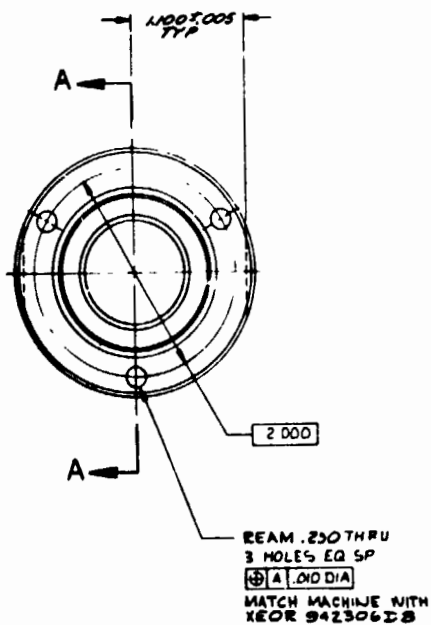


Figure 6-11. Check Valve Body



SECTION A-A
SCALE 4/1

ORIGINAL PAGE IS
OF POOR QUALITY

5. 6/ ALL MACH SURF
4. FILLETS .010 R MAX
3. BREAK CORNERS .001 ± .004
2. MACHINE PER RADIO3-002
1. CLEAN PER RADIO3-018

FOLDOUT FRAME /

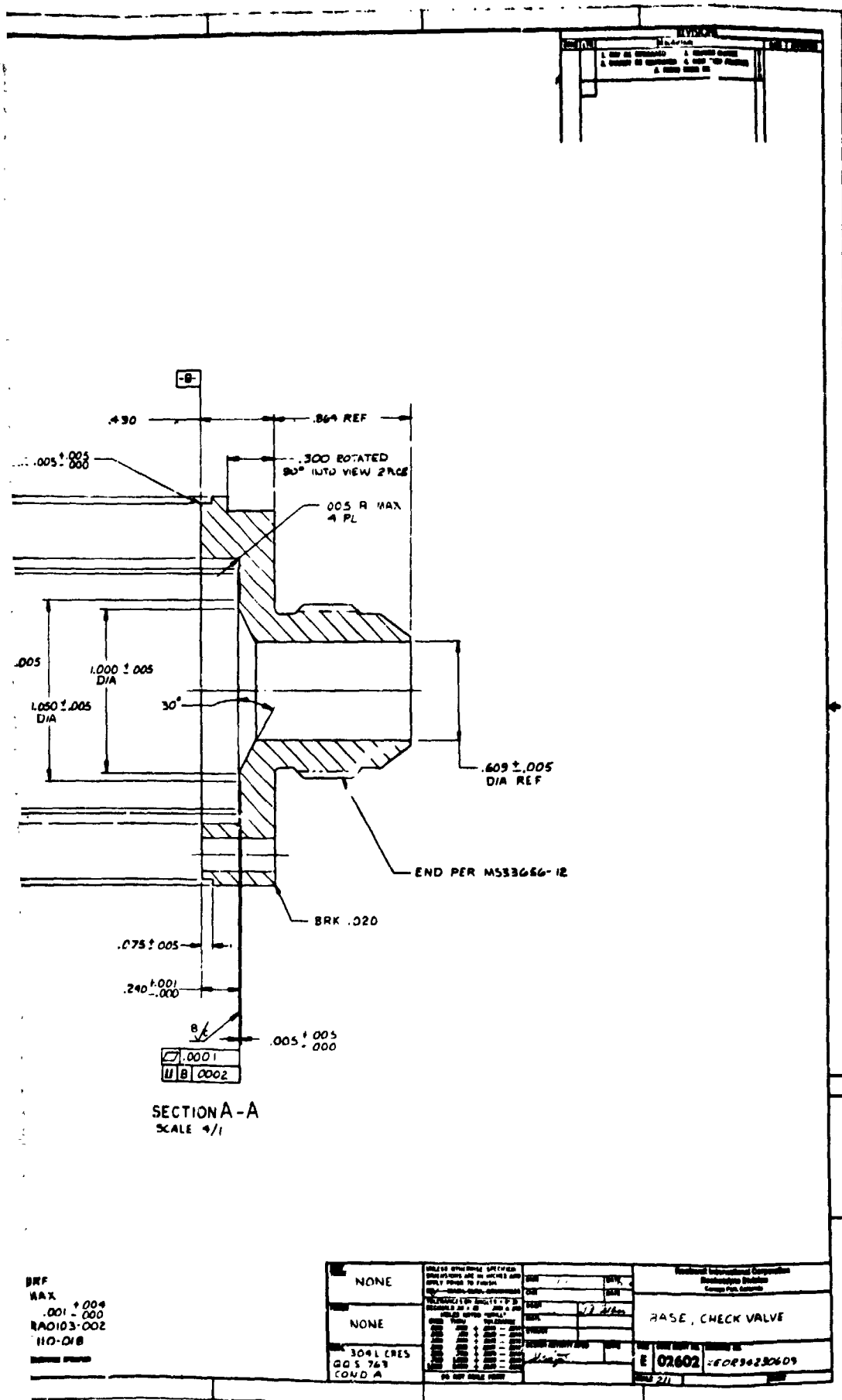
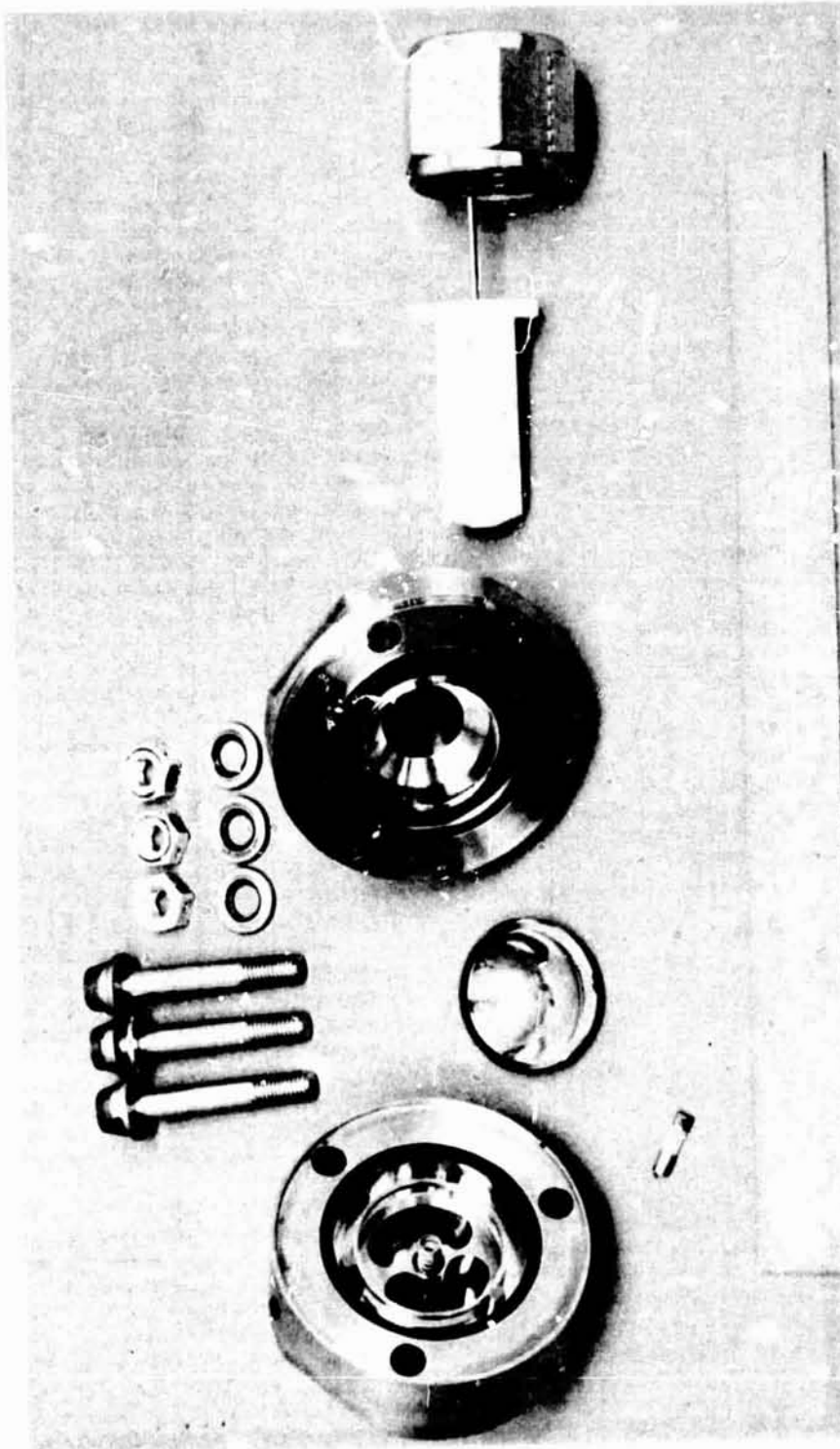


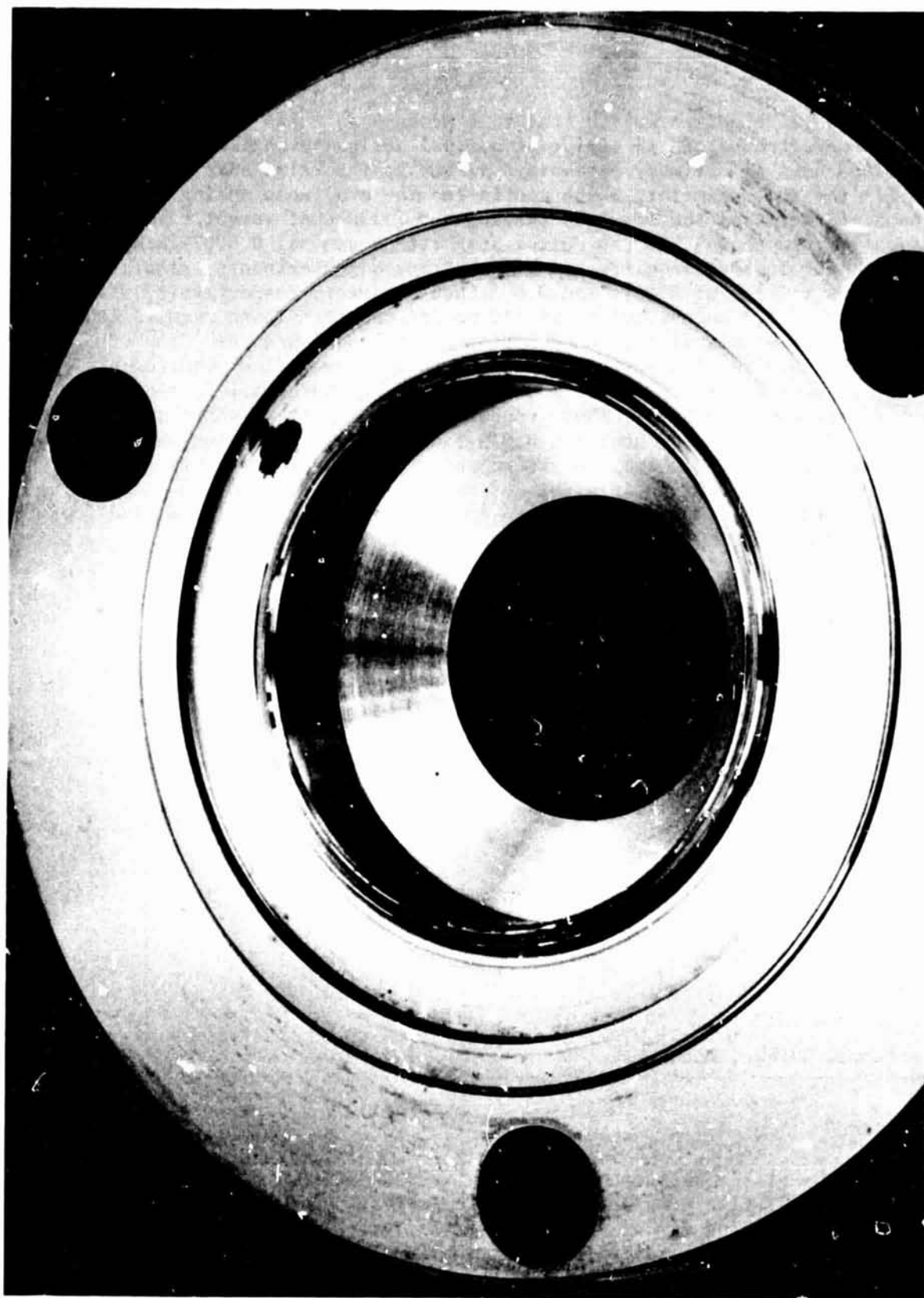
Figure 6-12. Check Valve Base



1S065-8/8/75 CIA

Figure 6-13. Prototype Valve Details

ORIGINAL PAGE IS
OF POOR QUALITY



IS065-8/8/75-CIB

Figure 6-14. Prototype Valve Seat

ORIGINAL PAGE IS
OF POOR QUALITY

PERFORMANCE ANALYSIS

The prototype valve design was an iterative process in which the basic dimensions and forces were traded off to arrive at a final design to satisfy the performance goals of Appendix A. Primary parameters affecting the valve size and function were: (1) the seat diameter, which controlled the available spring force; (2) the flow capacity defining the required stroke; and (3) poppet weight. The sealing investigation had shown that the cutter seat with a nominal 0.0002-inch-wide land could meet seat leakage requirements with entrapped contaminants, simulated by CRES and copper wires of 0.001- and 0.003-inch diameter, respectively, with a closure force of 1.3 pounds acting at the poppet center. These results led to the selection of a nominal 1.5-pound spring force. Goal pressure drop of 3.5 psid indicated the need for low cracking pressure to meet open flow requirements. Moreover, without angular guidance a short stroke was necessary to minimize closure edge impact stresses. These combined prerequisites led to selection of a nominal 1.0-inch-diameter seat and 0.029-inch stroke. Selection of a 1-pound lateral spring force was based on the poppet weight and required vibration resistance. A summary of the nominal design data for the prototype check valve is listed in Table 6-1. Analysis of the functional performance predicted for the valve is covered in the following paragraphs.

TABLE 6-1. PROTOTYPE CHECK VALVE DESIGN DATA

| | |
|--|---------------|
| Seat diameters (2), inch | 1.02 and 1.08 |
| Stroke, inch | 0.029 |
| Seating spring force, pounds | 1.48 |
| Seating spring rate, lb/in. | 8.5 |
| Lateral spring force, pound | 1.0 |
| Lateral spring rate, lb/in. | 63.0 |
| Lateral spring friction coefficient (estimated) | 0.25 |
| Cracking pressure area, in. ² | 0.92 |
| Open flow effective area (estimated), in. ² | 1.0 |
| Poppet weight, pound | 0.021 |

Force Balance

Analysis of the static balance of forces is used to approximate cracking and reseal pressures and full-flow pressured drop. The analysis also indicates the ability of the installed spring forces to resist acceleration loads that would cause the poppet to unseat or slide on the seat.

Cracking and Reseat Pressures. Without a lateral spring the check valve cracks and reseats at the same pressure. This occurs when the cracking pressure drop (ΔP_c) acting over the outer seat area (A_2) just balances the spring force (F_s) reducing seat force to zero; thus,

$$\Delta P_c = \frac{F_s}{A_2} = \frac{1.48}{0.92} = 1.61 \text{ psi}$$

If the closure spring is eccentric with the seat diameter then cracking pressure is reduced in proportion to the eccentricity (e) and seat diameter (D_2) as follows:

$$\Delta P_c = \frac{F_s (D_2 - 2e)}{A_2 D_2}$$

For $e = 0.05$ inch, $P_c = 1.46$ psi

Incorporation of the lateral spring force (F_c) will produce axial friction at each guide pin to create a differential pressure between crack and reseat. For straight axial opening or pivot about two pins:

$$\Delta P = \frac{F_s + 3\mu F_c}{A_2}$$

Assuming a friction coefficient (μ) of 0.25 and 1.0 pound lateral spring force indicates a cracking pressure

$$\Delta P_c = \frac{1.48 + 0.75}{0.92} = 2.42 \text{ psi}$$

and reseat pressure

$$\Delta P_r = \frac{1.48 - 0.75}{0.92} = 0.79 \text{ psi}$$

Acceleration Resistance. The axial and lateral springs provide resistance and damping to vibration induced acceleration forces acting on the poppet of weight (W). The g-force level required to unseat the poppet with a 0.5-psi closing pressure drop acting over the inner seat area (A_1) is given by:

$$\begin{aligned} \frac{a}{g} &= \frac{F_s + \Delta P A_1 + 3\mu F_c}{W} \\ &= \frac{1.48 + 0.5 \times 0.817 + 0.75}{0.021} = 126 \text{ g} \end{aligned}$$

Similarly, the lateral g force level required to slide the poppet on the seat is calculated from

$$\frac{a}{g} = \frac{F_c + \mu (F_s + \Delta P A_1)}{W}$$

$$= \frac{1.0 + 0.25 (1.48 + 0.5 \times 0.817)}{0.021} = 70 \text{ g}$$

The preceding g levels indicate the relative resistance of the valve to vibration. However, dynamic analyses involving vibration inputs were not performed and are a major consideration in valve performance and life expectancy.

Flow Capacity

Worst condition requirements from Appendix A guidelines are for a 2.4 lb/min helium flow through a quad valve or 1.2 lb/min/element (or 116 scfm).

Assuming a nominal inlet pressure of 245 psig and 70 F gas temperature provides sufficient data to compute the pressure drop for each check valve element, and thus the prototype valve. All flow areas through the prototype valve are significantly larger than the seat restriction. Therefore, assuming discharge coefficient (c) of 0.6 and the orifice equation (see Leakage Analysis section for nomenclature), the valve pressure drop is given by:

$$\Delta P = \left(\frac{12 \dot{w}}{CA} \right)^2 \frac{1}{2g\bar{\rho}}$$

where

$$A = \pi D_1 h = \pi \times 1.02 \times 0.029 = 0.0929 \text{ in.}^2$$

$$\bar{\rho} = \frac{\bar{P}}{RT} = \frac{259 \times 144}{386 \times 530} = 0.182 \text{ lb/ft}^3$$

and, therefore:

$$\Delta P = \left(\frac{12 \times 1.2/60}{0.6 \times 0.0929} \right)^2 \frac{1}{2 \times 32.2 \times 0.182} = 1.58 \text{ psi}$$

Thus, the predicted pressure drop lies between crack and reseal. Assuming flow noise provides sufficient dither to negate the lateral spring friction, the force balance for full open pressure drop is given by:

$$\Delta P = \frac{F_s + K_h}{A_e}$$

$$\Delta P = \frac{1.48 + 8.5 \times 0.029}{1.0} = 1.73 \text{ psi}$$

It would appear that the valve design is capable of meeting the goal pressure drop of 3.5 psi for the quad configuration with only one leg flowing. However, flow tests are required to establish effective flow areas and losses through split flows, etc.

Seat Leakage

Leakage has been the primary subject of study in the program. Test models have been evaluated and results presented in the Model Seal Tests section. Theoretical analyses based on laminar and molecular flow equations have been performed for the prototype valve seal to correlated measured and predicted performance for a hypothetical parallel plate leak path. The results, presented in the Leakage Analysis section, show more or less acceptable propellant leak rates but higher N₂O₄ vapor leakage because of high driving pressure of the vapor (14.8 psia at 70 F) without added closing force. This correlation has been performed for the prototype check valve test results to be subsequently presented.

FABRICATION

Parts for one complete prototype assembly were fabricated, along with spare poppets and seats. Conventional shop practices were employed in fabrication with exception of the poppet and seat. Special processing and handling of these parts is described.

Seat

Two seats (No. 1 and 2) were machined from Carmet CA315 micrograin tungsten carbide. The carbide blanks were diamond ID ground and wrung to an arbor for OD and face grind between centers. This produced concentricity and squareness within 50 microinches. Face grooves were formed by EDM in preparation for seat corner grinding. Seat No. 1 was completed as follows and seat No. 2 was used in subsequent spare parts testing.

Seat corners were ground to form nominal 0.001- to 0.002-inch-wide lands with a 60-degree included angle. This was accomplished on an ID grinder with the part wrung on a shouldered arbor and chucked in a hydrostatic head. Corners were individually ground by a formed diamond wheel in high-speed air bearing spindle. Material removed was constantly monitored using a 40X microscope and fiber optic light. Land width was limited to the maximum chip size produced at the seat face.

Final forming of the seat lands was produced by a combination of spherical and flat lapping with reduction in diamond compound size from 1 to 5 microns to 0.1 micron. Lapping progress was intermittently viewed using a 500X interference

microscope. This allowed correction for eccentricity in the land edges as the land width was reduced to a nominal 0.00015 to 0.00025 inch width. The final lands were continuous and without any significant abridgment from grinding or lapping flaws.

Seat No. 1 was cleaned, inspected, and vapor-deposit coated with a nominal 0.0012-inch thickness of CM-500 tungsten carbide over the land crests. The process was performed by Chemetal Corporation. The seat was induction heated to high temperature with tungsten and carbon bearing gases flowing over the surfaces to be coated. Buildup was preferential over corners and areas of maximum gas velocity. Examination of sectioned trial parts revealed that exposed corners received about two to three times the coating thickness as adjacent recessed fillets.

Final finishing of seat No. 1 was accomplished by OD, ID grind and flat lapping to produce continuous surfaces. Seat corners were spherically and flat lapped to a finished condition, as before. During this process, dimensions of the coating were continuously monitored to ensure coating thickness of not less than 0.0003 inch.

Extreme trouble was had with this part during initial lapping. Corners seemed to chip easily (in a very small way - on the order of 20 to 50 microinches) and material removal rate, even with coarse diamond (No. 20), was almost nonexistent. The problem was traced to a Vickers hardness well in excess of 2200. Desired coating hardness during this trial period was on the order of 1500 Vickers but no requirement was specified. Poppets received earlier were about 1400 to 1600 Vickers, so hardness measurements were not made on the seat. Discussions with Chemetal revealed that deposit hardness is variable with temperature, gas chemical composition, gas mixture ratio, flow rate, and time-at-temperature. Moreover, the coating can be softened with reheating to a high temperature. This was attempted with the coated seat and produced a coating hardness of about 1200 Vickers.

Poppet

Three poppet blanks of CM-500 tungsten carbide were chemically vapor deposited over molybdenum mandrels. Process control was developed by trial coating and sectioning several graphite parts. Two poppets were successfully formed. Part No. 1 required spherical ID grinding to produce print thickness requirements. Part No. 3 ID was finished by direct ball lapping. Sealing faces and the OD were diamond ground prior to acid etching the part from the mandrel. The latter was accomplished using 4/1 nitric to sulphuric acid at about 190 F. The shell poppets were then flat lapped to obtain spherical flatness within 10 μ in.

Before grinding the poppets the surface hardness of both parts was on the order of 1500 Vickers. However, to develop the required land width, ~ 0.015 inch was removed from the face of poppet No. 1 for a final thickness of 0.037 and 0.007 inch from poppet No. 3 with final thickness of 0.025 inch. Microhardness tests were made on the sealing and rear surfaces of each poppet. It was found that the thicker poppet (No. 1) was too soft for testing as the sealing surface was about 1000 Vickers and the rear side was only about 700. Poppet No. 2 was somewhat harder at around 1200 Vickers in the sealing area and 1000 on the rear side.

The cause of hardness variations was traced to a condition of variable hardness through the part depending on thickness, which is a function of deposition time. The thicker part (No. 1) was at temperature longer so a greater degree of softening was produced within the poppet compared with part No. 3. Thus, it was evident that material removal must be controlled in conjunction with deposition hardness gradient to produce the proper hardness at the final sealing surface.

In terms of structural strength the hardness gradient through the part is a significant advantage because the potential of brittle fracture is reduced compared with a through-hard part.

Guide Pins

Three solid carbide guide pins were ground per print to a 0.001- to 0.002-inch-wide edge. Preliminary evaluation, however, revealed excessive bearing stress from the lateral spring pin. To reduce the stress level, the solid pins were assembled into the body and cylindrically lapped to a 1.158/1.159 diameter and 0.003- to 0.005-inch width.

Two lateral spring guide pins were fabricated. Each pin was permanently bent to a predetermined deflection to produce an installed force on the poppet of 0.41 pound for one pin and about 1 pound for the second pin. The combination of the harder K602 carbide rubbing on the softer CM-500 poppet caused excessive scratching with the 1 pound spring. Consequently, all tests were performed with the 0.41-pound spring guide pin.

TEST PROGRAM

Evaluation of the prototype check valve consisted of a series of tests and measurements to establish basic functional performance. Leakage was thoroughly investigated in combination with crack and reseal pressures. Flow stability was also demonstrated. However, limited program scope precluded flow capacity and vibration tests.

Test Setup and Methods

The helium pressure feed system used in the model test program was adapted for testing the prototype check valve. As shown in Fig. 6-15, a dual level system, capable of controlling helium pressure from 0 to 30 and 0 to 600 psig with 0.1-percent sensitivity, provided precision control for leakage, crack, and reseal tests.

Cracking and reseal pressures were defined by flow increase or decrease from 0 to 10 scim with readings repeatable well within 0.1 psi.

Leakage measurements were made using a Teflon plug (Fig. 6-13) in the downstream port to reduce volume and provide for leakage collection to a 1 cc buret and leveling bulb apparatus. The technique employed was identical to that used in the model tests (described in Appendix D) and provided a leak rate sensitivity of less than 10^{-4} scim (0.1 scc/hr).

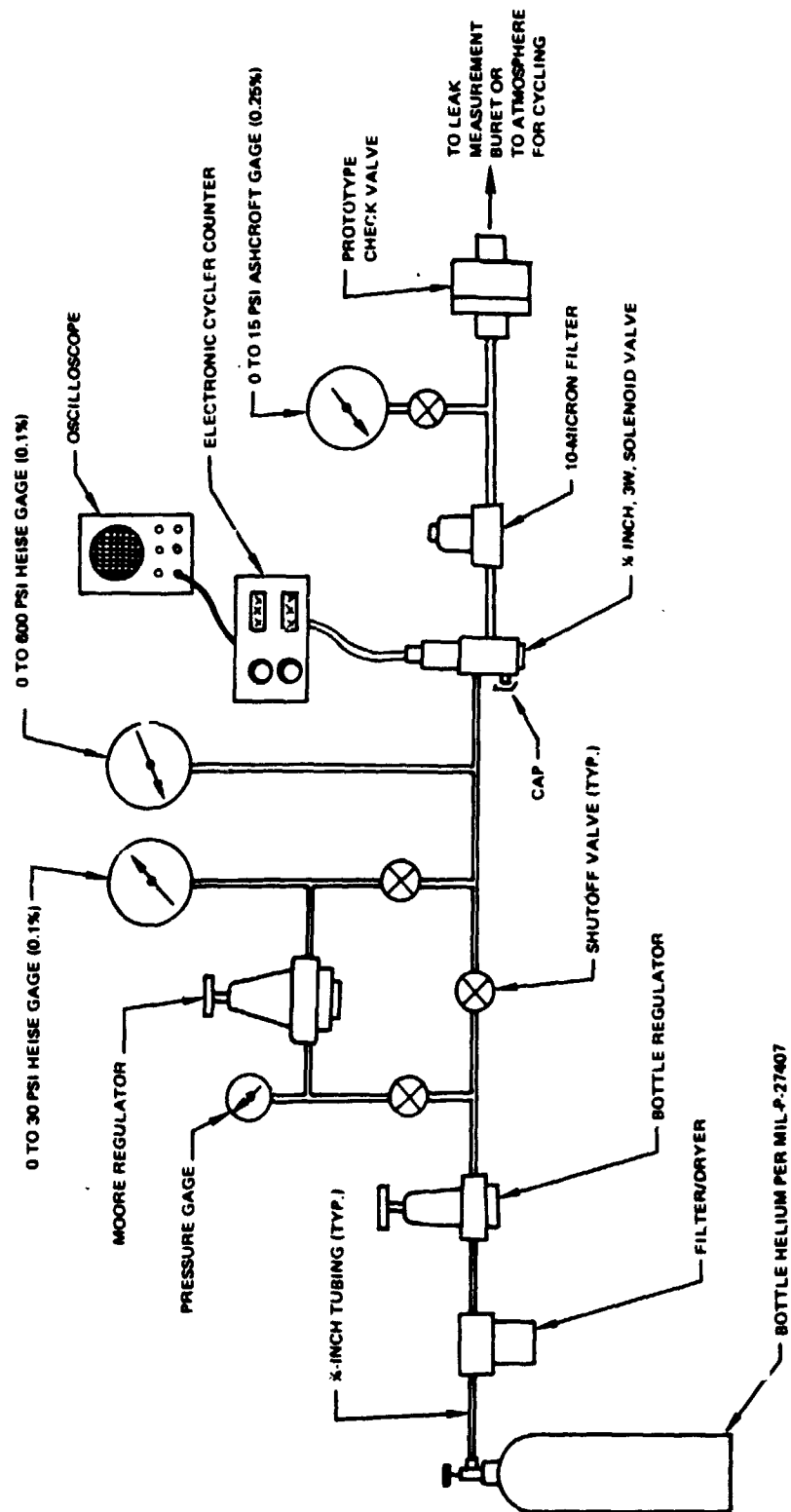


Figure 6-15. Leak and Cycle Test Setup

ORIGINAL PAGE IS
OF POOR QUALITY

Cycle testing was performed by pulsing the check valve open with 33 psig feeding a 1/4-inch, close coupled solenoid valve. Cyclic rate and pressure were established to ensure full opening and impact reseal of the check valve. The cyclic rate was on the order of 300 cycles per minute (0.5 ms open, 0.15 ms close). Full open was verified by direct measurement on the poppet through the outlet port. Impact reseal was evident by an audible click that could be varied by changes in supply pressure and cyclic rate. The solenoid valve supply pressure of 33 psig was set for maximum reseal impact. Cyclic rate was limited by the solenoid valve response. Capping the solenoid valve vent port did not significantly reduce the reseal click intensity, which indicated that the gas pressure pulse duration was probably considerably shorter than the poppet travel time. Consequently, the test method was probably more severe than the intended service in which closure occurs with a cessation in flow. The capped vent port did, however, reduce gas consumption.

Cracking and Reseat Pressure Tests

Crack and reseal pressure tests were performed initially with solid guide pins and then repeated with the 0.41-pound lateral spring guide pin; results were as follows:

| | <u>Crack, psi</u> | <u>Reseat, psi</u> |
|------------------------|-----------------------|------------------------|
| Without lateral spring | 1.4 | 1.4 |
| With lateral spring | 1.7 | 1.1 |

Leakage Tests

Several assemblies were made and numerous tests performed to 500 psid. Maximum leakage usually occurred between 0.1 and 1.0 psig reverse pressure with higher pressures producing increased seat loading and leakage reduction. Values ranging from less than 10^{-4} scim (0.1 scc/hr) to 0.003-scim helium were obtained up to 1.0 psid; higher pressure leakage was usually less than 10^{-3} scim (1.0 scc/hr).

During the test program a condition of apparent excessive leakage of up to 0.03 scim was observed for a seal normally about 0.003 scim at 0.5 to 1.0 psig or a ratio of about 10/1. The condition was determined to be caused by molecular flow at partial pressures. By purging the valve in one port with helium a helium pressure drop of 14.7 psia would be developed. Because air was present on the opposite side of the seat there was likewise an air pressure drop of 14.7 psia in the opposite direction. The noted 0.03 scim was, therefore, only an indication of the differential flow of helium into the leak apparatus and air in the opposite direction. Thorough helium purging of the downstream cavity and leak collection apparatus was required to establish true pressure drop leak rates and an indicated zero helium flow (i.e., less than 10^{-4} scim) at zero apparent pressure drop.

Analytical correlation of the leak results is provided by laminar and molecular flow leakage equations utilizing test data in which leakage is known for a given

load; typically for the prototype check valve: helium inlet pressure 1.0 psig (15.7 psia), downstream helium pressure 14.7 psia and actual leakage 0.00217 scim (2.1 scc/hr). Assuming a parallel plate leak path of length equal to 0.0002 inch and circumferential periphery of 3.20 inch indicates an equivalent gap between the poppet and seat of 1.0 μ in. This model can be used to evaluate the previously described cross flow of helium and air (or nitrogen) at apparent zero pressure drop. With a 14.7 psia differential of each gas on opposite sides, the predicted flows are 0.0317 scim helium and 0.0121 scim nitrogen or a difference of 0.02 scim or about 10 times the 1.0 psid observed leakage.

Full-Flow Stability Test

The check valve was directly connected to a feed regulator and slowly cycled from closed to full open to closed, with the outlet port dumping directly to atmosphere. There was no audible indication of chatter or unstable flow. Full open was verified by direct measurement of poppet position at the outlet port.

Cycle Tests

Two cycle tests were performed on the prototype check valve. The poppet and seat were refinished between each test.

For prototype cycle test No. 1, the seat land width was 0.00021 inch and outer land was 0.00028-inch wide. The results of cycle test No. 1, displayed in Fig. 6-16, show an increase in leakage with cycles with a maximum leakage of about 0.06 scim at 0.5 psid after 20,000 cycles. Disassembly inspection of the sealing surfaces revealed that the seat was grooving the poppet by several microinches and upset metal on the poppet caused small depressions in the seat. This is shown in Fig. 6-17 and 6-18. It was apparent that the combination of approximate 1200 Vickers hardness poppet and seat was cause for the deformed surfaces.

The sealing surfaces were refinished with the seat lands widened to about 0.00028 inch. Although performance was somewhat improved, cycling again caused leakage to increase, Fig. 6-19; inspection again revealed minor surface upset (Fig. 6-20 and 6-21).

In all tests, crack and reseal pressures were within 0.1 psi of previously noted values. Examination of guide pins and mating surfaces on the poppet showed up evidence of wear on the guide pins (2200 Vickers) and only minor scratching on the poppet rim (1200 Vickers).

Analysis of Test Results and Data Correlation

Crack-Reseat Hysteresis. Actual dimensions of critical details were measured to allow correlation of crack and reseal pressures and thus provide a reasonable estimate of the guide pin bearing coefficient of friction. Installed force of the axial spring was 1.34 pounds. Mean seat land diameters were 1.024 and 1.077 inch. From preceding analyses the theoretical cracking pressure without lateral spring is given by

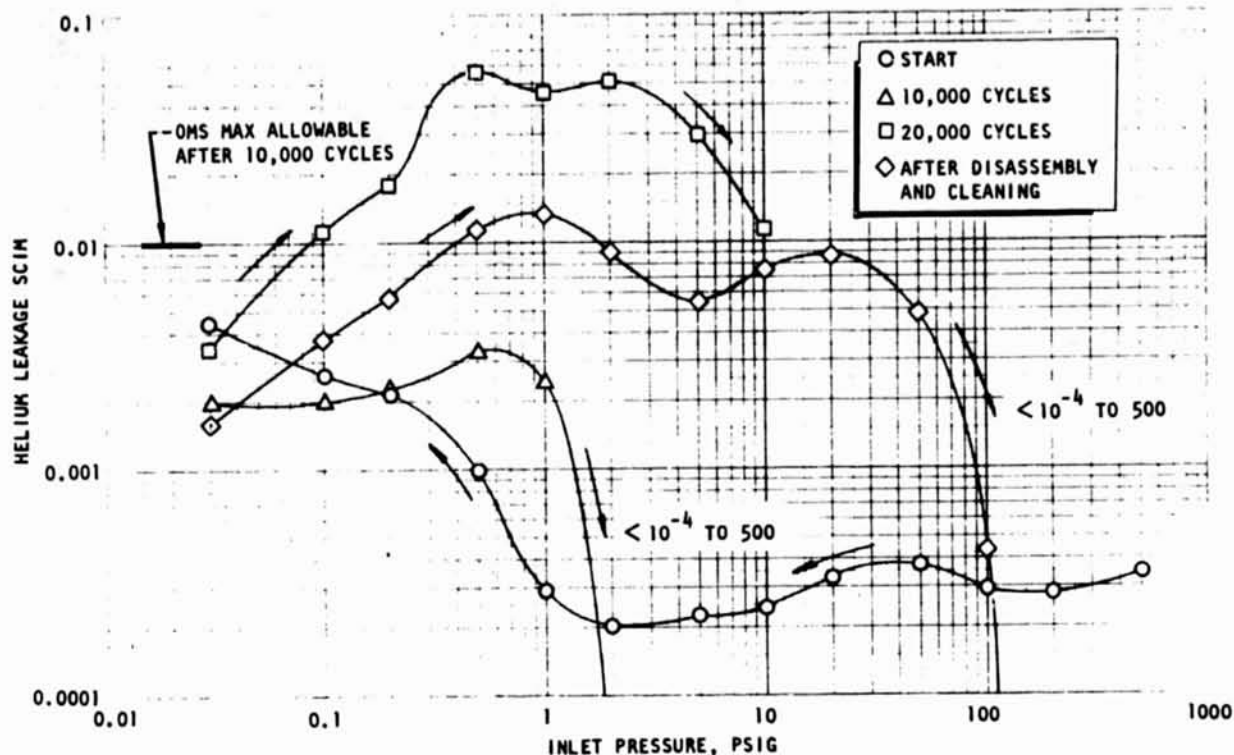


Figure 6-16. Prototype Cycle Test No. 1

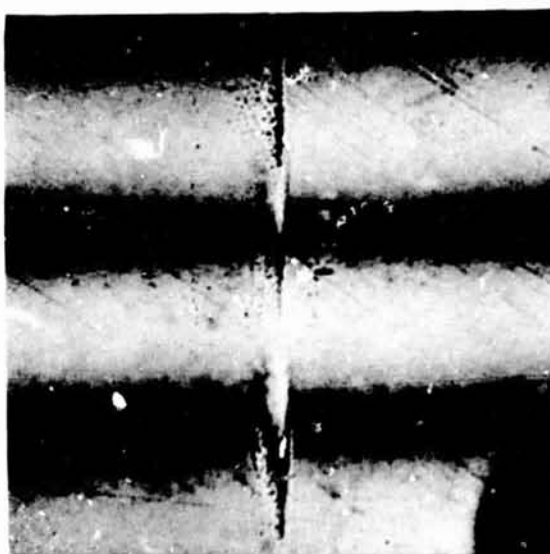


Figure 6-17. Test No. 1 Poppet
Showing Groove From Seat
(462X Interference Photo)

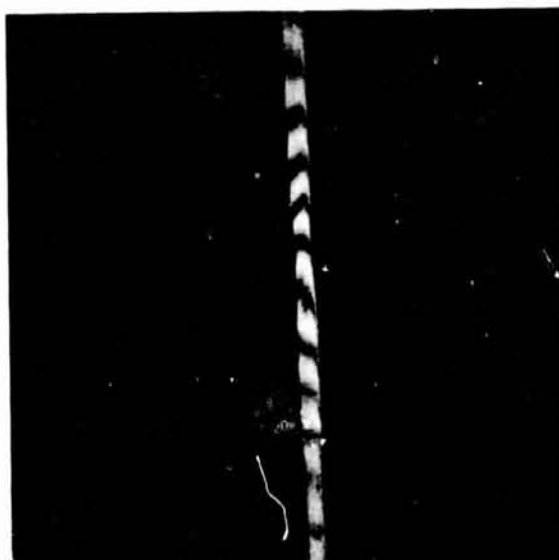


Figure 6-18. Test No. 1 Seat
Showing Deformed Land
(462X Interference Photo)

ORIGINAL PAGE IS
OF POOR QUALITY

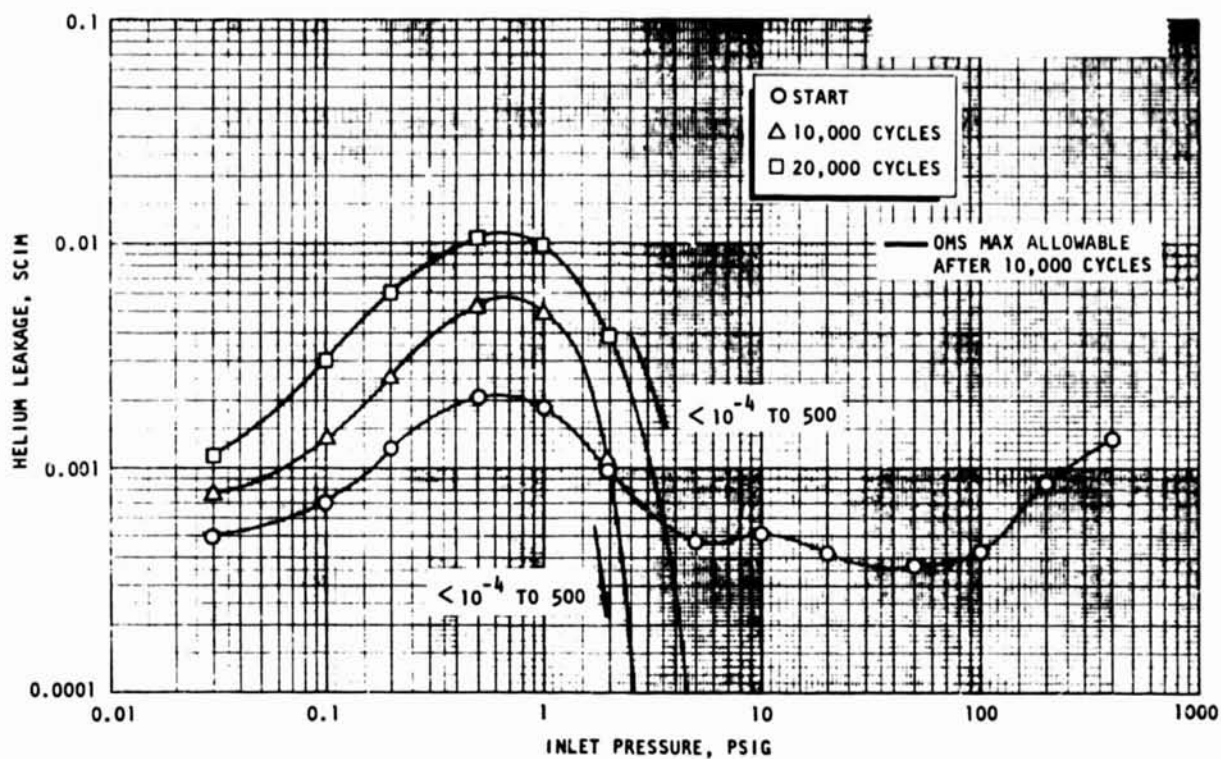


Figure 6-19. Prototype Cycle Test No. 2

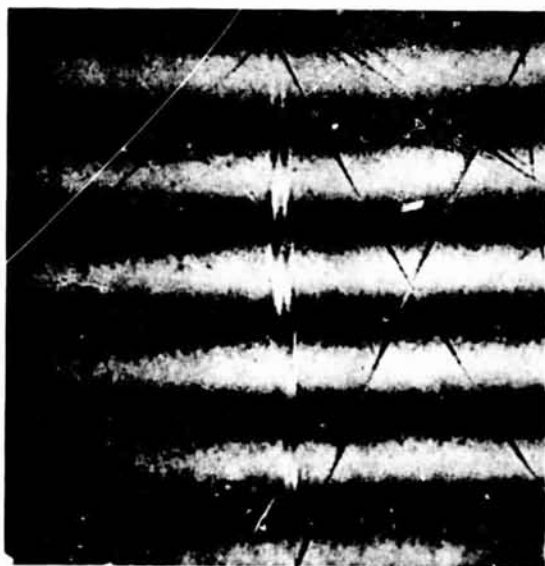


Figure 6-20. Test No. 2 Poppet Showing Groove From Seat (462X Interference Photo)



Figure 6-21. Test No. 2 Seat Showing Deformed Land (462X Interference Photo)

$$\Delta P_o = \frac{F_s}{A_2} = \frac{1.34}{0.7854 \times 1.077^2} = 1.47 \text{ psi}$$

or fairly close to the measured value of 1.4 psi.

The difference between cracking pressures with and without a lateral spring can be used directly to compute guide friction coefficient as follows:

$$\Delta P = \frac{F_s + 3\mu F_c}{A_2}$$

$$\Delta P_o = \frac{F_s}{A_2}$$

$$\mu = \frac{(\Delta P - \Delta P_o) A_2}{3F_c}$$

$$\mu = \frac{0.3 \times 0.7854 \times 1.077^2}{3 \times 0.41} = 0.222$$

It was expected that this friction coefficient and the corresponding +0.3 psi hysteresis would decrease with a harder poppet.

Cyclic Life. In review of the cycle test results, it was evident that the poppet and seat were too soft. As a basis for comparison, cutter model poppets and seats from the APS program (Ref. 4, and used herein) sustained several tests of 1 million cycles at 250 pounds impact with gradual reduction in leakage with cycles. Land wear was evident on the sealing surfaces (mostly the outer land) at about 1 to 3 μ in. but there was no evidence of upset metal. Hardness of these models was about 1500 to 1600 Vickers.

As shown in the Test Model section, the cutter model is exceedingly stiff and thus the load is more or less uniformly distributed over both lands. For 0.0002-inch-wide lands, the average seat stress at 250 pounds load is:

$$S = \frac{250}{\pi \times 0.00^2 (0.470 + 0.7000)} = 340,000 \text{ psi}$$

In comparison, at 500 psi the prototype check valve seat stress is:

$$S = \frac{500 (0.7854 \times 1.02^2)}{\pi \times 0.0002 (1.02 + 1.08)} = 310,000 \text{ psi}$$

However, measured deflection of the poppet dome at 500 psi was approximately 0.0003 inch, indicating most of the load was concentrated on the inner seat land. Consequently, excessive bearing stress on the softer surfaces was probably the cause of the observed surface degradation. Therefore, it is concluded that with the poppet and seat of suitable hardness, the design should be capable of sustaining many millions of cycles (or hours) of vibration in which small motion exists between the sealing surfaces.

Leakage. Experience with several refinishings and tests of the poppet and seat have demonstrated the capability of the cutter seal to achieve a low leak level at near zero loads (e.g., poppet weight). This characteristic stems from the extreme flatness of the sealing surfaces which mate to produce a maximum gap on the order of 2μ in. At pressures from 0.1 to 1.0 psig this gap theoretically corresponds to helium leakage between 0.001 and 0.01 scim (1 to 10 sec/hr). This is best illustrated by the theoretical correlation of actual leak data from prototype valve test No. 2 (Fig. 6-22). The plot presents computed seat force and gap obtained from measured leakage data versus inlet pressure. The results show the theoretical gap to be about 2μ in., which corresponds with the flatness produced. As pressure and load increase, slight waviness is pressed out and the gap is reduced to a dimension commensurate with the roughness level.

The advantage of the low load sealing characteristic is shown by Fig. 6-23 graph of predicted NO_2 vapor leakage versus seat load derived from the model gap data of Fig 6-22. Assuming decreasing seat load to the minimum value, NO_2 leakage rises to a maximum of about 0.08 scim. Extreme low seat force may result from near-cracking pressure drop across the check valve. Combined with the high vapor pressure of NO_2 and near zero seat load, the valve gap is thus controlled by the free position flatness produced on each surface, i.e., 1 to 2μ in. With polymer seals under the same conditions, a significantly greater waviness/roughness would produce a relatively greater gap (and therefore higher leakage) than the cutter seal, although leakage under a light load was comparable with the cutter seal.

SPARE PARTS TESTING

As the program progressed, requirements for the OMS/RCS quad check valve were firmed up by Space Shuttle contractors and commonalty became a major consideration. Sealing requirements for the OMS check valve were most stringent whereas long cyclic life was required in the RCS application. To verify the prototype check valve for both OMS and RCS applications, an additional (spare) poppet and seat were ordered (by NASA) with the object of completing 100,000 cycles. While meeting this objective, this effort uncovered significant new data in both fabrication and test experience with the CM-500 cutter seat and poppet. Seat No. 2 was completed for this effort.

Design and Fabrication

Results from previous testing showed that the poppet must be harder than the seat to preclude poppet damage being transferred to the seat upon high loading. Furthermore, it was believed that seat hardness should be near that of the Carmet CA315 cobalt-based tungsten carbide used in the previous APS program (about

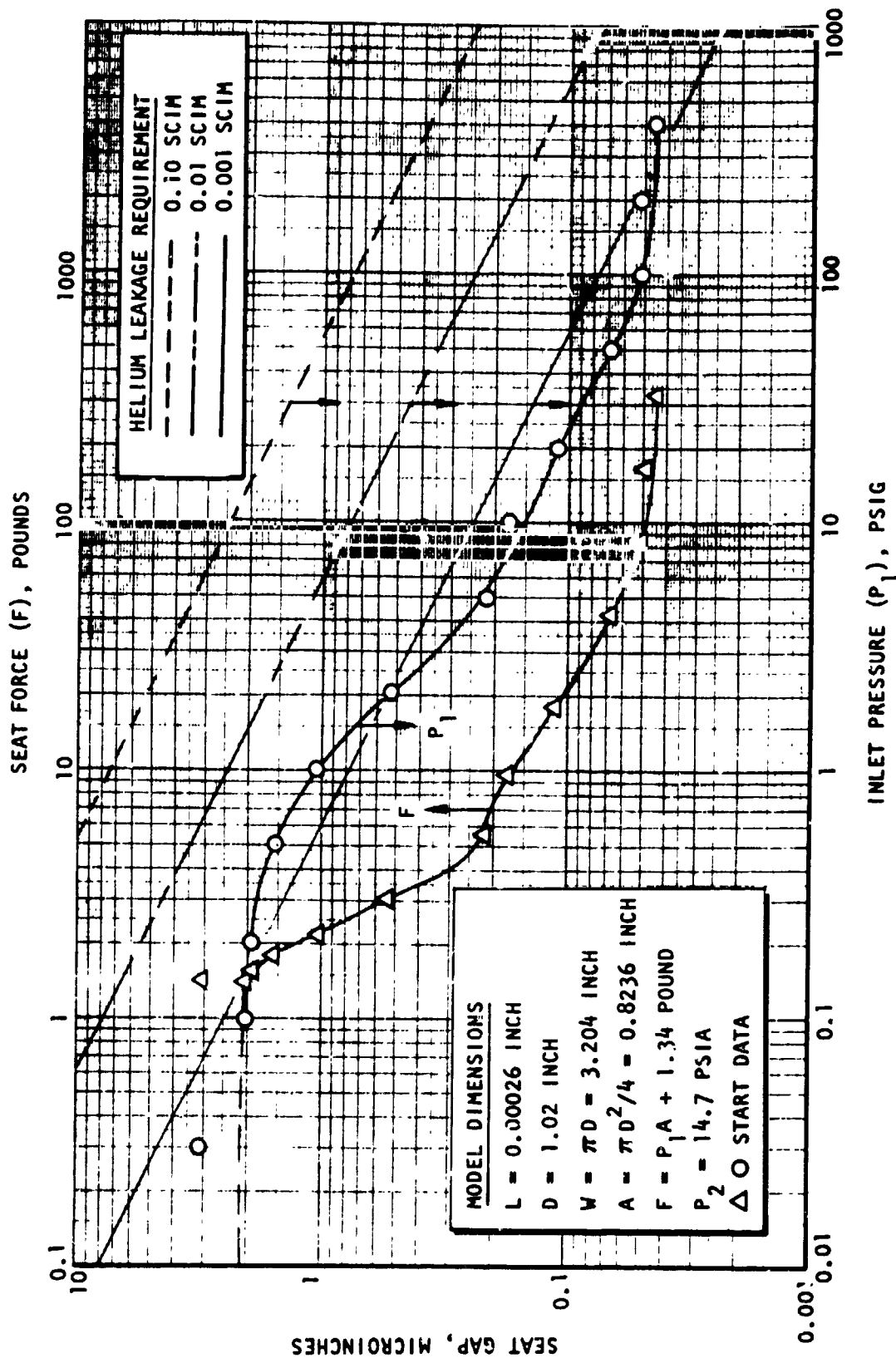
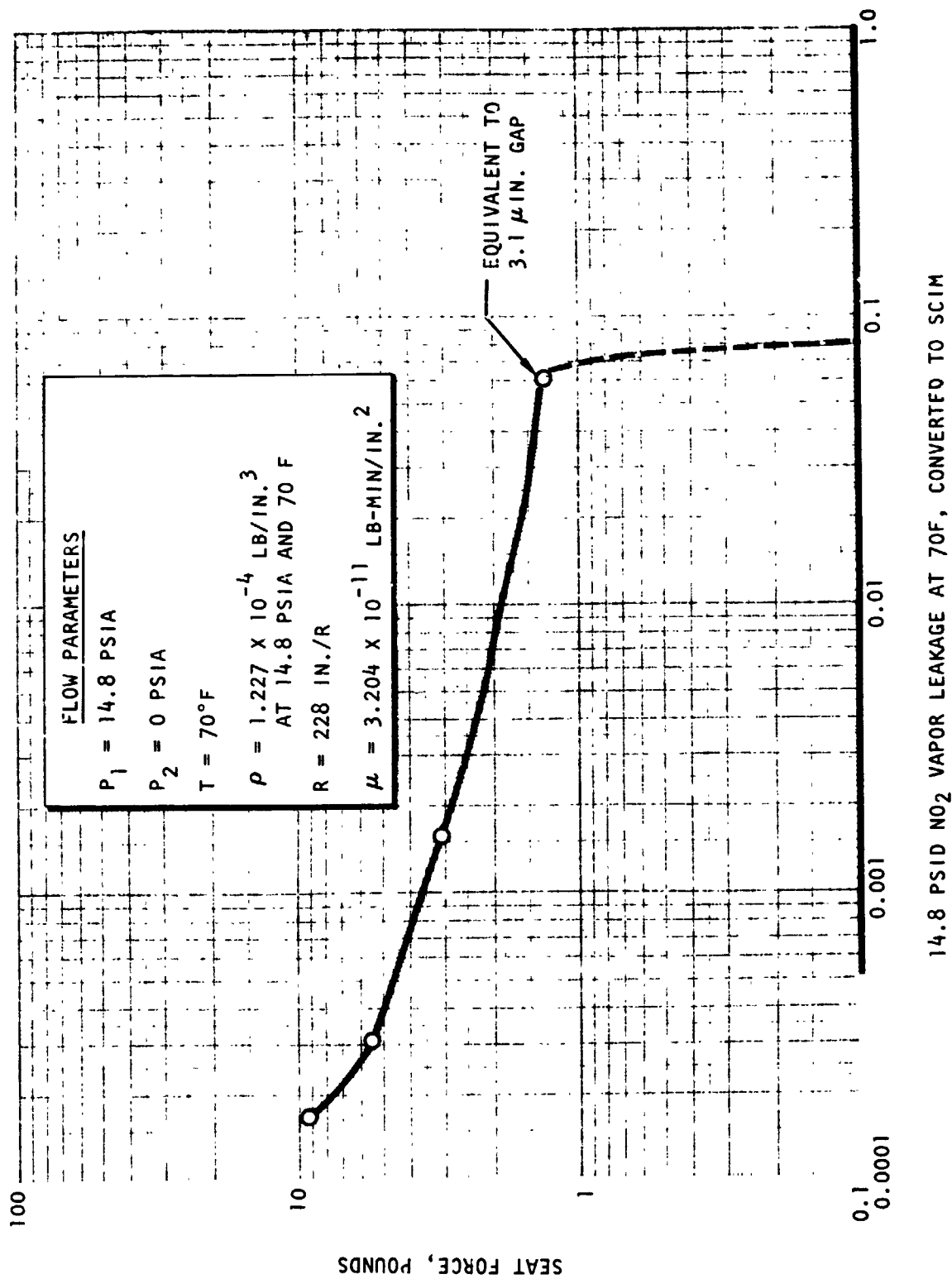


Figure 6-22. Prototype No. 2 Computed Seat Gap (Start)



14.8 PSID NO₂ VAPOR LEAKAGE AT 70F, CONVERTED TO SCIM

Figure 6-23. Predicted NO₂ Vapor Leakage (Prototype Check Valve, Test No. 2)

1600 Vickers). Hardnesses of 1600 to 1800 and 2000 to 2200 Vickers were selected for the seat and poppet, respectively.

To preclude the need for excessive removal of sealing face material to develop the necessary land width, the poppet mandrel was redesigned to incorporate a flat on the rim face rather than the previous full radius. The resulting poppet design is shown in Fig. 6-24 as an "A" change to the previous poppet (Fig. 6-6). The basic seat design was the same as shown in Fig. 6-8, except that final hardness was required to be 1600 to 1800 Vickers.

The Chemetal coating on each part as received was 1850 on the seat and 2300 Vickers on the poppet. Hand lapping the seat proved exceedingly difficult and tedious because of the extreme material strength and hardness. During flat lapping, the seat slipped off the edge of the lap, which caused a chip out of the base carbide material. The seat was then completely stripped and refinished for recoating. Hardness of the second coating was again about 1850 Vickers; however, the coating was only 0.0007-inch thick.

Considerably more effort was taken in lapping the second seat coating but great difficulty was again encountered because of the extremely slow material removal rate, even with relatively coarse diamond compound (6 to 12 microns). Adding to this problem, spherical lapping produced occasional minute chips on the land edge, believed caused by circumferential scratches produced by the coarse compound and the circular mode of lapping. To alleviate these problems, it was decided that a softer seat would reduce brittleness (and thus chipping) while allowing the use of finer compound. The seat was subjected to an anneal cycle. Although several runs were made to arrive at the desired 1400 to 1600 Vickers hardness, the final run of 60 seconds at 1000 C produced a hardness of 1200 or about the same as seat No. 1, which also had been annealed. Nevertheless, the seat was completed to obtain inner and outer lands of 0.00024 to 0.00028 and 0.00024 to 0.00030 inch, respectively. Further reduction of the lands to the desired 0.0002 inch was not made because of the initially thin coating. Final coating thickness over the sealing lands was 0.00032 inch. During spherical lapping to reduce the outer land to the noted dimension, the sharp edge of an inner lap was inadvertently placed over the outer land. Rotation produced 13 damaged areas, 2 of which were about 0.01 inch long and several ten-thousandths-inch deep. As a result, only the inner land was capable of sealing.

The first spare poppet (No. 4) fabricated was set up in an OD grinder for face and OD grinding. Grinding proved difficult and caused surface spalling on the poppet face. About 0.004 inch was removed by grinding, followed by 0.003 inch removed by flat lapping to eliminate the noted grind pits. This excessive material removed resulted in reduction of the sealing face hardness to 1700 Vickers.

Distribution of deposited material on poppet No. 4 was unlike previous poppets because of process variables and flow over the sharper face corners. Consequently, material buildup in the spherical cavity was heavier near the rim and thin near the center. Rim and center thickness, as deposited, were 0.035 and 0.019 inch,

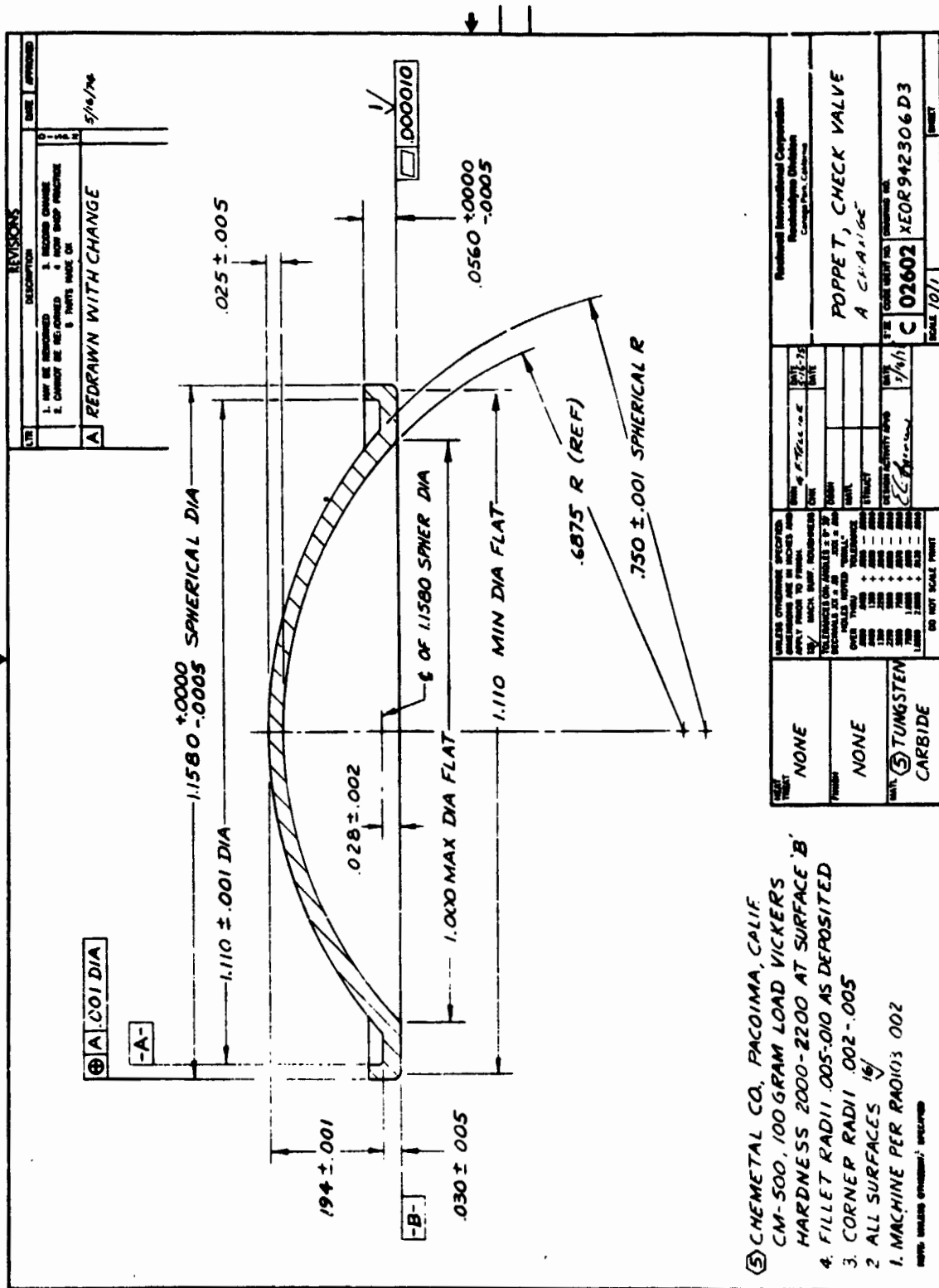


Figure 6-24. Check Valve Poppet ("A" Change)

respectively. Final thicknesses after face grinding and partial cleanup of the spherical cavity by ball lapping were 0.028 and 0.017 inch, respectively. Thus, the poppet center thickness was under that specified per blueprint.

Lapping poppet No. 4 to an adequately flat condition proved difficult because of a significantly wider land and harder material than previous poppet No. 3. These problems were eventually understood and corrected but led to further refinement in poppet land design. The design of poppet NO. 5 was varied from that of No. 4 (Fig. 6-24) as follows:

| <u>"A" Change (No. 4)</u> | <u>"B" Change (No. 5)</u> |
|---------------------------------------|--------------------------------|
| 0.194 | 0.200 |
| 0.030 <u>+</u> 0.005 | 0.030 +0.005 -0.000 |
| 0.005 to 0.010 inner fillet radius | 0.020 +0.010 -0.000 |
| 1.110 inch diameter minimum | 1.100 inch diameter minimum |

The purpose of these changes was to provide a narrower flat land without the sharp inner corner which produced an edge buildup at the entry to the spherical cavity. Furthermore, poppet No. 5 was to have a hardness of 1800 to 2000 Vickers to match with the desired seat hardness of 1400 to 1600.

Process variables and human error resulted in unusable parts for both poppets No. 5 and 6. With poppet No. 5 the rim mask was incorrect resulting in too short an axial length (0.056 dim.). Compounding this error the part was OD ground using a machine of inadequate stiffness that produced chips around the OD, which led to cracks across the face discovered during preliminary tests. It should be noted that even with numerous surface cracks this part sustained 500-psi pressure drop, which can be attributed to the relatively soft back side of about 500 Vickers (R_C 50).

Poppet No. 6 thickness was excessive (0.044-inch rim, 0.026-inch center) and would have required chordal and face grinding to obtain the desired thickness. This may be a necessity in production but so would an adequate process for grinding. Economies precluded further experimentation and all additional effort was expended using poppet No. 4

Cycle Test Results

Two cycle tests were performed in spares testing. In the first test of 50,000 cycles, poppet No. 4 was assembled with seat No. 1 which was refinished from previous testing. At this point in time, parts hardnesses were not as desired (1700 Vickers poppet, 1200 seat) but the pair had sufficient differential hardness to demonstrate long cyclic life. Guide pins and the lateral spring of 0.41 pound side force was identical with that used for the last 20,000-cycle test. After flat lapping the seat, land widths were 0.00031 to 0.00032 inch

(inner) and 0.00038 to 0.00040 inch (outer). The lands were not spherically lapped to narrow the seats because of coating thickness estimated at 0.0004 inch.

Results from the 50,000-cycle test are summarized in Table 6-2. Difficulty was experienced in obtaining the leakages noted. This was finally traced in the subsequent 100,000-cycle test to flatness errors in the poppet. These errors also helped explain the trend of increased leakage above 50 psi indicated in Table 6-1 and the phenomena of varying leakage with poppet orientation shown following the test.

Seat No. 2 was used with poppet No. 4 to demonstrate cyclic capacity to 100,000-cycles. The poppet was relapped to obtain peripheral flatness within an estimated 2 μ in. The guide pins were cylindrically lapped in place to produce lands 0.008/0.009 inch wide. The resulting increased diameter between pins was compensated by rebending the lateral spring to produce a side load of 0.45 pound.

Precycling conditions were: $P_C = 1.6$ psig; $P_R = 1.2$ psig; leakage less than 1.0 scc/hr helium for pressures noted in Table 6-1. These data were repeated at 10,000-cycle intervals through 100,000-cycles. Cracking to reseal hysteresis increased up to $P_C = 2.25$ psig, $P_R = 0.8$ psig at 20,000-cycles, whereupon the valve was disassembled. Guide pins 1 and 2 (the lateral spring) were worn over the entire width. The poppet was rotated and the valve reassembled with crack and reseal pressure returning to the original 1.6 and 1.2 psig. Leakage remained less than 1.0 scc/hr.

From 30,000 through 100,000-cycles the crack and reseal pressures remained at 1.55 to 1.6 psig and 1.2 psig, respectively. Numerous leak tests uncovered several heretofore unknown variables that led to the conclusion that the "noise level" of the test was on the order of 0.5 scc/hr. Variables identified were: (1) thermal effects from cycling, pressurization to 400 psig and venting to low pressure; (2) molecular flow and diffusion interactions between gases upstream and downstream of the seat, which included the air and water vapor in the buret column; and (3) torque from the outlet port B-nut, which could cause a significant level of creep in the TFE volume-reducing and leak-collection plug. It was found that after cycling or pressurization, thorough purging of the entire system with helium was necessary and up to several hours stabilization was required to establish a "zero" indicated flow (i.e., less than 0.1 scc/hr) at zero pressure drop, as defined by a vented upstream line and buret water level differential within 0.01 inch of atmospheric.

At the test conclusion the valve was allowed to stabilize as noted for several hours and indications were that leakage at the noted pressures was significantly less than 1.0 scc/hr with values measured at about ± 0.2 scc/hr. These results point up the variables and difficulty in accurately measuring leak rates between 10^{-5} and 10^{-3} scim (0.01 to 1.0 scc/hr). Moreover, it is imperative that the noise level for any system be thoroughly defined before it can be used to establish low level leak rates.

Valve disassembly and inspection showed that the guide pin wear had not progressed significantly beyond that observed after 20,000-cycles. Apparently, the initial wear matched the guides to the poppet OD, and when combined with a new

TABLE 6-2. 50,000-CYCLE TEST

| Cycles → Pressure, psig | 0K | 10K | 20K | 30K | 50K |
|---|-----------------------|------|-----|------|---------------|
| | | | | | |
| P_c → | 1.65 | 1.84 | -- | 2.1 | 2.15 |
| P_r → | 1.3 | 1.2 | -- | 0.9 | 1.0 |
| P_l | scc/hr helium leakage | | | | |
| 0.1 | 4.1 | 1.3 | 1.1 | 2.2 | 5.9 |
| 0.2 | 3.7 | 1.2 | 1.0 | 2.1 | 4.8 |
| 0.5 | 3.1 | 1.2 | 1.0 | 1.9 | 4.5 |
| 1 | 2.5 | 1.2 | 1.0 | 1.7 | 3.4 |
| 2 | 1.7 | 1.0 | 0.8 | 1.4 | 3.4 |
| 5 | 0.7 | 0.3 | 0.3 | 0.5 | 1.3 |
| 10 | 0.4 | <0.1 | 0.2 | 0.2 | 0.4 |
| 20 | 0.4 | <0.1 | 0.4 | 0.2 | 0.3 |
| 50 | 0.7 | 0.7 | 1.0 | 0.6 | 0.5 |
| 100 | 1.4 | 1.4 | 1.3 | 1.1 | 1.9 |
| 200 | 3.1 | 2.7 | 2.8 | 2.4 | 5.5 |
| 400 | 4.6 | 5.4 | 6.0 | 5.0* | 16.6** *** |
| <p>*Valve disassembled following this test to inspect for guide wear--none visible; poppet rotated 180 degree with $P_c = 1.68$ psig, $P_r = 1.2$ psig</p> <p>**Valve disassembled and found two solid guide pins worn with matching grooves in the poppet; wear depth was <0.0001 inch. There was no visible (500X) sealing surface wear or deformation.</p> <p>***Valve reassembled with poppet reoriented and leakage from 0.1 to 400 psig was <1.0 scc/hr</p> | | | | | |

unworn area on the poppet OD, there was little further wear. There was no visible wear of the poppet OD for the final 80,000-cycles. Similarly, there was no visible wear or deformation of the sealing lands or poppet surface at 500X.

Wire Cutting Tests

The damaged outer land of seat No. 2 was used with poppet No. 4 to measure the force required to cut or mash CRES and copper wear. The outer land width was nominally 0.00027 inch. The valve was assembled without lateral or axial springs so that closure force was simply inlet pressure times seat area plus the poppet weight (0.024 pound). Wires evaluated were 0.0004- and 0.001-inch CRES and 0.001-inch copper. For the 0.0004-inch CRES wire a loop was laid over the outer land so that two wires were mashed. Only a single strand was used in evaluating the 0.001-inch wires. Results of the tests are summarized in Table 6-3. Note that the force tabulated is the total force applied and is equivalent to a centrally applied spring force. The actual load applied to the wire was one-half the tabulated force.

The data of Table 6-3 indicate that higher loads were required to mash or cut the 0.0004 inch CRES and 0.001-inch copper wires than observed in model testing. However, with a 1.5-pound spring there is sufficient force to meet the 10 scc/hr requirement for low (less than 1.0 psid) pressure drop conditions. The leakage condition is improved with higher pressure drop. Also, it is certain that a narrower land would reduce the required load.

Disassembly and inspection of the valve seat at 500X indicated that the maximum load applied of 8.26 pounds was insufficient to cause any permanent deformation of the sealing land.

Analysis of Test Results

The spare parts tests served primarily to underscore the fabrication variables while demonstrating the potentially indefinite life of the cutter seal. The cycle and wire cutting test results have indicated that 1200 Vickers may be a suitable lower hardness limit for the seat. These tests also verified the cutting ability of the cutter seal and reaffirmed the need for a narrow land on the order of 0.0002 inch.

PROJECTED QUAD VALVE PERFORMANCE

Comparison between the prototype valve actual performance and that projected for a quad configuration is presented based on the goals and requirements set forth in Appendix A. It is expected that a flightweight quad valve incorporating the shell poppet-cutter seal design would simply be four prototype valves housed in a lightweight series-parallel configuration. Secondary static seals at each seat would contribute to seat seal leakage.

Application

Ability to minimize propellants from leaking past the valve to the upstream system is predicted for prototype model seals in the Leakage Analysis section.

TABLE 6-3. WIRE CUTTING TEST RESULTS

| P ₁ psig | F, * pounds | 0.0004 inch CRES Wire | | 0.001 inch Copper Wire | | 0.001 inch CRES Wire | |
|------------------------|----------------|-----------------------|------------------|------------------------|---------------|----------------------|---------------|
| | | Q, scc/hr He | hp, μ in. ** | Q, scc/hr He | hp, μ in. | Q, scc/hr He | hp, μ in. |
| 1.0 | 0.847 | 87.0 | 7.1 | 60.0 | 5.9 | 39.0*** | 4.8 |
| 1.5 | 1.26 | 82.0 | 5.6 | 21.0 | 2.9 | 15.0 | 2.5 |
| 2.0 | 1.67 | 63.0 | 4.3 | 13.0 | 2.0 | 7.3 | 1.5 |
| 3.0 | 2.49 | 41.0 | 2.9 | 4.4 | 1.9 | 2.0 | 0.6 |
| 4.0 | 3.32 | 21.0 | 1.8 | 2.2 | 0.6 | 0.6 | 0.3 |
| 5.0 | 4.14 | 16.0 | 1.4 | 1.3 | 0.4 | <0.1 | <0.1 |
| 7.0 | 5.79 | 2.8 | 0.5 | 0.8 | 0.3 | <0.1 | <0.1 |
| 10.0 | 8.26 | <0.1 | <0.1 | 0.7 | 0.2 | <0.1 | <0.1 |

*F = $(\pi/4 \times 1.02392) P_1 + 0.024 = 0.8234 P_1 + 0.024$ pound

**Mathematical Model: Parallel plate ($h_p = \text{GAP}$) laminar-molecular flow, $L = 0.00027$ inch

***Just prior to 1.0 psi, audible click indicated wire cut

While all liquid leakage is probably negligible, it is shown that there is the potential of significant NO₂ vapor leakage, depending on the allowed level of helium leakage.

Fluid Media Compatibility

Propellant compatibility was a major consideration in selection and evaluation of model seals. Materials were selected based largely on results of prior compatibility studies. However, little data were available on cutter materials and broad assumptions were necessary to provide concrete evidence of compatibility, particularly with N₂O₄ and its acid byproducts. Limited time and budget allowed study of only one compatibility parameter and cutter seal materials were therefore selected based on resistance to RFNA, as described in the Materials Investigation section. Propellant combinations and residues thereof were not evaluated and could constitute a leakage hazard if such residues were to build up on the sealing surfaces and agglomerate sufficient solids to withstand the cutter seal. However, if such were the case, it is difficult to imagine any other seal concept more capable of performing a comparable sealing function.

Contamination

Contamination tolerance was demonstrated with metal wire particles from 0.0004- to 0.003-inch diameter. It is certain that much larger organic or polymeric particles would have negligible effect on the seal. On the other hand, very hard metal or ceramic particles could cause excessive leakage if entrapped between the poppet and seat. It has been demonstrated, however, that the probability of cyclic entrapment is a direct function of the seal land width (Ref. 2). With a land only 0.0002 inch wide the probability of closing on a comparably sized hard particle is quite small because the incidence of such particles is very low in filtered gaseous systems. Furthermore, the probability of both series check valves entrapping a particle on the same closure cycle is even more remote. Because the cutter seat cannot permanently embed particles, it is concluded that the potential for particle derived leakage is negligible with the cutter concept in a filtered helium system.

Previous check valves have failed to crack or reseal because of contaminants entrapped in guide bearings. This problem has been completely overcome with the shell poppet guided by three narrow lands, one of which is a movable lateral spring.

Service Life

The service and cyclic life of the cutter seal has been shown to be greater than the 100,000-cycle RCS requirement. Redesign of the pin guides will be necessary to prevent a granular type of wear between the guides and poppet OD (particularly with a 1-pound side load) so that cracking and reseal pressures will remain constant throughout the cycle life.

Moisture Sensitivity

Very thin ice films coating the sealing surfaces or guide bearings will cause virtually any check valve to fail. Although not tested in this program, it is expected that under icing conditions causing conventional check valves to fail, the prototype valve would function satisfactorily.

Mechanical Design Characteristics

Previous valve failures have led to concepts for advanced component design, as defined in Appendix A under the above heading. The prototype valve does not have any critical flow passages. Sliding contacts were purposely incorporated to provide stable operation but were designed to minimize wear. Precision guidance is not required by the cutter seal and may, in fact, derive some benefit from closure scrubbing in reducing cutting loads and leakage.

Thermal Environment

Provided the valve body structure does not warp the carbide seat, +150 to -150 F temperatures will have negligible effect on the valve functions.

Flowrate, Pressure Drop, Cracking Pressure

With a large poppet diameter and short stroke the valve capacity is determined more from the cracking pressure than basic flow area. Computations shown in the Check Valve Development section indicate adequate capacity. However, full flow tests of a quad valve are required to accurately establish pressure drop.

Operating, Proof, Burst and Surge Pressures

The prototype valve was proofed to 600 psig and each poppet tested to 500 psi. One poppet with numerous surface cracks sustained 500 psid without failure. However, burst tests were not performed and are needed to establish real safety factors. Opening surge pressure testing was not performed (as described in Appendix A) but such operation should have negligible effect on the poppet or the mating impact surfaces.

Stability

Stable operation of the valve was demonstrated in cycling between closed and full open with discharge to atmosphere. Furthermore, the valve was continuously stable throughout 150,000 cycles discharging to atmosphere.

Leakage

The cutter seal has demonstrated the capability of meeting 0.1 scc/hr helium leakage from 0.1 to 400 psig. However, the program results have clearly indicated several problems in attempting to accurately measure this very low level of leakage by volumetric means. Unavoidably large internal volumes in the quad valve will necessitate extended stabilization periods and repeated evaluation of the apparent background leakage caused by molecular flow-diffusion and pressure-temperature effects.

In the quad valve, leakage will result from the cutter seal and a secondary static seal between the seat and valve body. Overall valve leakage therefore will be comprised of two static and two seat seals. Based on the work herein, the design goal of 1.0 scc/hr is considered a reasonable goal for a new quad valve.

With welded construction, external leakage will be ascertained with a mass spectrometer and should present few problems.

Vibration

Vibration was the major consideration in arriving at the shell poppet and lateral spring design. As shown by computations in the Check Valve Development section, the combination of poppet weight, friction, and spring forces provides considerable resistance to acceleration loads. Vibration testing was not performed and valve performance could be seriously affected by poppet-to-seat impacts or fretting due to lateral scrubbing.

RCS Commonalty Considerations

These considerations have been satisfied by demonstrating long life and ability to function stably under very low flow conditions.

REFERENCES

1. Tellier, G. F.: Poppet and Seat Design Data for Aerospace Valves, AFRPL-TR-66-147, DDC AD 488480, Rocketdyne Division, Rockwell International, Canoga Park, California, July 1966.
2. Tellier, G. F. and J. W. Lewellen: Poppet and Seat Design Criteria for Contaminant-Particle Resistance, AFRPL-TR-70-1, DDC AD 878212, Rocketdyne Division, Rockwell International, Canoga Park, California, April 1970.
3. Tellier, G. F. and T. R. Spring: Contaminant Particles in Metal-to-Metal Closures, AFRPL-TR-7-112, Rocketdyne Division, Rockwell International, Canoga Park, California, December 1971.
4. Smith, G. M.: High-Performance Space Shuttle Auxiliary Propellant Valve Program, NASA CR-120976, Rocketdyne Division, Rockwell International, Canoga Park, California, June 1973.
5. Anon.: Space Shuttle Seal Material and Design Development for Earth Storable Propellant Systems, 22539-6001-RO-00, TRW Systems Group, TRW, Inc., Redondo Beach, California, October 1973.
6. Howell, G. W., Weathers, T. M.: Aerospace Fluid Component Designers Handbook, RPL-TDR-64-25, TRW Systems Group, TRW, Inc., Redondo Beach, CA, Rev. D, Feb. 1970.
7. Design Guide for Pressurized Gas Systems, Contract NAS7-388, IIT Research Institute, Chicago, Ill., March 1966.
8. "Leakage Testing Handbook", Contract NAS7-396, General Electric R&D Center, Schenectady, N.Y., July 1969.
9. Dushman, S., et al: Scientific Foundations of Vacuum Technique, John Wiley & Sons, New York, 1962.
10. Binder, R. C.: Fluid Mechanics, Prentice-Hall, N.J., 1962.
11. Shapiro, A. H.: The Dynamics and Thermodynamics of Compressible Fluid Flow, Vol. 1, Ronald Press, N.Y., 1953.
12. Blair, A. W., et al: Measurement and Correlation of Helium and Fluid Leak Rates, D2-114258-1, Rev. A, Boeing Co., Houston, Texas, July 1968.

APPENDIX A

GENERAL TECHNICAL GUIDELINES

The following guidelines were extracted (in part) from the contract statement of work. They were defined as optimum design objectives and, with a few noted exceptions, not considered as firm requirements. Consequently they were subject to change in accordance with technology limitations and reliability considerations. One of the primary objectives in the work was to help define realistic requirements for check valves and general poppet sealing for the Space Shuttle and thus help avoid component and system problems that result from unrealistic performance requirements. The intent of this effort was to develop new technology, but sufficient similarity between this program and the flight program was required to allow utilization of the results.

APPLICATION

The Space Shuttle OMS propulsion system will utilize earth-storable propellants that will be pressure fed to the rocket engine(s) with gaseous helium. A check valve will be located between each propellant tank and a common helium pressurization system. The function of the propellant check valves is to minimize propellant vapor mixing, reduce vapor exposure of the pressurization system, and prevent any liquid exposure of the pressurization system.

CONFIGURATION

The propellant check valves will be a quad redundant configuration. This means that one valve will consist of four independent check valve subassemblies that will provide two parallel flow paths to each propellant system with two series check valve subassemblies in each path and either path will be capable of satisfying the flow requirements.

FLUID MEDIA COMPATIBILITY

The valves must be compatible for exposure to the following propellant vapors, liquids, and combinations of oxidizer and fuel vapors. Although a separate check valve will be utilized for each propellant, each valve must be compatible with both propellants to prevent propellant leakage through one valve from failing the other valve. The propellants will be nitrogen tetroxide (N_2O_4), unsymmetrical dimethylhydrazine (UDMH), 50-50 blend of hydrazine and unsymmetrical dimethylhydrazine (N_2H_4 -UDMH), and monomethylhydrazine (MMH). The valves must also be compatible with anticipated flushing and cleaning fluids.

In evaluating propellant compatibility, propellant and moisture combinations must be evaluated since once a valve is exposed to propellants it is unreasonable to assume that the unit will remain free of moisture for the remaining service life. Propellant decontamination of components to extend the service life is not allowed since cleaning of hardware between missions is improbable and will result only when required to ensure personnel safety during system repairs. Propellant

compatibility is a primary design requirement for this program. Conclusive data must be supplied or generated for each material that is considered for use, and all data sources or test data must be documented.

CONTAMINATION

Contamination tolerance is a major design objective for these valves. As a design goal, the design should be insensitive to particles of 150 microns and smaller. Limitation of self-generated contamination will also be a primary design goal. The contractor will take appropriate measure to limit self-generated contamination. These measures, as well as the contamination sensitivity tolerance, will be documented in detail during this contractual effort. Contamination failures were a major failure mode during the Apollo program and significant improvements in both component tolerance and self-generated contaminants will be required for the Space Shuttle program. In evaluating the component contamination tolerance, the contractor will trade off the penalties associated with the 150-micron contamination capability.

SERVICE LIFE AND REFURBISHMENT

A design goal is to obtain valves capable of a minimum shelf life of 7 years and a service life of 5 years with no maintenance other than minor adjustments or recalibration allowed. As a guideline, the contractor will assume that 1 year of service life consists of 520 minutes of flow time. This will consist of 16 minutes per mission for 20 missions and 10 minutes of ground checkout per mission. The design will be refurbishable and the possibility of critical subassembly replacement in the field should be evaluated.

MOISTURE SENSITIVITY

The contractor will take appropriate design measures to minimize the sensitivity of the valves to moisture and propellant vapor freezing.

MECHANICAL DESIGN CHARACTERISTICS

To enhance component performance potential and to ensure a technologically advanced component design, the following mechanical design characteristics should be incorporated into the design unless significant design penalties are involved:

1. No critical flow passages or orifices that could be susceptible to particulate contaminate or propellant reaction residue fouling
2. No sliding contact surfaces to eliminate frictional wear, self-generated contaminants, and sources of contaminate fouling
3. Precision guidance to reduce scrubbing at the seal interface to a level defined as acceptable in the analytical sealing tradeoff studies
4. Simplicity of design to minimize failure sources

THERMAL ENVIRONMENT

The valves will be required to function nominally for helium inlet temperatures varying from a maximum of +150 F to a minimum of -150 F and for unit temperatures that will vary from +150 to -20 F at the initiation of helium flow through the unit.

FLOWRATE

As a sizing design point, a flowrate of 1.2 lb/min of helium at 70 F will be used. However, the contractor should maintain an awareness during his design effort that the flowrate requirements for a flight qualified valve for the Space Shuttle OMS are not firmly derined. Three possible cases exist:

1. Nominal operation: Approximately 1.2 lb/min at 70 F
2. Simultaneous propellant supply to two OMS engines (cross feed lines from one OMS pod or payload bay kits): Approximately 2.4 lb/min at 70 F
3. Emergency OMS propellant dump: Requirement presently not defined but may require dumping of total OMS pod propellant supply in 100 to 200 seconds

OPERATING PRESSURE

The unit will be capable of operating as specified for nominal operational pressures from a minimum of 200 psi to a maximum of 275 psi and will be capable of withstanding full tank pressure (i.e., 275 psi) across the valve in the reverse flow direction for extended periods of time.

PRESSURE DROP

Minimum pressure drop is a desirable valve characteristic but consistent pressure drop is essential to propulsion system mixture ratio control. As a design goal, the pressure drop should be limited to less than 5 psi (with 3.5 psi as a target goal), but this value is subject to evaluation with respect to increased performance (i.e., dynamic stability, contamination tolerance, leakage, extended life, etc.).

CRACKING PRESSURE

The cracking and reseal pressure for the valve poppets will be controlled only to the extent that the valve satisfies the other requirements and not interfere with OMS or RCS operations by imposing unacceptable propellant tank pressure variations. The valve will be required to crack and relieve the pressure downstream of the regulators prior to the possibility of overpressurization of any regulator element.

PROOF PRESSURE

The unit will be capable of withstanding a proof pressure of one and one-half times the maximum operating pressure without failure, distortion, or subsequent variation of any of the valve performance parameters.

BURST PRESSURE

The unit will be capable of withstanding a burst pressure of two times the maximum operating pressure without rupture.

SURGE PRESSURE

The unit will be capable of withstanding, without subsequent performance degradation, a helium surge pressure of one and one-half times the maximum operating pressure that will occur within 100 milliseconds of flow initiation. Since this surge will vary depending on the specific regulator and pressurization system characteristics, as well as operational modes, the design should not depend on surge pressure for check valve operation.

STABILITY

The unit will perform stably throughout the preceding pressure and flowrate ranges. The unit will stabilize within a maximum of 2 seconds after flow initiation. During "stable" operation, limited poppet movement will be acceptable but no contact with the poppet sealing interface will be permitted. As a design goal, poppet movement during a flow cycle should be limited to a minimum and no poppet movement is considered a desirable design feature. Under no circumstances, including regulator flow initiation transients, should the valve originate or amplify pressure perturbations that could be detrimental to regulator performance or possibly result in life degradation or damage to the check valve unit or surrounding hardware. In evaluating unit stability, consideration should be given to the possibility of life degradation resulting from low flowrate operation of the valve during system purges for propellant decontamination, brazing operations, or other system maintenance tasks.

INTERNAL LEAKAGE

Minimum reverse flow leakage is a primary design objective of this contract. The intent of this valve is to minimize the propellant vapor exposure of the components upstream and to ensure that absolutely no liquid propellant is allowed to leak upstream of the valve. A detail evaluation and tradeoff study will be performed to define the optimum valve leak rate as a function contamination tolerance, pressure drop, compatibility, service life, weight, complexity, and exposure potential for upstream hardware. An initial design goal for internal leakage is 1 scc/hr of helium, at any pressure differential from 0.5 to 275 psig and at any temperature as previously specified. Under no circumstances will leakages in excess of 10 scc/hr be considered acceptable.

EXTERNAL LEAKAGE

The design goal for external leakage is a maximum of 5×10^{-6} scc/hr helium.

RANDOM VIBRATION

Vibration insensitivity is critical to the check valve if it is to achieve an extended service life. The check valve will be required to operate satisfactorily

during an OMS helium flow cycle for both the OMS engine burn and orbiter main engine burn vibration environments. The valve will be required to seal and not be damaged by repeated exposures to the vibration environments associated with orbiter main engine burns, liftoff, transonic, and max q. As well as valve stability in the presence of vibration, vibration induced wear, fretting and seal damage, particularly for low or zero pressure differential across the valve will be evaluated. These vibrations will not exceed the following.

Orbiter Main Engine Burn

Acceleration spectral density constant at $0.025 \text{ g}^2/\text{Hz}$ from 20 to 280 Hz, 6 db/octave increase to $0.15 \text{ g}^2/\text{Hz}$ at 700 Hz constant $0.16 \text{ g}^2/\text{Hz}$ from 700 to 2000 Hz.

OMS Engine Burn

Acceleration spectral density constant at $0.004 \text{ g}^2/\text{Hz}$ from 20 to 340 Hz, 6 db/octave increase to $0.01 \text{ g}^2/\text{Hz}$ at 500 Hz, constant $0.01 \text{ g}^2/\text{Hz}$ from 500 to 2000 Hz.

Liftoff

Acceleration spectral density increasing at the rate of 9 db/octave from $0.004 \text{ g}^2/\text{Hz}$ at 20 Hz to $2.0 \text{ g}^2/\text{Hz}$ at 160 Hz, constant at $2.0 \text{ g}^2/\text{Hz}$ from 160 to 1000 Hz, 9 db/octave decrease to $0.25 \text{ g}^2/\text{Hz}$ at 2000 Hz.

Transonic

Acceleration spectral density increasing at the rate of 9 db/octave from $0.002 \text{ g}^2/\text{Hz}$ at 20 Hz to $1.0 \text{ g}^2/\text{Hz}$ at 160 Hz, constant at $1.0 \text{ g}^2/\text{Hz}$ from 160 to 1000 Hz, 9 db/octave decrease to $0.12 \text{ g}^2/\text{Hz}$ at 2000 Hz.

Max q

Acceleration spectral density increasing at the rate of 9 db/octave from $0.001 \text{ g}^2/\text{Hz}$ at 27 Hz to $0.2 \text{ g}^2/\text{Hz}$ at 160 Hz, constant at $0.2 \text{ g}^2/\text{Hz}$ from 160 Hz to 1000 Hz, 9 db/octave decrease to $0.025 \text{ g}^2/\text{Hz}$ at 2000 Hz.

Test Duration For 500 Missions

Liftoff 1.5 hours, transonic 1.5 hours, max q 7.0 hours, orbiter main engine burn 67.0 hours, OMS engine burn 50.0 hours.

RCS COMMONALITY CONSIDERATIONS

The reaction control system (RCS) for the Space Shuttle will have a requirement for a check valve with basically the same requirements that will be required for the OMS. The primary difference will be a variable helium flowrate as the pressurization system response to the helium requirements for different combinations of RCS engine firings.

APPENDIX B

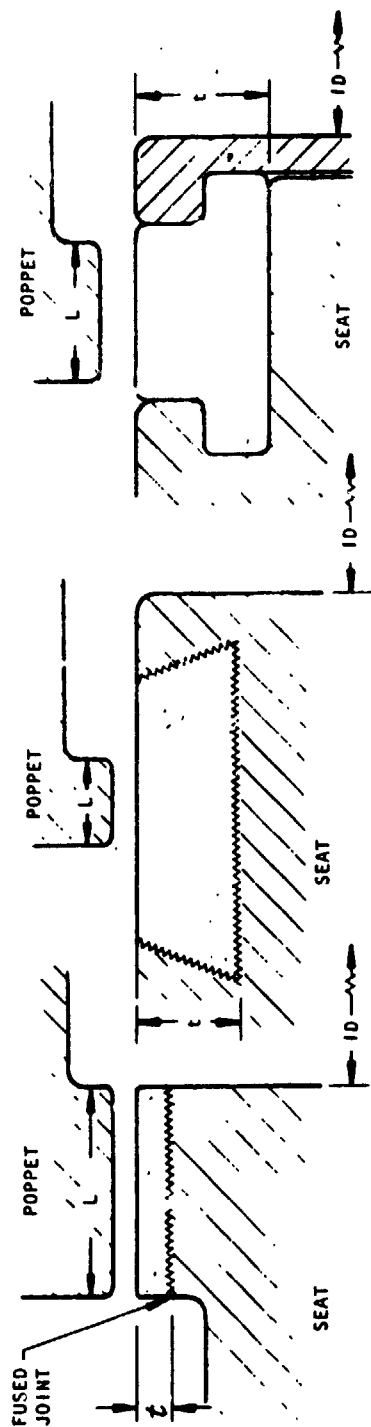
SEAL MODEL CONCEPTS AND DETAIL DESIGNS

Seal concepts studied for application in the OMS check valve are shown in Fig. B-1 through B-9. Design considerations are presented along with advantages and disadvantages based on judgment and previous experience. These concepts led to selection of a basic flat polymer seal, a captive seal, and the flat cutter concept for the test program. Assembly and detail drawings for these designs are displayed in Fig. B-10 through B-28.

The flat and captive seal models included provisions for a poppet loading spring so that load-leakage tests could be performed with constant inlet pressure. This assembly is shown in the captive model assembly drawings (Fig. B-20).

Cutter models fabricated for the SS/APS program* were modified for this program to remove the outer land (Fig. B-28). Detail drawings for the poppet and seat are reproduced in that report.

*Smith, G. M.: High-performance Space Shuttle Auxiliary Propellant Valve Program, NASA CR-120976, Rocketdyne Division, Rockwell International, Canoga Park, California, June 1973.

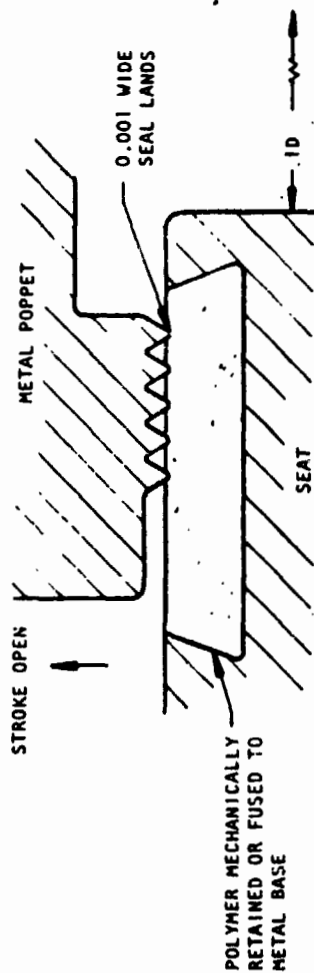


| Design No. 1 | Design No. 2 | Design No. 3 |
|--|--|---|
| <ol style="list-style-type: none"> 1. Polymer fused to metal base 2. Thickness (t) and land width (L) are variables 3. Sealing surface may be obtained by mold or machining 4. Maximum contact stress at poppet center | <ol style="list-style-type: none"> 1. Similar to No. 1, but provides edge protection 2. Edges may distort seal face at temperature extremes 3. Maximum contact stress at poppet corners | <ol style="list-style-type: none"> 1. Requires seal at base; may use sealant grease? 2. Variable squeeze from dimensional tolerances 3. May require surface machining after assembly |

Figure B-1. Polymer Seal Designs for Parametric Evaluation of Geometric Variables and Particle Effects

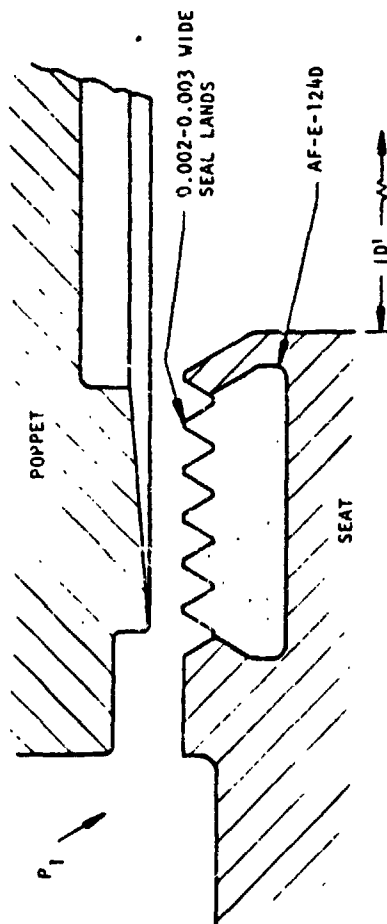
ORIGINAL PAGE IS
OF POOR QUALITY

ORIGINAL PAGE IS
OF POOR QUALITY



| Advantages | Disadvantages |
|---|---|
| <ol style="list-style-type: none"> 1. Redundant sealing 2. Particle displacement volume provides greatest particle envelopment capacity of any known seal 3. Minimum load sealing 4. Short stroke | <ol style="list-style-type: none"> 1. Cannot cut metal wire 2. Low-temperature hardening and distortion of polymer 3. Requires close concentricity and alignment 4. High contaminant entrapment probability 5. Cold-flow problem with Teflon |

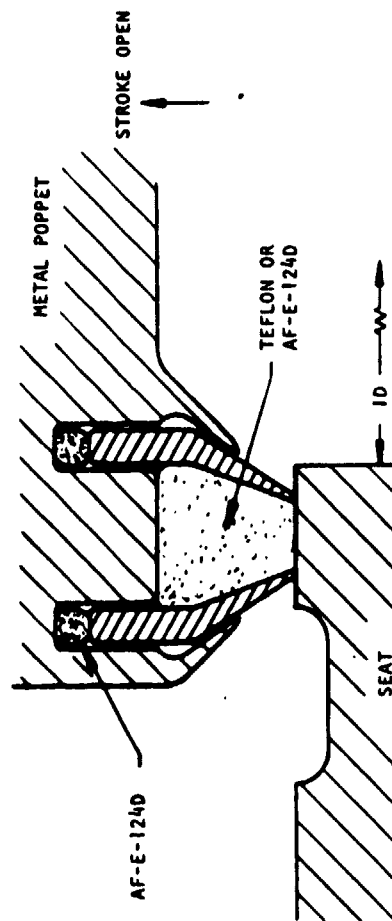
Figure B-2. Multiland Polymer Seal (Grooves in Metal Poppet)



| Advantages | Disadvantages |
|---|---|
| <ol style="list-style-type: none"> 1. Similar to metal poppet version except does not require tight concentricity 2. Optional taper feature provides maximum bearing stress at minimum load to ensure full circumferential contact 3. Polymer seal face more easily finished than wide continuous land | <ol style="list-style-type: none"> 1. Similar to metal poppet version 2. Single-land sealing at minimum seal load |

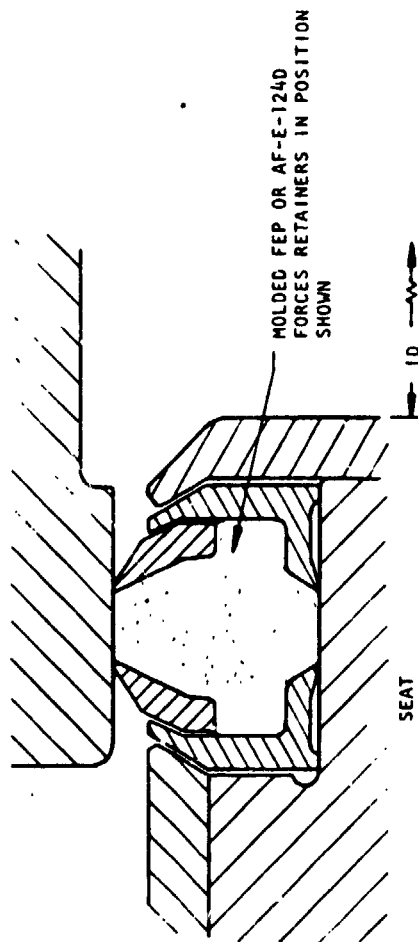
Figure B-3. Multiland Polymer Seat (Grooves in Polymer Seat)

ORIGINAL PAGE IS
OF POOR QUALITY



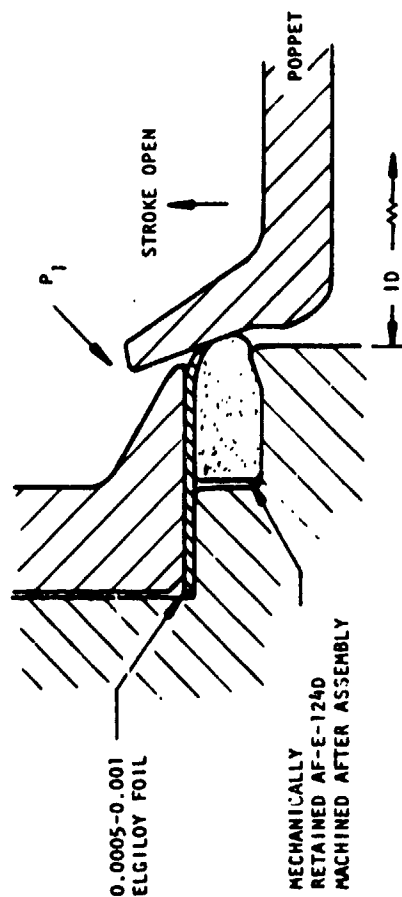
| Advantages | Disadvantages |
|---|---|
| <ol style="list-style-type: none"> 1. Retains Teflon from cold-flow at high loads 2. Does not require tight concentricity 3. Can tolerate high impact loads 4. Polymer absorbs particles 5. Short stroke | <ol style="list-style-type: none"> 1. Relatively complex assembly 2. Polymer retainers could cause leak with particle or wire entrapped 3. Low-temperature hardening and distortion of polymer 4. Single sealing land |

Figure B-4. Captive Polymer Seal



| Advantages | Disadvantages |
|--|---|
| <ol style="list-style-type: none"> 1. Separable seal can be parallel flat finished as sub-assembly 2. Does not require tight retention | <ol style="list-style-type: none"> 1. Complex and expensive 2. Doubles leak path 3. High-risk design 4. Single sealing land |

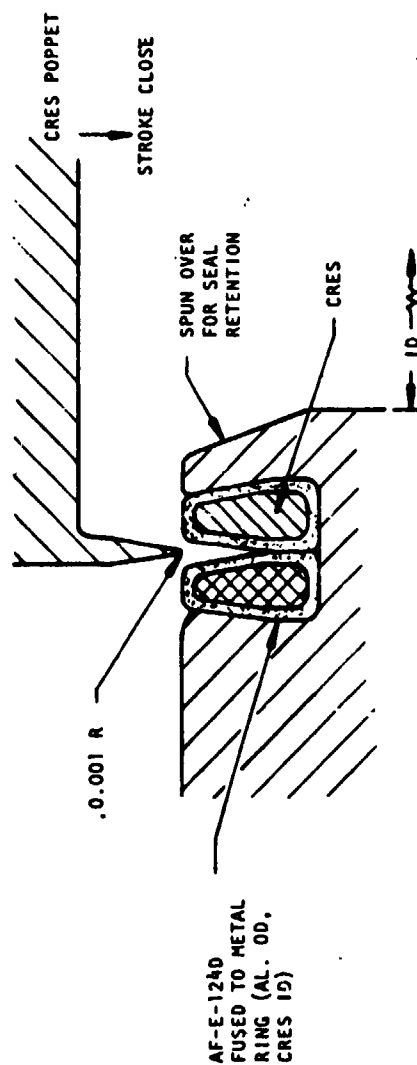
Figure B-5. Captive Sealing Element Concept



| Advantages | Disadvantages |
|---|---|
| <ol style="list-style-type: none"> 1. Essentially same as flat seal except seat load is increased by conical angle 2. Elgiloy foil disc forces elastomer into poppet 3. Does not require precise angular alignment as does flat seat | <ol style="list-style-type: none"> 1. Essentially same as flat seal except requires tight concentricity control 2. Radial crack required, so could not fully retain Teflon as do retainers on flat seal 3. Relatively difficult analysis 4. Long stroke required 5. High-risk design 6. Single sealing land |

Figure B-6. Conical Captive Elastomer Seal

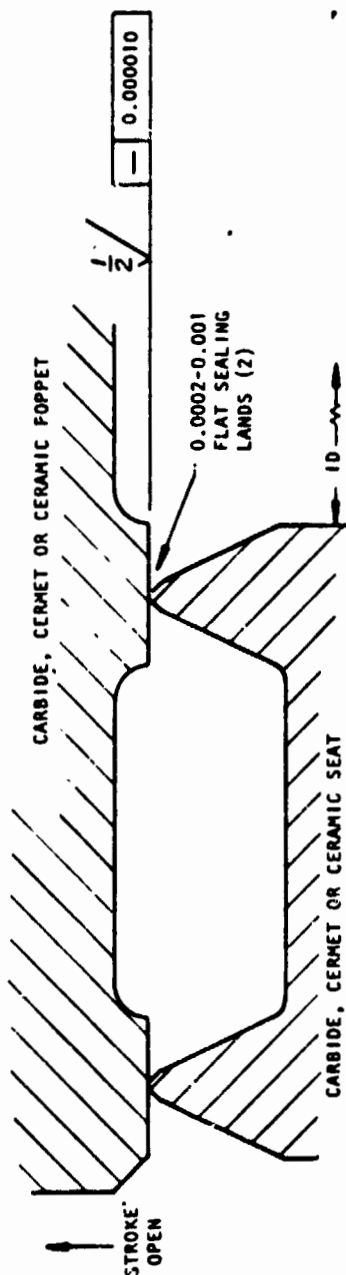
ORIGINAL PAGE IS
OF LOWER QUALITY



| Advantages | Disadvantages |
|---|--|
| <ol style="list-style-type: none"> 1. Long leak path with high load should give very low leak rate 2. Load concentration should give great resistance to contamination 3. Does not require precise angular alignment as does flat seat | <ol style="list-style-type: none"> 1. Requires close concentricity 2. Unproven high-risk design 3. Long stroke required 4. Potential of high cracking pressure from stiction |

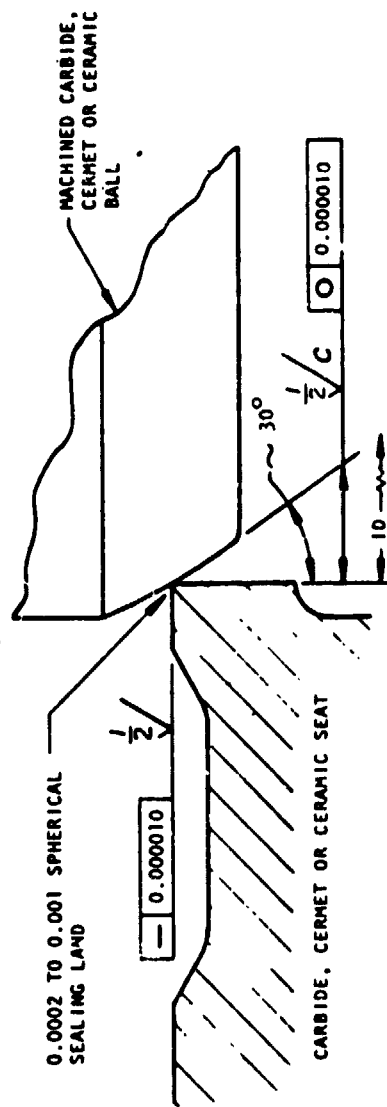
Figure B-7. Knife Seal

ORIGINAL PAGE IS
OF POOR QUALITY



| Advantages | Disadvantages |
|---|---|
| <ol style="list-style-type: none"> 1. Greatest wear resistance of any known seal (1,000,000 impact cycles) 2. Low contaminant entrapment probability and will cut particles with low load 3. Does not require tight concentricity 4. Proven low leakage at light loads 5. Temperature-insensitive sealing 6. Short stroke | <ol style="list-style-type: none"> 1. Limited fabrication sources; expensive 2. Potential land corner fracture with excessive impact or too hard particle entrapment 3. Must have uniform peripheral loading; requires pressure load or ball joint to provide for self alignment. This requirement dictates design |

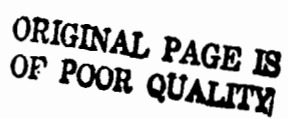
Figure B-8. Flat Cutter Seal



| Advantages | Disadvantages |
|--|--|
| <ol style="list-style-type: none"> 1. Similar to flat cutter seal except is much easier to fabricate 2. Self aligning 3. Geometrically simple | <ol style="list-style-type: none"> 1. Similar to flat cutter seal except requires close concentricity 2. Only one sealing land 3. Greater stroke required than with flat seat 4. Probably would experience greater scrubbing and edge impact than flat seat design |

Figure B-3. Spherical Cutter Seal

DRILL #43(.089) T.
CSK 90° .112 ±.00
4-40 NC-3B THC
4 HOLES



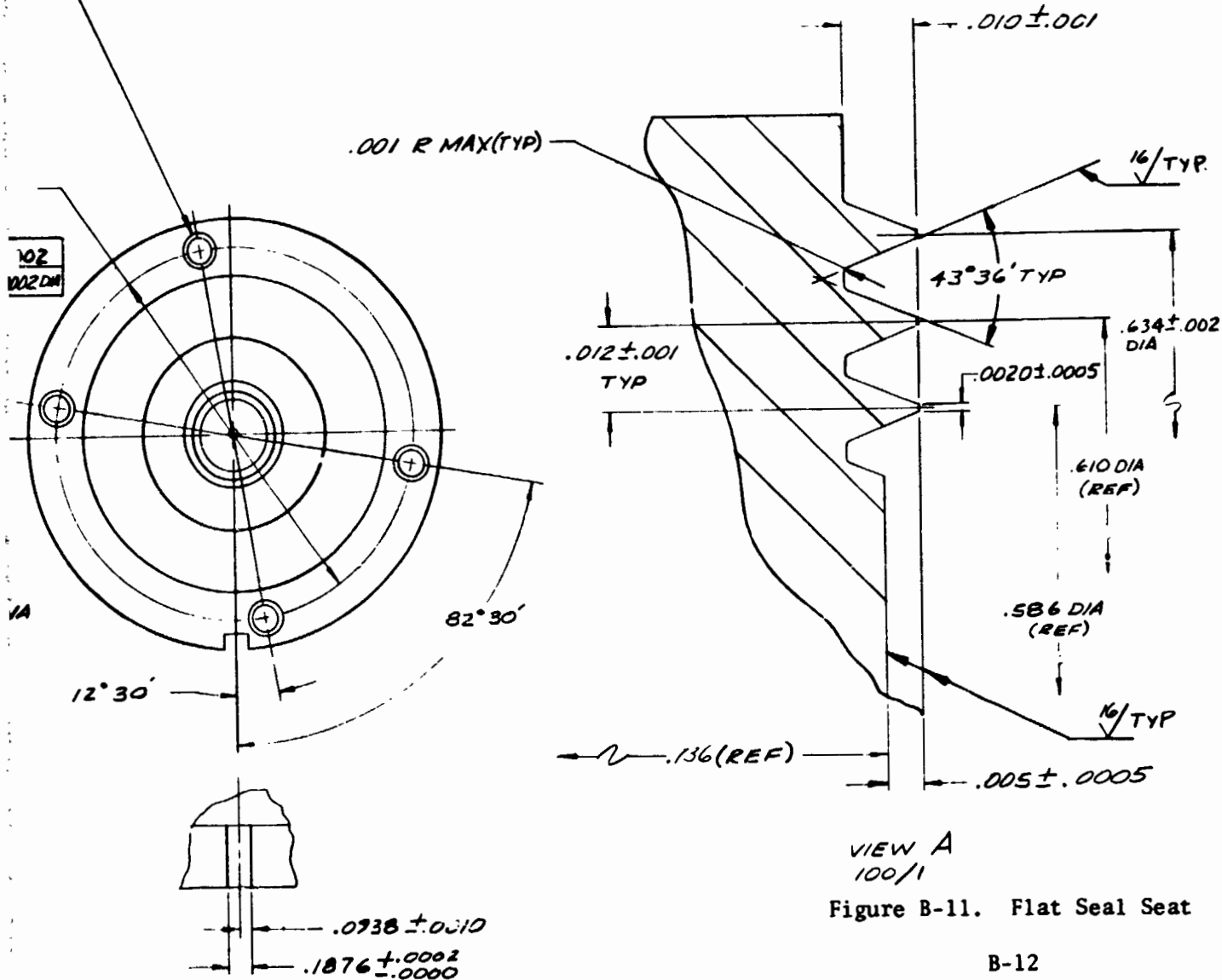
4. \checkmark ALL MACHINE SURFACES
3. DIAMETERS CONCENTRIC WITHIN .001 TIR.
2. BREAK EDGES .005 MAX
1. FILLETS .005 R MAX

NOTE: UNLESS OTHERWISE SPECIFIED

OLDOUT FRAME

| REVISIONS | | | |
|-----------|--------------------|------|----------|
| LTR | DESCRIPTION | DATE | APPROVED |
| 1. | MAY BE REWORKED | | |
| 2. | CANNOT BE REWORKED | | |
| 3. | RECORD CHANGE | | |
| 4. | NOW SHOP PRACTICE | | |
| 5. | PARTS MADE ON | | |

DRILL #43(.089) THRU
CSK 90° .112 ± .000 DIA
4-40 NC-3B THD THRU
4 HOLES



VIEW A
100/1

Figure B-11. Flat Seal Seat

B-12

SURFACES
TRIC WITHIN .001 TIR.
MAX

| | | | | | |
|--|--|--|--|--|--|
| HEAT TREAT TO COND H300 (R _e 42 MIN) | | UNLESS OTHERWISE SPECIFIED DIMENSIONS ARE IN INCHES AND APPLY PRIOR TO FINISH. | | Rockwell International Corporation Rockaldyne Division Canoga Park, California | |
| FINISH | | 120/ MACH. SURF. ROUGHNESS | | SEAT, FLAT SEAL | |
| MATERIAL 17-4 PH | | TOLERANCES ON ANGLES $\pm 9^\circ 30'$ DECIMALS $\pm .001$ | | SIZE CODE IDENT NO. DRAWING NO. D 02602 XEOR940771D4 | |
| DO NOT SCALE PRINT | | SCALE 1/1 | | SHEET | |

FOLDOUT FRAME 2

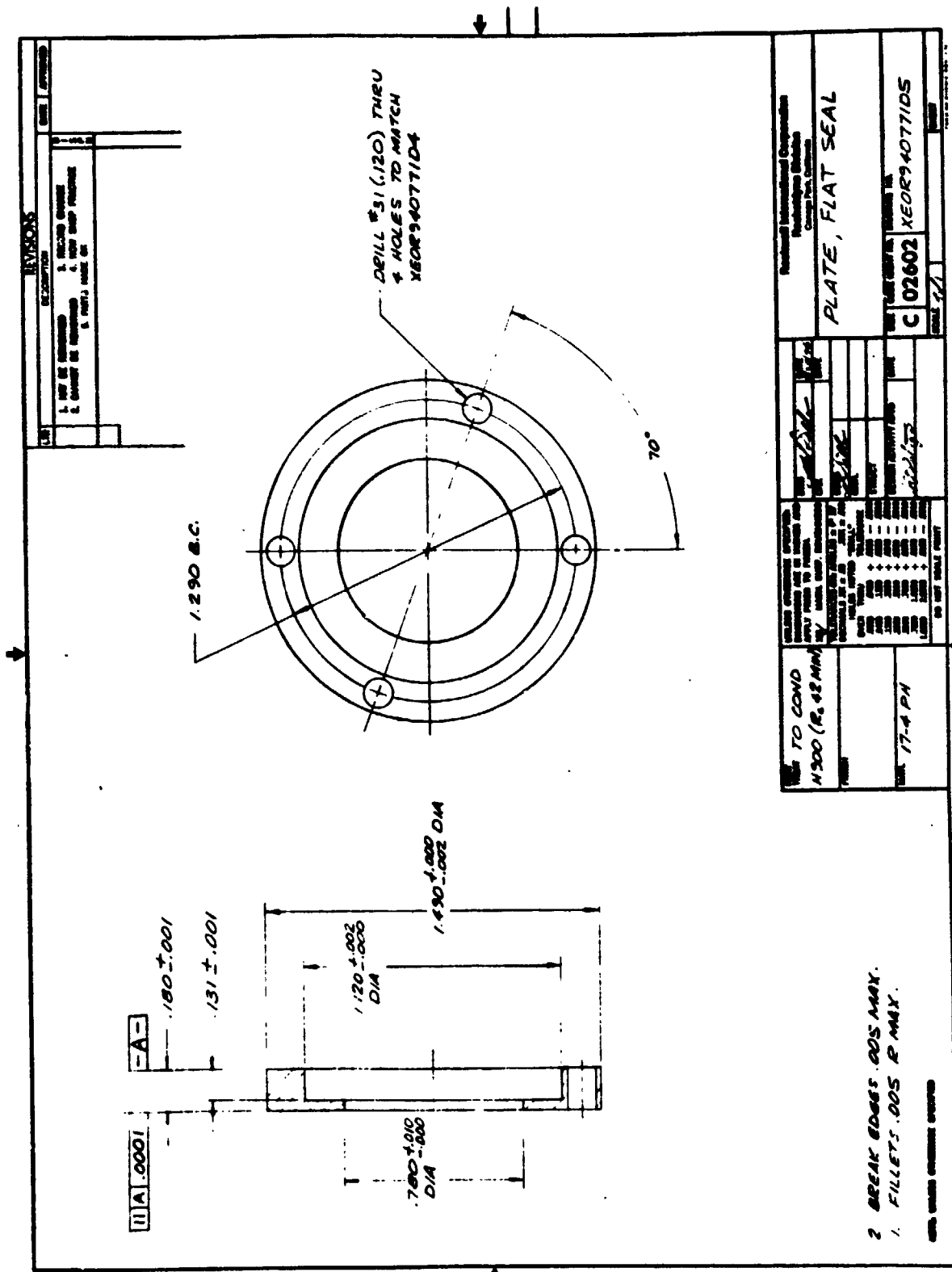


Figure B-12. Falt Seal Plate

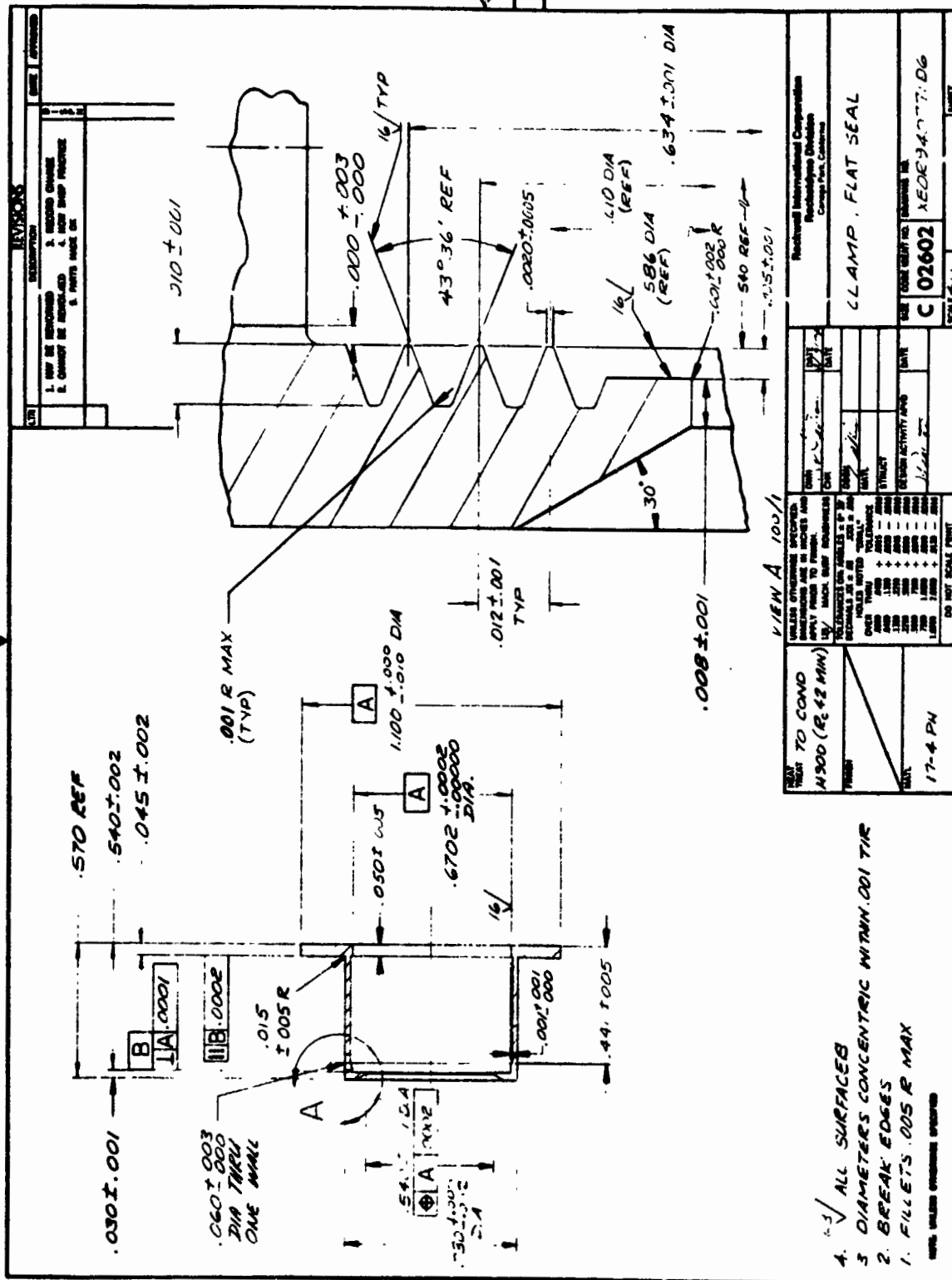


Figure B-13. Flat Seal Clamp

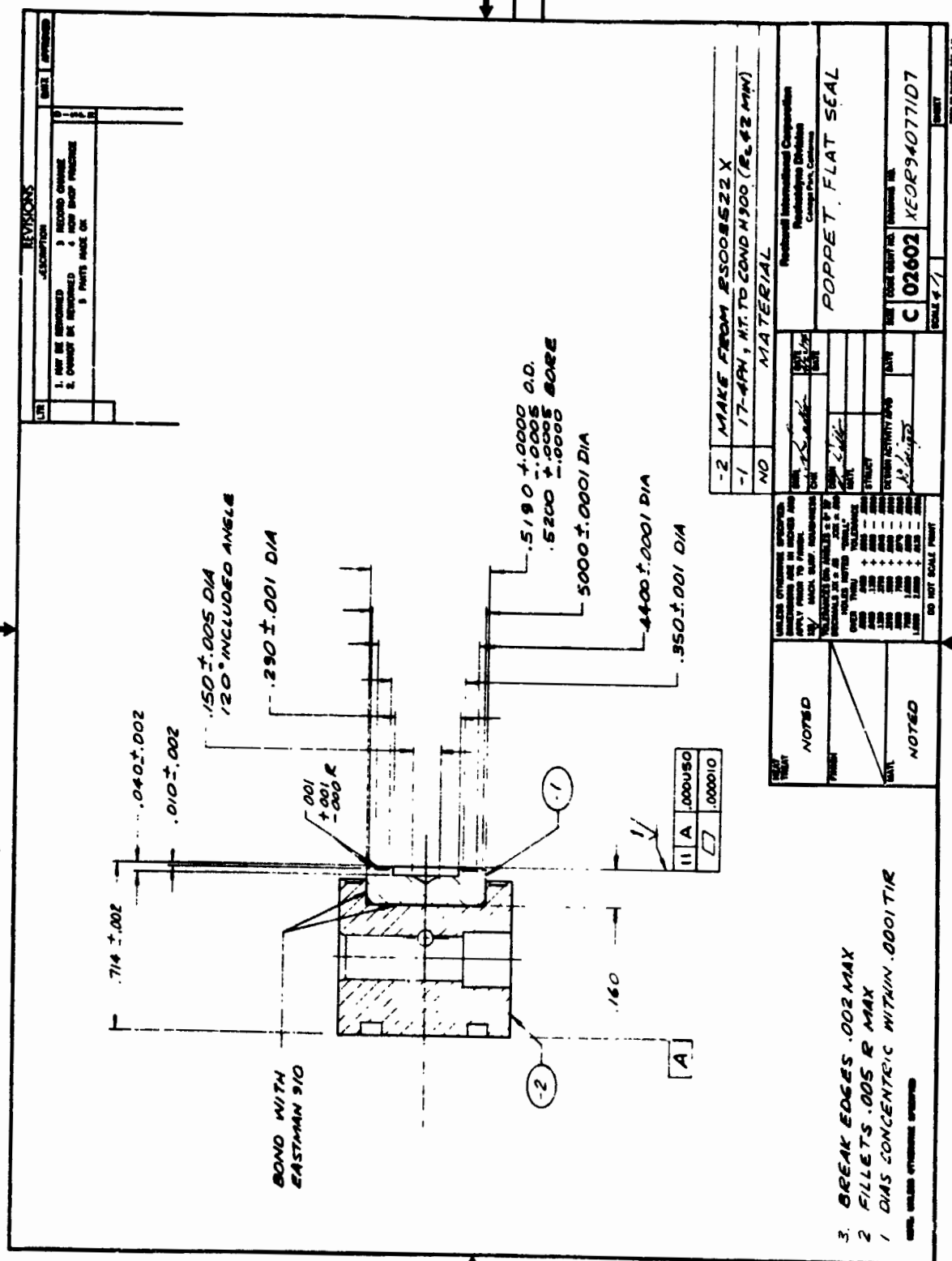


Figure B-14. Flat Seal Poppet

ORIGINAL PAGE IS
OF POOR QUALITY

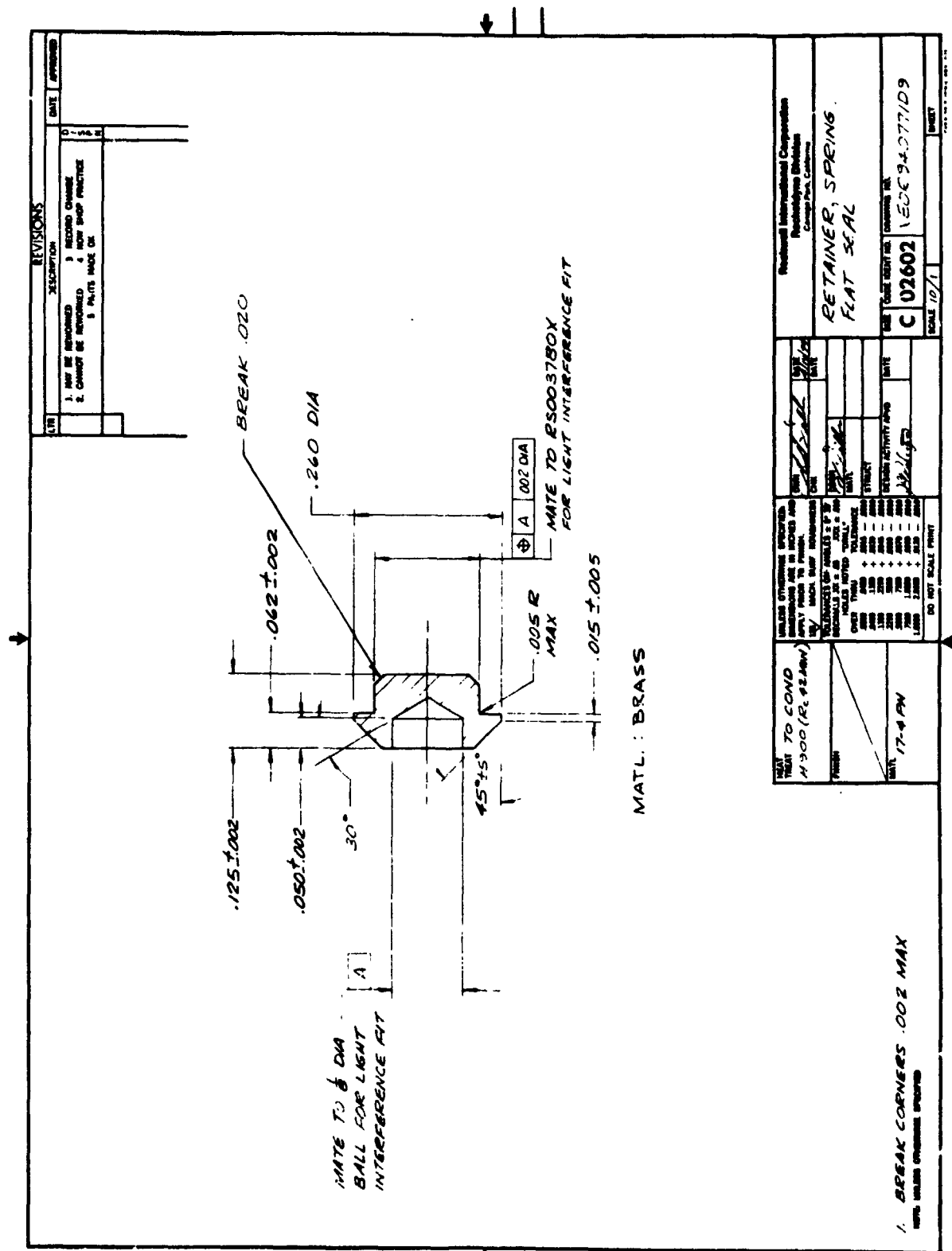


Figure B-16. Flat Seal Spring Retainer

ORIGINAL PAGE IS
OF POOR QUALITY

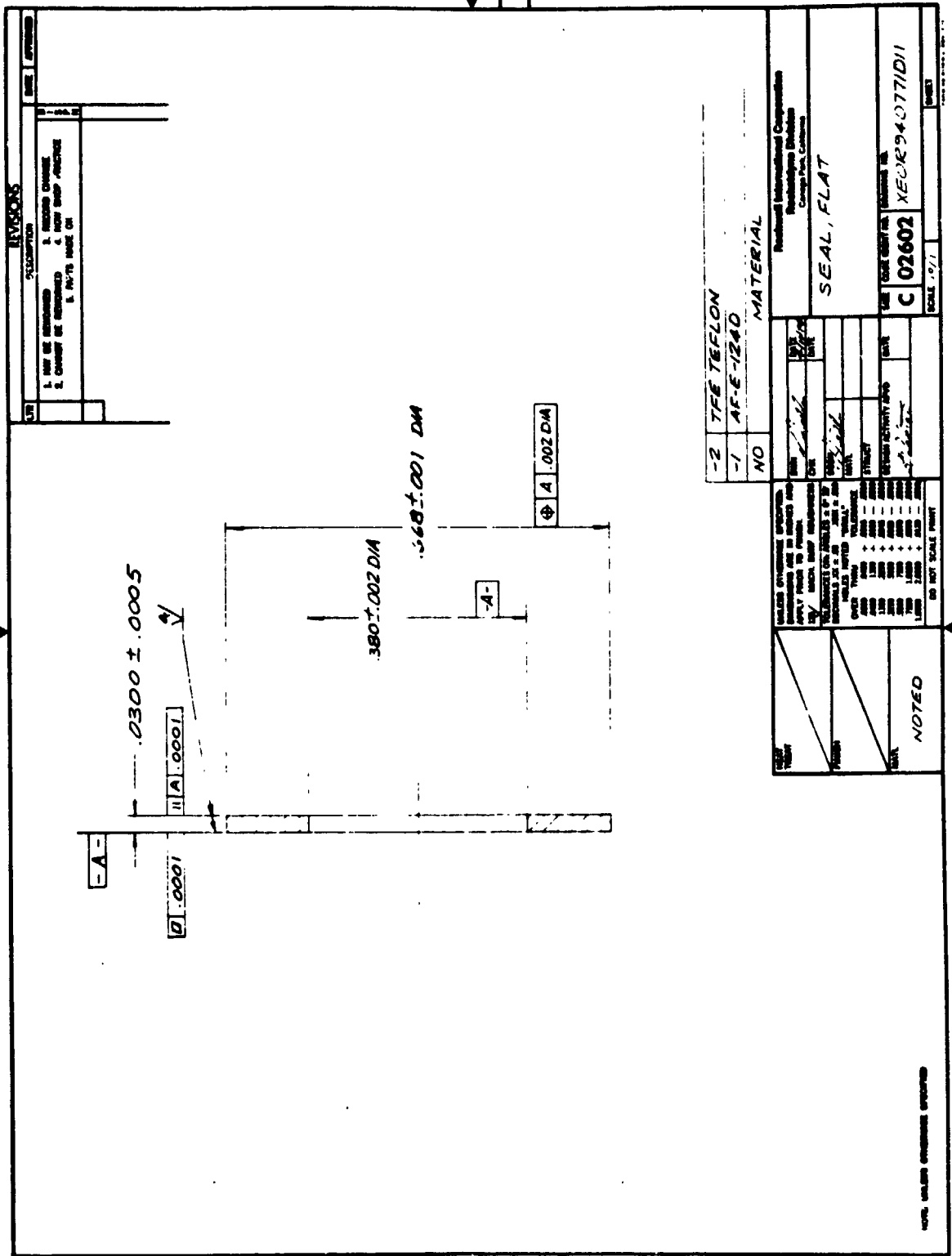
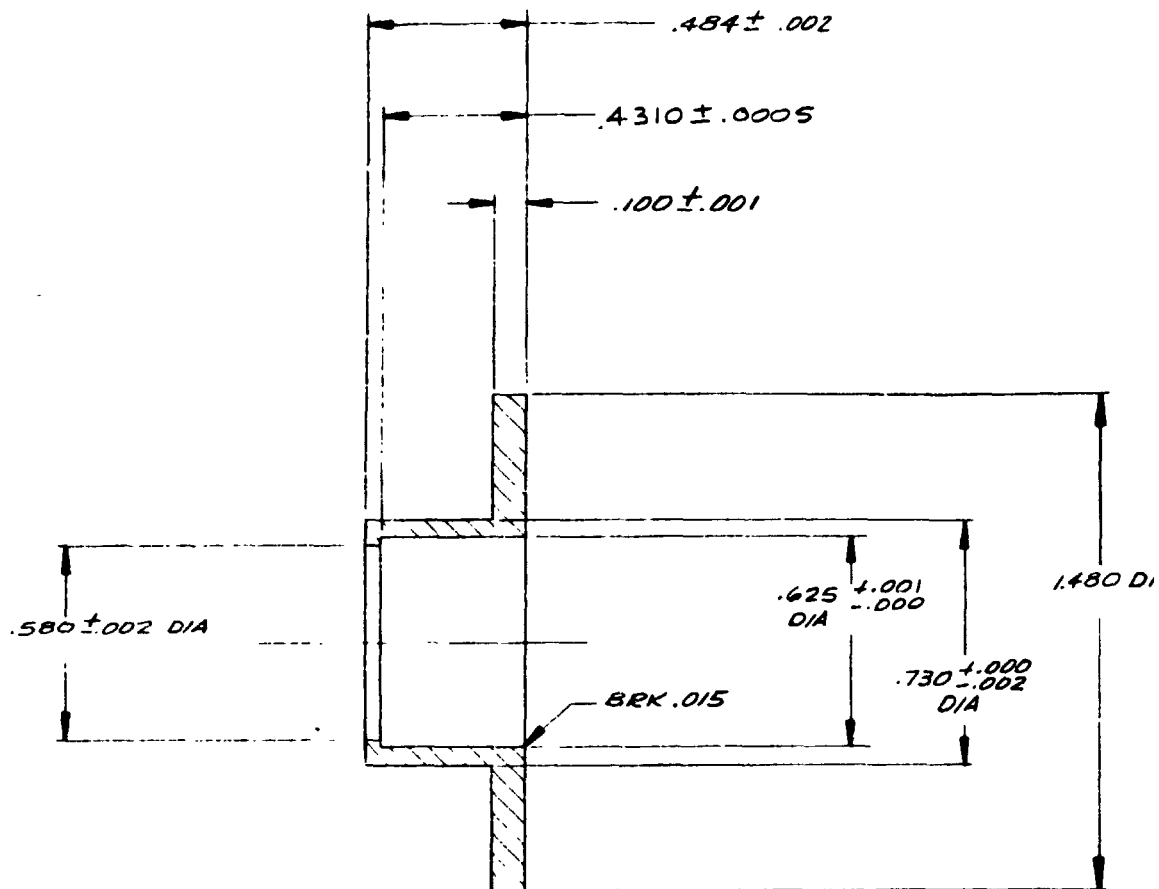


Figure B-18. Flat Seal

ORIGINAL PAGE IS
OF POOR QUALITY



ORIGINAL PAGE IS
OF POOR QUALITY

3. ALL DIAMETERS CONCENTRIC WITHIN .002 TH
2. BREAK EDGES .005 MAX
1. FILLETS .005 MAX

NOTE: UNLESS OTHERWISE SPECIFIED

FOLDOUT FRAME 1

| REVISIONS | | | |
|-----------|--------------------|---------------|-------------------|
| LTR | DESCRIPTION | DATE | APPROVED |
| 1. | MAY BE REWORKED | 3. | RECORD CHANGE |
| 2. | CANNOT BE REWORKED | 4. | HOW SHOP PRACTICE |
| | 5. | PARTS MADE OK | |

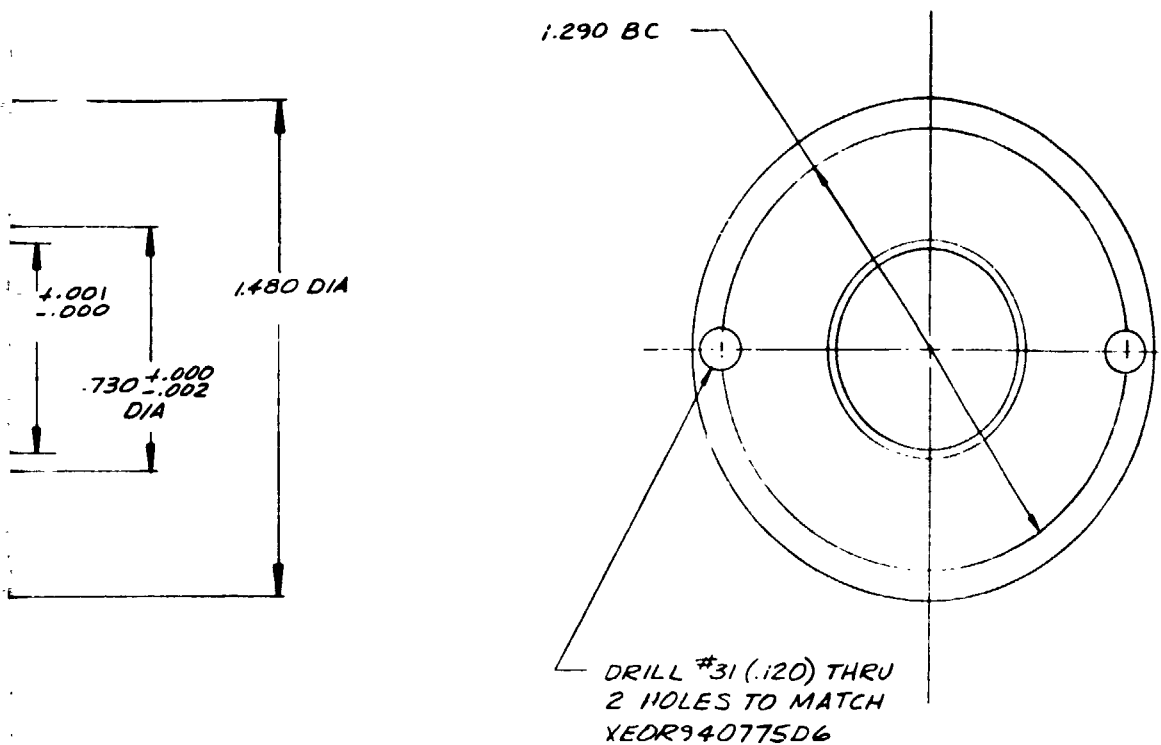


Figure B-24. Captive Seal Outer Stop

B-25

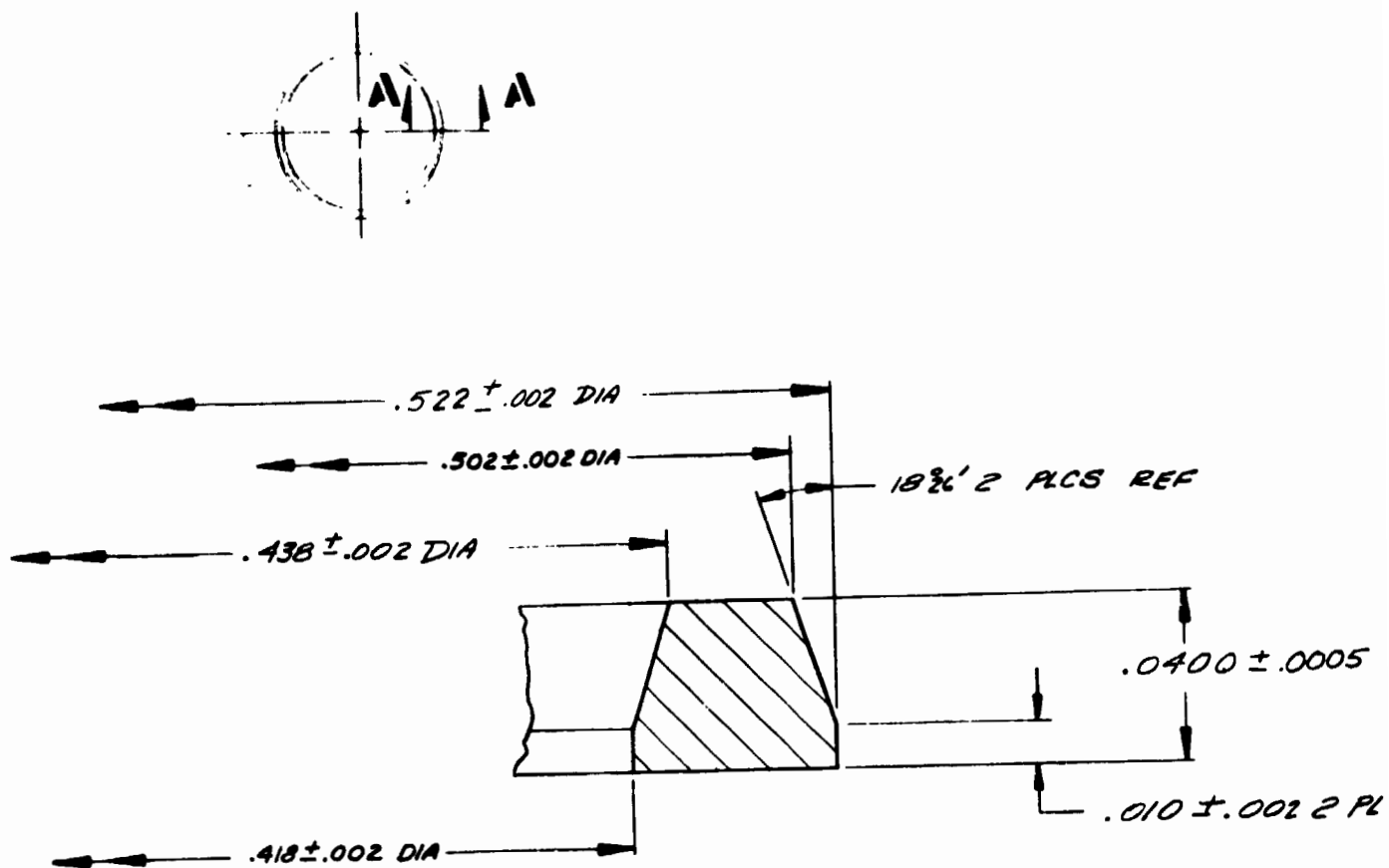
XEOR940775D4

CENTRIC WITHIN .002 TIR
MAX

SPECIFIED

| | | | | | |
|--|--|--|--|--|--|
| HEAT TREAT TO COND H900 (Rc 42 MIN) | | UNLESS OTHERWISE SPECIFIED: DIMENSIONS ARE IN INCHES AND APPLY PRIOR TO FINISH. 125/ MACH. SURF. ROUGHNESS TOLERANCES ON ANGLES \pm 9° BY DECIMALS \pm .01 .001 \pm .005 HOLES NOTED "DRILL" OVER THRU .0000 .0020 + .0015 - .0010 .0400 .1300 + .0030 - .0010 .1300 .2250 + .0045 - .0010 .2250 .5000 + .0060 - .0010 .5000 .7500 + .0070 - .0010 .7500 1.0000 + .0090 - .0010 1.0000 2.0000 + .0120 - .0010 | | Rockwell International Corporation Rocketdyme Division Canoga Park, California | |
| FINISH 17-4 PH CRES | | STOP-OUTER, CAPTIVE SEAL | | | |
| DO NOT SCALE PRINT | | DESIGN ACTIVITY APPROVED | | | |
| DATE | | DATE | | | |
| SCALE | | SIZE | | | |
| CODE IDENT NO. | | DRAWING NO. | | | |
| D 02602 | | XEOR940775D4 | | | |
| SHEET | | SHEET | | | |

FOLDOUT FRAME 2



SECTION A-A SCALE 50/1

1. DIAMETERS CONCENTRIC WITHIN .002 DIA

NOTE: UNLESS OTHERWISE SPECIFIED

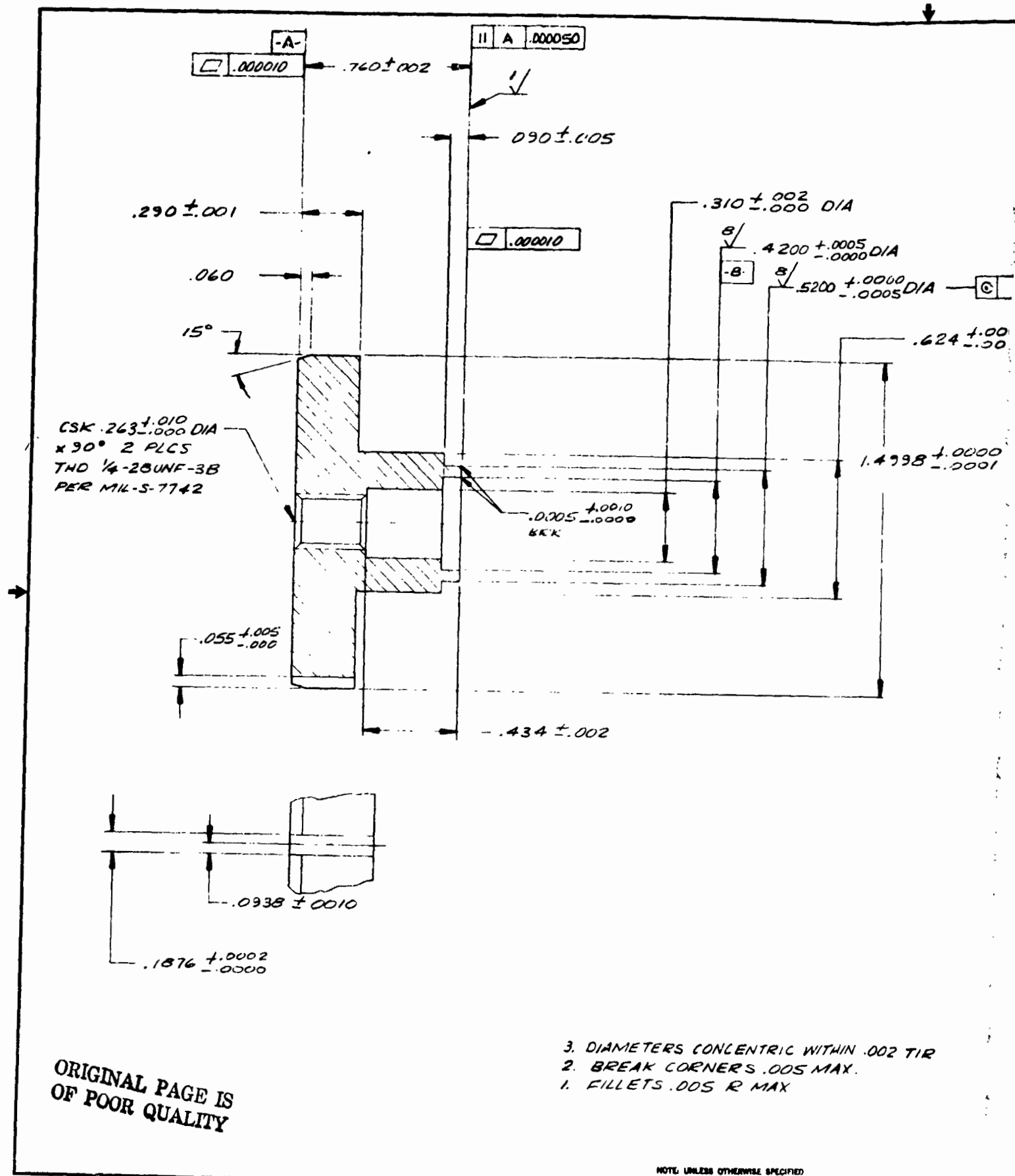
OLDOUT FRAME)

$.0400 \pm .0005$

B-26

| | | | | | | |
|---------------------------------|---|-------------------------------------|--|-----------|-------------------------|-------------------------------|
| HIGH TIGHT | UNLESS OTHERWISE SPECIFIED: DIMENSIONS ARE IN INCHES AND APPLY PRIOR TO FINISH. SURF. FINISH: BACH, SURF. ROUGHNESS TOLERANCES ON ANGLES $\pm 0^{\circ} 30'$ DECIMALS .XX $\pm .00$.XXX $\pm .005$ HOLES NOTED "DRILL" | DATE 2-13-75 DATE | Rockwell International Corporation Rockolayne Division Canoga Park, California | | | |
| | | | SEAL, CAPTIVE | | | |
| PART NAME | OVER THRU TOLERANCE .000 .000 + .010 - .010 .000 .120 + .000 - .000 .120 .220 + .000 - .010 .220 .300 + .000 - .010 .300 .700 + .000 - .010 .700 1.000 + .000 - .010 1.000 2.000 + .010 - .010 | DESIGN ACTIVITY APVD [Signature] | DATE | SIZE D | CODE IDENT NO. 02602 | DR. WIPED NO. XEOR940775D5 |
| MATL. AF-E-124D BLASTOMER | DO NOT SCALE PRINT | SCALE 1/1 | | SHEET | | |

FOLDOUT FRAME 2



ORIGINAL PAGE IS
OF POOR QUALITY

FOLDOUT FRAME

XE0R940775D6

FOLDOUT FRAME

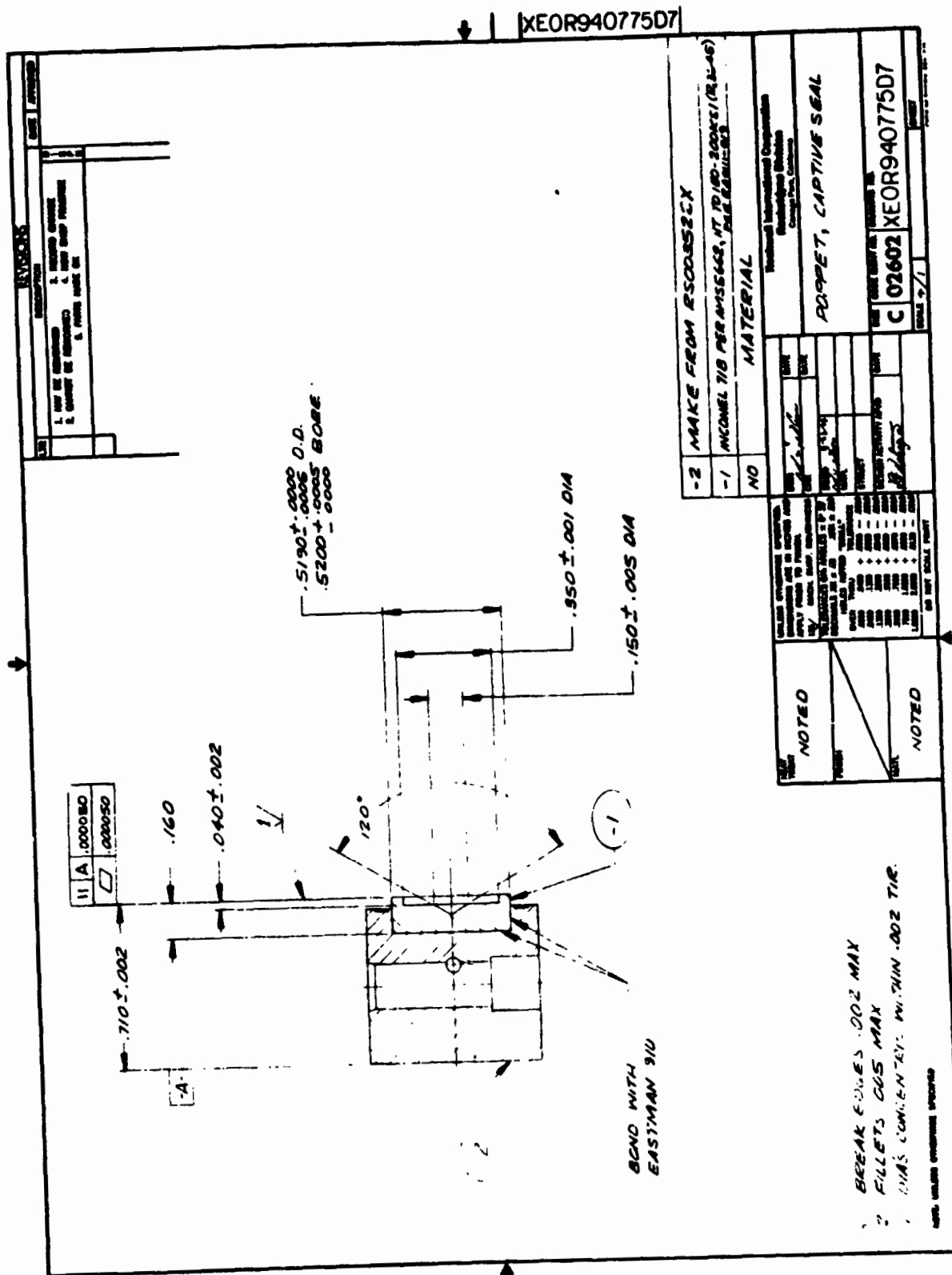
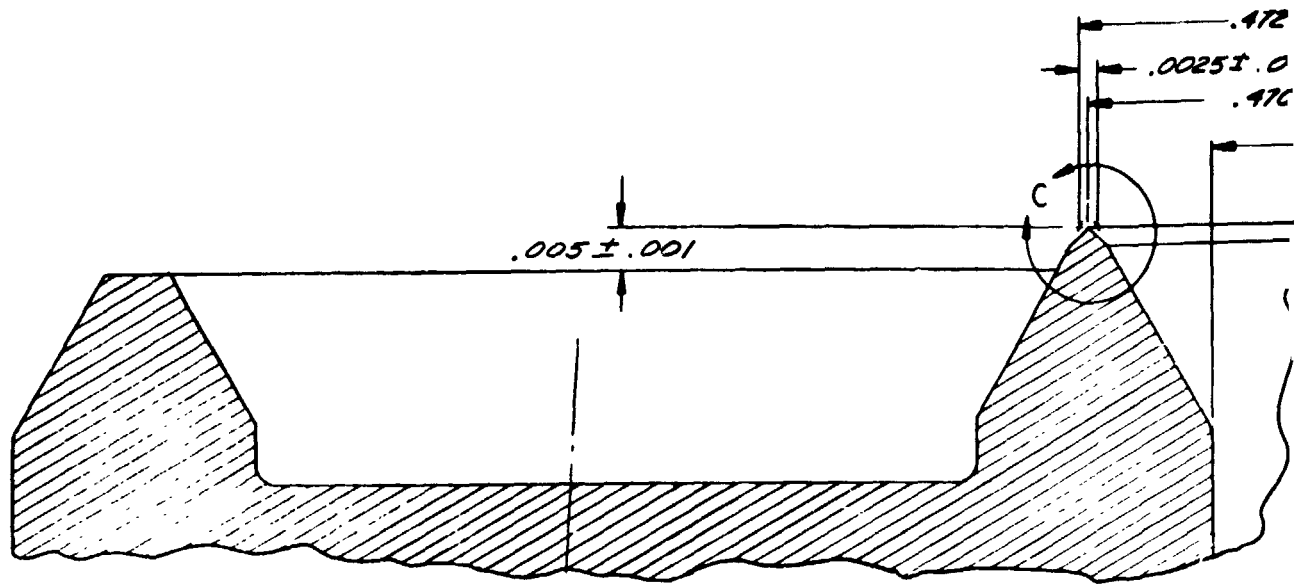
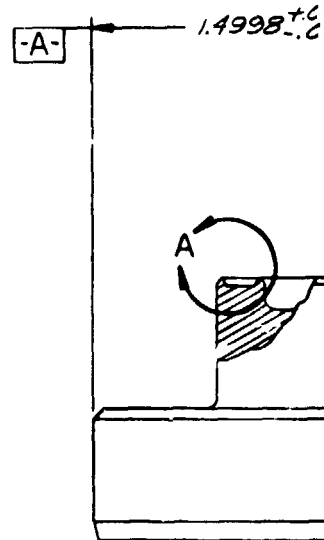


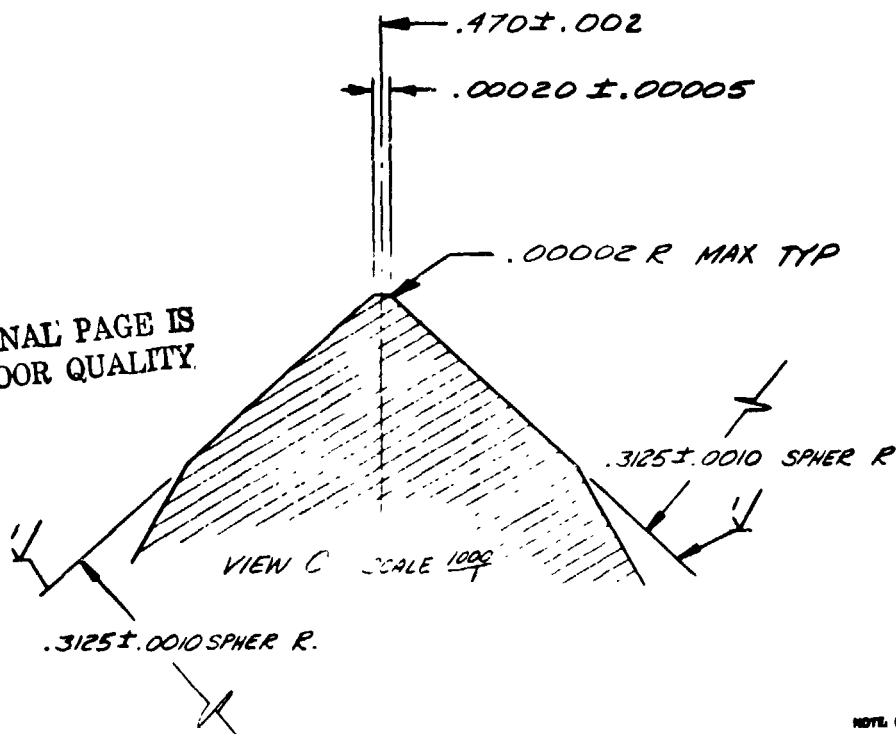
Figure B-27. Captive Seal Poppet



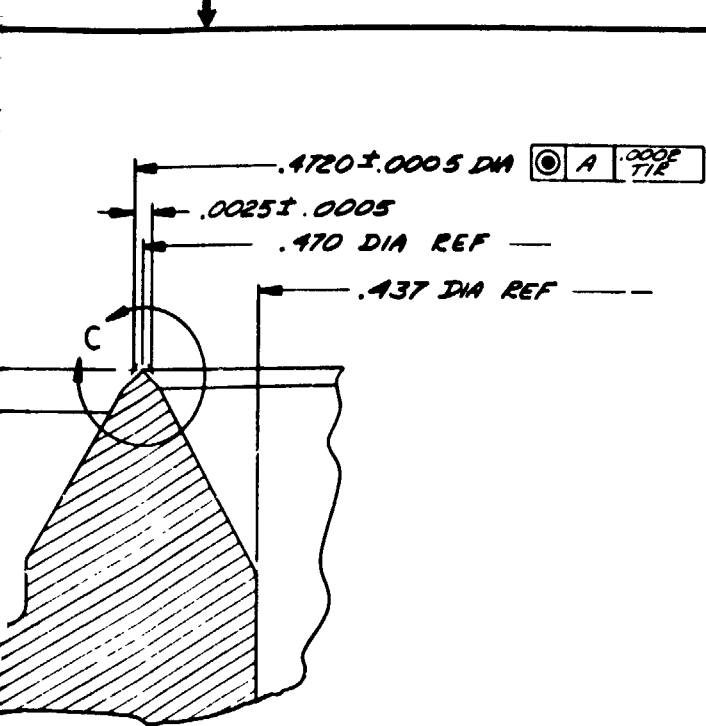
VIEW A SCALE $\frac{100}{1}$



ORIGINAL PAGE IS
OF POOR QUALITY.



NOTE: UNLESS OTHERWISE SPECIFIED



| REVISIONS | | | |
|-----------|--------------------|------|----------|
| LTR | DESCRIPTION | DATE | APPROVED |
| 1. | MAY BE REWORKED | | |
| 2. | CANNOT BE REWORKED | | |
| 3. | RECORD CHANGE | | |
| 4. | NOW SHOP PRACTICE | | |
| 5. | PARTS MADE OK | | |

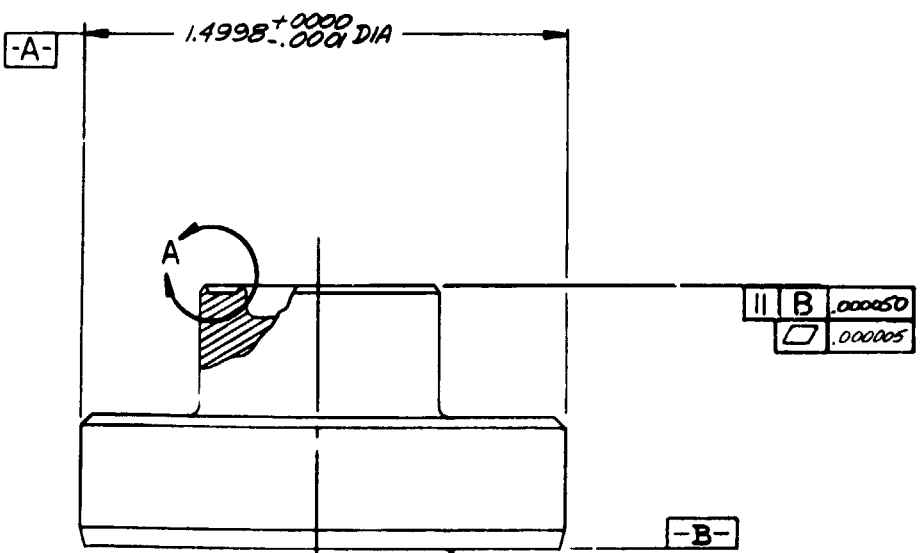


Figure B-28. Model Seat Seal Cutter

B-29/B-30

MAKE FROM RS003933X

| | | | | |
|--------------------------|---|------|---|--|
| HEAT TREAT | UNLESS OTHERWISE SPECIFIED, DIMENSIONS ARE IN INCHES AND APPLY PRIOR TO FINISH. | DATE | Rockwell International Corporation Rockadyme Division Gage Park, California | |
| | | DATE | | |
| FINISH | TOLERANCES ON ANGLES $\pm 9^\circ$ BY DECIMALS $\pm .01$ $\pm .005$ | DATE | | |
| | | DATE | | |
| MATERIAL | TOLERANCES ON ANGLES $\pm 9^\circ$ BY DECIMALS $\pm .01$ $\pm .005$ | DATE | | |
| | | DATE | | |
| DESIGN ACTIVITY APPROVED | DO NOT SCALE PRINT | DATE | SIZE CODE IDENT NO. DRAWING NO. | |
| | | DATE | | |
| | | DATE | D 02602 | |
| | | DATE | SCALE | |
| | | DATE | SHEET | |

APPENDIX C

POLYMER SEAL FABRICATION

Polymer seals of perfluoroelastomer (AF-E-124D, AF-E-124X, ECD-006), TFE and FEP, were cut from sheet stock. The elastomers were initially molded and then flycut on one or two sides to obtain parallel and smooth surfaces. TFE and FEP Teflon sheet stocks were too rough for use and were flycut on both sides. Methods and tooling developed to prepare the sheet stock and cut seals from it are described herein.

AF-E-124X POLYMER MOLDING

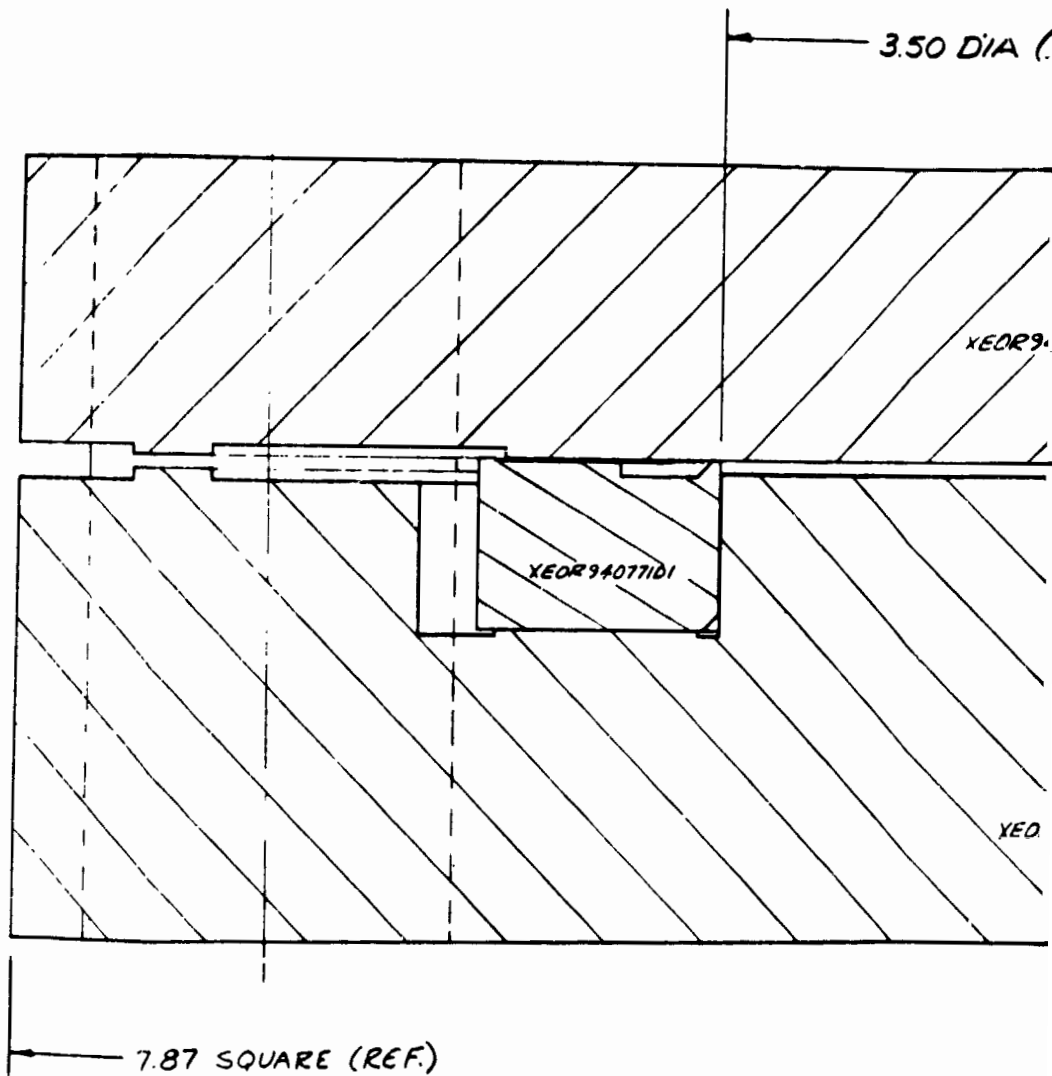
A precision molding die was fabricated for use by TRW in supplying sheet stock for flat and captive seals. The mold assembly and details are shown in Fig. C-1 through C-4. The mold surfaces were lapped before and after plating to produce a mirror-like, corrosion-resistant finish. The ring (Fig. C-2) provides a valving effect to contain the raw stock under high pressure. Overload protection is provided by a wider land between the excess material well and the inner seal land.

The composition and specific molding process for the white titanium dioxide filled AF-E-124X polymers are proprietary to TRW Systems. Specifics for molding and post-curing AF-E-124D elastomer were documented by TRW.* Briefly, raw stock is milled between heated rolls (similar to a wringer washer) to a prescribed thickness near the mold size. A slightly excess quantity is cut out and placed between the die plates, which are closed and brought up to temperature in a heated platen press. At appropriate intervals, the press is unloaded (but not opened) to allow evolved gases to escape and excess material to flow into the peripheral well. When the "done" light comes on, the press is opened and the "molded" material is removed for an elevated temperature postcure extending several days. Because this process involves many variables, including the raw stock composition, precise repeatability between molded parts proved difficult.

POLYMER FLYCUTTING

Early experiments with molding AF-E-124D produced rough surfaces and means for obtaining flat, smooth sealing surfaces on elastomer and plastic materials were required. As noted in the Materials Investigation section, various methods were examined leading to a relatively new process made possible by the high-speed air bearing. A sample of AF-E-124D given to Westwind Air Bearings (Division of Federal-Mogul) was flycut down to 0.03-inch thickness from 0.075 inch by alternately removing several thousandths from each side at a pass. The 1- by 2-inch sample was double-back taped to an air table that could be traversed under the high-speed air bearing spindle. Cutting was performed by a 1/2 carat diamond. Surfaces produced were parallel within 0.0001 inch and had a nominal 4-8 AA roughness. Waviness on the order of ± 50 μ in. per 0.1 inch was thought to be transference from the tape surface.

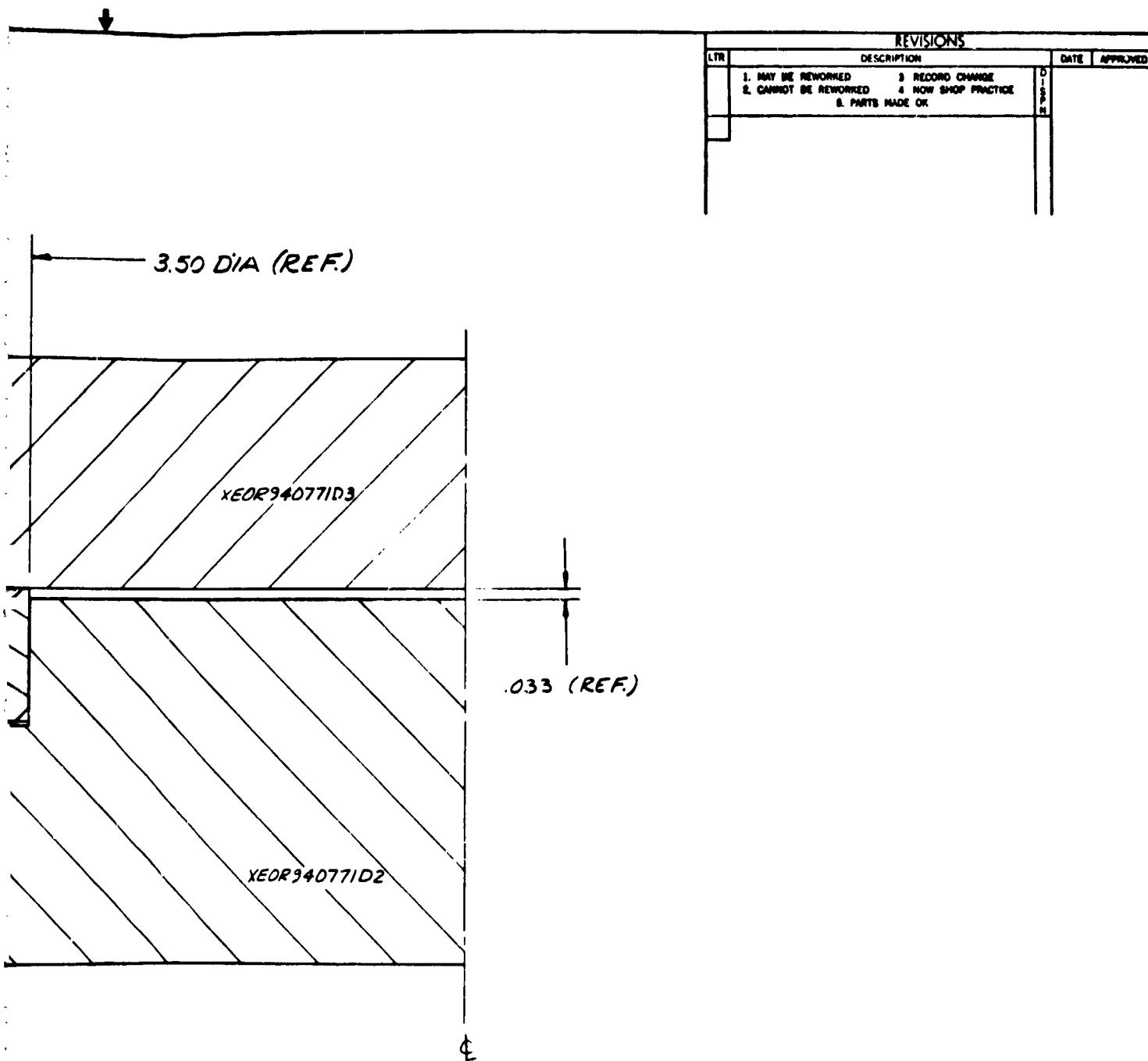
*22539-6001-RO-00, Space Shuttle Seal Material and Design Development for Earth Storable Propellant Systems, TRW Systems Group, TRW, Inc., Redondo Beach, California, October 1973.



ORIGINAL PAGE IS
OF POOR QUALITY

NOTE: UNLESS OTHERWISE SPECIFIED

FOLDOUT FRAME)

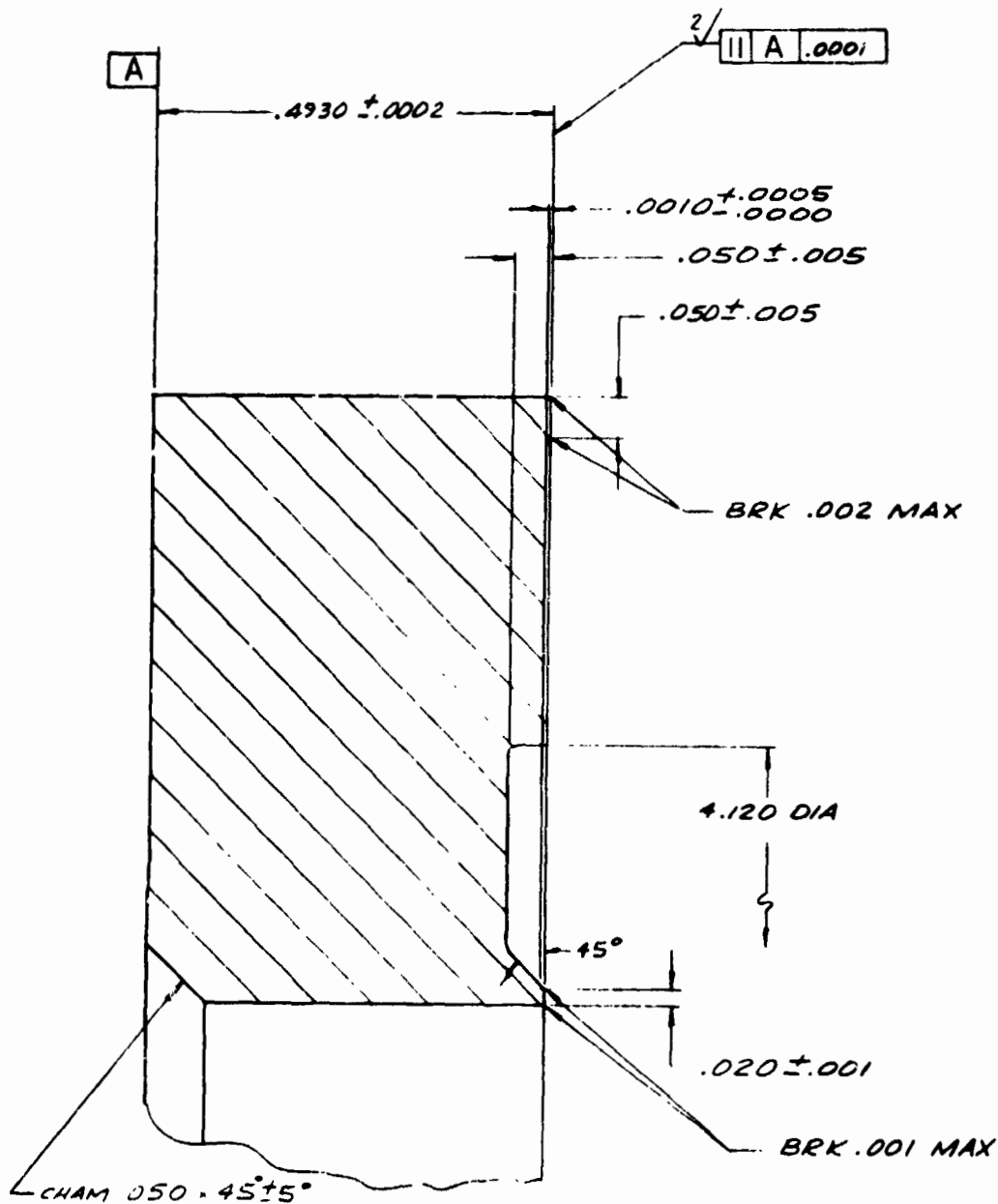


| REVISIONS | | | |
|-----------|--------------------|------|-------------------|
| LTR | DESCRIPTION | DATE | APPROVED |
| 1. | MAY BE REWORKED | 2 | RECORD CHANGE |
| 2. | CANNOT BE REWORKED | 4 | NOW SHOP PRACTICE |
| | 3. PARTS MADE OK | | |

C-2

Figure C-1. Molding Die

| | | | | | |
|-----------------------------------|---|--|--|--|--|
| FINISH FINISH MATL. | UNLESS OTHERWISE SPECIFIED: DIMENSIONS ARE IN INCHES AND APPLY PRIOR TO FINISH. 125/ MACH. SURF. ROUGHNESS | DWN DATE | Rockwell International Corporation Rockwell Division Torrance Park, California | | |
| | TOLERANCES ON ANGLES ± 6° IF DECIMALS .XX ± .05 .XXX ± .04 HOLES NOTED "DRILL" | CHG DATE | DIE, MOLDING | | |
| | OVER THRU TOLERANCE .000 .000 + .005 - .010 .000 .120 + .000 - .005 .120 .220 + .000 - .010 .220 .500 + .010 - .010 .500 .750 + .010 - .010 .750 1.000 + .010 - .010 1.000 2.000 + .010 - .010 | DESG DATE | | | |
| | DESIGN ACTIVITY APVD DATE | SIZE CODE IDENT NO. DRAWING NO. D 02602 | | | |
| DO NOT SCALE PRINT | | SCALE | SHEET | | |

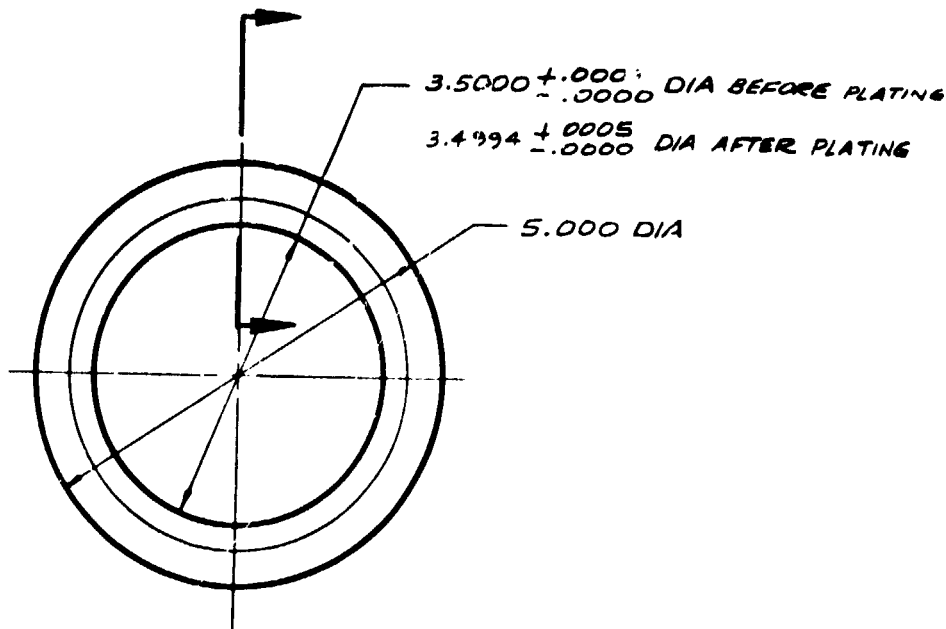


ORIGINAL PAGE 1-
OF POOR QUALITY.

- 5 ALL SURFACES $32/$
- ④ ELECTROLIZE .0002 TO .0003 THICK -
ELECTROLIZING CORP, L.A. CAL.
- ③ HEAT TREAT TO 200-220 KSI (R_c 42 MIN)
PER RA0111-015.
2. BREAK EDGES .005 MAX
1. FILLETS .010 \pm .005 R

NOTE: UNLESS OTHERWISE SPECIFIED

| REVISIONS | | | |
|-----------|--------------------|---------------|-------------------|
| LTR | DESCRIPTION | DATE | APPROVED |
| 1. | RAW BE REWORKED | 3. | RECORD CHANGE |
| 2. | CANNOT BE REWORKED | 4. | HOW SHOP PRACTICE |
| | 5. | PARTS MADE OK | |



C-3

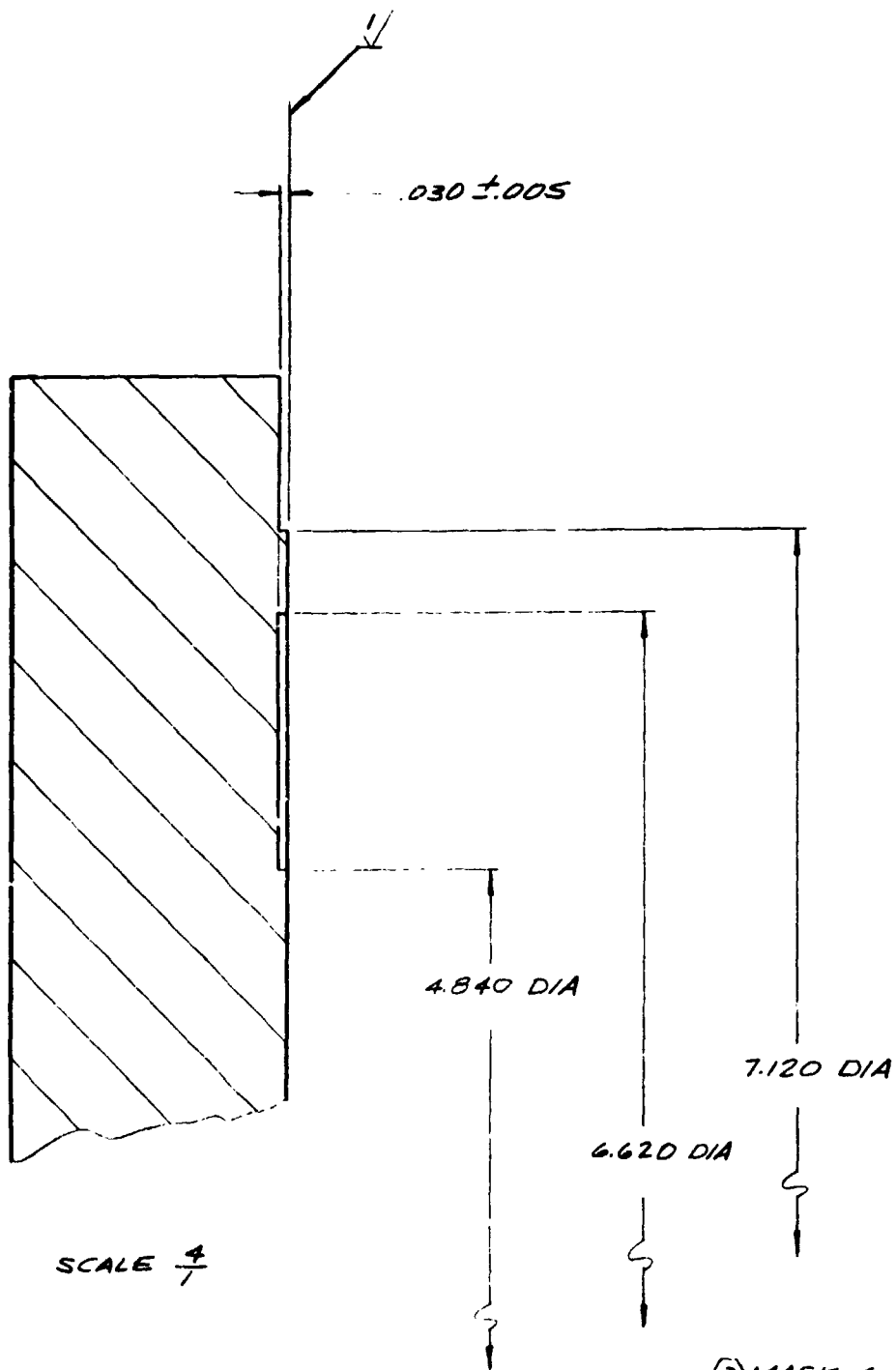
Figure C-2. Retainer Set, Rubber Die Ring

TO .0003 THICK-
P, L.A. CAL.
-220KSI (R_c 42 MIN)

3 MAX
S.R
BRED

| | | | |
|---|--|--|---|
| <div style="text-align: center;">3</div> | UNLESS OTHERWISE SPECIFIED, DIMENSIONS ARE IN INCHES AND APPLY PRIOR TO FINISH. | | <div style="text-align: center;">Rockwell International Corporation Rocketdyne Division Canoga Park, California</div> |
| | 125 / MACH. SURF. ROUGHNESS | | <div style="text-align: center;">RING - RETAINER SET RUBBER DIE</div> |
| <div style="text-align: center;">4</div> | TOLERANCES ON DIMENSIONS ± .005 IF BY DECIMALS OR ± .005 IF BY FRACTIONS | | <div style="text-align: center;">D 02602</div> |
| | HOLES NOTED "HOLE" | | <div style="text-align: center;">X EOK 34077101</div> |
| <div style="text-align: center;">+340 STEEL BAR</div> | OVER THRU TOLERANCE | | <div style="text-align: center;">SCALE 1/1</div> |
| | .000 .000 + .005 - .000 .000 .000 + .005 - .000 .000 .000 + .005 - .000 .000 .000 + .005 - .000 .000 .000 + .005 - .000 .000 .000 + .005 - .000 .000 .000 + .005 - .000 .000 .000 + .005 - .000 | | <div style="text-align: center;">SHEET</div> |
| DO NOT SCALE PRINT | | | |

FOLDOUT FRAME 2

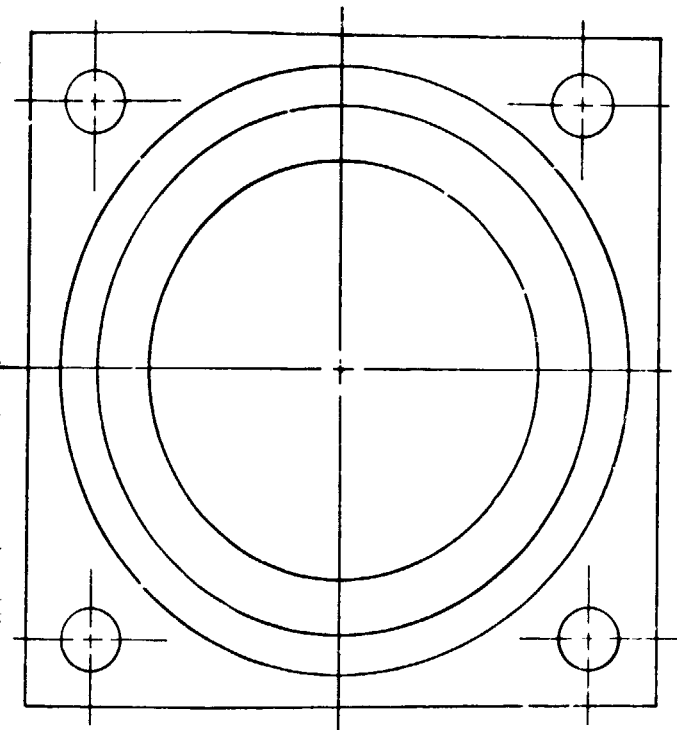


(3) MASK 4 HOLES AND ELECTROLIZE
 .0007 TO .0010 THICK-
 ELECTROLIZING CORP, L.A., CAL.
 2 BREAK EDGES .005 R MAX
 1 FILLETS .010 ± .005 R

NOTE: UNLESS OTHERWISE SPECIFIED

FOLDOUT FRAME

| REVISIONS | | | |
|-----------|-----------------------|------|----------|
| LTR | DESCRIPTION | DATE | APPROVED |
| | 1. MAY BE REWORKED | | |
| | 2. CANNOT BE REWORKED | | |
| | 3. RECORD CHANGE | | |
| | 4. NOW SHOP PRACTICE | | |
| | 5. PARTS MADE OK | | |



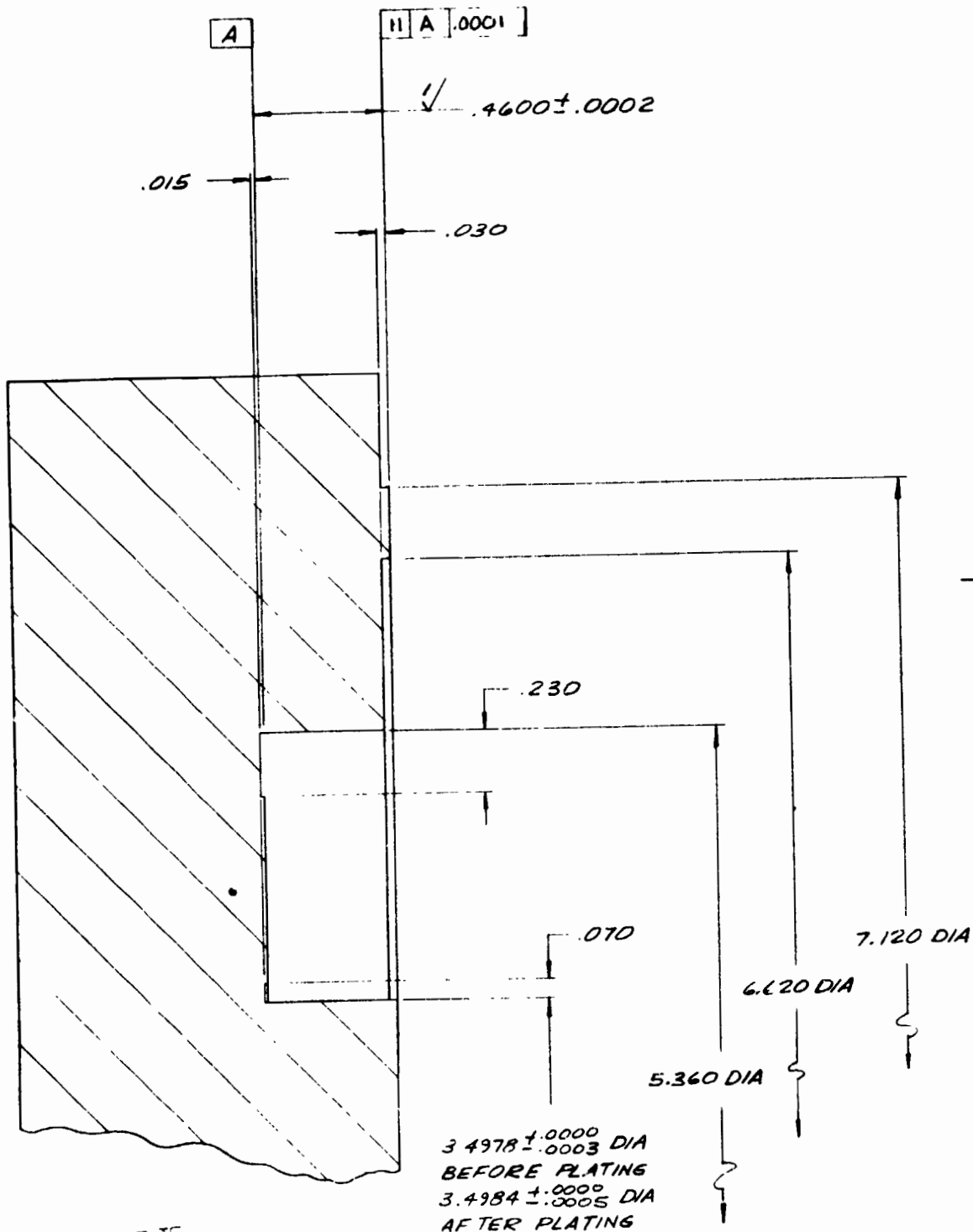
C-4

Figure C-3. Rubber Die "A" Plate

AND ELECTROLYZE
THICK-
CORP., L.A., CAL.
205 R MAX
205 R

| | | | | | |
|--|--|------------------------------------|----------------|--|-----------------------------|
| MEAS THREAT FINISH (3) | U-ESS OTHERWISE SPECIFIED: D. DIMENSIONS ARE IN INCHES AND APPLY PI FOR TO FINISH. 125/ MACH. SURF. ROUGHNESS TOLERANCES ON ANGLES $\pm 0^\circ 30'$ DECIMALS $\pm .001$ $\pm .010$ HOLES NOTED "DRILL" OVER THRU TOLERANCE .0000 .0000 + .0000 - .0010 .0000 .1300 + .0000 - .0010 .1300 .2250 + .0000 - .0010 .2250 .3000 + .0000 - .0010 .3000 .7500 + .0070 - .0010 .7500 1.0000 + .0000 - .0010 1.0000 2.0000 + .0120 - .0010 TO NOT SCALE PRINT | DWN CHK <i>[Signature]</i> | DATE 2/1/77 | Rockwell International Corporation Rocketdome Division Canoga Park, California | |
| | | DESG MATE <i>[Signature]</i> | DATE 2/1/77 | "A" PLATE, RUBBER DIE | |
| MATL MAKE FROM A" PLATE RETAINER | | DESIGN ACTIVITY APVD DATE | SIZE D | CODE IDENT NO. 02602 | DRAWING NO. XEOR940771D3 |
| | | | SCALE 1/1 | SHEET | |

FORM NO. 010-1-1 REV. 7-73



ORIGINAL PAGE IS
OF POOR QUALITY

SCALE $\frac{4}{1}$


- (3) MASK & PIN HOLES AND ELE
.0007 TO .0010 THICK -
ELECTROLIZING CORP, L.A. C
2 BREAK EDGES .005 MAX
1. FILLETS $.010 \pm .005 \text{ R}$

NOTE: UNLESS OTHERWISE SPECIFIED

FOLDOUT FRAME 1

Technical drawing of a square plate. The plate has a square outer boundary. Inside, there are three concentric circles. The innermost circle has a small horizontal arrow pointing to the right from its center. The middle circle is larger. The outermost circle is the largest of the three. In each of the four corners of the square, there is a circular hole. Each hole is represented by a solid circle and a dashed circle, indicating a hole. There are also dashed lines extending from the centers of these holes towards the center of the plate. A vertical line with an arrow pointing upwards is located on the right side of the plate, passing through the center of the concentric circles.

Figure C-4. Rubber Die "B" Plate

| | | | | | |
|--|---|--|---|------------------------|--|
| HEAVY THREAT  | UNLESS OTHERWISE SPECIFIED: DIMENSIONS ARE IN INCHES AND APPLY PRIOR TO FINISH. 1/8" MAX. SURF. ROUGHNESS TOLERANCES ON ANGLES \pm P 3P DECIMALS .XX \pm .03 .XXX \pm .010 HOLES NOTED "DRILL" OVER THRU TOLERANCE .0000 .0000 + .0015 - .0000 .0000 .1000 + .0030 - .0010 .1000 .2000 + .0045 - .0010 .2000 .5000 + .0060 - .0010 .5000 .7500 + .0070 - .0010 .7500 1.0000 + .0080 - .0010 1.0000 2.0000 + .0120 - .0010 | DWN <i>1/2" x 1/2"</i> DATE <i>1/27/79</i> CHN DATE DSGN <i>1/27/79</i> MAIL STRUCT DESIGN ACTIVITY APD | Rockwell International Corporation Rockfodyne Division Canoga Park, California B' PLATE, RUBBER DIE | | |
| | | MAKE FROM B' PLATE RETAINER | SIZE CODE IDENT NO. DRAWING NO. D 02602 XEOR940771D2 | SCALE <i>1/1</i> SHEET | |

FOLIOUT FRAME 2

For further experimentation, a setup similar to the preceding was made using an ID grinder to provide spindle mount and precision rotary head in lieu of an air table (Fig. C-5). Shown are a vacuum chuck and flycutter designed and fabricated for cutting 2.5 inch OD sheets of polymer material. The vacuum chuck (Fig. C-6) was made from a standard Hardinge faceplate. A hardened tool steel outer ring contains a 1/2-inch-thick section of Crystolon grinding wheel of suitable porosity. The three parts are epoxied together. The chuck face was lapped flat and parallel to the rear face within 25 μ in. Excessive pits were filled with quick-drying cement, which was lightly lapped flush with the basic surface. Within 0.01 inch of the porous surface OD, the tool steel ring was ground down 0.0038 inch to accommodate a band of double-back tape, which was cut in place with a razor blade and provided an air-tight seal. A sheet of machined elastomer is shown in Fig. C-6, which includes a flat model seal that was inset for thickness reduction.

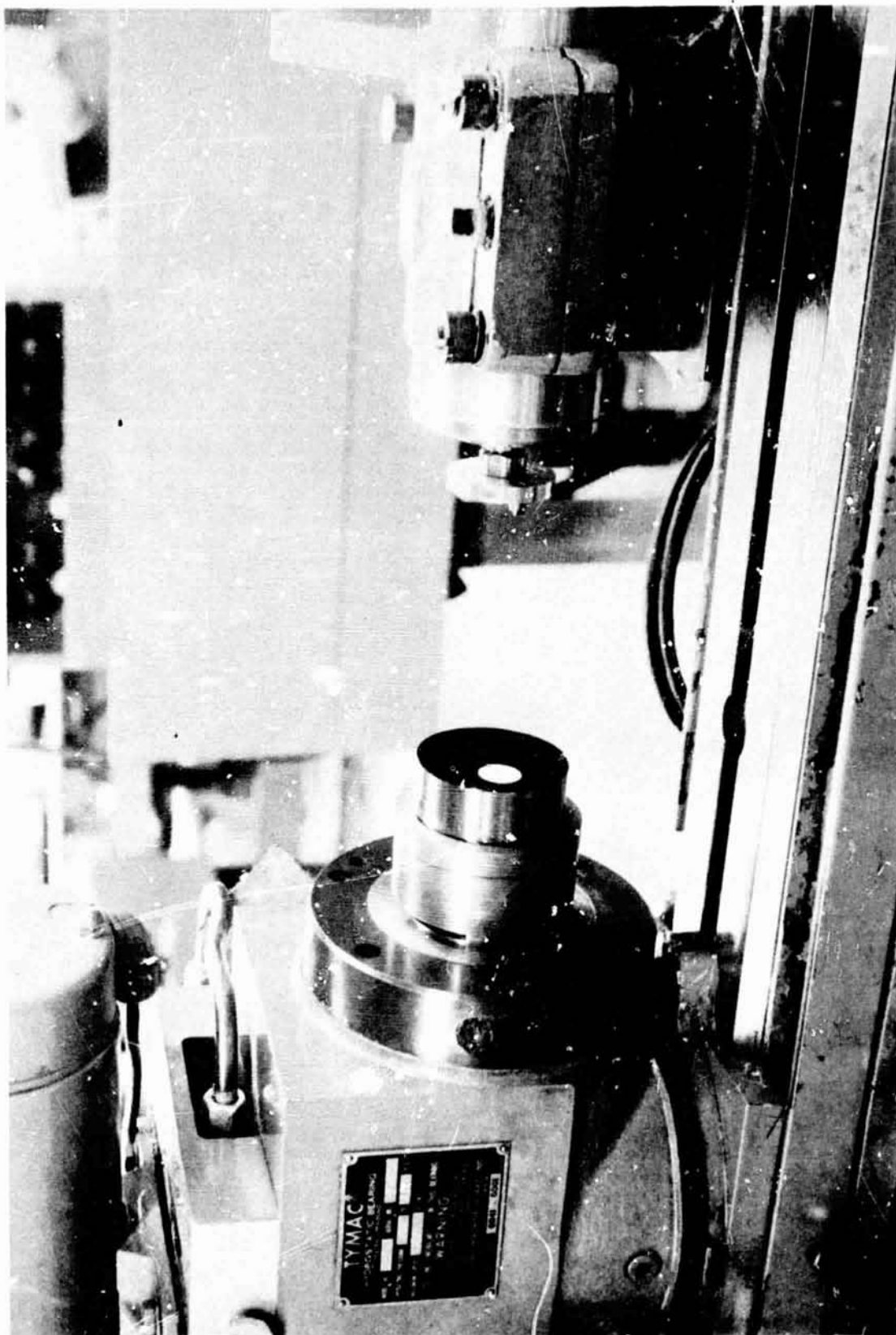
Initial attempts at flycutting were made using carbide tooling fashioned after the Westwind diamond tool. However, it was found that a one-pass cut of 0.001-inch depth increased the tool edge from an initially sharp condition (less than 50 μ in. break) to several ten thousandths inch. A diamond tool, subsequently purchased from Westwind, remained sharp for numerous cuts throughout the remainder of the program. The 1/2 carat diamond (Fig. C-7) has a 0.1-inch radius with 5-degree rake and clearance angles; as shown, the face plane passes through the wheel center. The diamond is inset into a steel post that is held into the wheel (at a 0.6875-inch radius) by a set screw. The aluminum wheel is balanced by a pin of equal weight on the opposite side and by precision machining.

The plane swept by the flycutter tool was made parallel to the chuck face within 50 μ in. The tool is positioned to pass through the center and over the material edge by 0.125 inch.

Many experiments were made in this setup to optimize material flatness and finish. Parameters were varied (and selected) as follows:

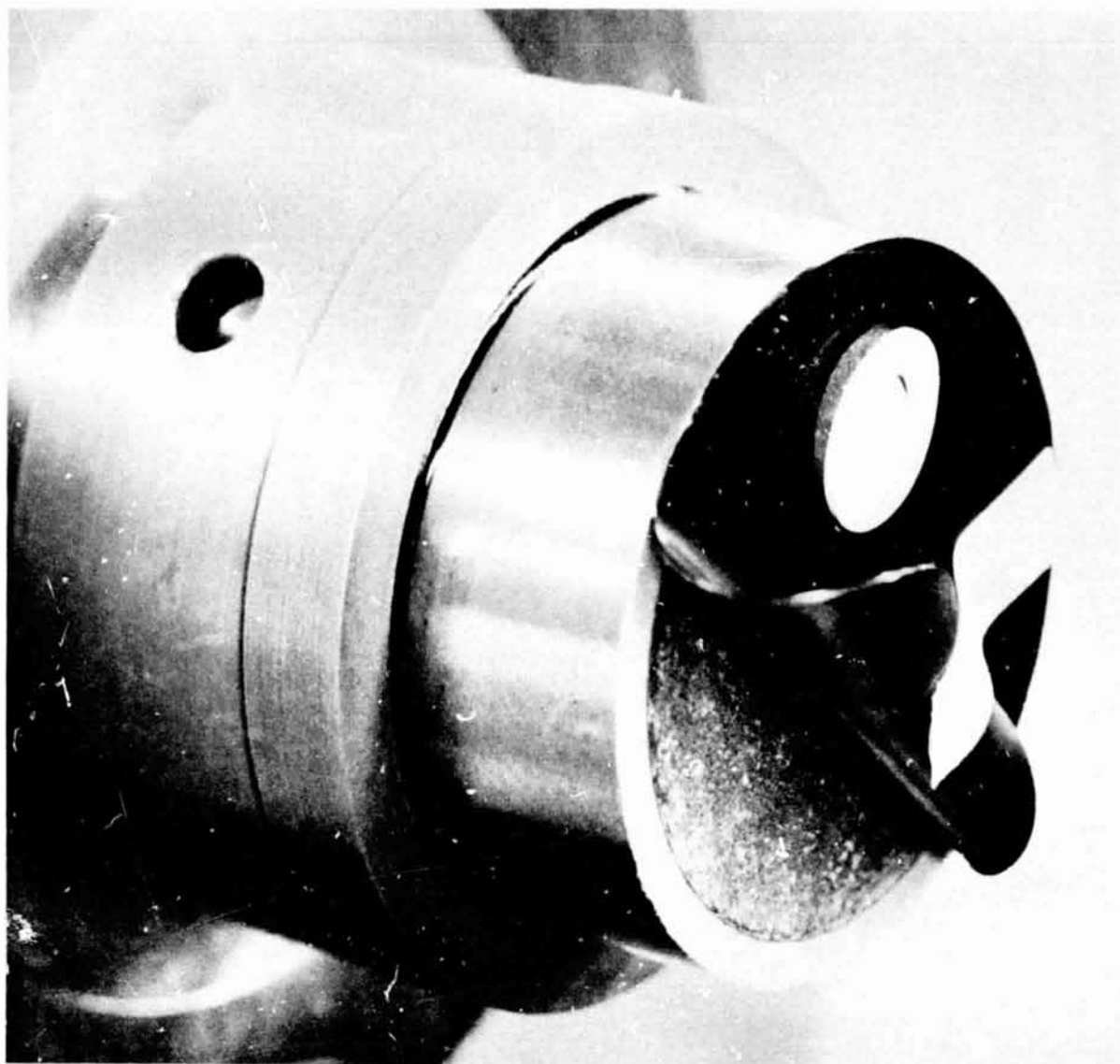
1. Tool geometry: diamond face angle ± 10 degrees off center (0 degree)
2. Cutter speed: 17 to 52K rpm (20K rpm)
3. Surface feed: 3 to 60 rpm (28 rpm)
4. Cut depth: 0.0005 to 0.005 inch (0.002 inch)
5. Overpasses: minimum one pass to several passes depending on item 3 (minimum)
6. Coolant: air, alcohol, water and soap solution (air)

Material cuts were made by plunging the rotating cutter into the rotating material to a preset depth at a rate of about 0.0005 to 0.001 in./sec. To minimize surface ripples, initial cuts on rough material were made using double-back tape over the entire chuck face. Subsequent cuts were made on alternate surfaces with each pass. Efficiency of the vacuum chuck was demonstrated by drawing a sheet of rubber down over a paper clip.



ISO62-10/24/74-C1F

Figure C-5. Flycutting Setup in ID Grinder



ISO62-10/24/74-C1E

Figure C-6. Flycutting Vacuum Chuck



ISO62-10/24/74-C1B

Figure C-7. Diamond Flycutting Tool

The best surface produced was on the white-filled AF-E-124X material and is estimated to have a surface roughness over 0.01 inch of about 4-8 AA. This finish is evident in the interference photograph (Fig. C-8). Thickness over the 2.5-inch sheet diameter was within 0.0001 inch. Waviness was produced on all machined surfaces on the order of 25 to 100 μ in. This may have been transference from the original surface or material relaxation after removal from the chuck face.

As previously noted, the process did not produce surfaces suitable for the OMS seal requirement. However, flat seal material of virtually any thickness was quickly produced and the process has potential for improvements over that indicated herein. To demonstrate the ability to cut thin material, one sheet of AF-E-124D material from AFML that contained numerous minute voids was machined down to 0.005 inch holding 0.0001 inch parallelism. At this thickness, the material was translucent and free of voids.

A major problem with the setup was the repeated cutting and variable feed from the rotary head and cutting process. A linear table wherein the cutter passes off each side of the cut material and only one cut is made would produce more uniform results. Even better for seals, the sealing surface should be single pointed with the diamond to produce a circular lay. This means that the material should be retained on the air spindle face and the diamond located in a crossfeed, similar to a conventional lathe. Ultimately, however, the sealing surface should be molded to provide a tough, glassy skin, inherent in the process, that machining cannot produce.

SEAL CUTOUT PROCESS

Flat and captive seals were cut from the flycut sheet stock using specially designed razor blade tooling. The setup, shown in Fig. C-9, is made in a Hardinge chucker lathe. Five razor blade tools are located on the rotary head.

Flat seal razor tools consisted of razor blade pieces wrapped around a brass rod and secured by a split collar and hose clamp. Sheet stock was held onto a rubber face plate by double-back tape. Seals were cut from the stock by plunging first the ID, then the OD blades through the stock with the faceplate rotating at slow speed; a water/green soap solution provided necessary lubrication. Diameters were sharp, square and well within ± 0.001 inch.

The captive seals required two angular cuts to a specific depth before ID/OD cut-out. This was accomplished with the razor blade tools shown in Fig. C-10 and illustrated in Fig. C-11. Because the razor formed an ellipse, the rod diameters were adjusted to minimize the circumferential amount of the blade (at its nominal 20-degree wraparound angle and cut depth) to within 0.0002 inch. Angular plunge into the stock was provided by the tool holders (Fig. C-9) with the carriage locked in place. Seals were initially cut by trial to establish dial settings. Dimensions were verified by measuring the hole ID in the stock and cutting a thin section from trial seals for microscopic inspection. Seal diameters were held well within ± 0.001 inch.

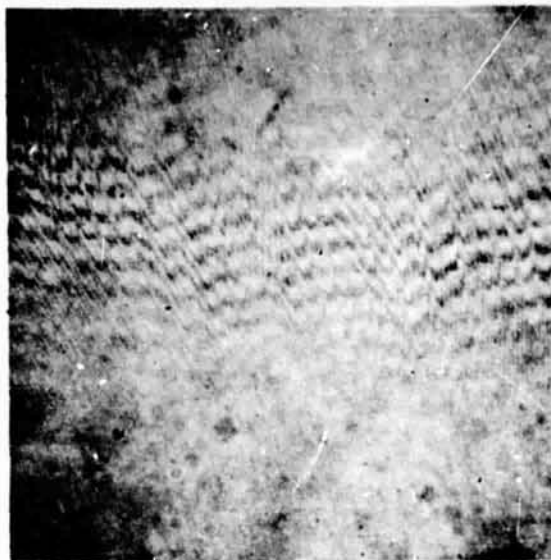


Figure C-8. Flycut AF-E-124X
Filled Elastomer (91X
Interference Photo)

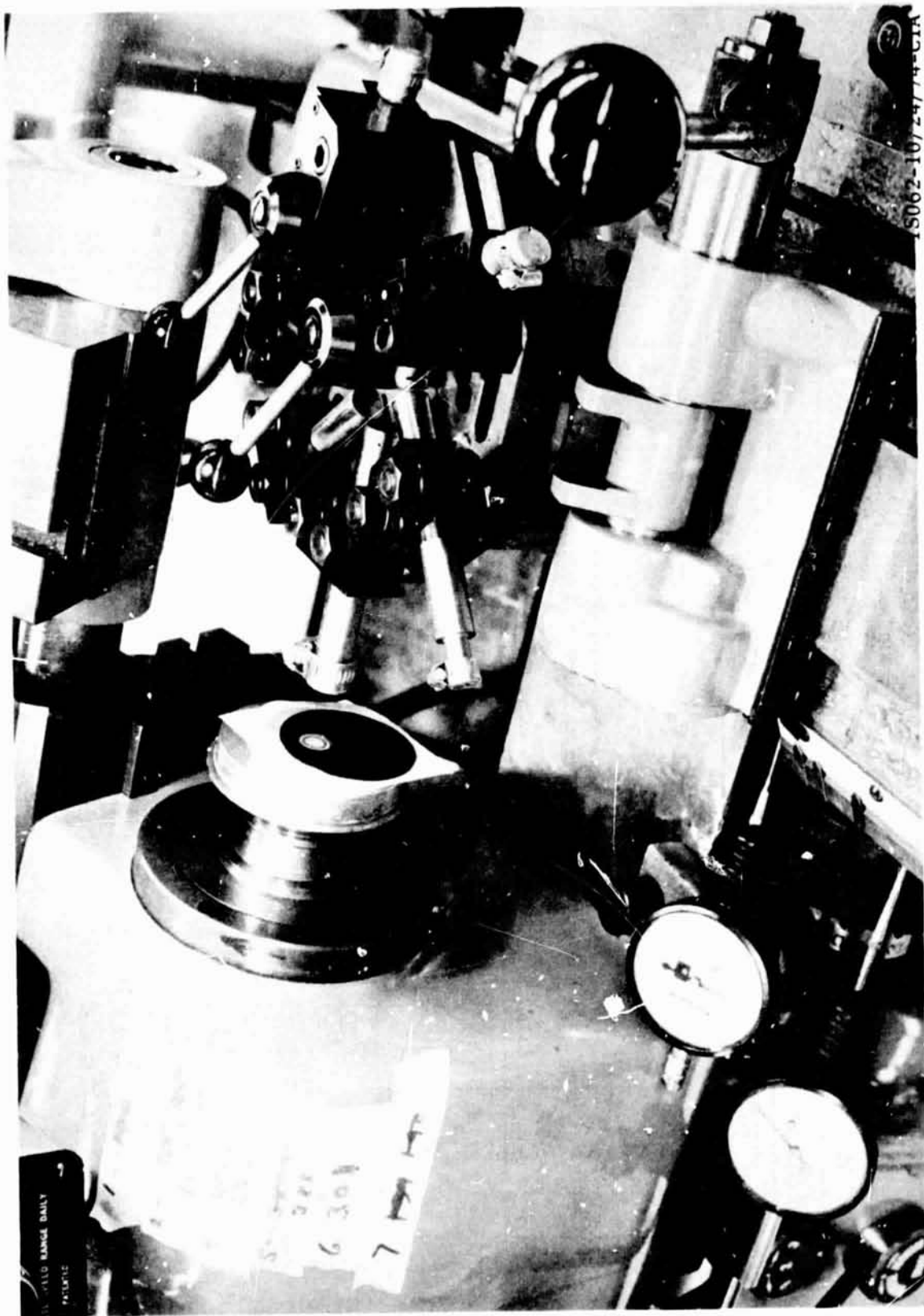


Figure C-9. Seal Cutout Setup in Turret Lathe

ORIGINAL PAGE IS
OF POOR QUALITY

| TOOL | A, OD $+.000$ -.000 | B, ID $+.002$ -.000 | $\theta \pm .25^\circ$ |
|----------|------------------------|------------------------|------------------------|
| -1 OUTER | .520 | .525 | $18^\circ 26'$ |
| -2 INNER | .450 | .455 | $18^\circ 26'$ |
| -3 OUTER | .518 | .523 | 0 |
| -4 INNER | .414 | .419 | 0 |

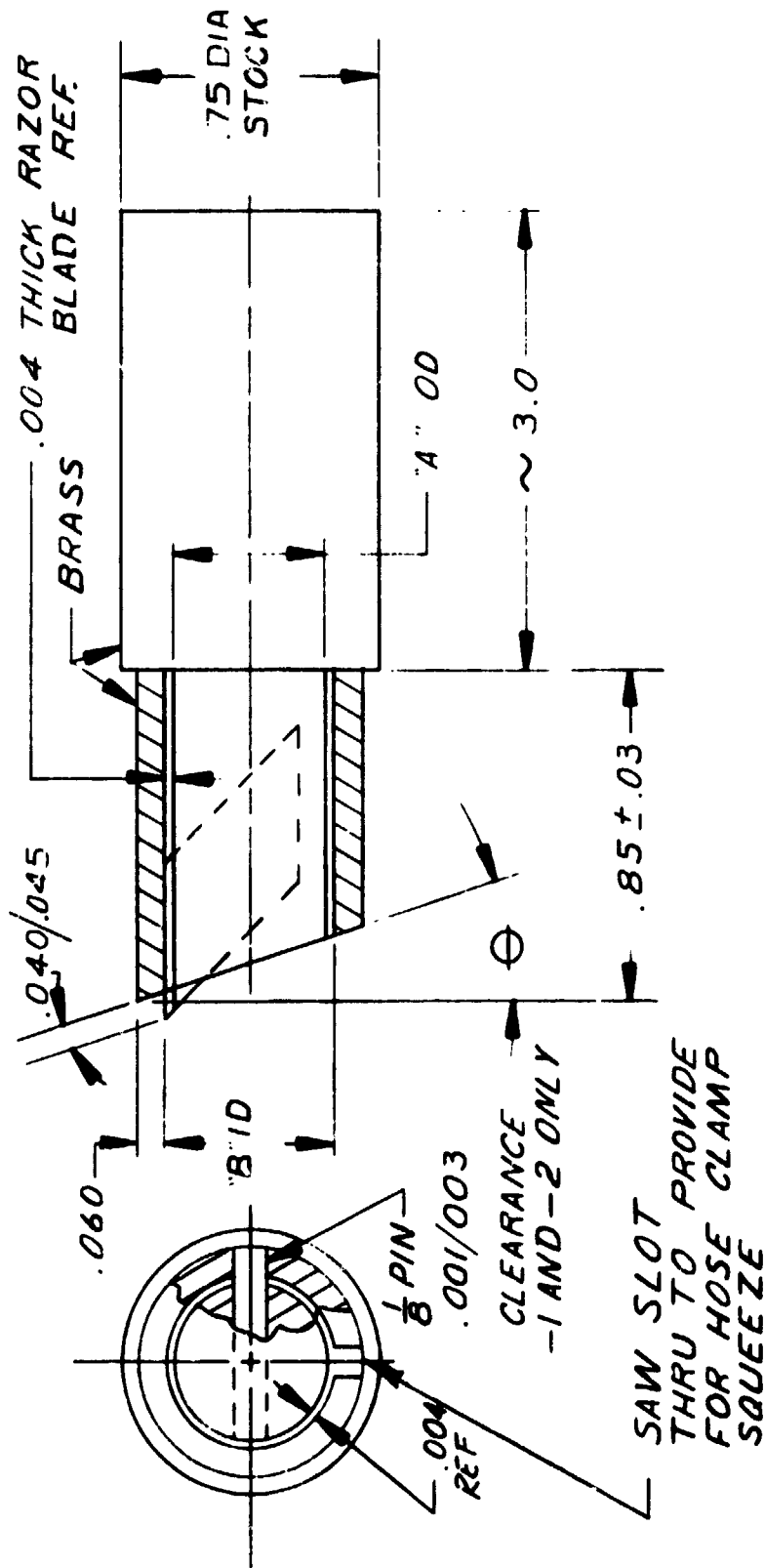
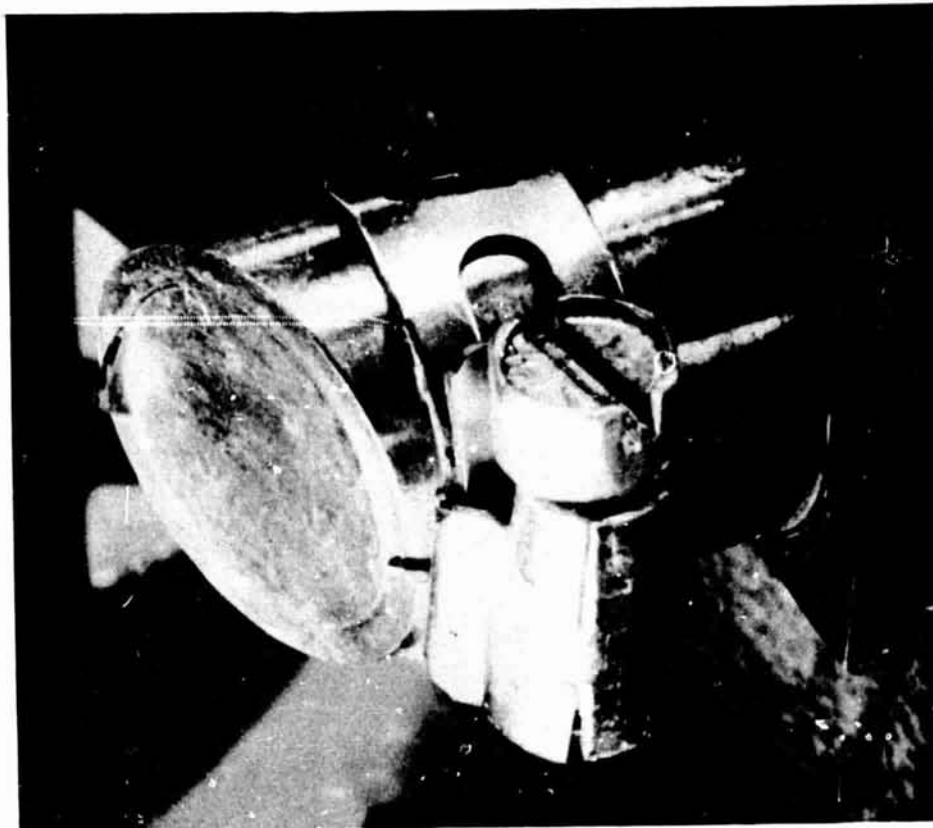


Figure C-10. Captive Seal Cutting Tools



IS062-10/24/74-C1D

Figure C-11. Captive Seal Cutout Razor Tool

ORIGINAL PAGE IS
OF POOR QUALITY

APPENDIX D

SEAL MODEL TESTER, SYSTEM AND OPERATIONAL PROCEDURES

Poppet and seat sealing characteristics are predominately affected by sealing interface closure positioning and loading. Precision control and repeatability of these parameters is fundamental for production of accurate data. The leak test provides the basic criterion of performance; therefore, accurate pressure control and leakage measurement are also required. Lastly, evaluation of cyclic performance calls for a tester capable of unlimited cycles over a range of temperature.

Poppet and seat model testers have evolved through several generations from past poppet and seat research programs. The first design consisted of a 440 C CRES body and 1.5-inch-diameter hydrostatic piston that provided accurate seal interface positioning, load control and leakage collection (Fig. D-1). This "static" tester was used to define the relation between surface geometry of metal-to-metal seals and load-leakage (Ref. D-1 and D-2).

The cyclic parameter was added in the second generation tester (Fig. D-2), which incorporated a hydraulic dashpot for seat impact control, and integral seat load cell to measure impact forces. This "dynamic" tester was used to evaluate cyclic impact closure effects in dry gases and in a Freon recirculation system containing precisely controlled distribution of artificial contaminant particles (Ref. D-2 and D-3).

Poppet and seat models in the dynamic tester were clamped in position and made parallel within about 10 μ m. Closure contacts were made with similar accuracy, which resulted in models demonstrating extremely long life. Recognition of tester precision not attainable in real valves led to the third tester design used in the Space Shuttle Auxiliary Propulsion System (SS/APS, Ref. D-4). In this tester, means were provided to vary the degree of interfacial scrubbing produced during closure. Additionally, refinements for improved performance and usage were incorporated into the design.

In all previous testers, inlet pressure was ported through the model seat with leakage collected at the periphery around the poppet and seat interface. Seat loading was developed by application of "control" pressure to the hydrostatic piston above that necessary to just balance piston weight and seat inlet pressure. Leakage versus net seat load data were thereby developed for a given constant inlet pressure, usually 100, 300, or 1000 psig. Net seat load accuracy was thus limited by the ability to discriminate between balance loads and incremental control pressure loading. Seat load error was on the order of ± 1.0 pound although 0.1-percent Heise gaging was employed.

OMS check valve seal requirements extend down to near zero seat load; therefore, previous methods were revised in the model test program. The APS tester was refurbished from the previous work (Ref. D-4) and modified to allow testing model poppets and seats in the check valve mode. The following paragraphs describe the modified APS tester with an analysis of load measurement methods and accuracy, the test system, and procedures employed in performance of specific tests.

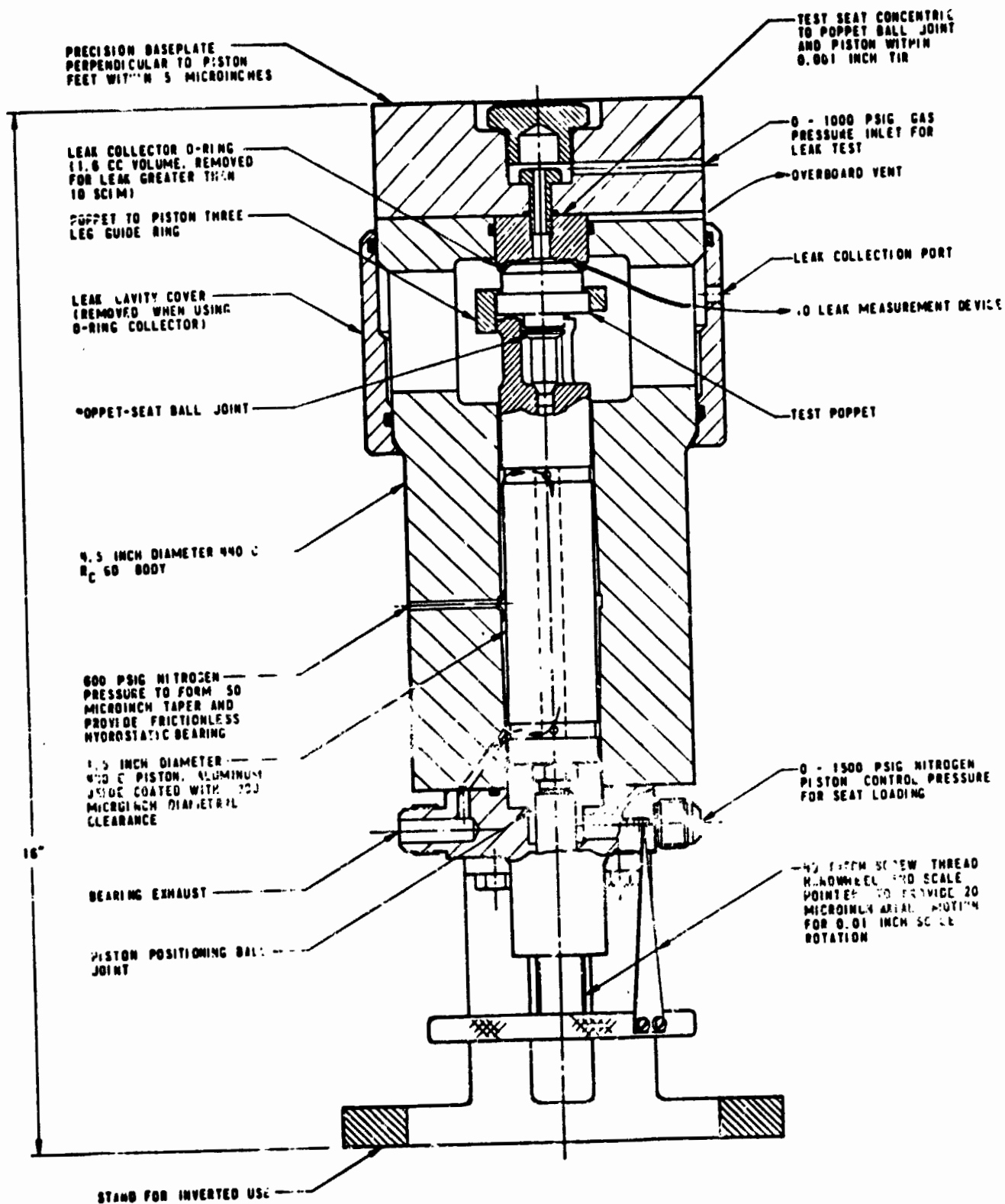


Figure D-1. Poppet and Seat Static Tester

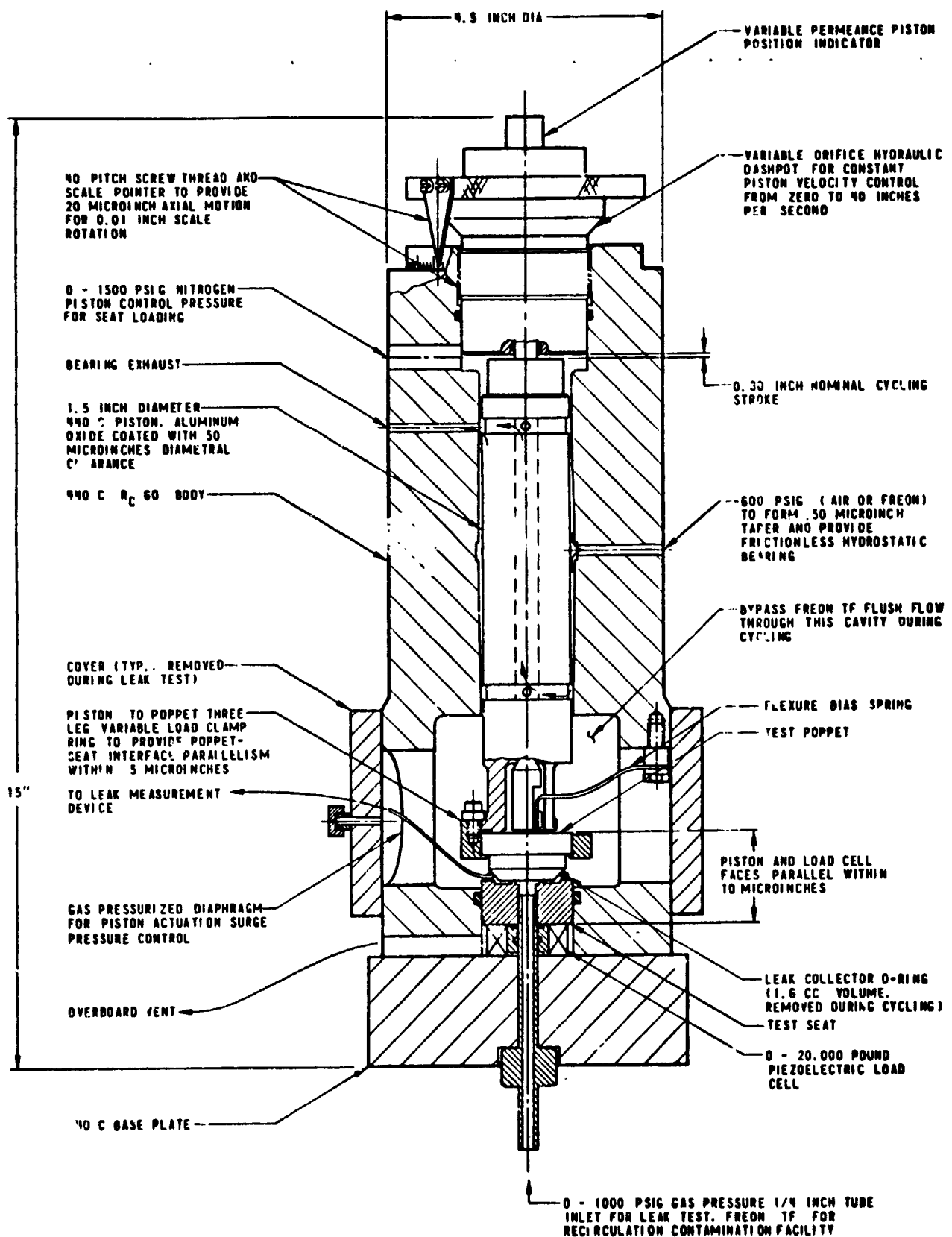


Figure D-2. Poppet and Seat Dynamic Tester

ORIGINAL PAGE 1
 C-7 POOR QUALITY

APS CLOSURE TESTER

General Description

The APS test fixture provided for (1) precision positioning and closure of poppet and seat models, (2) inlet pressure application around the poppet for check valve type loading, (3) augmented seat loading via piston control pressure, and (4) low-volume leakage collection. Tester functions are schematically shown in Fig. D-3 and D-4, and detailed in Fig. D-5 and D-6. The tester and parts are shown in Fig. D-7 through D-10.

In operation, the poppet is positioned between 8 carbide tipped, 120 pitch, set screws on a "wobbler" bearing, which provides for self-alignment by clamshell or scrubbing closure. The seat is retained in a separable cap by a quick-release spring. These features allow short turnaround time between model tests.

Frictionless translation of the poppet onto the seat is provided with a positional accuracy controlled by the piston to body clearance (about 0.0001 inch) and poppet to set screw clearances. The latter were set at 0.0002 inch diametral at top and 0.002 inch on the bottom for clamshell closure. A 40-pitch screw in the tester base with pointer and 0.010-inch scale allowed accuracy prepositioning of the poppet relative to the seat before applying inlet pressure to preclude inadvertent closure impacts. A welded metal bellows between the base and piston prevents piston rotation. The poppet was similarly retained by a pin in the holder. Poppet-to-seat contact was indicated by a Kistler piezoelectric load cell under the seat, which was capable of sensing load applications of less than 0.01 pound. Readout was by an oscilloscope.

The poppet retention beam shown in Fig. D-9 was used in previous tests (Ref. D-4) to retain the poppet onto the wobbler bearing during cycling. This beam and associated bearing parts were omitted for all tests described herein. The poppet was thus simply guided by the poppet holder during closure. After closure, the poppet holder and piston were retracted a few thousandths inch to prevent any possible influence of the test results.

Tester Refurbishment and Modification

The APS closure tester underwent millions of cycles from -320 to +390 F in the previous program (Ref. D-4). Tester cyclic function at -320 F was marginal due to piston binding. To complete this prior program effort, the diametral clearance was substantially increased. As a consequence, bearing stiffness was reduced to the point of allowing contact between the body and piston. Excessive clearance also caused a much greater consumption of piston bearing gas.

Original clearances were established between the body and piston by lapping the piston to a straight condition with the center section 100 μ in. smaller than the ends. The body was hard dense chrome plated 0.001 inch and rod lapped to produce a final bore of 1.127650- and 0.00011-inch diametral clearance. With this condition, the piston could be spun free at all bearing pressures to 800 psig. Leakage at 600-psig operation was between 50 and 100 scfm helium. Piston stiffness was such that the piston could not be made to rub the body with application of about 100 pounds between the poppet holder and body.

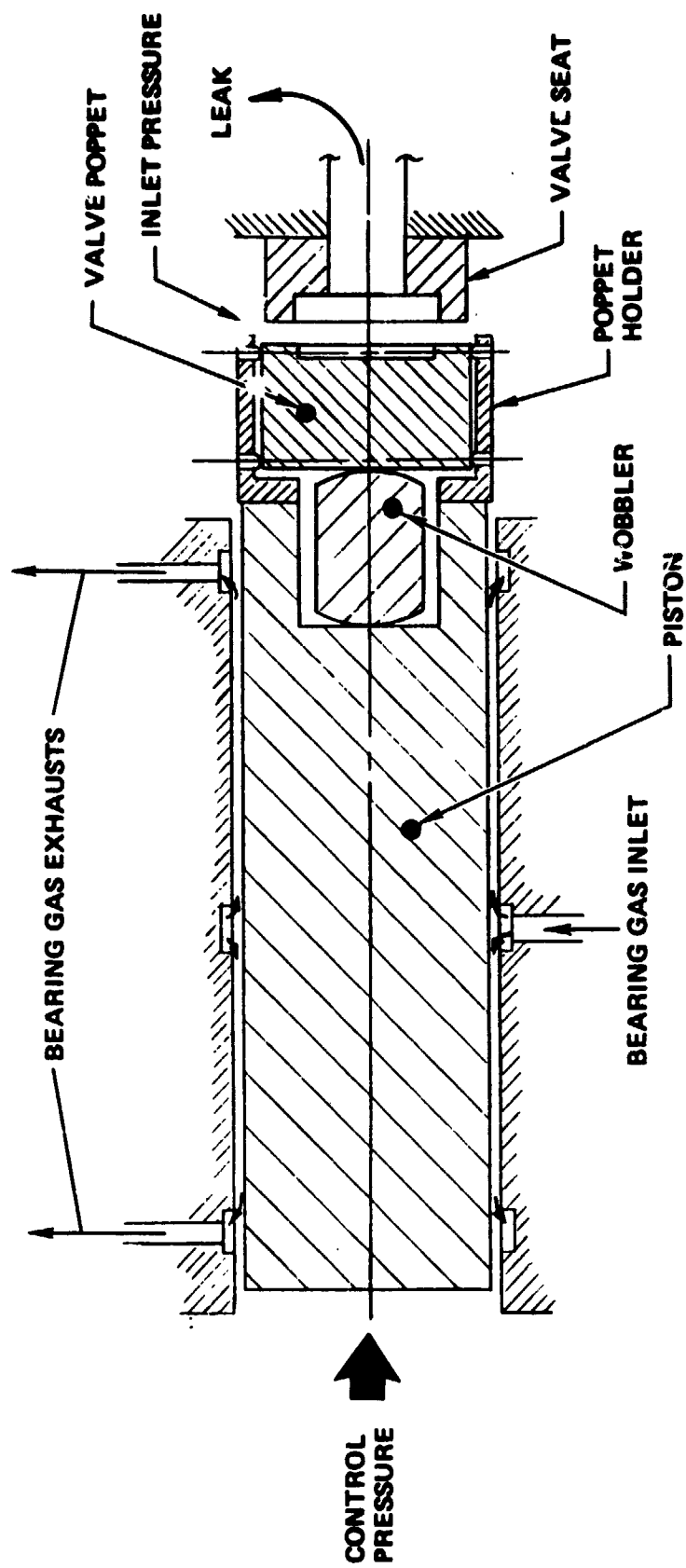
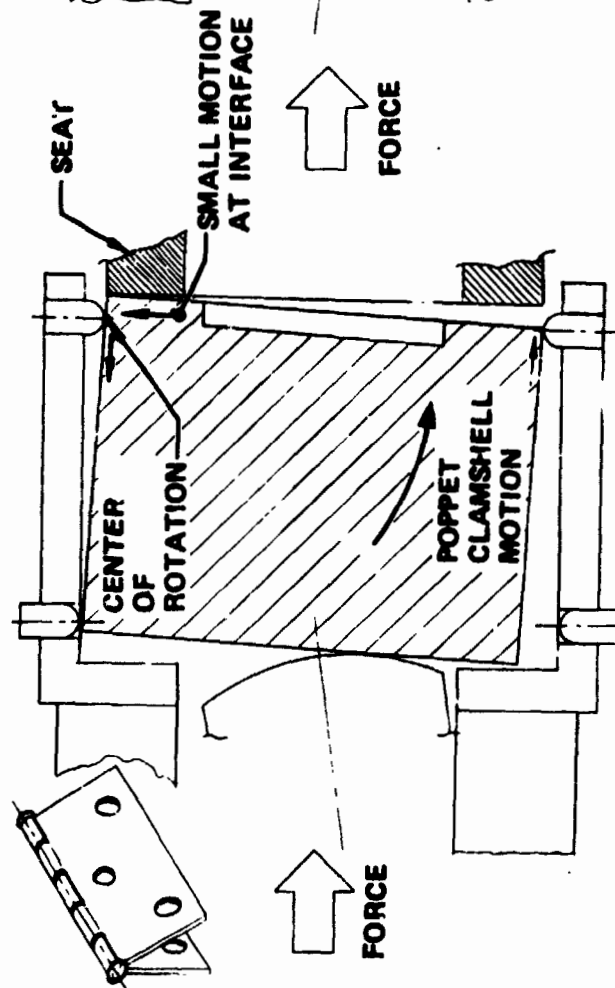


Figure D-3. Closure Tester Schematic

CLAMSHELL CLOSURE



SCRUBBING CLOSURE

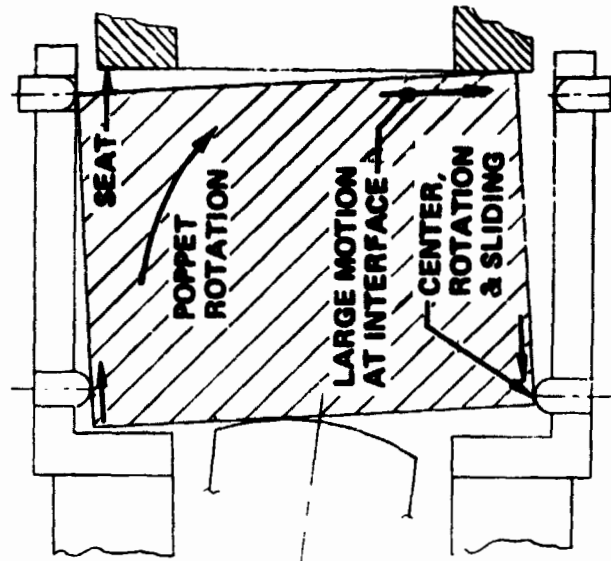


Figure D-4. Closure Mode

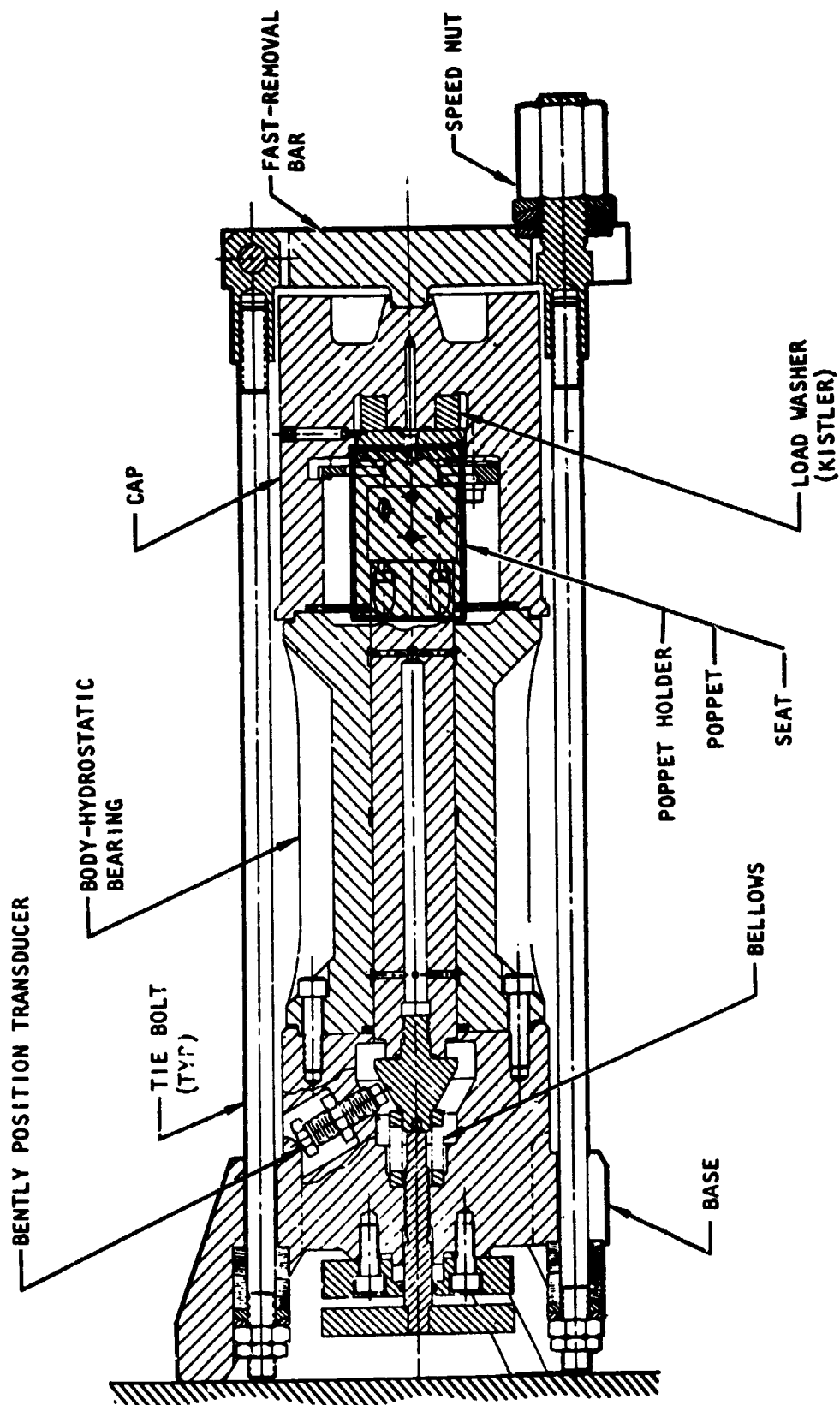


Figure D-5. Closure Tester

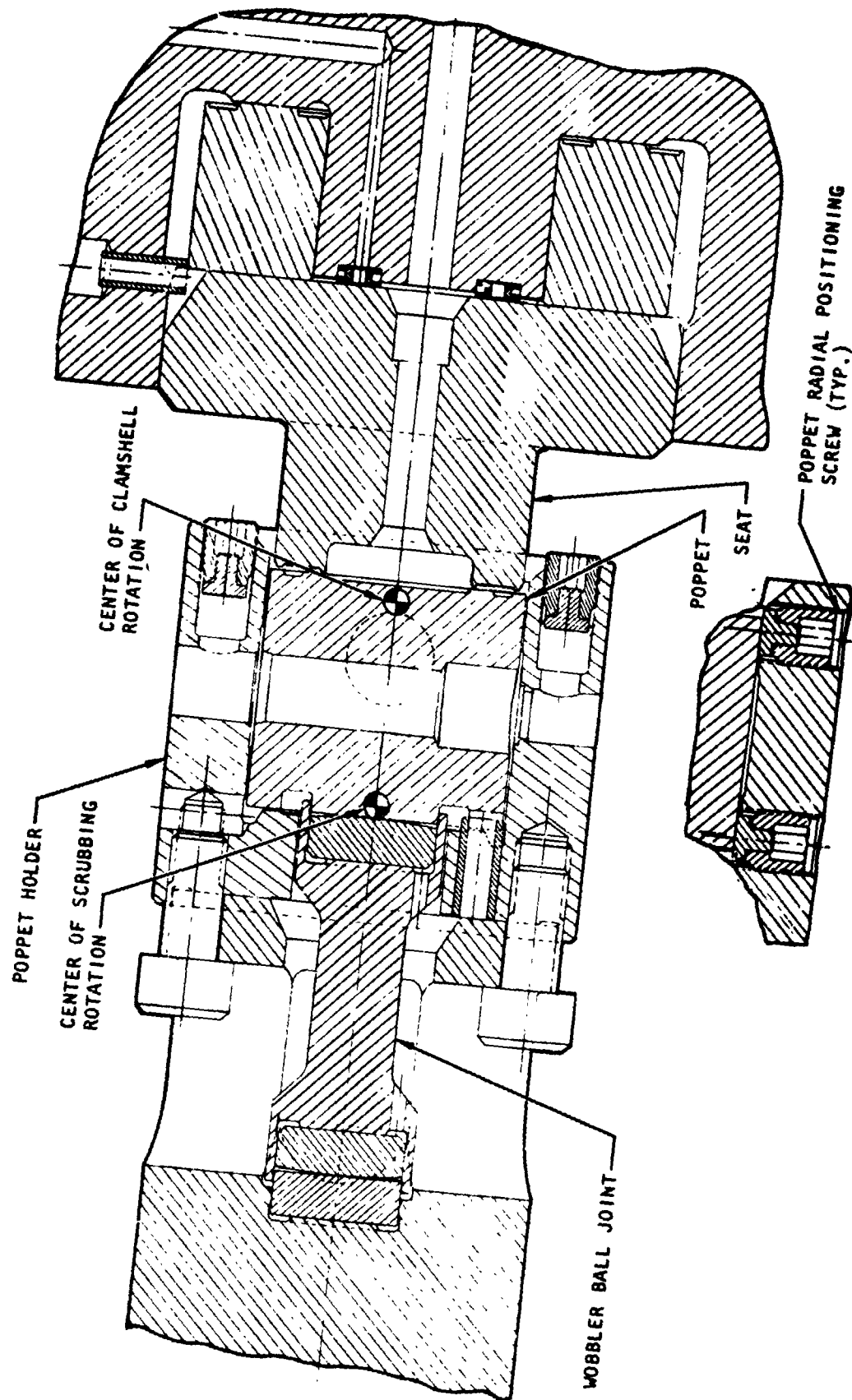
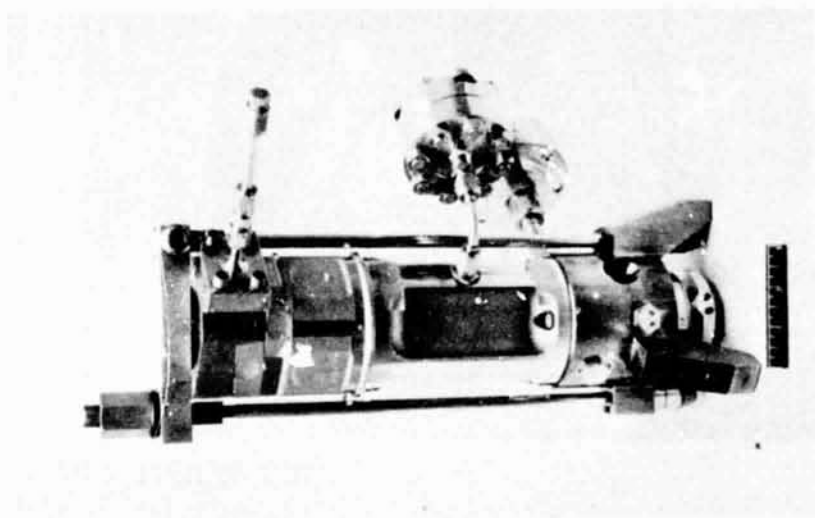
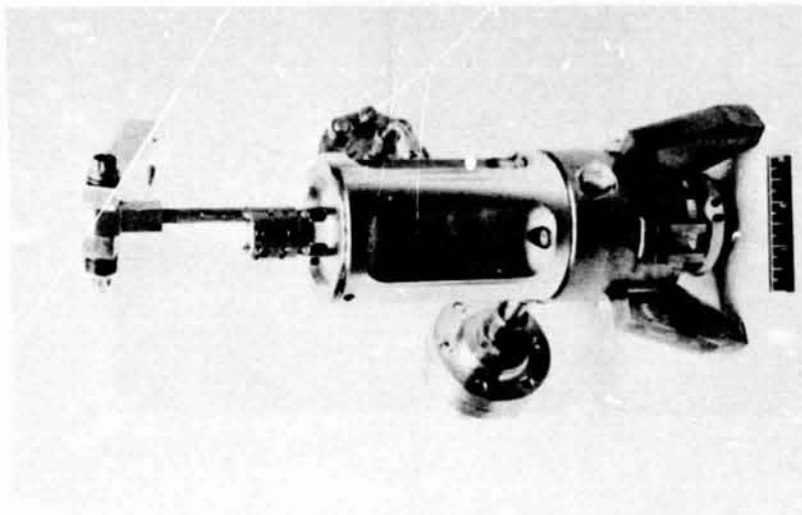


Figure D-6. Poppet Holder



1ST91-5/21/71-C1F

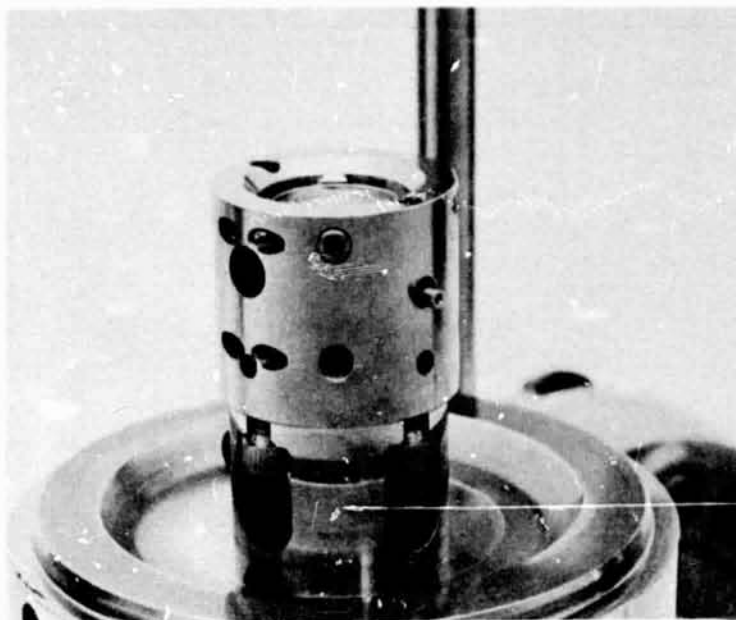
Figure D-7. APS Closure Screening Tester



1ST91-5/21/71-C1E

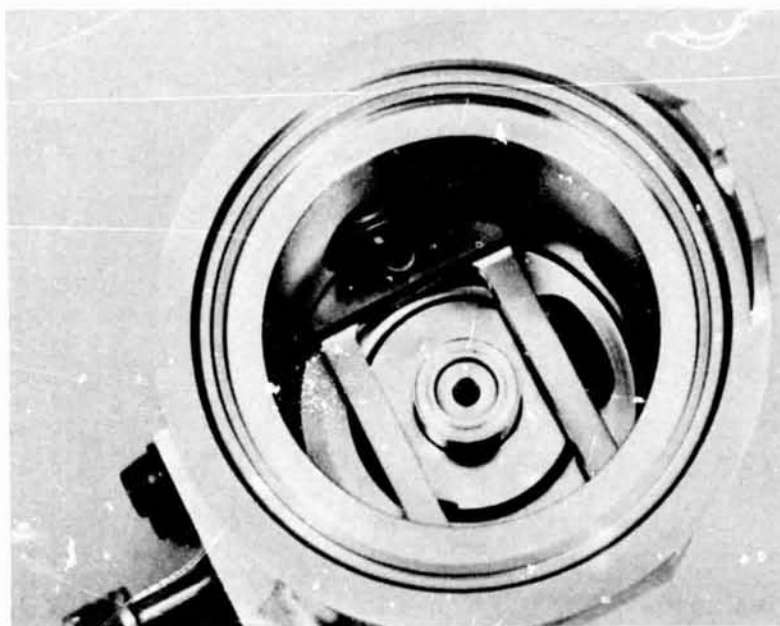
Figure D-8. APS Closure Screening Tester
With Cap Removed

ORIGINAL PAGE IS
OF POOR QUALITY



1ST91-5/21/71-C1A

Figure D-9. Poppet Holder With Poppet



ST91-5/21/71-C1D

Figure D-10. Cap With Seat

A new Kistler load washer was assembled into the tester cap. The load cell electrical leads were sealed at the cap with silicone rubber to prevent both external leakage and leakage into the coaxial cable.

To allow pressurization of the tester cap and thus provide inlet pressure around the model poppet, the normal inlet port filter assembly was removed. A small bore tube was epoxied into the cap below the seat and also out the inlet port, which provided for low-level leakage collection. Supply pressure was ported to the tester cap through a 0.5-micron membrane filter. A test was performed to prove that up to 500 psig could be introduced inside the tester cap without separation occurring between the cap and body.

Seat Load Analysis

Poppet-to-seat closure was initially obtained by slowly raising piston control pressure to the balance pressure required to just contact the seat, as indicated by a 0.01-pound output from the Kistler load cell. Inlet and control pressures were then sequentially increased to establish 1.0-psi inlet pressure to the poppet. Piston control was then dropped and the piston retracted if leakage was less than 1.0 scim (1000 scc/hr); otherwise, piston control pressure was raised to gradually decrease leakage to about 0.01 scim, holding inlet pressure constant at 1.0 psig. Measured back pressure through the discharge system was 0.1 psid at 2.0 scim and 0.5 psid at 11.0 scim. Closure loading was thereby produced by single application of inlet pressure acting over the effective seat area or was augmented by force from the control piston. Piston control pressure was used to measure the load required to either cut a contaminant wire or reduce leakage to a measurable value. Analysis of each loading method follows.

Check Valve Closure. With simple check valve closure the net seat force (F) is simply the pressure drop acting over the seat effective area (A_e) less the poppet weight; thus:

$$F = \Delta P A_e - W$$

With laminar flow, the pressure distribution across the seat land is parabolic (Ref. D-1) and

$$A_e = \frac{\pi}{4} \left(D_s - \frac{L}{3} \right)^2$$

where D_s is the seat mean diameter and L is the land width. With leakage less than 1.0 scim, the pressure drop was essentially equal to the inlet gage pressure as back pressure was less than 0.1 psid.

Error in computed seat force stems from pressure drop error and variation in effective area with load. A dual pressurization system provided pressure reading and control from 0 to 30 psig and 0 to 600 psig with setting and accuracy within 0.1 percent of full scale. With the cutter seat, effective area variation was

negligible. However, with soft polymer seals, the poppet and seat were not sufficiently parallel to ensure constant area and some (unknown) variation in effective diameter was probable. The maximum variation would be equivalent to a change in effective diameter from ID to OD, or reverse. The corresponding force change for $D_s = 0.0470$ inch and $L = 0.03$ inch is ± 29 percent from the actual value.

For the cutter seal, the nominal effective area was very nearly 0.173 sq in. From 0 to 30 psig, the maximum load variation from gage error was less than 0.01 pound. Above 30 psig, the maximum load variation was less than 0.1 pound.

Poppet weight was about 0.088 pound for all models. Therefore, simple check valve tests were essentially performed with a negative closure force, equivalent to an inlet pressure drop of 0.503 psid for the cutter seat. At 1.0 psid, the net seat load was 0.085 pound and at 10 psid the load was 1.64 pounds.

Check Valve Closure With Piston Loading. For most wire cutting tests, piston loading was necessary to cut the wire or reduce leakage to a measurable level. Force balance of the tester piston and poppet with control pressure (P_c) above balance control pressure (P_{CB}) is given by:

$$\Sigma F = 0 = P_c A_p + P_1 A_e - P_1 A_p - F - W - W_p$$

where W_p = piston weight + bellows force

$$P_{CB} = (W + W_p) / A_p \text{ at } P_1 = 0$$

$$A_p = \frac{\pi}{4} \times 1.12765^2 = 0.99871 \approx 1.0 \text{ sq in.}$$

Reducing gives

$$F = (P_c - P_1 - P_{CB}) A_p + P_1 A_e$$

Maximum seat force error is computed as before for the low-pressure range system; thus from the preceding equation, assuming 30-psi gages with 0.1 percent accuracy:

$$\Delta F = (0.03 + 0.03 + 0.03) \times 1.0 + 0.03 \times 0.173$$

$$\Delta F = \pm 0.095 \text{ pound maximum}$$

The rms average of the noted gage errors indicates a probable error of about 0.05 pound (assuming negligible seat area variation).

LEAKAGE MEASUREMENT

In all testing, closure leakage as a function of sealing load was a prime performance parameter. Gas leakage measurements made during various phases of seating investigations ranged from about 11 scim to 10^{-4} scim (0.1 scc/hr). Specifically calibrated, float-type flowmeters were used for flows down to 0.05 scim. Leakage was collected at the seat outlet and directed to the appropriate range flowmeters.

Lower range flow was measured with a leveling-bulb water buret system (Ref. D-1 through D-3). As shown in Fig. D-11, the leak is introduced into the top of the buret at atmospheric pressure, which is maintained by moving an interconnected water leveling bulb to hold buret capillary height constant. This procedure eliminates head pressure and surface tension effects associated with conventional bubble-under buret measurements. It also provides for self-leak checking by differential vacuum head testing to ensure a tight system. Computation of leak rates is determined from the following equation:

$$Q = \frac{3.66 \Delta V (P_a - P_v) T_s}{T t P_s}$$

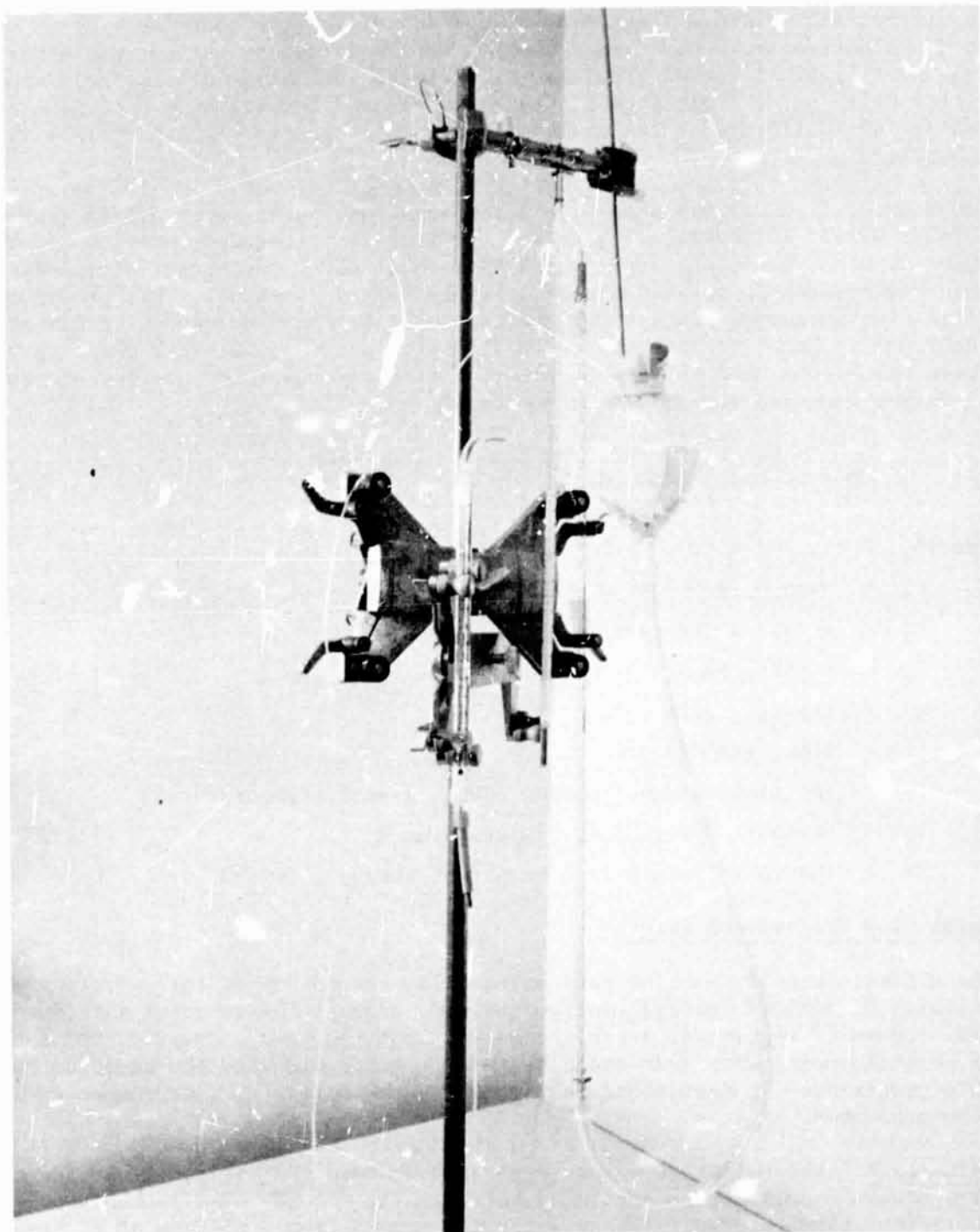
where

- P_a = atmospheric pressure, psia
- P_s = standard atmospheric pressure, psia
- P_v = vapor pressure of water at temperature, psia
- Q = leakage, scim
- t = time, seconds
- T = gas temperature (assumed equal to water temperature), R
- T_s = standard atmospheric temperature, R
- ΔV = change in volume as a result of leakage, cc

Buret Flow Measurement Errors

The ultimate use of the flow data is to allow comparison of the performance capabilities of various seating configurations. Because the range of data spans several orders of magnitude, great accuracy is not required. However, consistency of point-to-point data and repeat hysteresis loops dictated the need for reasonable precision. To meet these requirements, the following measurement errors were evaluated.

Volumetric. Where leakage values were greater than 10^{-3} scim, volume and time errors were made small by obtaining suitably large buret displacements over a sufficient time interval. These intervals ranged from a minimum of 30 seconds to several minutes. When leakage was measured between 10^{-3} and 10^{-4} scim, a



6AL42-11/6/69-C1J

Figure D-11. Leveling Bulb Leak Measurement Setup and
Low-Range Rotameter Tube

ORIGINAL PAGE IS
OF POOR QUALITY

minimum volume of 0.01 cc was displaced from the 1.0 ml buret (five 0.002 cc divisions). Because burets have precision bore tubes, the significant source of error is in the reading accuracy of the displaced water levels at start and stop. For the minimum leak of 10^{-4} , the length of displaced water was 0.200 inch which, for an estimated $\Delta h = 0.02$ inch (± 0.01 at each level), results in a maximum error of 10 percent.

Leveling. Errors in leveling cause the volume of gas being leaked into, as well as the leak volume, to be at a pressure other than atmospheric. Leveling errors stem from two sources:

1. Capillary action results in a differential height between the tube and bulb level. Variations in this height differential (due to film contamination of the glass) over a given span will result in pressure changes during a test run if a constant capillary height is assumed. This error was nullified by calibration over a specific span. (Thorough detergent cleaning of the tubes usually eliminated any noticeable error.)
2. Basic comparison reading errors of the levels in the bulb and buret

The equation for leakage error caused by pressure variations from variable head is.

$$\text{Error} = \frac{\rho_L \Delta h (V_L + \Delta V + V_1)}{(P_a - P_v + \rho_L \Delta h) \Delta V}$$

where

- Δh = leveling head error, inch
 V_1 = initial volume in buret, in.³
 V_L = leak volume external from the buret, in.³
 ρ_L = water density, lb/in.³

In the modified APS tester, external leak collection volume was comprised of 48 inches of 0.03-inch ID plastic tubing (0.034 in.³) and about 0.019 in.³ volume in the seat model (typical for the cutter seat) or about 0.053 in.³ for V_1 . Initial volume in the buret was usually less than 0.02 cu in. Assuming a leveling error of 0.1 inch differential from start to finish for a minimum collection volume (ΔV) of 0.01 cc indicates a volumetric leveling error of 3.0 percent.

Temperature. Variations in air temperature surrounding the external leak volume and buret induce changes in the final leak volume. The equation for leakage error caused by a change in system temperature is:

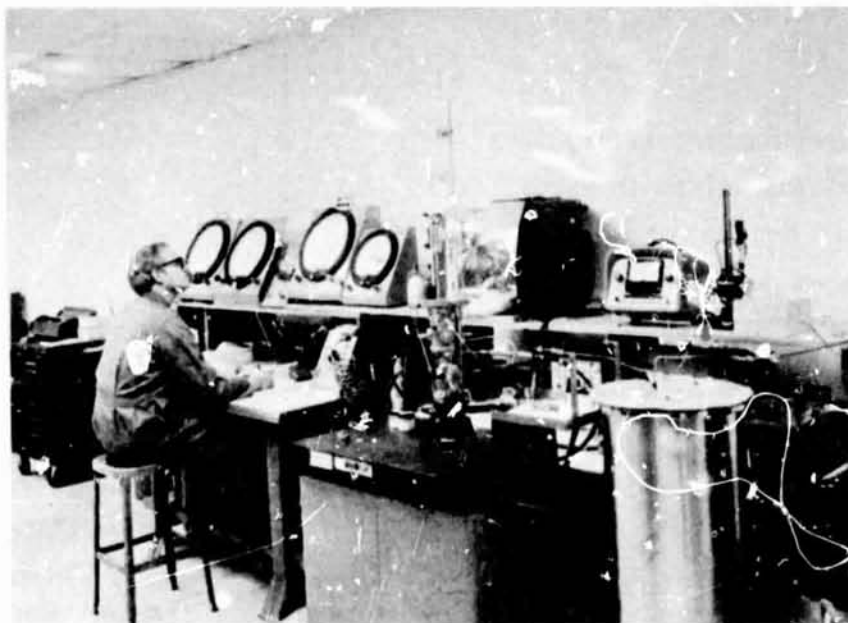
$$\text{Error} = \frac{V_L \Delta T}{\Delta V T}$$

where (ΔT) is the temperature variation, and (T) is the mean absolute temperature. Temperature variations were estimated to be generally less than 0.1 R. Consequently, for a minimum leak of 0.01 cc (6.1×10^{-4} in.³), maximum leak volume of 0.0736 in.³ and mean temperature of 530 R, the maximum (calculated) error in leakage is 2.3 percent.

Summary of Errors. From the preceding discussion, it can be seen that probable leakage measurement error down to 10^{-4} scim (0.1 scc/hr) was less than 15 percent. Around the 10^{-3} to 10^{-2} scim level (1 to 10 scc/hr), leakage measurement error was negligible.

TEST SYSTEM

The APS tester and system were set up in an air-conditioned room containing all of the tools, pressure-, temperature-, flow-, dynamic-, linear-measurement devices necessary to the test effort and microscopes for visual surface inspection. Figure D-12 shows the assembled system with four Heise pressure gages for high-low piston and inlet pressure control, the APS tester on granite gaging surface in front of the leak measurement buret and oscilloscope, a Cleveland electronic indicator, and a dewar for providing cold gas to the tester, as required. The system schematic is shown in Fig. D-13.



1S062-10/24/74-C1C

Figure D-12. Test System

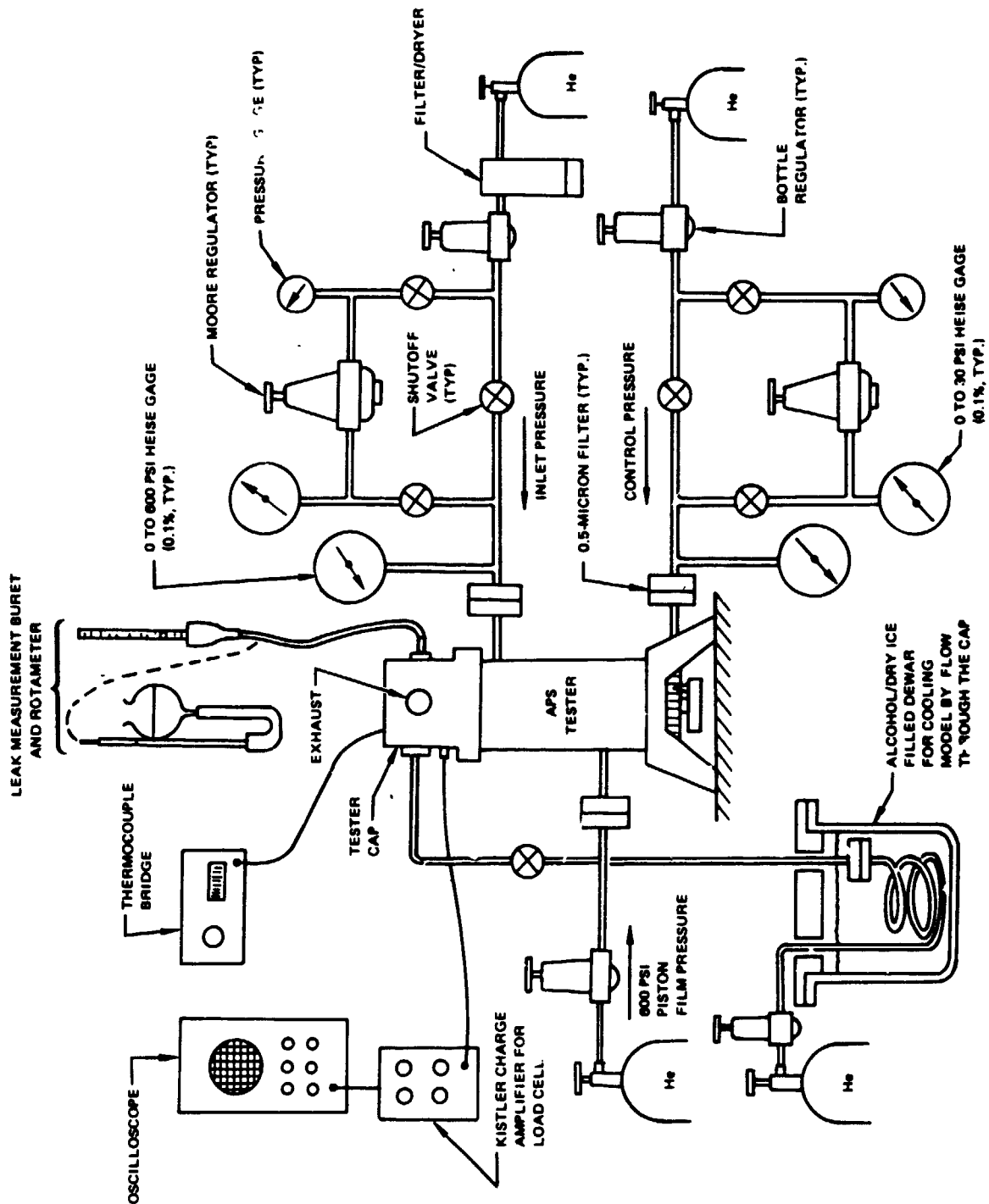


Figure D-13. Test System Schematic

ORIGINAL PAGE IS
OF POOR QUALITY

Pressurization Subsystems

Five pressurization sources were used, three for tester operation, one for cooling polymer test models by purging through the cap and one source (not schematically shown) for manual purging. Helium gas was used exclusively for tester operation (supplied as GFP, per MIL-P-27407).

First-stage inlet and control pressure regulation was obtained with commercial bottle regulators (Hoke, Airco, etc.). These devices have exceptional stability under low-flow conditions to provide pressure control within 1.0 psi from a few psi to over 1000 psig. For precision pressure control from 0.1 to 30 psig, Moore Nulmatic regulators were used. These valves proved capable of incrementing and holding pressure constant within 0.03 psi. All operating gas supplies to the tester were filtered through 0.5-micron millipore membranes.

Inlet pressure and seat closure load accuracy was established by 0.1 percent compensated Heise gages. Prior to performing any tests, all gages were connected to a common pressure source and sensitivity and common readings were verified to be within 0.1 percent of full scale.

Instrumentation

Poppet position relative to the seat was initially established in the tester using the 40 pitch screw and pointer built into the tester base. Actual contact between the poppet and seat were indicated on an oscilloscope by the output from a Kistler load cell located under the seat. This was the sole purpose of the load cell; therefore, sensitivity of the charge amplifier was increased to indicate contact for loads less than 0.01 pound.

Low-temperature conditioning of the polymer poppet and seat models was monitored using a thermocouple contacting the seat with readout by a thermocouple bridge.

Cold Test System

Low-temperature (-15 F) conditioning of polymer seals was accomplished by purging cold gas through the tester cap, across the closure model. The gas was chilled through a coil submerged in alcohol and dry ice at about -90 F. Supplemental cooling during chilldown and test was provided by surrounding the tester cap with dry ice. A thermocouple was used to continuously monitor the seat temperature. Several trail test runs were made with the thermocouple embedded in the seal material to establish temperature stabilization characteristics of the seal relative to surrounding metal.

TEST PROCEDURES

The sealing performance of all test models was determined by a check valve mode of testing. Because of the vertical position of the tester, the poppet weight acted as a negative closure force. As a consequence, the force required to cut or mash most (larger) wires was determined by application of a gradually increased

load from the tester piston. Reduction of the closure gap produced by wire cutting was ascertained from leakage produced by a constant inlet pressure of 1.0 psig. Because cutting or mashing contaminants is a plastic process, it was necessary to carefully control the sequence of load applications so that low load data were not lost. In other cases, sealing performance was much more simply obtained by repeated pressure loops from 1 to 500 psig to verify leak performance repeatability. In those cases where low-pressure leakage was excessive, pressure loops were run using the piston to simulate a constant spring load between 1 and 2 pounds.

The sequential steps in operating the tester and performing the preceding tests are covered in the following sections.

General Pretest Sequences

1. Turn on electronics and verify load cell operation
2. With all regulator valves in the closed position, slowly raise supply pressure to each regulator by gradually opening gas bottle valves
3. Raise tester film pressure to 600 \pm 25 psig
4. Ensure tester piston position screw is backed off at least two turns to provide 0.05-inch space between poppet and seat upon assembly
5. Assemble test model seal as necessary and clean sealing surfaces with solvent and blow dry with filtered gas; inspect for foreign films and particles and remove same
6. Assemble model seat into the tester cap and place poppet in the poppet holder; reinspect sealing surfaces for particles and blow off with filtered gas
7. Place cap on tester and advance tie-bolt nut one and one-half turns after taking up slack
8. Place all manual valves in position for low-pressure (0 to 30 psig) operation
9. Raise inlet pressure to each Moore regulator to 25 psig
10. Using the Moore regulator, raise tester inlet pressure to purge cap cavity with helium for 10 seconds; shut off purge
11. Slowly raise P_C to bring poppet into contact with the seat, as indicated by load cell output of about 0.01 pound on the oscilloscope. Bellows rate allows the piston to advance with increasing pressure; P_C to touch varies with the length of the poppet and seat (about 5.6 psig for the cutter model to 2.6 psig for the captive polymer model). The P_C obtained is the balance pressure (P_{CB}) at zero inlet pressure and represents the combined piston and poppet weight and the bellows force at the poppet to seat contact point. Bellows rate at contact deflection is 0.063 pound per 0.001 inch travel; therefore, seal deflection at light loads will have negligible effect on P_{CB} and thus net seat load.

At this point, procedure varies with the model and test objective. With initial test of each model, the piston handwheel is advanced to just contact the seat as indicated by the load cell. The scale reading indicated by the pointer is recorded as the contact point. The handwheel is then retracted 1 scale inch to provide 0.00441-inch gap between the poppet and seat.

Clean Model Leak Test

1. Raise P_C to 1.0 psi greater than P_{CB} , which places a 1.0 pound force on the poppet and seat
2. Raise P_1 to 1.0 psig and reduce P_C to zero
3. Raise inlet pressure in a logarithmic sequence of pressures (1.0, 2.0, 5.0, 10.0, 20.0, etc.) to 500 psig and similarly back to 1.0 psig, recording leakage at each pressure level. Repeat as required to verify consistency of data. (Note: At P_1 of 25 psig, appropriate shutoff valves must be switched so as to maintain inlet pressure constant within 5 psi.) The Moore regulator is left open for descending switchover.
4. Back off handwheel two turns if model is to be removed from tester

Cutter Seal Model Leak Test With Entrapped Wire

1. Place clean wire radially across one land of poppet
2. Verify that handwheel position from contact is backed off two turns
3. Assemble cap containing seat onto tester
4. Establish P_{CB} to contact wire
5. Advance P_C an additional 0.6 psi to provide 0.6 pound load on the seat
6. Raise P_1 to 0.2 psig, reducing net load to 0.435 pound
7. Raise P_C an additional 0.3 to 0.9 psi over balance; net load is now 0.735 pound
8. Raise P_1 to 0.5 psi and record leakage for net load of 0.487 pound
9. Raise P_1 to 1.0 psi and reduce P_C to zero if leakage is less than 1.0 scim; net load is now 0.085 pound. If partial reduction of P_C causes excessive leakage, raise P_C in 0.1 psi increments (recording data) until leakage is reduced to 0.01 scim (10 scc/hr) or less
10. Advance handwheel to within 1 scale inch of contact
11. Reduce P_C to zero and proceed as with clean test (step 3) except do not reduce P_1 below 1.0 psi until the test conclusion
12. Back off handwheel two turns and remove poppet and seat from tester for sealing surface inspection

Polymer Seal Test

Polymer seal test procedures were similar to cutter model methods except that an initial 1.0 pound P_c load was applied with P_1 raised to 1.0 psi to stick the poppet onto the seat. P_c was then either raised to reduce leakage below 0.01 scim or dropped and P_1 incrementally changed as above.

Cold test procedures were the same as ambient tests except that the model was closed ($P_1 = 1.0$ psig) with a net seat load of 2.5 pounds for the captive and 1.0 pound for the flat model during chilldown. A thermocouple was placed on the seat base to ascertain temperature stabilization. The time relation between chilling the metal and polymer seal was determined by comparison of chilldown times required for both materials during an initial calibration test. The -15 F model temperature was obtained by blowing cold nitrogen gas over the model through the tester cap. Additional cooling was provided by surrounding the cap with dry ice.

APPENDIX D REFERENCES

- D-1. Tellier, G. F.: Poppet and Seat Design Data for Aerospace Valves, AFRPL-TR-66-147, DDC AD 488480, Rocketdyne Division, Rockwell International, Canoga Park, California, July 1966.
- D-2. Tellier, G. F. and J. W. Lewellen: Poppet and Seat Design Criteria for Contaminant-Particle Resistance, AFRPL-TR-70-1, DDC AD 878212, Rocketdyne Division, Rockwell International, Canoga Park, California, April 1970.
- D-3. Tellier, G. F. and T. R. Spring: Contaminant Particles in Metal-to-Metal Closures, AFRPL-TR-7-112, Rocketdyne Division, Rockwell International, Canoga Park, California, December 1971.
- D-4. Smith, G. M.: High-Performance Space Shuttle Auxiliary Propellant Valve Program, NASA CR-120976, Rocketdyne Division, Rockwell International, Canoga Park, California, June 1973.